Electrostatic Precipitation of Fine Airborne Particles and Biological Decontamination: Efficiency and Energy Consumption Tendencies

Yihan Liu

Department of Electronic and Electrical Engineering

University of Strathclyde

A thesis presented in fulfilment of the requirement for the degree of

Doctor of Philosophy

2018

I would delicate this thesis to my parents, who have been supporting me during the whole period of my study. This PhD means a lot to me. It is not only study and research, but also an important experience of my life. I have been chasing my dream since I left my hometown at 16. As your son, I am deeply aware of your sacrifice.

I would also delicate this thesis to my wife, Dr Tong Qiao. Our marriage in Glasgow during our PhD period makes a wonderful ending to the 8-year love race. Everything in this city we love has witnessed our love. Our PhDs will not be successful without the associated effort and our tacit understandings to each other. For the time being abroad, it is good to have you along the journey.

谨以此文，献给我的父母。

感谢你们一直以来对我学业上的支持，博士对于我来说意义重大，它不仅仅是学习和研究，更是一段重要的人生经历。从十六岁背起行囊离开家乡那天起，追梦的路上，儿子深知您二老为了这一切的牺牲。

此文也送给我的妻子乔彤博士。

八年的爱情长跑在我们的博士期间划下句点，格拉斯哥的一草一木见证我们的爱情。博士生涯一路顺利，与我们的共同奋斗和彼此的心照不宣是分不开的。漂泊海外，在人生路上的重要时间里，有人相伴同行，真好。

DECLARATION

This thesis is the result of the author's original research. It has been composed by the author and has not been previously submitted for examination which has led to the award of a degree.

Signed:

Date:

ACKNOWLEDGEMENT

The past years of my PhD life are amazing and unforgettable. My sincere thanks are going to the people who helped me during this period.

First, I would like to thank my supervisor Dr. Igor Timoshkin, who believed my potential and gave me an opportunity to be a PhD. I would like thank for his guidance and support, not only as an excellent supervisor, but also as a mentor. His academic knowledge and his professional attitude of researching both influence me. I have learnt a lot from him during my PhD which I will benefit from them in the future in my life.

Besides, I would like to thank Dr. Mark Wilson, Dr. Michelle MacLean and Dr. Tracy White. Whenever I have problems, they are always keen to suggest possible solutions for me. I can still remember my first discussion with Mark and his encouragement. The time working in biological laboratory with the guidance and support of Michelle and Tracy was a valuable experience to me.

I would also like to thank David Griffin, Andy Carlin and Sean Doak from the High Voltage Mechanical Workshop, for their support on producing different test cells for my experiments.

Moreover, I also wish to thank my friend Dr. Si Qin. The proverb “A friend in need is a friend indeed” probably describes the friendship between us. I can still remember the days we worked in the same office, the encouragement during difficult time, the beer we drank, and the football games we watched together. Wish him all the best in the future.

Last, my special thanks go to Glasgow, the city I love. Having lived in this city for years, it has become my second hometown. Now I have to leave this city, and everything here will become my homesickness.

ABSTRACT

Particulate matter poses serious health problems to human beings. Electrostatic precipitation, which utilises high voltage energised plasma, has been proved to be one of the most effective and efficient method to solve the problems caused by particulate matter. However, there are issues of the electrostatic precipitation which have been noticed. One of the most critical issues of the electrostatic precipitation is the efficiency. There are two meanings of the efficiency, which are particulate matter precipitation efficiency and energy using efficiency. There are reports that the electrostatic precipitation in certain cases is with low particulate matter precipitation efficiency and high energy consumption. Therefore, the first objective of this thesis is to solve the problems of low efficiency and high energy consumption. The first solution is to design and develop a novel system with unique topology, which is the hypodermic needle-mesh system in this thesis. The second solution is to make suggestions on the electrostatic precipitation system which has already been widely used (coaxial topology). The two suggestions are the increase of electrostatic precipitation stage and the increase humidity of the inner environment. Both solutions have been compared with typical state-of-the-art researches and both solutions have been proven to be with high precipitation efficiency and with low energy consumption.

In addition to the electrostatic precipitation effect by plasma, the effect of biological decontamination by plasma has also been investigated. A biological decontamination system has been designed and developed. The objective of the research is not only to control particulate matter, but also to decontaminate pathogenic microbes.

Finally, a model which is able to simulate particle dynamics in electrostatic precipitators and calculate particle collection efficiency has been designed. The model has considered the parameters which are neglected by classical approaches and is more accurate. The particle dynamics characteristics and the particle collection efficiency influenced by the dynamics can be used to make suggestions to the electrostatic precipitators in practice.

TABLE OF CONTENTS

1. Introduction

1.1. Motivations and Aims of Research

Particulate matter (PM) is the pollution of particles with the complex mixture of solid particles and liquid droplets. PM emissions into the atmosphere have become an important issue with modern industrial development which involves a significant increase in pollution levels in industrialised countries. The compositions of PM emitted by diesel engines, coal power stations, steel production plans and other sources of air pollution is complex and carries a wide range of chemical elements including sulphates, nitrates, ammonium, organic and elemental carbon, heavy metals, for example, depending on the source of emission and type of industry. Particulate matter may also include organic compounds, contaminated water droplets and biological agents, such as bacteria viruses and other microorganisms. Particulate matter is generally classified into three groups: PM 10, PM 2.5 and PM 0.1 according to the aerodynamic diameter of the relative particulate. Particular matter with average dimensions of 10 μm and less (PM 10) classes as coarse particles, PM with 2.5 μm particles are fine particles and PM 0.1 μm particles are ultrafine particles. The sources of PM include combustion of fossil and biomass fuels, particles from photoreactions, condensation of atmospheric gases, evaporation of water (may contain dissolved gases), industrial processes (smelters, steel mills, mining, refineries) and others. Multiple published studies, [1] [2] [3] [4] [5] [6] [7] [8] [9], illustrate that both long and short exposure to PM can cause health problems to humans from cardiovascular, respiratory, cancer, neurological, development, reproduction and allergy issues. The health problems which may be caused by PM include cardiovascular-related mortality, asthmatic symptoms, lung cancer mortality, neurological disorders, lung development problems, adverse birth outcomes, exacerbation of allergies and other significant medical problems. Due to these associated risks which PM poses, the control of PM emission of all particle size ranges is essential in industrial processes.

There are four basic methods of controlling PM emission in industry: cyclones, wet scrubbers, fabric filters (bag houses), and electrostatic precipitators. Each of these methods has their own advantages and disadvantages. Cyclones have low construction and operation costs and are effective with larger particles (PM 5), however, the cyclones cannot be used to remove smaller particles because of the unsatisfactory performance. For wet scrubbers, although provide better performance when compared with cyclones, the particle removal efficiency for smaller particles (PM 1) can be much lower and there is a requirement of waste water treatment for reuse as it is often difficult to separate particulate matter from water. So, the above two methods are used for larger PM emission control. In modern industry, fabric filters and electrostatic precipitators are used for fine and ultrafine PM emission control. The particle removal efficiency for fabric filters for fine and ultrafine particulate is satisfactory, however, the increase of concentration of particles can cause the decrease of particle removal efficiency. Air pressure is the key factor which influences the performance of fabric filters, therefore, a certain pressure drop must be maintained and gas flow rates must be limited to certain values to achieve a good performance. This potentially limits the use of fabric filters. The greatest weakness of fabric filters is that they cannot be used to control PM with increased humidity, even in oil forms of PM. Since the emission of PM can be in liquid form, the use of fabric filters is limited. Electrostatic precipitators overcome the listed problems with fabric filters with fine and ultrafine particles, and the particle removal efficiency for electrostatic precipitators is very high when controlling emissions of fine and ultrafine particles. Therefore, electrostatic precipitators are widely used for PM emission control in modern industry.

The electrostatic precipitator is a device that uses both non-thermal plasma discharges to generate ions that charge the airborne particles and electric fields to remove these charged particles from the gas flow: to precipitate particles on the collection plates by electric force on charge particles under electric field. Although electrostatic precipitators show a good performance and high degree of control on PM, there are several problems with electrostatic precipitators which may potentially limit their use in practice.

First, it is found that there is a particle size range (0.2-0.4 μm) which makes it difficult for electrostatic precipitators to control. The reduced performance of electrostatic precipitators is due to the dominant charging mechanism for this range is changing from field charging to diffusion charging. Optimisations of design of electrostatic precipitators are required for increased particle removal efficiency, particularly for fine and ultrafine particles.

Second, energy consideration is an important consideration as electrostatic precipitators use high voltage to generate plasma to removal particles, where the evaluation of precise energy consumption is needed.

Third, several factors can influence the performance of electrostatic precipitators, including particle electric parameters (conductivity and relative permittivity), particle size, particle initial displacement in electrostatic precipitators, ion mobility, current level, etc. It is important to understand the influence of these parameters and how they influence the performance of electrostatic precipitators. Since it is difficult to capture particle dynamic behaviours during experiments, a model which simulates particle dynamics and calculates particle collection efficiency is required. The model should be capable of investigating the influence of the listed factors on the performance of electrostatic precipitators. Besides, in classical theoretical charging approaches, only relative permittivity of particles are considered, so it is important to take the relative permittivity and conductivity of both particle and medium into consideration.

Fourth, and final, it is known that pathogenic microorganisms can be present in liquid aerosol particles in indoor conditions (such as in hospital environment or other public spaces) or potentially can be emitted into atmosphere by some industrial processes. These pathogenic microorganisms can cause health problems, as mentioned previously. It is important to investigate the efficiency of removal of such airborne contaminated particles by non-thermal plasma and the potential bio-decontamination effect of plasma discharges

used in the electrostatic precipitation systems. If the non-thermal plasma generated in the precipitation system is capable of decontaminating microorganisms while removing particles from gas flow, both the potential practical applications of the electrostatic precipitators can be expanded and the plasma precipitation systems will provide another option to control microorganism emission.

The research presented in this thesis aims at improving efficiency of electrostatic precipitation, investigating the influence of various factors (electrical and environmental) on precipitation efficiency and investigating the possibility of bio-decontamination by non-thermal plasma of corona discharges. In summary, the objectives are defined as follows:

1. To develop an electrostatic precipitation system with high particle precipitation efficiency using novel topology designs of an electrostatic precipitation system.

2. To improve the performance of an electrostatic precipitation system with common coaxial topology by increasing both the number of stages and humidity.

3. To investigate the microorganism decontamination effect by non-thermal plasma developments in electrostatic precipitation systems.

4. To investigate and optimise energy consumption for the electrostatic precipitation system and microorganism decontamination system developments.

5. To develop a model to simulate particle dynamics and particle collection efficiency using Matlab.

1.2. Main Contributions of This Research

In this thesis, several approaches have been proposed and implemented in order to develop novel techniques for improved PM electrostatic precipitation. This thesis also

investigates decontamination of airborne microorganisms by non-thermal plasma as developed in the precipitation topologies. The analytical studies conducted in the framework of the present research project were focused into development of a novel model which simulates the dynamics of the airborne particles in electrostatic non-thermal plasma precipitation systems. The main contributions of this thesis are later outlined in order to address the main objectives, as listed in Section 1.1. The research programme has been developed and implemented and the main contributions this research project to the current field of study are listed as follows:

1. An electrostatic precipitation system based on the needle-mesh topology has been designed and developed. A hypodermic needle and two metallic meshes are used for this design. Both positive and negative DC energisation has been used with the needle-mesh electrostatic precipitation system. The precipitation performance of the developed system was investigated in particle precipitation experiments and this performance was focused on two main aspects which are particle precipitation efficiency and energy consumption. Four types of particles were used in this study: airborne particles which are present in ambient laboratory air, particles generated by burning bee wax candles, particles present in cigarette smoke and airborne particles present in air collected on a city street with busy traffic. To collect street air contaminated with particles emitted by traffic a designated system was developed which was based on a bicycle pump and air balloons. Particle precipitation efficiency in the developed needle-mesh electrostatic precipitation system energised with positive and negative voltages was obtained and it was shown that 100% precipitation efficiency can be achieved for particles as small as 0.25 μm in dimension (PM 0.25 particles). The energy consumption for the developed precipitation system is as low as 0.1 Wh/m^3 for both positive and negative energisation.

2. A comprehensive investigation was conducted within the framework of this project that also focused on the capability of the non-thermal plasma not only to charge and to remove particles from the air but also to inactivate airborne microorganisms. The non-thermal

plasma test cell used for air decontamination (inactivation of airborne microorganisms) has been designed and developed. This test cell has a topology which is similar to the needle-mesh electrostatic precipitation topology. Unidentified microorganisms grown on mouldy wheat bread were used as a model microorganism in the decontamination studies. The obtained results show that the non-thermal plasma developed in the precipitation system energised negatively (with the applied voltage in the range from -10 kV to -16 kV) is capable of decontaminating these naturally grown microorganisms while removing airborne particles from the air flow. The efficiency of decontamination achieved in the present work was ~90%. The energy consumption of the bio- decontamination process achieved in the present study was in the range from 0.02 Wh/m^3 to 0.2 Wh/m^3.

3. A larger electrostatic precipitation system has been developed and its precipitation efficiency has been investigated. This system is based on the coaxial topology and has a modular design which includes both single stage and double stage topologies. The influence of the second stage and the influence of the increased humidity of air on the particle precipitation efficiency have been investigated. Both positive and negative DC energisation was used in the precipitation tests. The precipitation performance of the system (its particle precipitation efficiency and energy consumption) has been obtained by conducting comprehensive precipitation tests using three different types of airborne particles: ambient particles naturally present in the laboratory air, bee wax candle particles introduced in air flow and cigarette smoke particles introduced in air flow. It was found that the particle precipitation efficiency of the developed system is high (up to ~100 %) even in the single stage configuration for particles with lower concentration (indoor particles and bee wax candle particles). The increase of air humidity in the system helps to increase the particle precipitation to ~100% for particles with higher concentration (cigarette smoke particles). The use of the double stage topology has increased the particle precipitation efficiency further where it showed that the particle precipitation efficiency in these cases are 100% for all types of particles used in the present study with dimensions as small as PM 0.25.

4. An accurate method of obtaining the energy consumption in the plasma electrostatic precipitation process was developed and used for calculating the energy consumption of the needle-mesh system and coaxial precipitation systems. This method is based on integration of the current wave shapes during particle electrostatic precipitation process.

5. A novel analytical approach for modelling the particle dynamics and the particle collection efficiency in the coaxial electrostatic precipitation systems has been developed. Particle dynamics includes particle velocity and particle displacement inside the electrostatic precipitator. The developed analytical model considers the space charge influenced electric field in the precipitation topologies. For particle charging, both field and diffusion charging mechanisms have been taken into consideration in the developed approach. Unlike a conventional field charging mechanism, which only considers the permittivity of airborne particles, the field charging mechanism used in the developed model considers both conductivity and relative permittivity of airborne particles and plasma/ionic wind environment. The mobility of ions in the air, which is an important parameter for the developed model, has been obtained for both positive and negative energisations in the needle-plane topology test cell. The ionic mobility has been obtained by using the experimental I-V curves and by fitting these experimental data with analytical I-V curves. The mobility of charge carriers was a free parameter in this fitting procedure. The influence of air humidity on ionic mobility has been investigated. Analytical analysis of the particle dynamics and particle collection efficiency has been conducted using practical particle parameters relevant to particles which are problematic for different industrial processes and should, therefore, be controlled. The particles include soot particles, salt particles, condensable organic compounds particles and water particles. The influences of different factors which may affect the performance and particle collection efficiency are discussed, and include, electrical and dielectric parameters of the particles (electrical conductivity and relative permittivity), particle initial displacements, ion mobility, current levels and particle size distributions. The model will help in optimisation of practical design of electrostatic precipitation systems.

1.3. Thesis Overview

This thesis is organised as follows:

Chapter 1 introduces the motivation for this research project, addressing the existing problems of electrostatic precipitation technology, particulate emission control methods, potential use of plasma on biological decontamination and particle dynamics modelling. Also, the main project objectives are provided and discussed.

Chapter 2 provides the background of the research topic. In this chapter the characteristics of PM suspended in atmospheric air are reviewed. The methods used in the industry for PM control are reviewed and their advantages and disadvantages are discussed. Electrostatic precipitation, which is one of the main emission control methods, is the focus of this thesis. The background of the electrostatic precipitation technology is presented by reviewing the mechanisms of precipitation and operation of electrostatic precipitators, including generation of corona discharges and the electric field, particle charging mechanisms and particle collection mechanisms. The classifications and designs of electrostatic precipitators are reviewed from different aspects. Factors which affect the performance of electrostatic precipitators and particulate penetration mechanisms are reviewed. An analysis of the particle collection efficiency and ion mobility, which play important roles in particle dynamics/efficiency model, are introduced and discussed in this chapter. Corona discharge, which is the key factor for particle charging, is also presented. Finally, both the problems of electrostatic precipitation by corona discharge and the mechanisms of microorganism decontamination by non-thermal plasma developed by corona discharges are reviewed.

Chapter 3 discusses the design of the electrostatic precipitation system (needle-mesh topology) and provides the results of the study of precipitation performance of this electrostatic precipitation system. The proposed design is based on the needle-mesh electrode topology. A hypodermic needle is used as HV corona electrodes and two metallic

meshes are used as the collection plate. Both positive and negative DC stresses were used in the precipitation tests. The performance of the system was evaluated from the point of view of two main aspects: particle precipitation efficiency and energy consumption. The particle precipitation efficiency was investigated based on comprehensive precipitation tests that were conducted using airborne particles of different nature and with different dimensions and characteristics: indoor particles, bee wax candle particle, airborne particles collected on a city street with a heavy traffic and cigarette smoke particles. The efficiency of particle precipitation for different particles and for both energisation polarities are compared and discussed. In order to obtain the energy consumption of the developed precipitation system, an accurate method for calculating energy consumption is introduced. This method is based on integration of the current-time curve obtained during the particle electrostatic precipitation tests. The results are compared with typical energy consumption obtained from the literature.

Chapter 4 introduces a coaxial topology for the electrostatic precipitation system. The precipitation performance of the electrostatic precipitation system developed in this chapter has been investigated. The design of the proposed system includes both one stage and double stage topology. Both positive and negative DC energisations were used in the conducted precipitation tests. Similar to the needle-mesh system in Chapter 3, the performance of the proposed coaxial system has been obtained from a point of view of two major aspects: the particle precipitation efficiency and the energy consumption of the precipitation. For particle precipitation efficiency, the results are based on precipitation tests for different sized particles and for three types of particles: indoor particles, bee wax candle particle and cigarette particles. The efficiency of particle precipitation for different particles and for both energisation polarities are compared and discussed. The influence of increased humidity on particle precipitation is investigated and discussed in this chapter with the analysis of particle precipitation results for increased humidity. Energy consumption is calculated based on the methodology, as developed in Chapter 3, and the energy consumption for one stage system, double stage system and single stage system

with increased humidity has been calculated and compared with typical energy consumption obtained from the literature.

Chapter 5 continues the study initiated in Chapter 3 and investigates not only precipitation of particles by non-thermal plasma discharges but also plasma bio-decontamination effects. The main aim of this chapter is to demonstrate that corona discharges used in the electrostatic precipitation systems are capable of not only charging airborne particles and aerosol droplets but can also be used for biological decontamination. The test cell used in the investigation of non-thermal plasma bio-decontamination effects is similar in its design to the electrostatic precipitation system used in Chapter 3 (needle-mesh). Airborne unidentified microorganisms naturally grown on mouldy wheat bread in ambient atmospheric conditions have been used to model the microorganism and the bio-decontamination tests as conducted in this chapter. Negative energisation, different voltage levels and different gas flow rates have been used in these tests. The energy consumption for the plasma bio-decontamination process has been obtained and the results are presented and discussed in this chapter.

Chapter 6 introduces a novel model for simulation of the particle dynamics inside the electrostatic precipitators and for calculations of the particle collection efficiency. The particle dynamics include particle velocity and particle displacement. The model considers the space charge influenced electric field and the electric field dependency on displacement. For particle charging, both field and diffusion charging mechanisms are taken into consideration. Unlike conventional field charging mechanism, which only considers the conductivity of particles, the field charging mechanism in this research includes conductivity and relative permittivity of both particles and medium. In the design of the model an important parameter, ion mobility, is measured and used. The measurement is conducted by I-V curve fitting of experimental data curve and a theoretical data curve. The experimental data curve is measured using a needle-plane topology test cell. Both positive and negative DC energisation has been taken into consideration, and influence of increased

humidity is also investigated. The simulation of the particle dynamics and particle collection efficiency are conducted using real particle parameters which are common in industry and require control. The particles include soot particles, salt particles, condensable organic compounds particles and water particles. The influences of different factors which may affect the performance and particle collection efficiency are discussed. These factors include particle electric parameters (particle conductivity and particle relative permittivity), particle initial displacements, ion mobility, current levels and particle size distributions.

The concluding chapter, Chapter 7, is the summary of this thesis and provides concluding remarks and discussion for potential future research work.

2. Background and Literature Review

2.1. General

This chapter reviews the background of electrostatic precipitation together with related topics. The literature review sections will focus on the review of typical problems related to the electrostatic precipitation and biological decontamination which will be introduced later in this chapter. The outcome of this thesis will be to resolve the problems found in the literature.

2.2. Particulate Matter and Associated Issues

2.2.1. Particulate Matter Component and Sources

Particulate matter consists of both primary components and secondary components. For primary components, PM is released directly from the source into the atmosphere. For secondary components, PM is formed in the atmosphere by chemical reactions. PM comes from both human-made and natural sources and contains a range of chemical compounds. [10] [11]

There are four types of primary components: sodium chloride, elemental carbon, trace metals and mineral components. The source of sodium chloride is the sea salt. The source of the elemental carbon is black carbon (soot) where the black carbon is formed during the high-temperature combustion of fossil fuels. These fossil fuels include coal, natural gas and oil. Biomass fuels such as wood chips are also the source of black carbon. The sources of trace metals are generated by metallurgical processes and by impurities found in additives mixed into fuels used by industry. A mechanical abrasion process (vehicle motion and break and tyre wear) can also generate metal PM. These metals include chromium, zinc, lead,

nickel, cadmium and manganese and have a low concentration. The source of mineral components is found in coarse dusts from quarrying, construction and demolition work and from wind-driven dusts. The mineral components include aluminium, silicon, iron and calcium. [10] [11]

There are three types of secondary components: sulphate, nitrate and water. Sulphate is formed by the oxidation of sulphur dioxide (SO_2) in the atmosphere. Sulphate can form sulphuric acid, and ammonium sulphate can be formed by the reaction of sulphuric acid with ammonia (NH_3). Nitrate is formed by the oxidation of nitrogen oxides in the atmosphere to form nitric acid. NO_x consists of nitric oxide (nitrogen monoxide, NO) and nitrogen dioxide (NO_2). Ammonium nitrate can be formed by the reaction of nitric acid and NH_3. Sodium nitrate is another type of nitrate PM. Water is also one type of secondary component of PM as some components of the aerosol form of PM, such as ammonium sulphates and ammonium nitrates, take up water from the atmosphere. [10] [11]

There is also one type of PM component (organic carbon) which derives from both primary and secondary components. Primary organic carbon results from traffic or industrial combustion sources, whereas secondary organic carbon is a result of the oxidation of volatile organic compounds (VOCs). Organic carbon can be several hundred individual components. Some of these trace organic compounds are highly toxic (for example certain polycyclic aromatic hydrocarbons). [10] [11]

Precursors of secondary PM are also important in terms of PM emissions. There are four types of precursors of secondary PM: SO_2, NO_x, NH_3 and VOCs. SO_2 is formed by the combustion of fuels which contains sulphur, such as coal, and ship fuels, such as heavy fuel oil. NO_x is formed by the combustion of fuels used in power generation and domestic heating and traffic. NH_3 is emitted mainly from agricultural sources, particularly livestock waste. VOCs Aromatic compounds such as benzene and toluene are generated by traffic

and solvents. Monoterpenes come from vegetation, especially conifers and heathers. [10] [11]

2.2.2 Particulate Matter Size Fractions, Components and Sources

As has been mentioned, PM is classified in to three groups: PM 10, PM 2.5 and PM 0.1. The classification is made on the basis of aerodynamic diameter of particulate. PM 10 is classed as coarse particles [12], PM 2.5 as fine particles [13] and PM 0.1 as ultrafine particles [14]. Relatively speaking, large particles with diameter larger than 30 μm (PM 30) have shorter periods of time being suspending in the atmosphere and will deposit quite rapidly [15]. So, the total suspend particles refers to particles with a diameter up to 30 μm or particulate matter up to PM 30 [16]. In general, the PM is measured using the unit $\mu g/m^3$. There are situations where ultrafine particles account for the majority of the part and the particle number is also used for measurement of PM [17].

Coarse particles (PM 10):

Coarse particles are generated by the following sources: construction, ash from combustion without emission control, re-suspension of road by traffic, erosion of land by wind, dust suspension, ocean spray, break-up of solids and droplets, surface disturbance (including agriculture, surface mining, quarry) and biogenic emissions (pollen and fungi spores). Therefore, the composition of coarse particles consists of sulphates, nitrates, chlorides, organic and elemental carbon, sea salt, biological debris and bacteria. Coarse particles are usually with large mass and the lifetime in atmosphere ranges from hours to days [18]. The lifetime in atmosphere for coarse particles is relatively short which makes travelling distance of particles less than tens of kilometres from the source [19] [20]. If no industrial emission control is conducted, coarse particles are removed by gravity or with the help of

rain. Medically speaking, coarse particles can land on upper airways which is the primary bronchi of humans [21].

Fine particles (PM 2.5):

Fine particles are generated by the following sources: combustion of fossil and biomass fuels, particles from photoreactions, condensation of atmospheric gases, evaporation of water (may contain dissolved gases), coagulation of ultrafine particles, and industrial processes (smelters, steel mills, mining, refineries) [22] [23]. Therefore, the composition of fine particles includes sulphates, nitrates, ammonium, organic and elemental carbon, heavy metals, organic compounds, water, bacteria and virus. Fine particles are usually with a large surface area which makes allows a greater ability for adsorption and absorption, and the lifetime in atmosphere for fine particles ranges from days to weeks. The travelling distance of fine particles is from hundreds to thousands of kilometres from the source [19]. If no industrial emission control is conducted, fine particles are removed by gravity, by the formation of clouds or with the help of rain. Medically speaking, fine particles could land on lower air ways which are the terminal bronchioles and alveoli of humans [21].

Ultrafine particles (PM 0.1)

Ultrafine particles are generated by the following sources: nucleation and condensation of atmospheric gases, high-temperature combustion, vehicle exhausts. Therefore, the composition of ultrafine particles includes sulphates, organic and elemental carbon, heavy metals and organic compounds. Ultrafine particles are usually with a high particle number and the lifetime in atmosphere for ultrafine particles ranges from minutes to hours. This is because ultrafine particles can easily and rapidly turn into fine particles through diffusion, coagulation, absorption and condensation. Therefore, the travelling distance of ultrafine particles is quite near to the source which is several kilometres [24]. If no industrial emission control is conducted, ultrafine particles are removed with the help of rain through

diffusion, coagulation, absorption and condensation. Medically speaking, ultrafine particles could land on the extra-pulmonary organs which are the tissues outside the lungs of humans [21].

2.2.3 Health Problems Caused by Particulate Matter

Exposure to PM will harm the health of humans. Both long- and short-term exposure are harmful. Medically speaking, the health effects for long- and short-term exposure to PM are listed as follows [21]:

Long-term exposure (months or years):

From a cardiovascular aspect, long-term exposure can cause cardiovascular-related mortality, atherosclerosis, ischaemic heart disease and complications of diabetes [1] [2] [3] [4] [5] [25] [26] [27] [28]. From a respiratory aspect, respiratory-related mortality, asthma symptoms, reduced lung function and respiratory infections in children can result [29] [30] [6] [7] [8] [9]. From a cancer aspect, lung cancer mortality can result [31] [32] [33]. From a neurological aspect, neurological disorders in adults and impaired cognitive function can result. From a development aspect, lung development and neurological development in children can be inhibited. From a reproduction aspect, there are potential adverse birth outcomes and low sperm quality and quantity. From an allergy aspect, exacerbation of allergies and allergic sensitisation can result.

Short-term exposure (daily):

From a cardiovascular aspect, short-term exposure can cause cardiovascular-related mortality, atherosclerosis, ischaemic heart disease, ischaemic stroke, myocardial infarction and congestive heart failure [1] [2] [3] [4] [5] [25] [26] [27] [28]. From a respiratory aspect, respiratory-related mortality, asthma symptoms, respiratory infections, bronchitis in

children and COPD (chronic obstructive pulmonary disease) symptoms can result [29] [30] [6] [7] [8] [9]. From an allergy aspect, exacerbation of allergies can result.

Therefore, it is very important to control particulate matter emission and the particulate matter should be controlled to a high standard (with high particulate matter precipitation efficiency) to prevent hazardous particulate matter to be contacted by human beings.

2.3 Methods of Eliminating Airborne Particles

There is a need for air pollution emission control in modern industry such as power plants, steel factories, refineries, etc. In fact, pollutants in the form of particulates, vapours, gases and aerosols are generated from these industries during different industrial processes. In order to control the emissions, a wide range of controlling devices or systems are applied and the selection of the devices and systems is determined by the certain pollution emission type. In this research, since the destination is to control particulate emission, four typical methods of particulate emission control which are widely used in industry are introduced and explained.

The four most commonly used methods for particulate emissions control include: wet scrubbers, fabric filters (bag houses), cyclones and electrostatic precipitators (wet and dry types).

2.3.1 Wet Scrubbing Equipment

Scrubbing equipment uses a physical process of liquid to control particulates vapours and gases with water being the most commonly used for the absorption of pollutants. The controlling process is through the contact of the liquid to allow pollutant absorption through the liquid. The process is conducted either by passing a gas stream through the liquid solution or spraying liquid into the gas stream. The pollutants controlled by the gas

absorption process should have high concentrations and be liquid absorbable, and the equipment for gas absorption is designed to maximise the highest possibility of gas-liquid contact [34].

Four types of gas absorption equipment are commonly used, which are packed towers, spray towers, tray towers and spray chambers. Packed towers are the most commonly used equipment for controlling gaseous pollutants. However, when packed towers are used to control pollutant gas which contains particulate with high concentration, the equipment can be plugged by PM. The PM controlling can be achieved by wet collection devices which include venturi scrubbers, bubbling scrubbers, spray towers and, in some instances, wet electrostatic precipitators. A typical wet scrubber is shown in Figure 2-1.

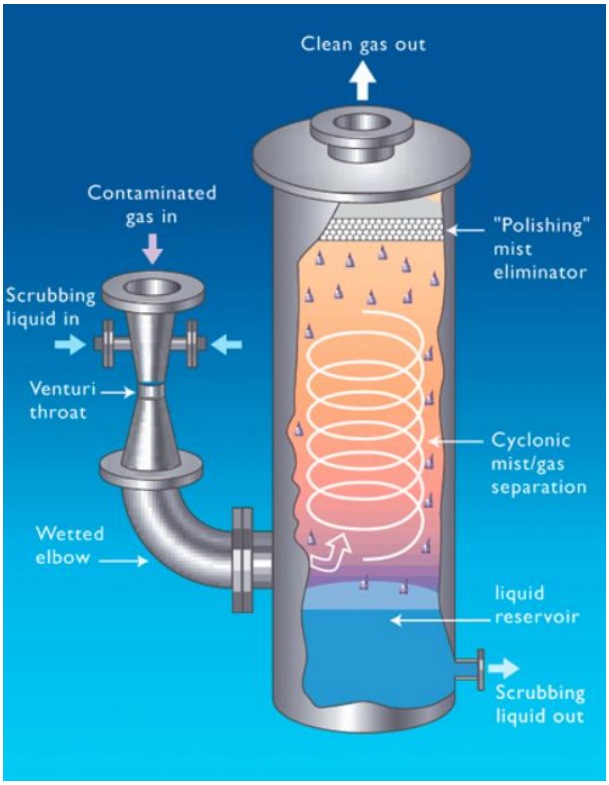

Figure 2-1. Figure of a typical wet scrubber. Picture is taken from [35].

In scrubber systems, liquid stream is used to remove solid particles from the gas stream. This process is conducted by spraying water droplets into the gas stream or mixing the gas stream into water directly. The purpose of this process is to make liquid droplets collide with PMs in the gas stream. The water, or liquid, is guided into the gas stream at either the point of or after the venture throat with reduced cross section. Due to the reduced cross section, the gas stream and water droplets can have high velocity in this space, and the difference in velocity and pressure can cause turbulence (which ultimately makes good contact of PMs and water droplets). The mixture of PMs and small water droplets then mix with large water droplets in the space with increased cross section. Subsequently, the final mixture of PM and water droplets is removed from the gas stream. In industry, it is common that a cyclonic part is designed and placed after the venture to improve the process of the PM droplets mixture removal process [34].

The PM removal efficiency of wet scrubbers can be as high as up to 99%. However, the efficiency for small particles can be much lower. Another disadvantage of using wet scrubbers is the requirement of waste water treatment for reuse as it is often difficult to separate PM from water [34].

In modern industry, scrubbers are used in power plants which are based on coal, asphalt plants and concrete plants. If the pollution of industry is PM based and with gases, which are easy for treatment such as sulphur oxides, scrubbers are also applied and used for controlling pollutants [34].

In this research, the principle of wet scrubbers is considered and included in the design of the particle precipitation system, and the details will be discussed in the main chapter.

2.3.2 Fabric Filters (Bag Houses)

In many industries, fabric filters (bag houses) are used as the working principle of fabric filters is relatively simple. Gas streams with particles pass through fabric filters, since the pore size of fabric filters is smaller than the size of particles, and dry PMs are blocked and captured by the filters on the surface. With increasing particles being captured and accumulating on the fabric filters, when the particles on the filters are saturated, the particles are removed by reversing gas flow direction through filters or shaking the filters themselves and, therefore, particles fall and are collected. When particles are accumulating on the surface of the filters, since the pores on the filters are gradually blocked by the particles, the particles themselves help increase the particle removal efficiency [36] [37].

There is a wide range of materials for fabric filters and the selection of fabric depends on particle type and need of application. In industry, materials such as paper, glass fibre, Teflon, stainless steel, etc. are commonly used. In this research, the principle of fabric filters is considered and included in the design of electrostatic precipitation system. The material used in this research was glass fibre and stainless steel and the details of the filters will be discussed in main chapters of this thesis.

Bag house is the configuration of the fabric filter combination. The purpose of bag houses are to increase the filter area and are designed as a series of fabric tubes (bags) in which small fabric filters are located. One feature of bag houses is that the bags can be removed from the system for cleaning while other bags can remain working. In industry tens, or even hundreds, of bags can be applied in one system, depending on the situation [36] [37]. A typical fabric filter system is shown in Figure 2-2. The circles are the dusts, and the filters are in parallel. The arrows show the dust moving direction.

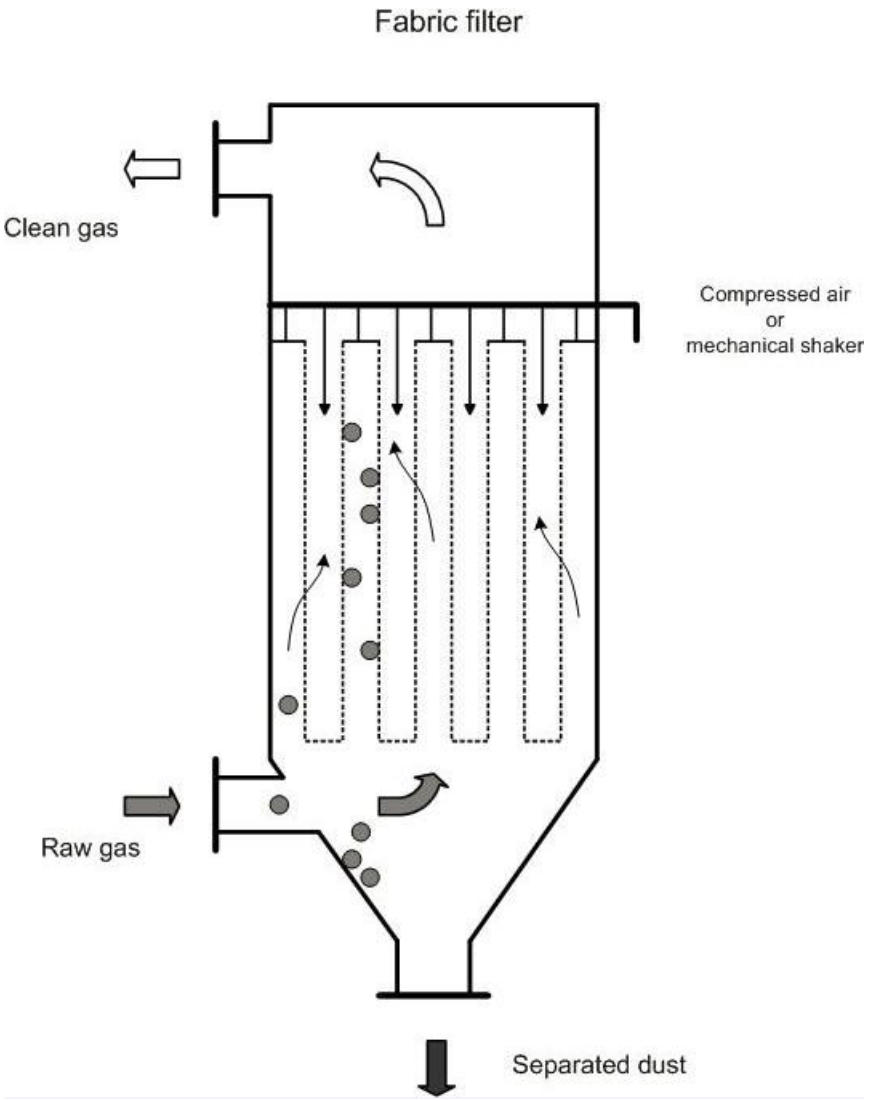

Figure 2-2. Figure of a typical fabric filter. Picture is taken from [38].

In modern industry, fabric and bag houses, used for PM removal, are used in power plants which are based on coal, steel factories, foundries, etc. The removal efficiency of fabric filters can be up to 99.9% and they have good performance when dealing with fine particles. In recent technological developments, the bag houses are equipped with a catalyst which makes the bag houses also available for the removal of chemical pollutions while the PMs are being removed [36] [37].

2.3.3 Cyclones

Cyclones use the principle of centrifugal forces on particles inside the cylinder container to remove particles from gas streams. As shown in Figure 2-3, when gas streams with particles are guided into the cyclone system with cylindrical topology, gas is swirling rapidly in the shape of a cyclone. The swirling motion provides particles with centrifugal forces and the particles are then removed from the inner wall of the system due to the centrifugal forces. These particles then drop to the bottom of the system and are collected. The gas streams are guided upwards and exit the cylinder from the gas outlet on the top [39]. A typical cyclone system is shown in Figure 2-3.

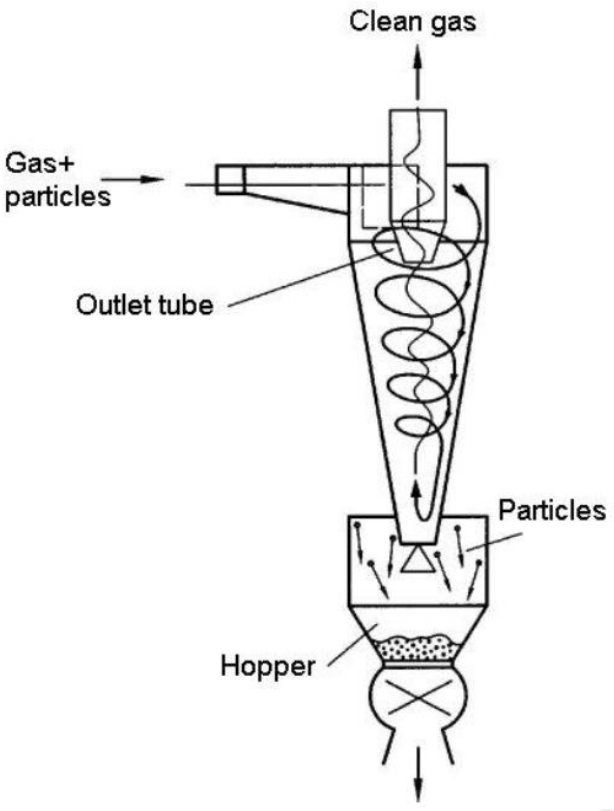

Figure 2-3. Figure of a typical cyclone. Picture is taken from [40].

Cyclones are used for the removal of particles with larger sizes from a gas flow and the removal efficiency can be up to 90% for particle dimension of 10 µm. The removal efficiency can be improved by increasing the pressure drop through the cyclone and also with the increase of particle size. In industry, cyclones are used for the removal of particle with dimensions larger than 50 µm [39].

Cyclones are used in cotton industry, rock crushers and industries where there is a need for the removal of particles with relatively large sizes from a gas flow. Both solid particles and liquid droplets can be removed when using cyclones. The problems with cyclones are: 1) When particle concentration is high, there is the problem of plugging the cyclone system, 2) Sometimes particles can recirculate through the system and 3) The inner walls of the cyclones can be corroded by the particles or droplets being removed [39].

2.3.4 Electrostatic Charging and Precipitation (Overview)

An electrostatic precipitator, as investigated in this research, is a device that uses electrical discharges to remove particles from a gas flow, and details discussed in later chapters. An electrostatic precipitator is a very efficient method of removing fine particles in a high volume and high efficiency system. The electrostatic precipitator applies energy only to PMs without significantly reducing the flow rate of gas due to the low flow rate difference through the electrostatic precipitator system.

In general, the working principle of electrostatic precipitators is that the electrostatically charged particles in the gas flow are attracted to collection plates or devices. There is high voltage drop from the charging electrode to the collection plates and the electric field is produced inside the electrostatic precipitator and the charging process is conducted through ionisation of gas. During ionisation the plasma forms and a high voltage discharge introduces charge on particles and, subsequently, the air after treatment passes out of the electrostatic precipitator. When particles on the collection plate are saturated, the plate is

stroked using devices, such as a hammer, to make particles fall into collection devices for final removal. Figure 2-4 shows a typical dry type electrostatic precipitator with all the essential parts shown in the figure.

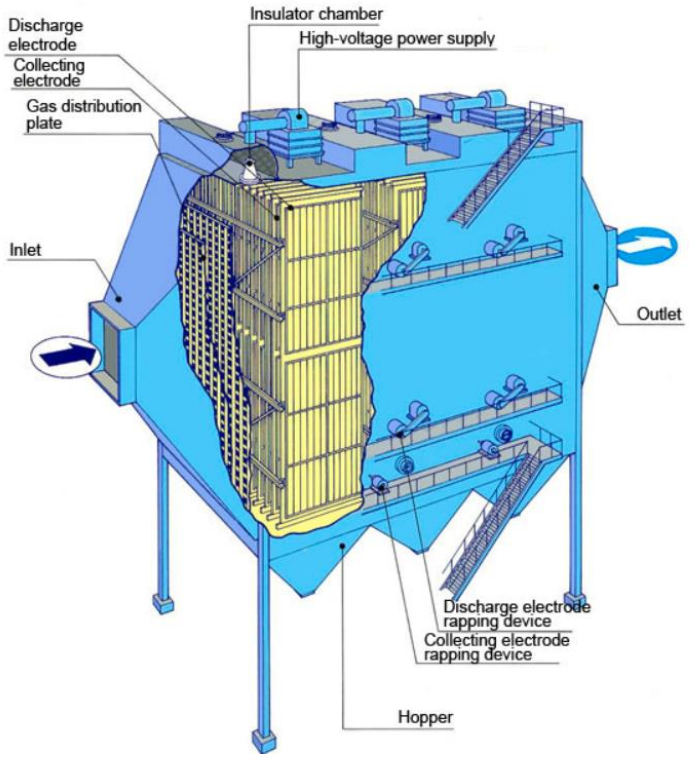

Figure 2-4. Typical electrostatic precipitator. Picture is taken from [41].

Electrostatic precipitators are available in many different sizes and types and are designed for various dust and water droplet characteristics and gas volume flows. Some types are designed to work with a gas streams with particular temperature and moisture characteristics. Dry electrostatic precipitators operate above the dew point of the gas stream to remove impurities from smoke and dust. Wet electrostatic precipitators, in contrast, operate with saturated airstreams that have 100% relative humidity. Wet precipitators are commonly used to remove liquid droplets, including oil, resin, tar and sulphuric acid mist, from gas streams in industrial settings. They are applied where the gases are laden with humidity, contain combustible particulates or have particles that can be sticky.

Very large power plants may have multiple precipitators for each unit, whereas residences may have a single precipitator which is often only slightly larger than a household vacuum cleaner. Some precipitators can collect 99.9%, or more, of the dust (which can contain arsenic, acids and other chemicals) from the gas exhaust depending on the temperature and flow rate of the gas, the size and chemical composition of the particles, and the precipitator design and voltage is applied to the gas. They have been used in the following industrial and household applications:

1) Removing dirt from flue gases in steam plants. 2) Removing oil mists in machine shops. 3) Removing acid mists in chemical process plants. 4) Cleaning blast furnace gases. 5) Removing bacteria and fungi in medical settings and pharmaceutical production facilities. 6) Purifying air in ventilation and air conditioning systems. 7) Material recovery from gas flow (including oxides of copper, lead and tin). 8) Separating rutile from zirconium sand in dry mills and rutile recovery plants [42].

The advantages of using electrostatic precipitators include: 1) collection efficiencies of ≥ 99.9% for coarse and fine particulates at relatively low energy consumption, 2) the ability to remove dry as well as wet particles, 3) typically a low pressure drop, 4) continuous operation with minimum maintenance and low operating cost, 5) relatively low operation costs, 6) flexibility in temperature (Can be operated at high temperatures (~700^{o}C)) and high pressure or under vacuum and 7) the capability to handle relatively large gas flow rates (~50,000m^{3}/min). [43] [44]

The disadvantage of using electrostatic precipitators include: 1) generation of dusts as secondary residuals 2) high capital cost (expensive to purchase and install, for example, U.S.$160/m^{2} of plate area), 3) high sensitivity to fluctuations in gas stream conditions (flow rates, temperature, particulate and gas composition and particulate loadings), 4) difficulties with the collection of particles with extremely high or low resistivity, 5) relatively large space requirements, 6) explosion hazard for combustibles, 7) safety requirements for personnel from high voltage exposure during ESP maintenance, 8) production of ozone by

the negatively charged electrodes during gas ionisation and 8) highly trained maintenance personnel required. [43] [44]

2.4 Process of Electrostatic Precipitation

The process of electrostatic precipitation in electrostatic precipitators includes the generation of electric field, corona discharge generation, particle charging and particle collection. Each aspect will be expanded in the following sections.

2.4.1 Electric Field

The electric field is important in electrostatic precipitators. The formation of electric field inside electrostatic precipitators is through the application of high voltage on charging electrodes of electrostatic precipitators. There are three purposes of applying electric field in electrostatic precipitators: 1) the electric field is the key to generate corona discharges, 2) the electric field helps charging ions collide with particles and transfer charge on particles (this is more important in field charging which will be discussed later in this chapter) and 3) the electric field provides electric forces on charged particles which subsequently helps remove particles from the gas flow [45].

The electric field in an electrostatic precipitator is affected by three factors: 1) the applied high voltage level, 2) total charge on particles and 3) space charge and free electrons. For different situations, each of the factors may become the most dominant affecting factor of the electric field.

In electrostatic precipitators the strength of an electric field can affect the performance of the system. In fact, the strength of the electric field is affected by two factors. First, the distance from ionisation region to collection region. For example, in a point-system, this distance can be assumed to the distance from the tip of the needle to the plane. In a coaxial

system this distance refers to the distance from the surface of the inner charging electrode to the surface of inner wall of electrostatic precipitator i.e. the collection plate. In general, the distance decides the working voltage range of electrostatic precipitators. The increase of the distance can increase the breakdown voltage of the system and also working range of electrostatic precipitators is increased. Second is the resistivity of the particles for collection. In fact, the high resistivity of particles can cause the decrease of corona current and the applied voltage, so the strength of electric field is reduced [45]. The influence will be discussed later in this chapter.

2.4.2 Corona Discharge

As has been mentioned in the above section, the generation of corona discharges take place in a highly non-uniform field if this field exceeds a critical value for specific gas.. When three main conditions are met, corona discharges can be generated: 1) There is an electric field inside the electrostatic precipitator; 2) the field is highly non uniform and 3) The strength of electric field exceeds the critical value: it is high enough for ionization of electrically neutral molecules or atoms of gas to form positive ions. The direction of movement of positive ions and free electrons are opposite. The corona discharge can be initiated through electronic avalanche mechanism, which will be introduced later in this chapter. In this case, free electrons are accelerated by electric field and gain sufficient velocity, so when electrons collide with neutral gas molecules or atoms they can ionize these neutral species to form new free electrons and positive ions. However, the electronic avalanche does not cross the inter-electrode gap as highly non-uniform filed reduces significantly away from the sharp HV energized electrode. Therefore, corona discharge is formed in the vicinity of this energized electrode only. The corona discharge can be generated by both positive and negative energisation [45].

2.4.3 Particle Charging

Corona discharge in electronegative gases such as air, produced negative ions through attachment of electrons to electronegative neutral species (oxygen molecules). These ions travel in the electric field in neutral gas and may collide with airborne particle. Thus the particles become charged. Thus particle charging occurs in the space free from corona discharge: between the active corona region and the collection plates of the electrostatic precipitator [45].

Particle charging in electrostatic precipitators is governed by both field charging and diffusion charging mechanisms. In the case of field charging, the charge transfer is due to the collision of particles and ions and the charging process is influenced by the external applied electric field. When particle is within an electric field where there are ions travelling along the electric field lines, the electric lines flow through particles and the ionic flux transfer charge on particles by collision. The ions continue to bombard the particle until the charge on that particle is saturated and at this point the saturation charge on particles is achieved. When the charge on particles becomes saturated, the electric field lines will be repelled from the particle and field charging process stops [45].

In the case of diffusion charging the charging mechanism is based on diffusing ions which collide with particles due to random Brownian motion. Thus the airborne particles are charged due to collision with ions. An externally applied field is not involved in the diffusion charging mechanism. The ionisation source ionises air or gas molecules and the ions collide with particles resulting in charge transfer. The charging rate decreases with the increase of charge on particles [45].

Details of the charging mechanisms, field charging and diffusion charging, will be discussed later in this chapter.

2.4.4 Particle Collection

After charging, airborne particles are ready for precipitation – removal from air flow. Typically there is a significant voltage drop between the charging electrode(s) and the collection plate(s). In some cases the collection plates have an energisation polarity opposite to that of the charging electrodes. Charged particles migrate towards the collection electrodes due to electric forces acting on these particles. Generally, larger particles (with dimension larger than 10 μm) and smaller particles (with dimension smaller than 10 μm) have the same direction of movement, which is towards the collection electrodes. However, due to turbulence of gas flow, the movement track for smaller particles is not exact the same as larger particles because smaller particles are much more easily influenced. This situation has been considered in this research in the simulation model, which will be discussed in later chapters [45].

2.5 Parameters Which Influence the Performance of Electrostatic Precipitation

Several operating parameters are indicative of a likely change in performance of electrostatic precipitators, and most of these parameters directly affect the performance of electrostatic precipitators. The following typical parameters are discussed: gas volume and gas velocity through the ESP; temperature, moisture and chemical composition of the gas; particle size distribution and concentration; resistivity of the particulate; and power input. Many of these factors are interrelated. [46]

2.5.1 Gas Volume and Velocity

Equations and models [47] for prediction of performance of electrostatic precipitators show that the gas volume is an important parameter which influences the performance of

electrostatic precipitators. In fact, the decrease in gas volume increases the collection efficiency of electrostatic precipitators. An important parameter, SCA (specific collection area) is introduced here. SCA is used for comparison of electrostatic precipitators and for estimating collection efficiency of electrostatic precipitators. SCA is defined as the collection plate area divided by gas flow rate and SCA is measured in units of s/m or $m^2/(m^3/s)$. SCA is very important in cost evaluation of electrostatic precipitators and the size of the electrostatic precipitation system is determined by SCA. The decrease of gas volume causes both the increase of SCA and the decrease of gas velocity, which means that the exposure time of particles to electric field and collection mechanism is increased. The increase of SCA and the increase of exposure time result in better performance of electrostatic precipitators.

Gas flow distribution also influences the performance of electrostatic precipitators. The gas flow distribution ideally should be uniform. However, in practical situations, the gas flow distribution inside the electrostatic precipitators is always non-uniform. In spaces where the gas flow is higher there is a decrease in collection efficiency, while in the spaces where the gas flow is lower there is an increase in collection efficiency. The decreased efficiency is not compensated by the increased efficiency so this non-uniform distributed gas flow causes the reduction of collection efficiency. As discussed, the non-uniform distributed gas flow can also potentially cause the gas sneakage (gas sneakage will be discussed later in this chapter), which also influences the performance of the electrostatic precipitators. In industry, devices such as perforated plates, turning vanes and good ductwork design can help to provide better gas distribution [47].

2.5.2 Chemical Composition

The chemical composition of both particulate and flue gas is also one of the factors which affects the performance of electrostatic precipitators. The compositions of particulates and flue gas affect the performance of electrostatic precipitators in two different mechanisms.

For particulates, the chemical composition of particulates affects the performance of electrostatic precipitators from the resistivity of the particulates aspect. Since resistivity is related to conductivity and conductivity shows the difficulty of particles to be charged, and charge on particles will influence the electric force on particles thus influence the particle precipitation efficiency. When the composition of particulates becomes complex, potentially, the range of resistivity of particulate which the electrostatic precipitator is controlling increases. For flue gas, since the operation of electrostatic precipitators depends on electronegative gases, such as oxygen, carbon dioxide, sulphur dioxide, etc., so the concentration of these gases can affect the performance of electrostatic precipitators. [47]

2.5.3 Particle Size Distribution

Particle size plays a very important role in the collection efficiency of electrostatic precipitators. It is found that the efficiency increases with particle size. Particles with diameters 0.2-0.4 μm are found to be the most difficult to collect due to the dominant charging mechanism for this range is changing from field charging to diffusion charging. Theoretically, field charging dominates particles with a diameter larger than 1 μm and diffusion charging dominates particles with a diameter smaller than 1 μm. Normally, the respective performance of electrostatic precipitators is well under these two charging mechanisms for particles in their domination range. However, in practice it is found that there is a range (between 0.1 and 1 μm) of particle sizes which makes most electrostatic precipitators difficult to collect. The reason for the reduced performance of electrostatic

precipitators on this range of particle size is that, in practice, neither of the charging mechanisms dominates. Therefore, it is important to investigate and increase the performance of electrostatic precipitation in this range.

2.5.4 Resistivity of Particles

The resistivity of particulates is a parameter which shows the difficulty for a given type of particulate to conduct electric charge, with levels shown in units Ω cm. A low resistivity level means that it is easy for particulates to transfer charge, and the resistivity of particulates is determined by the chemical composition of particulate and the temperature. Humidity level of the gas stream also plays an important role in resistivity because water mist can help with the charging process.

Different levels of resistivity on the operation of electrostatic precipitators show different characteristics. For typical electrostatic precipitator operation parameters (energisation voltage: 30-70 kV, current density: 5-50nA/cm^2, dust layer thickness: 0.6-2.5 cm), there are four different resistivity levels to be considered: 1) for resistivity level less than 10^8Ω·cm, electrostatic precipitators maintain normal operation voltage and current levels (the voltage drop across the dust layer is negligible). Under this resistivity level, the retaining electrical force on the collected particulates is low, which means that the probability of particle reentrainment (particle reentrainment will be discussed later in this chapter) is high and, therefore, the performance of electrostatic precipitators is reduced. 2) For resistivity level between 10^8Ω·cm and 10^{10}Ω·cm, electrostatic precipitators are within normal operation voltage and current levels. The voltage drop across the dust layer is negligible. Under this resistivity level, the retaining electrical force on the collected particulates is sufficient. Therefore, the performance of electrostatic precipitators is high. 3) For resistivity level around 10^{11}Ω·cm, electrostatic precipitators are with reduced operational voltage and current levels and there is a high probability of sparks occurring sparks. There is significant

voltage loss across the dust layer. Under this resistivity level, the retaining electrical force on the collected particulates is moderate. With the reduced operation voltage and current, the high probability of sparks and the voltage loss reduce the performance of electrostatic precipitators. 4) For resistivity more than $10^{12}\Omega\cdot cm$, electrostatic precipitators are with reduced operation voltage and, if the power supply controller is not operated properly, the current is high during the operation process. There is significant voltage loss across the dust layer and the voltage loss is higher than the voltage loss in situations when the resistivity level is around $10^{11}\Omega\cdot cm$. Under this resistivity level, the retaining electrical force on the collected particulates is high. However, due to the reduced voltage, high current and significant voltage loss the performance of electrostatic precipitators is significantly reduced. There is also a relatively higher probability for back corona (back corona will be discussed later in this chapter) to occur which also reduces the performance of electrostatic precipitators. [47]

2.5.5 Gas Temperature

Gas temperature influences the resistivity and the previously discussed resistivity influence affects the performance of electrostatic precipitators. At times the effect of temperature on the performance of electrostatic precipitators is dramatic because temperature is closely related to the resistivity (conductivity) of particles and the resistivity of particles will influence the performance of the electrostatic precipitators as discussed. [47]

2.6 Typical Types of Electrostatic Precipitators in Industry

Generally, electrostatic precipitators are divided into two types: dry electrostatic precipitators and wet electrostatic precipitators. The distinction between dry and wet electrostatic precipitators is the method of cleaning collection plates. From an internal

design point of view, electrostatic precipitators are divided into two typical types which are wire-plate electrostatic precipitators and wire-pipe electrostatic precipitators. The details will be discussed in this section. [48]

2.6.1 Cleaning Mechanisms: Dry and Wet Electrostatic Precipitators

Dry electrostatic precipitators can be used for particle emission control in different environments for many different temperatures or pressures and for a wide range of gas & particle types. In general, dry electrostatic precipitators follow the working principle of electrostatic precipitators which has been discussed. The feature of dry electrostatic precipitators is that a rapper system, either hammers, electric vibrators or even sonic energy systems, is used to remove particles collected on collection plates. The performance of the electrostatic precipitators can be adjusted by changing the vibration rate or frequency. After the rapper system, a hopper system is then used for final collection and disposal of the particles. Therefore, the main components for dry electrostatic precipitators are: high voltage source, charging electrodes, grounded collection plates, rapper system and hopper system.

Dry electrostatic precipitators are very efficient in solid particulate control with an efficiency of over 90%. However, dry electrostatic precipitators are not quite effective for gaseous emissions, such as condensables.

The year 1907 saw the development of wet electrostatic precipitators by Dr. Cottrell. Since then, wet electrostatic precipitators are developed and used in many industries. Although wet electrostatic precipitators are widely used, the technology itself is relatively unknown. Wet electrostatic precipitators are used for fine particle emission control and for condensable gas control in an environment such as chemical processing. Similar to dry

electrostatic precipitators, the working principles of wet electrostatic precipitators are also from particle charging to particle collection and to the cleaning of the system. The difference is that the cleaning of the system uses the water spray instead of the rapper system [48].

Since the wet ESP works by collecting particles electrostatically charged by way of a dry electrostatic precipitator within a liquid film formed on a collecting electrode (CE), it is normally found following a wet scrubbing device, where the gases are at, or near, saturation temperatures. Given that the materials collected are often corrosive in a saturated gas environment, this results in the materials used for construction need to be highly corrosion resistant and, thus, can be very expensive [48].

The wet ESP cleaning mechanism significantly affects the nature of the particles that can be captured, the performance efficiencies, the design parameters and operating maintenance of the equipment. Since the dust is removed from a wet ESP in the form of slurry, the dry ESP hoppers are typically replaced with a drainage system. Given that a wet ESP creates a slurry mixture that flows down the collecting wall to a recycle tank, the collecting walls never build up a layer of particulate matter, thus, there is no deterioration of the electrical field due to particulate matter build-up. Wet ESPs have several advantages over dry ESPs: 1) they can adsorb gases, causing some pollutants to condense, 2) they are easily integrated with scrubbers and 3) they eliminate reentrainment of captured particles. Additionally, wet ESPs are not limited by the resistivity of particles since the humidity in a wet ESP lowers the resistivity of normally high resistivity particles. It should be noted that power levels within a wet ESP can be significantly higher than in a dry ESP [48].

Wet ESPs, or any of the previously described ESPs, can be operated with a wet spray to remove collected particles. Wet ESPs are used for industrial applications where the potential for explosion is high (such as collecting dust from a closed-hood Basic Oxygen Furnace in the steel industry), or when dust is very sticky, corrosive or has a very high

resistivity. The water flow may be applied continuously or intermittently to wash the collected particles from the collection electrodes into a sump (a basin used to collect liquid). The advantage of using a wet ESP is that it does not have problems with rapping reentrainment or with back corona. [48]

2.6.2 Typical Design of Electrostatic Precipitators

2.6.2.1 Wire-Plate

The most common design of electrostatic precipitators uses wire-plate electrostatic precipitators. The most important feature of wire-plate electrostatic precipitators is the topology where electric charging wires are suspended from a frame at the top of the electrostatic precipitator. The wires are kept straight by hanging some weight at the bottom of the wires. The space between wires is kept by the application of a frame at the bottom. The collection plates for this design are large parallel plates with the space between collection plates used for flow to pass through (the wires are designed to be in the central section of this space). This space is named ducts in the electrostatic precipitator industry. In practice, the height for ducts is between 6 and 14 metres. Wire-plate electrostatic precipitators can be used for dry cleaning or wet cleaning. For wet cleaning, the washing system is located on the top of the system above the charging electrodes. [48]

2.6.2.2 Rigid Frame-Plate

The working principle of rigid frame-plate electrostatic precipitators is similar to that of wire-plate electrostatic precipitators. In rigid frame-plate electrostatic precipitators, the charging electrodes are a rigid frame instead of a series of wires and, in the pulp and paper industry, this topology is more preferred. The rigid frame-plate electrostatic precipitators can also be used for both dry cleaning and wet cleaning. The rigid frame is used as the supporter of the system. The advantages of rigid frame-plate electrostatic precipitators are:

1) higher efficiency. Compared with conventional wire-plate electrostatic precipitators, the rigid frame-plate electrostatic precipitators have larger spacing. The width of spacing is between 0.2 m to 0.3 m for wire-plate topology and 0.5 m for rigid frame-plate topology. The larger space offers a larger electric field strength because of the increase of space charge. With the increase of current, a higher migration velocity can be achieved and the precipitation efficiency which is dependent on migration velocity is increased. 2) The increase space between collection plates gives the system a more flexibility design to make the system adaptable for different situations. 3) The higher precipitation efficiency reduces the needs for larger collection area, so the application of rigid frame-plate electrostatic precipitators reduces the total footprint of the system. Finally, 4) rigid frame-plate electrostatic precipitators are more durable when compared with wire-plate electrostatic precipitators. However, the expense for the initial construction for rigid frame-plate electrostatic precipitators is higher. [48]

2.6.2.3 Wire-Pipe (Coaxial)

The wire-pipe electrostatic precipitator, which also refers to coaxial topology electrostatic precipitators, is also a common design of electrostatic precipitator. In this topology design, a cylindrical metallic tube is used as collection plate. A wire is fixed along the central axis of the cylindrical tube, and the wire is used as the charging electrode. Typically, the cylindrical tube is placed vertically, and the wire is suspended from a frame on top of the cylindrical tube and weighted at the bottom to be fixed. The space between the charging wire and the inner wall of the tube is used for particle charging and particle migration. Although cylindrical tubes are used, there are other topologies developed in recent years where square or hexagonal tubes are used as collection plates. The advantage for either square or hexagonal tubes is that each of the electrostatic precipitator can be attached closely to each other and, therefore, the inner wall of one electrostatic precipitator can be designed to be the outer wall of another one, which may potentially reduce the costs and footprint

of the system. For wire-pipe topology, the system is very efficient in particle precipitation for low gas flow rate. It is also very effective to precipitate mists in which the humidity is relatively high using this topology. The wire-pipe topology electrostatic precipitators in industry are typically between 0.15 m to 0.30 m in tube diameter and 1.8 m to 4.6 m in height. Dry cleaning and wet cleaning can both be applied in this topology, however wet cleaning is more widely used in industry. [48]

2.6.3 Number of Stages: Single and Double Stage Electrostatic Precipitators

Electrostatic precipitators are also grouped by the number of stages. In general, particle charging and particle collection for a single stage electrostatic precipitator occur in the same location. However, for a double stage electrostatic precipitator, particle charging and particle collection occurs in different locations. Particles are charged in the first stage and then collected by the second stage.

All designs of electrostatic precipitators as discussed are single stage electrostatic precipitators. Typically, the voltage level used for single stage electrostatic precipitators is between 50 to 70 kV.

Double stage electrostatic precipitators separate particle charging and particle collection into two stages. In the first stage, which serves as a charging stage, the particles are charged as they pass through the charging electrodes with the voltage level between 12 to 13 KV. Then, in the second stage which serves as collection stage, particles migrate to the collection plates which have opposite charging polarity with the charging electrodes in the first stage and, eventually, particles are collected. Double stage electrostatic precipitators are designed and used for the control of fine particles or liquid aerosols, such as metal

coating industry, high smokehouses, etc. Double stage electrostatic precipitators can also be used for cleaning the air of inner environments in buildings.

The use of double stage electrostatic precipitators is considered in this research to increase the particle precipitation efficiency and there are some differences in the design compared with double stage electrostatic precipitators in industry. The two stages of the double stage electrostatic precipitators in this research are both energised with charging electrodes, and the details of the design and performance will be discussed in Chapter 4. [48]

2.6.4 Gas Temperature: Hot and Cold Electrostatic Precipitators

According to the temperature of flue gas, electrostatic precipitators are divided into cold electrostatic precipitators and hot electrostatic precipitators. In general, the temperature of flue gas for cold electrostatic precipitators is 204°C or lower, and the temperature of flue gas for hot electrostatic precipitators is from 320 °C to 420°C.

Cold electrostatic precipitators have been used for over 50 years in industry. As discussed, cold electrostatic precipitators generally use collection plates for particle collection. The volume of flue gas controlled by cold electrostatic precipitators is lower than that of hot electrostatic precipitators due to the temperature difference (temperature can influence the volume of gas). Therefore, the overall footprint of the system for cold electrostatic precipitators is smaller, which potentially reduces the cost. [48]

Hot electrostatic precipitators, which control the emission of flue gas with higher temperatures, helps reduce corrosion and plugging of the hopper. However, due to the temperature difference, the volume of flue gas controlled by hot electrostatic precipitators is larger when compared with cold electrostatic precipitators. Therefore, the overall footprint of the system for hot electrostatic precipitators is larger, which potentially

increases the cost. Another disadvantage for electrostatic precipitators is the structural and mechanical problems in the system due to thermal expansion.

Since a higher temperature results in lower resistivity, the charging efficiency is higher in the case of hot electrostatic precipitators. Therefore, in the 1970s, hot electrostatic precipitators became widely used, especially for the flue gas which is difficult for cold electrostatic precipitators to control. However, since the 1980s, many of these units did not operate reliably, so operators have generally decided to use cold electrostatic precipitators along with conditioning agents to make cold electrostatic precipitators adaptable for different situations. In modern industry, hot electrostatic precipitators are used in the cement industry, steel refining industry, etc. [48]

2.6.5 Electrostatic Precipitator with Impulsive Energisation

All the electrostatic precipitators discussed previously are high voltage DC energised. These electrostatic precipitators are conventional electrostatic precipitators which use a constant base voltage to generate a corona and electric field.

For impulse energisation, the high voltage that is applied to the charging electrodes is in the form of pulses which last for a short duration (several micro seconds). The voltage level for the pulses is typically in the order of 100 kV as opposed to 50 kV which is used in conventional DC energisation. Theoretically, the pulses can provide the current distribution with better uniformity on the collection plates to charge particles evenly. The impulsive energisation can be used in two ways: 1) the impulsive energisation can be applied as the only energisation of the electrostatic precipitator. 2) The impulsive energisation can be applied with another DC voltage component base. Impulsive energisation has proven to be successful in the electric utility industry. The Ion Physics Corp. has performed tests at Madison Gas and Electric, Madison, Wisconsin. Although there is still gaps in the understandings of impulsive energisation and the application of impulsive energisation, the

efficiency of energy used may increase when impulsive energisation is applied as there is potentially a lower electric energy consumption that can be achieved during the process of using impulsive energisation when compared with conventional DC energisation. [48]

2.7 Penetration Mechanisms

Penetration of particles in electrostatic precipitators means that particles which are not collected by electrostatic precipitators penetrate from the system. Penetration of electrostatic precipitators reduces the effectiveness of electrostatic precipitators, and the particle pollution to be controlled will be emitted into the atmosphere and cause environmental problems. There are three types of penetration mechanisms which will be discussed in this section: Back corona, particle sneakage and particle reentrainment. [49]

2.7.1 Back Corona

Back corona is the mechanism in which breakdown occurs inside the electrostatic precipitators. As discussed previously, the corona in an electrostatic precipitator forms at the charging electrodes and particles are charged in the space between charging electrodes and the collection plates. The electric force on charged particles by electric field separates the particles from the gas flow and particles move towards collection electrodes due to the electric force and are finally collected. If the corona forms at the collection plates the situation is reversed (this mechanism is called back corona). For example, if the charging electrodes generates negative ions and electrons from ionisation, the collection plates are electric positive. In back corona, the collection plates start to generate positive ions and the positive ions move towards to the charging electrodes.

There are two mechanism of back corona which influence the effectiveness of electrostatic precipitators: 1) the positive ions which move towards the charging electrodes collide with negative ions, electrons and particles with negative charges. The collision can cause the

charge neutralisation on particles. When total charge on particles is reduced, the electric force on particles is also reduced. Therefore, the reduced electric force may be not large enough to move particles to the collection plates and particles which are not collected on collection plates penetrate from the electrostatic precipitators. 2) The positive ions which move towards the charging electrodes can cause the charge neutralisation of space charge and reduce the amount of total space charge. In electrostatic precipitators, space charge is exceptionally important as the space charge contribute to the electric field of the electrostatic precipitator, especially in the region near the collection plates. In back corona, the neutralisation of space charge reduces the amount of total space charge and, therefore, reduces the electric field inside the electrostatic precipitators. Therefore, the electric force is reduced due to the reduced electric field. The effectiveness and efficiency of electrostatic precipitators are influenced and there are potential opportunities for particles to penetrate from the system. [49]

2.7.2 Particle Sneakage

The particle sneakage mechanism is where particles sneak from electrostatic precipitators with gas flow. The sneakage of particles is caused by gas flow with particles which flows to the non-electrical region of electrostatic precipitators. Since there is no electric field in this region, there is no electric force on particles in this region. Particles which are not driven by electric force will flow with gas instead of being collected by collection plates. The non-electrical region in electrostatic precipitators is inevitable due to the construction of the electrical distribution system, the rapper system, the support system, etc., should be non-electric. Therefore, there are certain opportunities for gas flow with particles flowing over these regions and cause particle sneakage. [49]

2.7.3 Particle Re-entrainment

Particle re-entrainment is the typical mechanism for dry electrostatic precipitators. In a dry electrostatic precipitation system, after particles are collected on collection plates, the collection plated is rapped for certain time intervals and particles fall to a hopper system which is used for final particle collection. During this process, there are certain opportunities for particle re-entrainment: 1) when particles move towards the collection plates, these particles may collide with the particle layer which is already collected on the collection plates. The collision of particles may loosen the layer and some particles may be circulated by the gas flow and re-enter the electrostatic precipitator. 2) When the collection plates are rapped, the mechanical forces raps particles back. Meanwhile there is still gas flowing inside the electrostatic precipitator, so particles may be circulated by the gas flow and re-enter the electrostatic precipitator. Finally, 3) when particles are falling into the hopper system these particles collide with the collected particles in the hopper and a potential particle cloud forms. The particle cloud may also be circulated by the gas flow and re-enter the electrostatic precipitator. [49]

2.8 Particle Collection Efficiency

Particle collection efficiency for electrostatic precipitators is determined by the Deutsch-Anderson equation, the equation is under ideal conditions. The simplest form of the equation is given by [50]:

$$\eta = 1 - \exp(-wA / Q) \quad (1)$$

where η is the collection efficiency, A is collection surface area of the plates, Q is the gas flow rate and *w* is the particle migration velocity.

The Deutsch-Anderson equation has been used for many years for the calculation and the determination of theoretical collection efficiency. There are three important assumptions which have been made: 1) the particle size is assumed to be uniform, so the velocity based on particle size is uniform. In fact, this is not true because the migration velocity for larger particles is higher than the migration for smaller particles. 2) The Deutsch-Anderson equation assumes the gas flow rate to be uniform, therefore, no gas and particle sneakage happens. As discussed, the sneakage of particles is caused by gas flow with particles which flows to the non-electrical region of electrostatic precipitators. Since there is no electric field in this region, there is no electric force on particles in this region. Particles which are not driven by electric force will flow with gas instead of being collected by the collection plates (i.e. this mechanism is inevitable. 3) Particle reentrainment is not considered. Because of the listed three assumptions, the Deutsch-Anderson equation can only be used for preliminary estimations of the collection efficiency [50].

In order to modify the Deutsch-Anderson equation to be more accurate, studies have been conducted by decreasing the calculation of collection efficiency by a factor of k, which is called Matts-Öhnfeldt equation. According to literatures, the factor k ranges from 0.4 to 0.8 depending on the certain conditions [50].

2.9 Overview of Atmospheric Air Gas Discharges: Mechanisms and Parameters

2.9.1 Townsend Discharge

The beginning of the twentieth century saw the development of the Townsend discharge theory. The Townsend discharge theory is the description of the breakdown process of discharge between electrodes at the distance of d and under the pressure of p. Townsend theory gives an accurate description of the breakdown process for the following conditions:

the product pd limitation is in a range of approximately 0.1–100 Pa·m (0.075–75 Torr·cm) and simple electrode geometries. [45] In general, the product of pd is limited to a range of 0.1-100 Pa·m.

A uniform electric field between metal parallel electrodes is assumed. A single electron from cathode will cause an electron avalanche towards the anode. The number of electrons in this electron avalanche, N_e, is given by:

$$N_e = e^{\alpha x} \tag{2}$$

where x the is the distance from the cathode and α is the First Townsend ionisation coefficient is defined as the number of electrons produced by an electron per unit length of path in the direction of field.

α/p depends on a reduced electric field strength E/p and types of gas. The ionisation coefficient α is described as

$$\frac{\alpha}{p} = A \exp\left(-\frac{Bp}{E}\right) \tag{3}$$

where the constants A and B are gas-specific parameters.

The number of ions, N_i, produced in an electron avalanche by ionising electron impact collisions is given by

$$N_i = e^{\alpha x} - 1 \tag{4}$$

The drift velocity of the electrons is much higher than the drift velocity of the ions. The drift process of ions has not started by the time the electrons reach the anode, nevertheless, the

ions will eventually drift towards the cathode. When ions reach the cathode surface there is a certain number of secondary electrons, γ, that will be emitted from the cathode surface.

The secondary electrons will each start a new electron avalanche, producing new electrons and ions between the discharge gaps. A criterion for self-sustainment of the electron avalanches can be derived. The situation is exactly self-sustaining when the ions resulting from a single electron avalanche produce a single electron by secondary emission at the cathode (when other production and loss processes for charged particles, such as photoionisation, field emission and electron attachment are neglected). This situation is given by [45]:

$$\gamma(e^{\alpha d} - 1) = 1 \tag{5}$$

which is known as the breakdown criterion. This criterion will be described in details later in this section.

Townsend discovered that, at first, the current increased proportionally as the voltage increased then remained constant at I_0 i.e. the saturation current. At even higher voltages the current increases exponentially. The exponential increase in current is due to the ionisation of gas by electron collision. As the voltage increases the electric field increases and the electrons are accelerated between collisions. Therefore, an increasing amount of electrons are knocked out [45].

In Townsend's earlier investigations he observed that the current in the parallel plate gap increased more rapidly with a voltage increase. To explain this departure from linearity, Townsend suggested that a second mechanism must be affecting the current. He postulated that the additional current must be due to the presence of positive ions and the photons. The positive ions will liberate electrons by collision with gas molecules and by

bombardment against the cathode. Similarly, the photons will also release electrons after collision with gas molecules and from the cathode after photon impact.

Let us consider the phenomenon of self-sustained discharge where the electrons are released from the cathode by positive ion bombardment. Let n_0 be the number of electrons released from the cathode by ultraviolet radiation, n^+ the number of electrons released from the cathode due to positive ion bombardment and n the number of electrons reaching the anode. Let γ, known as Townsend's second ionisation coefficient, be defined as the number of electrons released from the cathode per incident positive ion [45], then

$$n = (n_0 + n^+)e^{\alpha d} \tag{6}$$

Now, the total number of electrons released from the cathode is $(n_0 + n^+)$ and those reaching the anode are n, therefore, the number of electrons released from the gas = $n - (n_0 + n^+)$, and corresponding to each electron released from the gas there will be one positive ion and, assuming each positive ion releases γ effective electrons from the cathode, in terms of current,

$$I = \frac{I_0 e^{\alpha d}}{1 - \gamma(e^{\alpha d} - 1)} \tag{7}$$

When the voltage between the anode and cathode is increased, the current at the anode is given by this equation above.

Therefore, Townsend breakdown the mechanisms are summarised as follows.

When

$$1 - \gamma(e^{\alpha d} - 1) = 0 \tag{8}$$

or

$$\gamma e^{\alpha d} \approx 1 \tag{9}$$

The current becomes infinite. Since

$$e^{\alpha d} >> 1 \tag{10}$$

Then, the anode current equals the external circuit current. Following the conditions mentioned previously, theoretically the current becomes infinitely large. However, practically speaking the current is limited by the external circuit resistance and the voltage drop in the arc. The condition $\gamma e^{\alpha d} = 1$ defines the beginning of spark and is known as the Townsend criterion for spark formation, or Townsend breakdown criterion. Therefore, the following three conditions are listed:

When $\gamma e^{\alpha d} = 1$, the sparking condition threshold is defined. The arc electron avalanche produces ion pairs in the gap and the number of ions is sufficiently large. The resulting positive ions on bombarding the cathode are able to release one secondary electron and a repetition of the avalanche process is caused. The discharge is self-sustained as the discharge will sustain itself even without the source producing I_0.

When $\gamma e^{\alpha d} > 1$, under this condition the ionisation produced by successive avalanche is cumulative. The spark discharge grows more rapidly.

When $\gamma e^{\alpha d} < 1$, under this condition the current I is not self-sustained, and when I_0 is removed, the flow stops. [45]

2.9.2 Streamer

Streamer is a type of transient electrical discharge. Assume that the field $E_0 = V/d$ is not affected by the space charges of electrons and positive ions. When the field between electrodes is uniform, it is known that charge between the electrodes (with distance d) increase by a factor of $e^{\alpha d}$. Raether has observed that the growth of an avalanche is weakened if the charge concentration is higher than 10^6 but lower than 10^8 ($dn/dx < e^{\alpha d}$). Whenever the concentration exceeds 10^8, the avalanche current is followed by steep rise in current and a breakdown occurs between the gaps. The weakening of the avalanche at lower concentration and rapid growth of avalanche at higher concentration has been attributed to the modification of the electric field E_0 due to the space charge field. [45]

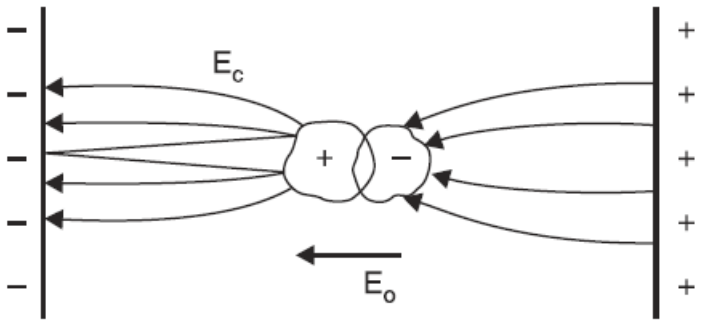

Figure 2-5. Field redistribution due to space charge. Picture taken is from [45].

Figure 2-5 shows the electric field around an avalanche as it progresses along the gap and the combined field (the superposition of the space charge field and the original field E_0) in which plus and minus shows the polarity of charge and the arrow shows the electric field. Since the electrons have a higher mobility, the space charge at the head of the avalanche is considered to be negative (assuming electrons are in a spherical volume). It can be seen from Figure 2-5 that the field at the head of the avalanche is strengthened. The field between the assumed electron charge centre and the positive ions centre is decreased at the field as the charge centres oppose the main field E_0. The field between the positive

space charge centre and the cathode is increased as the space charge field is added to the main field E_0 in this region. It has been observed that if the charge carrier number exceeds 10^6, the field distortion becomes noticeable. The distortion does not have a significance influence on discharge, however, if the charge carrier exceeds 10^8 the space charge field becomes almost of the same magnitude as the main field E_0 which may lead to the initiation of a streamer. Therefore, the space charge field is very important in the mechanism of electric discharge in a non-uniform gap which will be included in the simulation chapter in Chapter 6 to make the model more accurate as compared with the classical approach shown in this section. [45]

According to Townsend's theory i.e. the ionisation of gas molecule by the electron impact results in electric spark discharge and positive ion bombardment at the cathode results in the release of electrons from cathode, the formative time lag of the spark should be at best equal to the electron transit time t_r. At pressures around atmospheric and above p.d. > 10^3 Torr cm, the time lags have been found in experiments to be much shorter than t_r. Some studies also show the space charge in avalanche can transform the avalanche into channels of ionisation (known as streamers) which can lead to rapid development of breakdown. Studies also show that the critical conditions of the transformation from avalanche to streamer is when the charge within the avalanche head reaches the value of $n_0e^{\alpha x} \approx 10^8$ or $\alpha X_c \approx 18$ to 20. Xc is the length of the avalanche path in field direction when it reaches the critical size. If the gap length d < Xc, it is impossible for the streamer to occur.

The studies of discharge development show that there is a secondary mechanism of streamer development which is related to the short time lag, as mentioned previously. This secondary mechanism of streamer development is called the Kanal mechanism and the streamer result from the secondary Kanal mechanism is only due to the photoionisation of gas molecules, which means that streamer resulting from the Kanal mechanism does not rely on electrodes. The key conditions for the Kanal mechanism are intensive ionisation and

excitation of gas particles in front of the avalanche head. To reach the key conditions, the gap distance required for the formation of avalanche should be a critical value and the applied field should reach the level for intensive ionisation. Under these conditions, photons are generated due to the recombination of electrons and positive ions. After photons are generated, these photons generate the secondary electrons by the photoionisation process. These secondary electrons reach the speed of light, therefore, form secondary avalanches extremely quickly under an external electric field. The process is shown in Figure 2-6. [45]

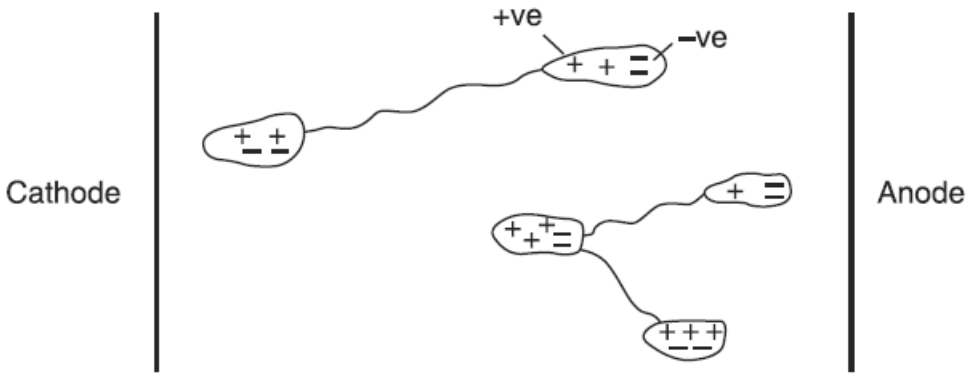

Figure 2-6. Secondary avalanche formation by photoelectrons. [45]

2.9.3 Mechanisms of Corona Discharge

Mechanisms of corona discharge will be introduced in this section. For a gradually increased uniform electric field, when the measurable ionisation begins, the ionisation leads to a complete breakdown of the gap. However, there are discharges which are visually and audibly available before the breakdown of the medium in non-uniform fields, also known as corona discharges. A corona discharge is a self-sustained electric discharge and the ionisation occurs only over a certain value of the distance (non-uniform fields) between the electrodes. A corona discharge frequency is usually between 20 Hz and 20 kHz

in air with ambient humidity and room temperature and is initiated with a hissing noise and ozone gas is formed. [45]

When the applied voltage reaches the critical voltage, the corona discharge starts. Corona discharge is not visually available at first as the charged ions in the air need to receive energy to cause further ionisation by collisions. For a radial field, a gradient g_v at the surface of the conductor should be reached to cause a gradient g_0, which is at a finite distance away from the surface of the conductor. The distance between g_0 and g_v is called the energy distance. According to Peek, for two parallel conductors this distance is equal to ($r + 0.301\ r^{1/2}$) and for coaxial conductors this distance is equal to ($r + 0.308\ r^{1/2}$). The electric field intensity for two parallel wires is given as [45]:

$$E = 30(1 + \frac{0.301}{1 + \delta\sqrt{r}})\delta \tag{11}$$

and for a coaxial wire

$$E = 30(1 + \frac{0.308}{1 + \delta\sqrt{r}})\delta \tag{12}$$

Electric field is in kV/cm.

Investigations with point-plane gaps in the air have shown that when the point is positive, the corona current increases steadily with voltage. At sufficiently high voltage the current amplification increases rapidly with voltage up to a current of about 10^{-7} A, after which the current becomes pulsed with a repetition frequency of about 1 kHz composed of small flashes. This form of corona is known as flashing corona. The average current then increases steadily with the applied voltage, leading to breakdown. [45]

With a point-plane gap in the air, when a negative polarity voltage is applied to the point and the voltage exceeds the corona ignition value, the current flows in vary regular pulses known as Trichel pulses. The corona ignition voltage is independent of the gap length and is numerically equal to the corona ignition of streamers under positive voltage for the same arrangement. The pulse frequency increases with voltage and is a function of the radius of the cathode, the gap length and the pressure, where a decrease in pressure decreases the frequency of the pulses. It should be noted that the breakdown voltage with negative polarity is higher than with positive polarity except at low pressure. Therefore, under alternating power frequency voltage the breakdown of non-uniform field gap invariably takes place during the positive half cycle of the voltage wave. [45]

2.9.3.1 Positive Corona (Flashing)

In order to study the mechanisms of the corona discharge, different configurations have been investigated. It is found that a point-plane configuration is the most suitable configuration for investigation as different degrees of field non-uniformity can be achieved by changing radius of the electrode tip and the localisation of space charge can be obtained using this configuration.

In terms of impulsive corona discharge and static state corona, it is easy to distinguish as the former is energised by an extremely short impulsive energisation duration, so no space charge is permitted to drift and accumulate.

For impulse energisation, at just above corona ignition voltage level, it is difficult to monitor the growth of discharge precisely due to the transient development of ionisation. However, the use of the 'Lichtenberg figures' and high-speed photographic techniques, which have recently been developed, make it possible to help understand various discharge stages preceding breakdown under impulse energisation.

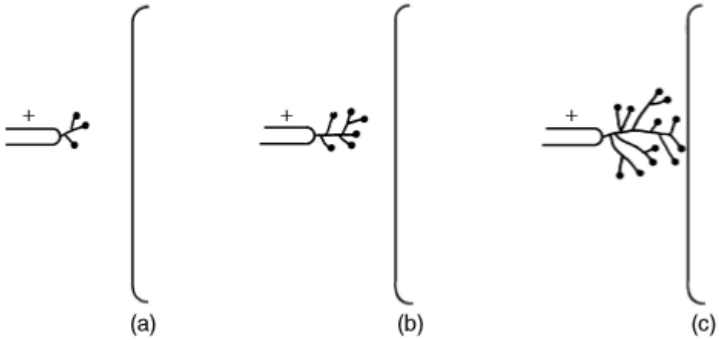

Figure 2-7. Schematic illustration of the formation of streamers under impulse voltage-progressive growth with increasing pulse duration-positive rod-plane gap. Picture is taken from [45].

As shown in Figure 2-7, for positive impulsive energisation which is applied to the point electrode, the first ionisation can be detected in a branch (shown in (a)). This discharge is a streamer. When the voltage level is increased the length of streamers grows and the number of branches increase (as shown in (b) and (c)). The branches never cross each other. The velocity of the streamers decreases rapidly as they penetrate the low electric field region. [45]

When the energisation is DC or with longer pulse duration time, a distortion in the original field will result as there is sufficient time for ionisation products to stay in the gap and accumulate in space.

To investigate the various discharge modes and the breakdown characteristics for this arrangement in atmospheric air, as shown in Figure 2-7, a tip-plane configuration with the tip radius of 1 cm is assumed. If the tip-plane distance is small (less than 2 cm), no appreciable ionisation is detected with the increase of voltage level till breakdown voltage. When the distance is increased, the field distribution becomes un-uniform and the situation is more obvious with the increase of distance. With the increase of voltage, transient discharge branches appear first. These discharges, which are called streamers, are shown to

be identical. The streamer develops with varying frequencies under steady state and the current is proportional to the distance. These streamers are called onset streamers or flashing pulses. The frequency of these streamers increases with the increase of voltage level until the transient process stops. The discharge becomes self-sustained and a steady glow appears close to the anode, with the current caused by the glow, where brightness also increases with increased voltage level, to be continuous and unstable. Further increase of the voltage level will cause increasing streamers until the breakdown in the gap. In order to explain the characteristics of the discharges, Figure 2-8 is plotted to show the ignition voltages of different discharge modes as a function of point-plane distance. [45]

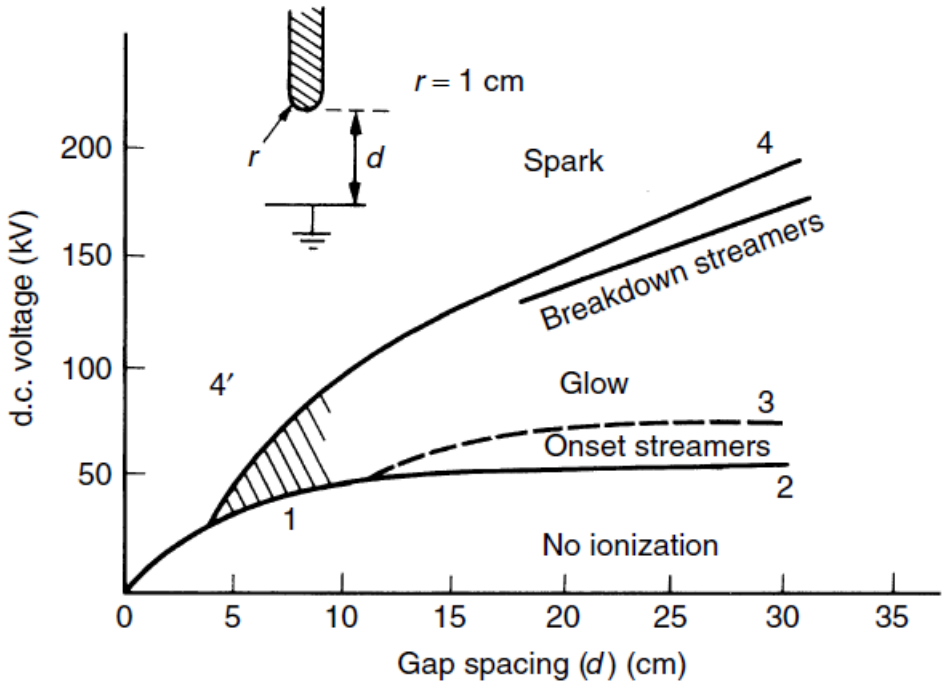

Figure 2-8. Threshold curves for various modes of anode corona and for spark breakdown for a hemispherically capped anode and plate cathode. Picture is taken from [45].

For shorter distances, the voltage can be assumed to be uniform. Therefore, similar to uniform cases, the streamer is capable of penetrating the electric field which is relatively weak. The streamers can reach the cathode and initiate breakdown. In Figure 2-8, this

situation is described in curve 1. Curve 2 describes the situation when streamers appear that do not cross the gap when a larger tip-plane distance above 10cm is reached. Curve 3 describes the transition from streamers to steady glow corona without sparking. When the tip-plane distance is larger, there is a situation that breakdown streamers develop preceding the complete breakdown of the gap and the corresponding voltage range is considerable. The region of uncertain transitions is described by the dashed area in Figure 2-8, in which portion 1 shows the onset of streamers followed immediately by a transition to spark. For a certain value of tip-plane distance when glow is first caused then reduced, if the voltage is kept constant, there is a certain value of voltage that the glow discharge is kept without breakdown. For this certain value of voltage, if this voltage is increased, a spark will be caused by the glow corona which is described by curve 4. On the other hand, if this voltage is decreased, a streamer breakdown will result. Curve 4 also shows that the glow corona sparking voltage can be set to lower value by decreasing the tip-plane distance and by increasing the voltage level. Therefore, when a steady corona glow is established, and the sparking voltage is increased, then the lower breakdown voltage for the streamer is prevented [45].

2.9.3.2 Negative Corona (Trichel Impulses)

The nature and characteristics of impulses for point-plane configuration with negative energisation and under static conditions are studied by Trichel. The current of these impulses, also known as 'Trichel impulses', are found to be in regular tendency above the ignition voltage. The corona ignition voltage, in negative energisation cases, is found to be independent of the tip-plane distance. For the same configuration and tip-plane distance, the value of the ignition voltage level for positive energisation and for negative energisation is close. The frequency of Trichel impulses increases with the voltage and depends on the pressure of the experimental environment, the radius of the cathode and the tip-plane distance. Studies show that 1) the increase of voltage causes the increase of frequency, 2)

the increase of distance causes the decrease of frequency for the same voltage level and 3) the decrease of experimental pressure causes the decrease of frequency.

According to [45], a typical example is shown to explain different coronas with negative energisation. Figure 2-9 shows the ignition voltage as a function of tip-plane distance (tip radius is 0.75 mm). As shown, the lowest curve gives the corona ignition voltage for Trichel impulses which are not significantly affected by the tip-plane distance. For a certain range of voltage levels, the mode of the Trichel impulses is not affected by the increase of voltage level. When the voltage level is increased further to a certain value, a steady glow discharge is obtained, however, the transition from Trichel impulses to glow discharge is not previously defined, so there is a wide transition range in the figure. Further increase of the voltage level maintains the glow discharge until breakdown at a certain value of voltage level. The breakdown voltage for negative energisation is higher than the breakdown voltage for positive energisation of the similar configuration and the similar experimental parameters, except at low pressures. Flashing corona impulses and Trichel corona impulses are very important to the research in this thesis, as they can provide transient electrical discharge for particle to be charged and removed, and they are the key factors of the establishment of electrostatic precipitators.

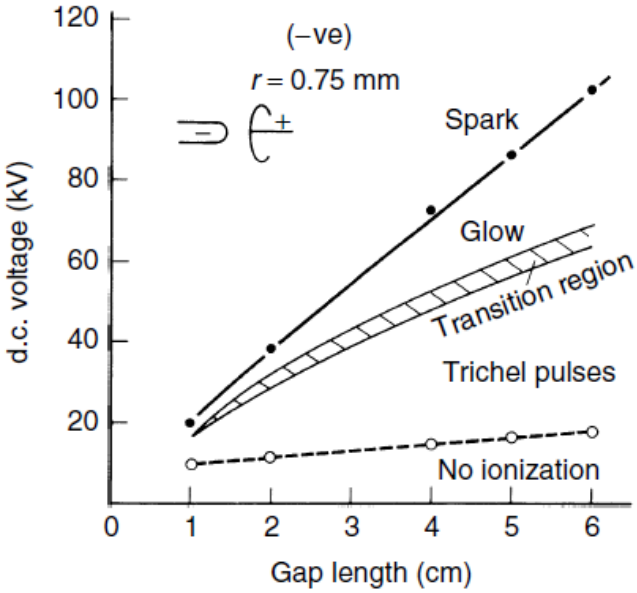

(a)

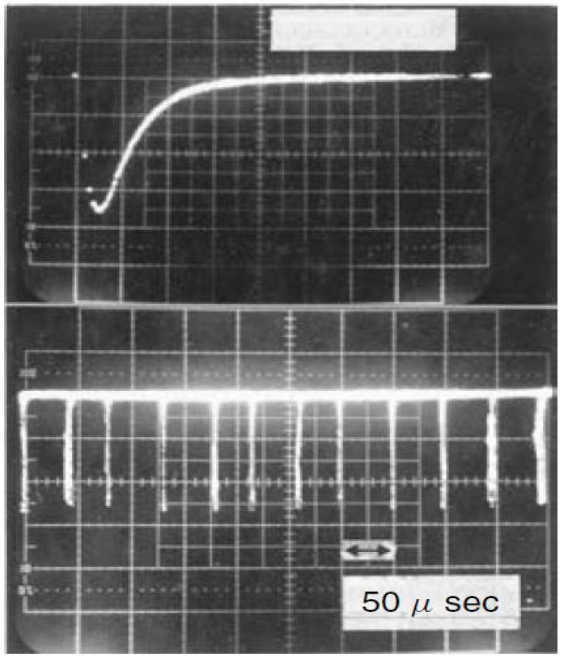

(b)

Figure 2-9. Negative rod-plane breakdown and corona characteristics in atmospheric air (a) discharge modes, (b) pulse pattern. Picture is taken from [45].

2.10 Particle Charging Mechanisms

Several particle charging mechanisms are used in electrostatic precipitation research and industrial processes, such as: 1) gaseous ions charging, i.e. the collisions of gaseous ions, generated by either unipolar or bipolar chargers, with aerosol particles results in particle charging. This type of particle charging mechanism, which includes field charging and diffusion charging, is very important for this study. For field charging, the collision of particles and ions is influenced by the external applied electric field. For diffusion charging, the collision of particles and ions is caused by Brownian motion. Field charging and diffusion charging will be illustrated in detail in this section. 2) Contact charging, the separation of particles from solid surfaces, can result in charge transfer between surfaces. The particles are dry and non-metallic for this type of charging mechanisms. The charge on particles is significant but uncontrolled and this type of charging mechanism is important for solid particles. 3) Inductive charging is the charge transfer through electromagnetic induction. 4) Thermionic emission charging is the charge transfer in the form of electron flow from a metal or metal oxide surface. The electrostatic force is not capable of holding electrons due to thermal vibration, so electron flow is generated from the metal or metal oxide surface and, finally, results in charge transfer. This type of charging mechanism is important for high-temperature environments (1000 K to 3000 K) due to the nature of thermal vibration and material of metal or metal oxide. 5) Spray charging is where liquid droplets are surface charged. 6) Electro kinetic streaming charging is caused by the generation of an electric field due to relative motion between a solid and a fluid. 7) Electrolytic charging is where the charged liquid droplets which are produced during the atomisation process of the separation of dielectric liquid from the solid surface [45]. Particle charging is very important in electrostatic precipitation because particles will be removed by the electric force on particles and the electric force is due to charge on particles in the electric field.

2.10.1 Field Charging and Diffusion Charging

For field charging, the charge transfer is due to the collision of particles and ions and the charging process is influenced by the external applied electric field. When a particle is within an electric field, where there are ions travelling along the electric field lines, the electric lines flow through particles and the ionic flux transfer charges on particles by collision. The ions continue to bombard the particle until the charge on that particle is saturated and, at this point, the saturation charge on particles is achieved. When the charge on particles becomes saturated, the electric field lines will be repelled from the particle and the field charging process stops.

For an electrostatic charging approach, the charge on particle as a function of time (Q(t)) is given by [51]:

$$Q(t) = 12\pi E_0 \varepsilon_0 \frac{\varepsilon_p}{\varepsilon_p + 2} (\frac{R_p}{2})^2 \frac{t}{t + \frac{4\varepsilon_0}{Ne\mu}} \quad (13)$$

where E_0 is the applied field, ε_0 is the relative permittivity, ε_p is the permittivity of particles, R_p is the radius of particles, N is ion number density (counts/m^3) and μ is ion mobility (m^2/Vs).

For the two types of charging mechanisms, diffusion charging is particularly important for smaller particles and for shorter charging times, whereas field charging is particularly important for larger particles and longer charging times. When a particle is in an electrostatic precipitator, the total charge is the sum of diffusion charge and field charge. In practical industrial cases, the particles to be controlled are large enough and the charging time is long enough, which makes diffusion charging less of a necessity than field charging. The saturation field charge (when the charge on particles is saturated and the electric field on particles repels extra charge, stop ions from bombarding particles) is given by [51]:

$$Q_s \approx \frac{3\varepsilon_p}{\varepsilon_p + 2}\left(\frac{ER_p^2}{4\pi\varepsilon_0}\right) \tag{14}$$

As shown in the classical charging approach, from a particle electric and dielectric property point of view, only permittivity of a particle is considered. This problem will be explained in detail later in this chapter. However, in reality, the electric and dielectric properties also include conductivity of particles, permittivity of media and conductivity of media. Therefore, in this case, the advanced charging approach is derived and used in this research. The influence of the consideration of conductivity and permittivity of both particles and media will be shown and discussed in Chapter 6 in detail. The advanced charging approach is shown in this section.

Diffusion charging is the charging mechanism where diffusing ions collide with particles due to random Brownian motion, and particles are charged due to collision with ions. In a diffusion charging mechanism, there is no external field applied. The ionisation source ionises air or gas molecules and the ions collide with particles resulting in charge transfer. The ions could be of the same polarity (unipolar) or both polarities (bipolar). The charging rate decreases with the increase of charge on particles.

The gas ions have a Boltzmann distribution of velocities so the collisions of ions with particles are expected to result in a Boltzmann distribution of charges. The charge for diffusion charging is given by [51]:

$$Q_{diffusion}(t) = \frac{2\pi\varepsilon_0 kTd}{e}\ln\left(1+\frac{e^2 Ntd}{2\varepsilon_0\sqrt{2m\pi kT}}\right) \tag{15}$$

where k is the Boltzmann constant (1.38 x 10^{-23} m^2 Kg $s^{-2}K^{-1}$), T is temperature (K), d is diameter of particle, m is the mass of particle and N is ion number density (counts/m^3).

The most significant difference between field charging mechanism and diffusion charging mechanism is that field charging is better suited for 1 μm and larger particles while diffusion charging is suited for 100's nm and smaller particles.

2.11 Typical Problems of Researches Reviewed for Electrostatic Precipitation

Based on the literature review of electrostatic precipitation approaches, several problems have been identified in these researches. The problems include: 1) low particle precipitation efficiency (or particle penetration after the electrostatic precipitation process) has been found in some researches. 2) High energy consumption has been found in the electrostatic precipitation systems. 3) In particle precipitation simulation researches, it has been found that the electric parameters of particles and medium have been neglected. These problems are introduced and discussed in this section.

2.11.1 Particle Precipitation Efficiency Problems

The first problem that has been found in literature research is low particle precipitation efficiency. When particles are charged and removed by the electrostatic precipitators some particles escape from the system instead of being precipitated and collected by the electrostatic precipitator. This phenomenon is called particle penetration and can lower particle precipitation efficiency. In the literature researches of electrostatic precipitation it has been found that some approaches have low particle precipitation efficiency. In other researches, although particle precipitation efficiency is high (up to 90%), there is still particle penetration of the system. It also has been found that particle precipitation efficiency is even lower for small particles (particle diameter smaller than 1 μm).

For example, the research in paper [52] illustrates a DC energised electrostatic precipitation system with needle-plate configuration. This research investigated ten cases of designs based on different types of filters and collection plates. The filters include glass fibre, polyethylene, bag filter media, polyester, polyethylene terephthalate, non-woven media and refined cotton media. The collection plates include iron plate, iron grid and activated carbon media. Fly ash is used as the pollution source of the research. Both positive and negative DC high voltage energisations have been used, and the precipitation results for larger particles (larger than 1 μm) can be as high as 99%. However, particle precipitation efficiency for particle diameters smaller than 1 μm is unstable (between 20% to 70%).

Paper [53] presented research of an electrostatic precipitation system based on the configuration of a single needle and a hole-punched plate. Carbon particles were used as the source of pollution with diameter from 0.03 μm to 3 μm. Negative high voltage energisation was applied to the needle hole-punched plate system with the voltage level from -4 kV to -15 kV. The research investigated the influence of the size of the hole, therefore, different sizes of holes were used in the research. Particle precipitation efficiency in this research for particle diameter of approximately 0.265 μm is around 65% for the best hole size. The particle precipitation efficiency for different cases are all below 80%.

High voltage energised plasma by gas discharge can be used both for particle precipitation and for biological decontamination at the same time. Paper [54] presented an approach of a system to improve the indoor air quality by particle collection, odour removal and sterilisation of *E.coli*. In particle collection section, the system designed was based on multiple needle electrodes (located on a plate) with the mesh filter. The high voltage supply used for the multiple needle system was negative energisation with voltage level of -5 kV. The particle collection efficiency was approximately 50% with the collection time of 80 minutes.

Another paper [55] investigated the behaviour of a double stage particle precipitation system with a co-flow particle pre-charger and a parallel plate collection stage. The particle diameter in the paper ranged from 0.2 μm to 4 μm. The co-flow particle pre-charger was energised with negative DC energisation and the working voltage levels were -12 kV and -16 kV. The parallel plate collection stage was energised with positive DC energisation and the working voltage level was 20 kV. Different voltage level combinations have been applied to the system for comparison. The particle precipitation results in the paper show that the system is with highest particle precipitation when -16 kV and 20 kV are applied to the pre-charger and the collection plate respectively. The highest particle precipitation efficiency for particles larger than 1 μm can be as high as 100%. However, particle precipitation efficiency for particles smaller than 1 μm was below 100% and approximately 80% when the particle diameter is around 0.2 μm. In other cases, particle precipitation efficiency was either around or below 80%.

Another paper [56] presented a research based on an electrostatic precipitator with discharge electrodes consisting of seven circular discs with zigzag-shaped edges for both particle charging and removal of increased humidity inside the electrostatic precipitator. The particle sources used for this literature were oleic acid particles, Al_2O_3 particles and SiO_2 particles. The particle size ranged around the hundreds of nanometres and below 1 μm. Water mist was used to increase humidity in the system as the paper established that increased humidity can improve the performance of the electrostatic precipitation system by increasing particle precipitation efficiency for the three types of particles. The voltage levels used were 21 kV for oleic acid particles and Al_2O_3 particles, and 18 kV for SiO_2. The particle precipitation efficiency in the paper for increased humidity is higher than 90%. However, the particle precipitation efficiency for particle smaller than 300 μm dropped below 90%.

From the reviewed researches on electrostatic precipitation, it is found that electrostatic precipitation system in these papers is either with low particle precipitation efficiency or with high particle penetration rate. Low particle precipitation efficiency can affect the performance of the electrostatic precipitator and the purpose of precipitating particles cannot be achieved. Although in some cases particle precipitation efficiency is high, as identified in some reviewed papers, there is still particle penetration. The particle penetration sometimes can be dangerous when particle precipitators are applied in environments such as hospitals, biological laboratories, chemical plants and so on. In such environments, particle precipitation efficiency for electrostatic precipitators must be as high as possible and, in most instances, a 100% precipitation efficiency is expected. The improved efficiency provides the motivations of the research in this thesis by improving the design, optimising the process and by changing the inside environment of the electrostatic precipitators.

2.11.2 Energy Consumption Problems

The second problem of electrostatic precipitation approach based on the reviewed researches is the high energy consumption during particle precipitation. High energy consumption of electrostatic precipitators can result in two problems: 1) increased cost of operation and 2) the lack of control of hazardous particles emitted into the atmosphere to protect the environment. However, high energy consumption means more electric power will be used which, as this needs to be generated, potentially means more fossil fuels will be used i.e. non-sustainable energy, or, even worse, the use of fossil fuel can cause more particle emissions. Therefore, high energy consumption will set up a vicious cycle.

Considering the two listed problems with high energy consumption, electrostatic precipitators should be designed to utilise low energy consumption. However, the

researches based on literature review show that high energy consumption is the typical remaining problem remaining when dealing with electrostatic precipitation.

For example, paper [57] presented a needle cylindrical electrostatic precipitation system. The needle cylindrical system was based on a central needle electrode (DC high voltage energised) and cylindrical collection plate. The design also included a soft X-ray emitter to help increase the particle precipitation efficiency. NaCl nanoparticles (~100 nm) were used for the particle source. Both positive (9 kV) and negative energisations (-9 kV) have been used for the needle cylindrical system to achieve maximum particle precipitation efficiency (98%). The energy consumption for the needle cylindrical system was 0.06 Wh/m^3 for positive energisation and 0.18 Wh/m^3 for negative energisation.

Another paper [55] presented a research on a multiple stage electrostatic precipitation system consisting of three stages; a streamer corona reactor (AC/DC energisation), a bipolar charging reactor (negative DC energisation) and an electrostatic precipitator (positive/negative DC energisation). The streamer corona reactor is with coaxial configuration whereas the bipolar charging reactor and the electrostatic precipitator are based on a wire-plate configuration. The particle source was styrene and the particle diameter ranged from 0.01 μm to 1 μm. The working voltage for the bipolar charging reactor stage was -17 kV and working voltage of the electrostatic precipitator stage was 29 kV for positive energisation and -32 kV for negative energisation. The research in the literature investigated different voltage combinations with different voltage levels and voltage polarities. The best particle precipitation efficiency of the paper was approximately 80%. Energy consumption was evaluated in the paper at 3.33 Wh/m^3.

There are also typical energy consumption values found in paper [58] [59] [60], with energy consumption values of 0.44 Wh/m^3 (10-17 kV voltage level), 0.1-0.5 Wh/m^3 (20 kV voltage level), and 0.1 Wh/m^3 (60 kV voltage level) respectively.

The energy consumption values that have been found in approaches on electrostatic precipitation are high. In other approaches, although the energy consumption value is not calculated, the working voltage levels are high (sometimes they can reach up to 30 kV) and can result in a high energy consumption value. Another important factor is that energy consumption increases as the particle precipitation efficiency increases (or voltage level increases as the particle precipitation efficiency increases). The minimisation of energy consumption provides one of the motivations of the research in this thesis where the aim is to minimise the energy consumption but to maintain high particle precipitation efficiency.

2.11.3 Simulation Problems on Electrostatic Precipitation

In order to investigate the particle behaviours (such as particle charging, particle dynamics, particle precipitation, etc.) In order to provide suggestions on improving the performance of electrostatic precipitators, a simulation is one of the most important methods to help understand the characteristics of electrostatic precipitation as well as investigate the influences of different parameters. One of the investigations is conducted through particle dynamics while inside electrostatic precipitators. Particle dynamics include particle acceleration, velocity and displacement and these values can be used for analysis and calculations to reflect the performance of electrostatic precipitators. In the reviewed approaches on simulation of electrostatic precipitation, two problems have been found; the neglect of space charge influence of electric field and the neglect of electric parameters of particle and medium.

The first problem discovered in literature is the neglect of space charge influence of electric field when a simulation is conducted. For example, space charge influence was not considered in paper [61] when the particle charging process was simulated, which is not as accurate as the space charge effect occurs during the process of ionisation and particle charging. The existence of space charge decreases the electric field of the charging

electrode and the particle collection efficiency can be reduced by the influence of space charge [62]. Therefore, it is extremely important to include the influence of space charge for simulations of electrostatic precipitators to reflect a more real environment inside electrostatic precipitators.

The second problem is the neglect of electric parameters of particle and medium. The electric parameters of particle and medium include conductivity of particle, relative permittivity of particle, conductivity of medium and relative permittivity of medium. For example, in a simulation approach presented in papers [62] and [51], the only electric parameter considered was the relative permittivity of particles. The conductivity of particles, the conductivity of medium and the relative permittivity of medium in the papers are neglected, which is not accurate as the conductivity and relative permittivity of particles and medium are the nature of particles and medium that cannot be neglected. Therefore, similar to the space charge influenced electric field, it is very important to include the conductivity and relative permittivity of particles and medium for simulations to reflect a real situation in electrostatic precipitators

It also has been discovered that there is no simulation approach that has included the influence of space charge and the influence of all electric parameters of both particle and medium at the same time, which provides another motivation of the research in this thesis to develop a model to simulate particle dynamics and the particle precipitation efficiency calculation based on particle dynamics. The model should include the influence of space charge and the influence of all electric parameters of both particle and medium (particle conductivity, particle relative permittivity, medium conductivity and medium relative permittivity).

2.12 Use of Non-thermal Plasma Discharges for Biological Decontamination

Another objective of this research is to investigate the probability of biological decontamination of the electrostatic precipitation system. If the electrostatic precipitation system can decontaminate microorganisms of the gas flow during the process of electrostatic precipitation, there is less probability for microorganisms to be emitted into atmosphere or to enter certain spaces controlled by electrostatic precipitation. With the decreased probability existence of microorganisms, pathogenic microorganisms can, potentially, be reduced. The probability of biological decontamination makes the technology of electrostatic precipitation more widely used, either as a method of controlling certain types of microorganism emission or as an extra advantage of using electrostatic precipitation for particle emission control.

Biological decontamination refers to the process of destroying or removing microorganisms, which include bacteria, viruses and eukaryotic organisms. Different levels of decontamination methods are defined by the efficiency and, when the efficiency reaches the status that all the viable forms are eliminated for the certain environment, the level is defined as sterilisation. The plasma (corona) generated by electric discharge is one possible method for decontamination or sterilisation, and has proven to be effective. Practically speaking, decontamination or sterilisation by non-thermal plasma is not widely used, however, this method is very important due to the following advantages: 1) decontamination or sterilisation by non-thermal plasma does not require a change in temperature and does not influence sensitive materials. 2) This method could be operated in an open chamber so there is more flexibility when using this method. 3) There are no side products generated during the process. 4) There is no problem with storage and preparation of a decontamination agent when compared with other types of methods. 5) The operational costs are low.

There are studies for decontamination or sterilisation by non-thermal plasma in which different types of discharges are used and the plasma generated are under different conditions and experimental parameters. In these studies, different microorganisms are selected as the experimental samples to be decontaminated. The physical and chemical process is very complex during the process of the discharge, so the possible mechanisms and causes of the decontamination or sterilisation are not fully defined. For decontamination or sterilisation by non-thermal plasma, action of Ultra-Violet (UV) radiation and action of charged particles and reactive particles are the three main potential possible mechanisms, which will be discussed in this section. In addition, the action of electric field will also be discussed.

2.12.1 Action of UV Light

The action of UV light has been known to allow biological decontamination. The wavelength of UV light usually ranges from 250 nm to 280 nm, with 260 nm being optimal for the decontamination effect. The mechanism of UV light decontamination includes: 1) the ability of UV light to inhibit the microorganism cell from replicating by the dimerisation of thymine bases of DNA. 2) Damage of UV light to proteins. 3) Hydrogen peroxide generated by UV light in an intracellular environment. 4) Ozone generated by UV light in air. Plasma can generate energetic photons, and UV light with different wavelengths can be generated by plasma depending on the environmental conditions [63], [64], [65], [66].

2.12.2 Action of Reactive Particles

Plasma is a state of ionised gas, in which there are electrons and ions generated during the process of electric discharge, both which play an important role in the decontamination of microorganisms. Electrons and ions can mechanically damage cell envelops. One possible cause of decontamination of microorganisms is due to the membrane damage of the

microorganism cells due to mechanical impact caused by the bombardment of electrons and ions. The effect of an external electric field is also one possible mechanism of decontamination of microorganisms. During the process of discharge, charges are generated and accumulate on the surface of microorganisms and electrostatic forces are caused by the application of external electric field. When the electrostatic force on microorganism surface exceeds the tensile strength of the surface, the membrane will be broken, and decontamination will occur. The decontamination mechanism of the external electric field is particularly effective for gram-negative bacteria [63], [64], [65], [66].

The action of reactive particles in an ambient atmosphere is very important in biological decontamination. In general, the decontamination of microorganisms is caused by the disintegration of the cell walls, coats and membranes which, subsequently, is due to the oxidisation effect of these reactive particles. The reactive particles include reactive oxygen species such as O, O_2 ($^1\Delta_g$), O_3, OH, and nitrogen species such as NO, NO_2. These reactive particles are either the products generated by discharge or the product of chemical reaction on microorganisms. In general, reactive oxygen species can destroy DNA due to the formation of adducts with nucleotide bases, oxidise proteins resulting in enzyme and structural damage and cause lipid peroxidation which may further lead to membrane damage. The effect of different reactive species is discussed as follows: 1) O_3 is a stable modification of oxygen and is well known for its effect of decontamination. In researches, O_3 is generated by electric discharges and is a strong oxidant and toxic in higher concentration. O_3 can also be decomposed to form atomic oxygen, O. 2) O is formed either by the decomposition of O_3 or by interaction of ions or electrons with oxygen molecules during the process of discharge. O has a strong etching effect on microorganisms and is very reactive. It oxidises extremely quickly and can react to O_2, O_3 and hydroxyl radical OH. 3) OH is highly reactive and is able to pass through the membrane of microorganisms and reach their internal sections. OH is very effective in decontamination of live cells as the enzyme of cells cannot eliminate it. 4) Singlet oxygen $^1O_2$ is the electron excited state of

oxygen which has two forms O_2 ($^1\Delta_g$) and O_2 ($^1\Sigma_g$). $^1O_2$ is the product of electric discharge in oxygen atmosphere and is a highly reactive species. 5) Superoxide anion O_2^- is also one of the species generated in discharges. It is not as reactive as other species, however, the reaction of O_2^- and other atoms and molecules can produce OH and O which are highly reactive. It is also important that both O_2^- and H can produce H_2O_2 in the cells by biochemical reactions, which is effective in biological decontamination [63], [64], [65], [66].

2.12.3 Action of Charged Particles

The action of charged particles on biological decontamination has been investigated by several researchers. When charged, a body the size of a bacterial cell (in the micrometre range) experiences an outward electrostatic force due to each charge being subjected to the repulsive forces of all the similar charges accumulated on the cell surface. This theory seems to provide a convincing explanation for some of the experimental results reported in the literature. Considering that the hypothesis holds well, the microorganism would certainly be ruptured, provided that the time of the charge accumulation is long enough. Another viewpoint is that the antimicrobial action of the charged particles seems to occur due to the chemical modification of the surface proteins in bacteria. More specially, in situ hydroxyl, radical formation on the surface of bacteria was proposed to be the leading mechanism underlying the protein damage caused by the charged particles. Another convincing mechanism of biological decontamination effects of the charged particles has been summarised by some researchers where the charged particles randomly absorb on the outside of the cell wall. One of the cases is that charged particles absorb on the cell wall and that a non-uniform electric field is generated between these charged particles. As the time of charge accumulation goes by, transmembrane potential increases. When the transmembrane potential reaches a certain threshold the protein of ion channel changes its form, allows the ion channel to open and makes certain ions, such as Na^+, K^+, Ca^+ and Cl^-, to pass through. However, the ions generated in the non-thermal plasma cannot pass through

the membrane and, therefore, charge accumulation is still proceeding. Previous studies have demonstrated that modest frequency and amplitude of an electric field that applied on the bilayer membrane can cause the protein conformational transitions. When the intensity of electric field generated by the charged particles is high enough, it can change the three-dimensional structure of the proteins so much as to separate the proteins from cell membrane, creates larger pores in the cell membrane and also weakens it. Hence, the charged particles generated in the non-thermal plasma can peculate into the cell and disturb the activity of proteins and enzymes. Most likely, cytoplasm can leak out of the cell through these holes which is the reason behind cell death. [63]

2.12.4 Action of Electric Field

In most indirect treatment cases reported in the literature, the electric field at the location of the microbe samples was too weak to have an influence on the inactivation process. However, in some direct treatment cases, the microbe samples were immersed within the plasma generation region where the electric field intensity could be high enough to take effect. The maximum electric field in the non-thermal atmospheric pressure glow discharge is known to range from a few kV/cm when helium is used as the operating gas, through 20-30 kV/cm in the atmospheric pressure dielectric barrier glow discharges over 50 kV/cm in the dc atmospheric pressure glow discharge. Under such a high electric field strength the process could be ruined, even if they are in the aqueous environment. For most non-thermal atmospheric pressure plasma, the electric field is unlikely to have a significant contribution on the inactivation of a microorganism. This is probably due to the maximum electric field that usually exits a nearby surface of the electrodes and then reduces to a fraction of its maximum magnitude in a very short distance (less than 300 mm). In most cases of the non-thermal atmospheric pressure plasma, there is a rare possibility to position the microbes within 300 mm from the electrodes, hence, the electric field cannot play a major role in microbial inactivation. [63]

2.12.5 Researches Reviewed on Biological Decontamination by Plasma

The paper [63] has reviewed different researches on biological decontamination of plasma and has summarised some general rules from different views. In this paper, five agents generated by plasma which have effects on biological decontamination have been summarised and listed as follows: 1) UV radiation, 2) charged particles, 3) reactive species, 4) heat and 5) electric field. This paper has also summarised conditions affecting the result of biological decontamination, which are the treatment surface and the humidity. These two conditions can influence the five agents generated by plasma and, thus, affect the result of biological decontamination, however, humidity influence was not investigated in the research work in this thesis.

The paper [67] has investigated the possibilities of using impulsive and steady-state corona discharges (plasma) for biological decontamination. The research in this paper has used a tube-mesh topology test cell for investigation in which a high tension tubular corona electrode was used and stressed with both positive and negative DC voltage levels up to 26 kV. *E. coli* and *S. aureus* were selected to be the microorganism source in this research. Different operational regimes of corona generators were investigated for the production of ozone in air flow. The results of this paper have shown that corona discharge has a strong effect in biological decontamination with ~94% efficiency within a 30–60-s time interval for positive energised flashing corona discharges, and with over 97% efficiency within a 120-s energisation interval for negative steady-state corona discharges.

The paper [64] has investigated the effect of H_3O^+, OH^-, O_2^- , NO_x^- and NO_x for *E. coli* inactivation in atmospheric pressure DC corona discharges. The effects of ionic and neutral species, such as H_3O^+, OH^-, O_2^- , NO_x^- (x= 2,3) and NO_x, inactivation in both gas and liquid phases has been investigated. The tests were based on point-plane configuration and were

stressed with DC energisation. The species listed above, together with OH and O_3, were irradiated selectively onto *E. coli* suspensions on agar plates using a needle angle of 45°with respect to the plates, airflow and a grid plate. The results of this paper have shown that positive ion H_3O^+ was not effective in inactivation, while negative ions NO_x^- and neutral species NO_x in gas phase had strong inactivation effects when compared to the cases in liquid phase. The results also show that liquid HNO_3 which formed during the process had a weak inactivation effect on *E. coli.* This paper has also determined the threshold amount of gas phase NO_x^- and NO_x for *E. coli* inactivation.

Another paper [65] investigated the effect of ions produced in a DC corona on the inactivation on the surface of agarose gel, and both positive and negative corona discharges in different gases at different levels of humidity were investigated. The results show that pure N_2, pure O_2 and an N_2 H_2O mixture had no inactivation effect. When oxygen and water containing mixture was ionised, the best result of inactivation has been achieved. The results have shown that the main role of charged particles may be related to the faster transport of active peroxide species OH^- $(H_2O)_n$ and $H_3O^+(H_2O)_n$. The efficiency of these radicals was much higher than that of the oxygen radicals and ions (including O_2^-, O_4^+ and O_3) and also higher than that of the nitrogen and argon ions.

The paper [66] has presented the research of inactivation of microorganism by plasma of positive and negative corona discharge in air. Both gram-positive (*S. aureus*) and gram-negative (*P. aeruginosa*) bacteria were selected to be the microorganism source. According to the research in this paper, ultraviolet radiation (UV), neutral reactive species (R), and electric field & charged particles (E) were the three types of agents generated by plasma, and the influence of each agent on inactivation of the two types of bacteria has been investigated. The research in this paper has shown that the joint action of UV, R and E has an effect on inactivation. The research in this paper has also revealed that the contribution of the electrophysical effect to the total streamer inactivation was 12% by

processing data. The electrophysical effect of negative ions in negative energisation was inessential, however, it provided strong synergy with R agents. The *P. aeruginosa* with two membranes was more resistant against the electrophysical influence of negative ions compared with *S. aureus* with one membrane. The paper has also concluded that the R agents had the most inactivation efficiency among UV, R and E agents in corona discharge for both positive and negative polarities.

Researches of plasma on biological decontamination have been reviewed. In these papers the decontamination effect for different types of microorganisms has been investigated. For example, in paper [68], microorganisms, such as *Pseudomonas fluorescens* vegetative cells, *Bacillus subtilis* var. *niger* endospores and *Penicillium brevicompactum* fungal spores, can be decontaminated by plasma with an efficiency of over 70%. Paper [69] shows that airborne pathogen such as *Escherichia coli*, *Pseudomonas alcaligenes* and *Staphylococcus epidermidis* can also be inactivated by plasma with efficiency ranging from 20% to 70% with negative high voltage energisation.

In practice, the purpose of inactivation or removal of microorganisms when particle precipitation process is conducted at the same time is desired. Paper [54] presented a study of a system to improve the indoor air quality by particle collection, odour removal and sterilisation of *E.coli*. The system developed for the sterilisation of *E.coli* is based on the topology of two perforated metals used for the generation of plasma and the system is energised with AC high voltage. The experimental results for *E.coli* sterilisation, in this paper, showed that plasma is effective in biological decontamination. The experimental results also showed that an increased voltage level can result in increased biological decontamination efficiency. The biological decontamination efficiency in this paper can be over 90% for the best case. The system developed for particle precipitation and the system developed for *E.coli* sterilisation were two different systems. The particle precipitation

system was based on multiple needle-plate topology with DC energisation and the *E.coli* sterilisation system was based on double perforated metal topology with AC energisation.

The literature review of these approaches shows that biological decontamination by plasma is effective. However, the efficiency is low. Another problem is that particle precipitation and biological decontamination occurs in different systems, which potentially increases the difficulties of operation which, ultimately, can influence the use of plasma in the environment in which both particle precipitation and biological decontamination are required at the same time. These problems have provided another motivation of the research in this thesis to develop a biological decontamination system with high biological decontamination efficiency, as well as allowing the particle precipitation process to be conducted using the same system. Energy consumption is also another consideration of the biological decontamination system to make the system more environmental friendly.

2.13 Conclusions on Literature Review

In this chapter, particle emission status and the influence of particle emission on human's health have been discussed. Methods for particle emission control have been reviewed, in which electrostatic precipitation has been discussed including corona discharge generation, particle charging and particle collection. Parameters that can influence the performance of electrostatic precipitation and penetration mechanisms of electrostatic precipitators have been listed and discussed, as well as the different types of electrostatic precipitators have been reviewed. Background knowledge of plasma and particle charging, which play very important roles in electrostatic precipitation, have also been discussed.

The approaches of electrostatic precipitation, including practical and simulation research, have been reviewed. Problems of electrostatic precipitation after the literature review include the following: 1) low particle precipitation efficiency and high particle penetration rate, 2) high energy consumption and 3) parameter neglect in the simulation. These three

problems have provided the thesis with motivations to develop an electrostatic precipitation system with high particle precipitation efficiency and low energy consumption. From a simulation aspect, a model with the consideration of parameters which cannot be neglected (space charge and electric parameters of particle and medium) is to be developed to simulate particle dynamics and to calculate particle precipitation efficiency.

The effect of plasma on biological decontamination has been discussed and approaches of biological decontamination by plasma have been reviewed. It is found that the biological decontamination efficiency is low and the system for both particle precipitation and biological decontamination is complicated. This problem has provided another motivation of the research in this thesis to develop a biological decontamination system with high biological decontamination efficiency and low energy consumption, as well as allowing for the particle precipitation process to be conducted using the same system.

3 Development of the Needle-Mesh Electrode Topology Electrostatic Precipitation System

3.1 Introduction

To solve the problems which have been outlined in Chapter 2, and to improve performance of the electrostatic precipitators in environmental applications and potentially in the power industry, several potential solutions have been proposed in the present study. The feasibility study which is based on the proposed approaches has been conducted in the present chapter which includes comprehensive particle precipitation tests. The first approach is to design an electrostatic precipitation system with the high particle precipitation efficiency. The system should be either innovative in its topology to avoid the disadvantages of traditional systems, or the new system should be designed to improve the performance of traditional systems on particle precipitation.

This chapter presents an electrostatic precipitation system based on the needle-double-mesh topology. This specific topology includes a sharp HV tip and two grounded meshes and this metal needle is connected to the high voltage source and two meshes are grounded, therefore, the voltage drop occurs between the needle tip and the two meshes. The tip of the needle is sharp and can be used to ionise the gas that passes by and it is this ionised gas which is the source of ions and electrons being the key factor of particle charging. Then, charged airborne particles are collected on the plane. The tip-plane topology electrostatic precipitation system is not widely used in industry as this topology is difficult to be applied in practice due to the specific needle-plane configuration and the low gas flow rate. However, the objective of the research in this chapter aims to provide a possible solution to the industry, especially for small volume gas or indoor applications.

The concept on particle precipitation of the system in this research is similar to the traditional tip-plane topology system, however, possess some slight differences. Typically, the needle electrode consists of a sewing pin, gramophone needle or a solid pin with a sharp tip. The needle used in the electrostatic precipitator developed in the present work is a hypodermic needle. Due to the specific topology of hypodermic needles, the gas with particles can pass through the needle and then be charged at the needle tip, where the better performance of particle charging is expected. In order to solve the problems of gas flow arrangement in traditional tip-plane topology, metallic meshes are used as collection plate (ground) instead of a metallic plane. There are two metallic meshes used in the electrostatic precipitator with different mesh pore sizes. The first mesh with larger pore size is used for measurement of current, and the second mesh with smaller pore size is used for particle collection. The charged particles can be collected on the metallic mesh and the cleaned gas can pass through and finally pass out of the system. A glass fibre filter is also used to achieve better precipitation performance. The detailed design of the electrostatic precipitator and the electrostatic precipitation system will be demonstrated in this chapter.

The source of particles is very important in this research. The air in University of Strathclyde is relatively clean, and is confirmed by the particle mass measurements presented and discussed in Section 3.6.3.2 (untreated air sample collected from the street with traffic). However, there are areas within cities in the UK and abroad with higher concentrations of PM 2.5 in atmospheric air, for example, the typical PM 2.5 particle mass value commonly seen on weather reports in China is over 1000 $\mu g/m^3$ which indicates that the air is heavily polluted. Thus, it is necessary to investigate the system performance in the case of heavily contaminated air conditions which can be found in practical cases. To test the performance of the developed electrostatic precipitation system different levels of pollution, depending on the concentration of particles, were simulated in the laboratory. Various types of airborne particles (indoor particles, street airborne particles, bee wax candle particles and cigarette smoke particles) have been used in the precipitation tests. The particle number

and particle mass for cigarette smoke particles is close to those as reported in heavily polluted areas in real world. Results show that the designed electrostatic precipitation system is capable of removing almost all the particles (with ~100% efficiency) from atmosphere which are heavily polluted.

The system can be operated under both positive and negative DC energisation and comparisons in the precipitation efficiency have been made. Energy consumption is also considered in this research as the design of the system also aims to be environmental friendly. In this research, a method of calculating energy consumption, based on the current-time waveform, is introduced and energy consumptions for different situations are calculated.

3.2 Design of the Electrostatic Precipitator

The key component of the air plasma cleaning system is an electrostatic precipitator with the detailed design based on a needle-double-mesh topology will be introduced in this section. The detailed design of the electrostatic precipitator will be shown in Section 3.2.2.

3.2.1 Materials

The materials used to build the electrostatic precipitator are introduced in this section. The electrostatic precipitator consists of the needle, two metallic grounded meshes and electrostatic precipitator body. Each part of the electrostatic precipitator is discussed in detail in this section.

3.2.1.1 HV Needle Electrode

The HV electrode in this design is the hypodermic needle used to develop the high electric field and to generate non-thermal plasma (corona) discharges. Due to design of the hypodermic needle, in which air flow can pass through the needle, the mixture of gas (air)

flow and particles can be close to the ionisation zone of the needle tip, so that particles will be easily charged which makes their removal from air flow more effective.

Based on the initial proposal, hypodermic needles have been chosen for the electrostatic precipitator as HV electrodes. Hypodermic needles are made of stainless steel which has a high electric conductivity (1.45×10^{6} S/m) and, also, hypodermic needles have a sharp edge which could be used for the ionisation of air. An advantage that hypodermic needles provides when used as HV electrodes is that the mixture of gas flow and particles could pass through the needle itself i.e. all the particles could be charged at the tip of the needle. The precipitation system designed in this study is sealed to make the mixture of gas and particles go through the needle without leaking elsewhere. Therefore, in this case, the area of the charging is decreased which is equal to the cross section of the needle. The use of the hypodermic needle allowed an increase in precipitation efficiency to be achieved by concentrating the effective charging area manually.

The hypodermic needle used in the developed topology is a gauge 14 hypodermic needle. The needle parameters are as follows: nominal outer diameter is 2.108 ± 0.025 mm, nominal inner diameter is 1.600 ± 0.076 mm and nominal wall thickness is 0.254 ± 0.025mm. Gauge 14 hypodermic needles have a relatively larger cross section which could allow the mixture of gas and particles to pass through without blocking. In routine precipitation tests, the needle worked very well.

Another advantage of the hypodermic needles is that they are readily available and easy to machine. The designed needle holder is shown in Figure 3-1.

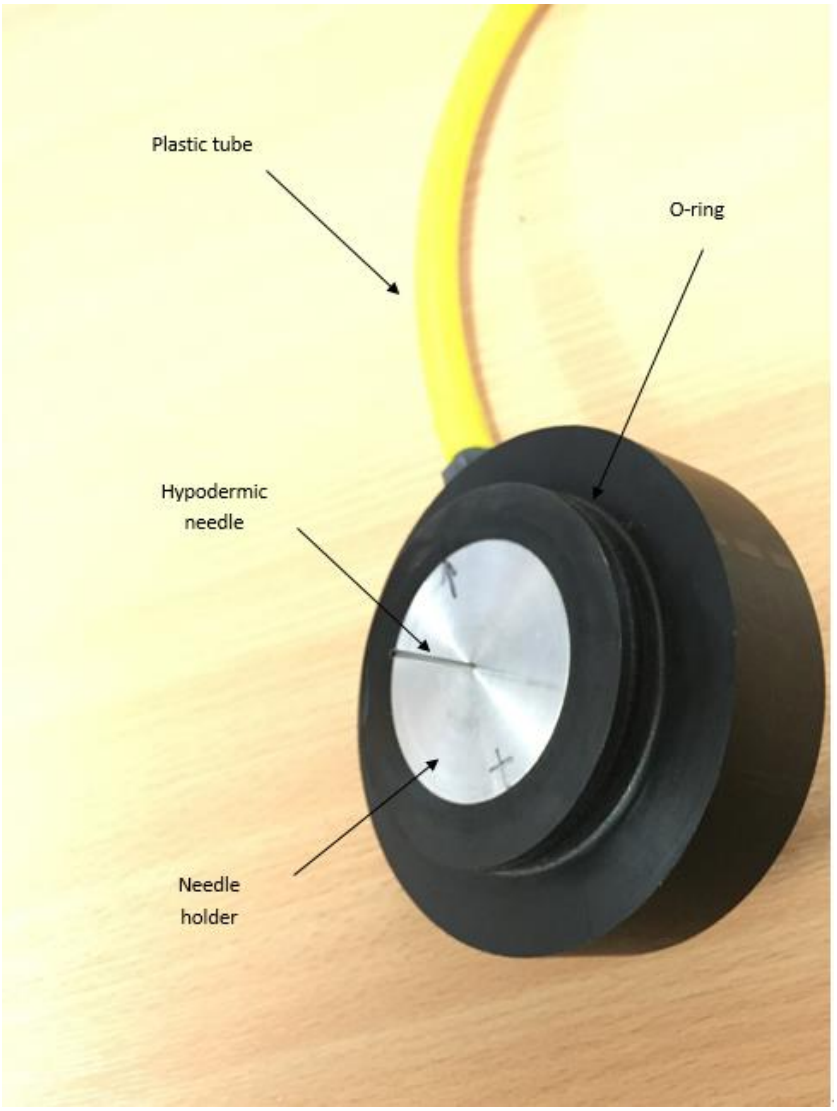

Figure 3-1. Hypodermic needle (HV electrode) and needle holder

3.2.1.2 Metallic Grounded Electrodes

Two metallic meshes made of stainless steel (conductivity of stainless steel: 1.45×10^6 S/m) were used in the electrostatic precipitator. The first mesh and the second mesh were both grounded, so there will be an electric field forming between the mesh and the needle which is stressed with higher voltages. Since there are open apertures in the mesh, gas flow freely passes through the open sections. The open section size of the first mesh is larger than the second mesh and also larger than the particles. The aperture of the first mesh is 0.31 mm

and the metallic wire diameter of the first mesh is 0.2 mm. The aperture of the second mesh is 0.099 mm and the metallic wire diameter of the second mesh is 0.028 mm. Therefore, most charged particles can pass through the first mesh, and remaining charge generated by plasma which is not on particles could be removed by the first mesh. The second mesh was also grounded, so all charged airborne particles which have passed through the first mesh will be attracted to the second mesh. There was a glass fibre filter close to the second metallic mesh and the pore size is relatively small. Therefore, all the charged particles attracted by the second mesh could be collected by the glass fibre filter.

There is another reason for the selection of the two meshes topology for this study. In the process of particle charging and removal inside the electrostatic precipitator, the total charge delivered into the precipitator could be calculated using the first mesh by integration of current on the first mesh over precipitation time. The charge on particles, which is important for calculation of precipitation efficiency, could be calculated by integration of current through the second mesh over precipitation time. The calculation of total electric charge will be discussed in detail in Section 3.8. Metallic meshes used in the precipitation topology are shown in Figure 3-2.

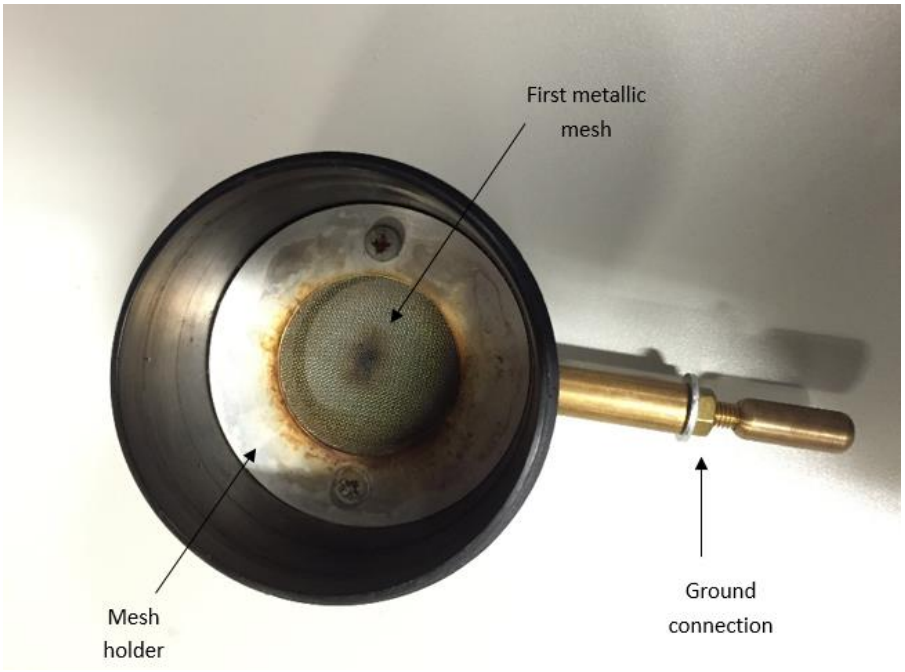

(a)

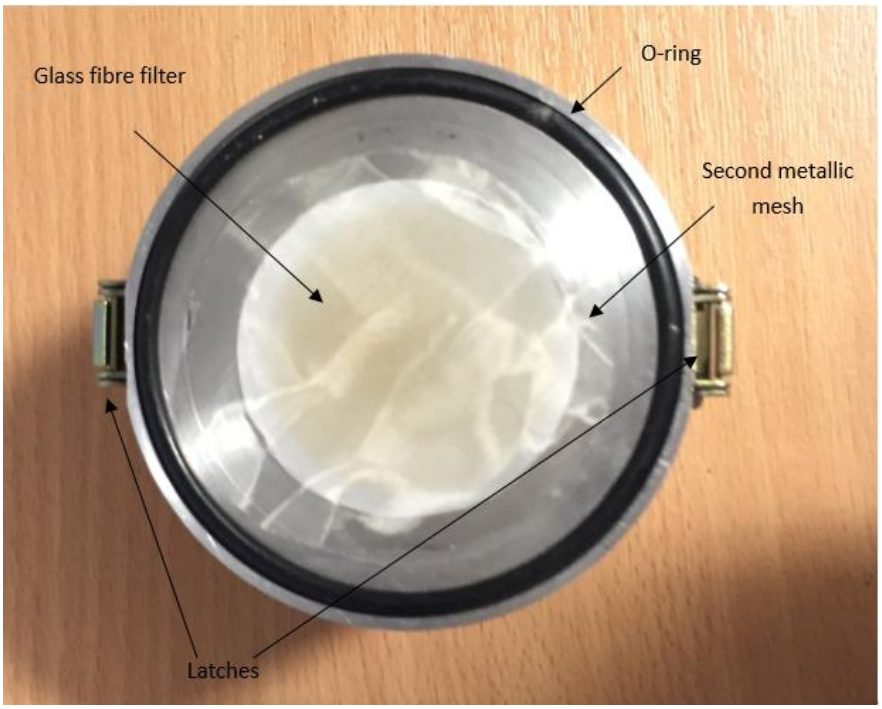

(b)

Figure 3-2. Metallic mesh (a) first mesh (b) second mesh

3.2.1.3 Electrostatic Precipitator Body

The body of the needle-mesh electrostatic precipitator consists of two parts. The first, which holds the hypodermic needle, is made of PVC (relative permittivity of PVC: 3.9). The reason for choosing PVC is due to electrical safety and for insulation, as a dielectric material is needed for the HV electrode holder. Since the first part of the electrostatic precipitator body holds both the needle and the first mesh, it requires a material which could be easily machined to accommodate both these. As it has been discussed, the electrostatic precipitator should be completely sealed to guarantee the mixture of gas and particles go through the hypodermic needle to increase precipitation efficiency. Therefore, two rubber O-rings have been used to prevent gas leakage from the electrostatic precipitator.

The second part of the electrostatic precipitator is made of aluminium (conductivity of aluminium: 36.9×10^6 S/m). The reason for two separate body parts is that the glass fibre filter should be replaced if there are too many particles on the filter causing the saturation of particle collecting of the filter. During tests, the fibre filters were replaced every 10 runs of the precipitation tests with particles with the highest concentration (cigarette smoke particles). The glass fibre filter used in this research is ADVANTEC GA-55 with a diameter of 47 mm, pore size of 0.6 µm and a thickness of 0.22 mm.

The second part of the electrostatic precipitator also holds the second mesh and the glass fibre filter which are used for removal and collection of all charged particles. If there are particles that penetrate the second mesh and the glass fibre filter, the body itself should remove the penetrated particles. Therefore, the second part of the electrostatic precipitator should be conductive. It should also be conductive in order to easily measure current. Aluminium is also readily available and easily accessible, the mesh and the glass fibre filter are needed, and the thickness of the second metallic mesh and the glass fibre filter are very thin.

During the test procedure, the glass fibre filter is replaced after 10 to 15 tests due to the short time required for each precipitation tests time and small electrostatic precipitation system scale. If the system is scaled up to a larger system with larger amounts of particles, the glass fibre filter should be replaced more often than the small-scale system in the laboratory. Another reason for the separate body parts is that the metallic meshes might need to be polished to prevent oxidation on the surface. In the precipitation tests, it was found that metallic meshes are more easily oxidised than when in an ambient environment due to the ionisation in the electrostatic precipitator. Therefore, the two separate parts of electrostatic precipitator body was designed to allow ease of access to appropriate parts.

In order to prevent gas leakage from the electrostatic precipitator and to create a completely sealed environment, one rubber O-ring was used between the two parts of the electrostatic precipitator body. The use of the rubber O-ring is also important as it pushes the second metallic mesh to the slot of the mesh to make very good contact, which is ideal for particle removal and current measurement.

Two metallic latches with springs were used to lock the two parts of the electrostatic precipitator body.

The electrostatic precipitator body is shown in Figure 3-3.

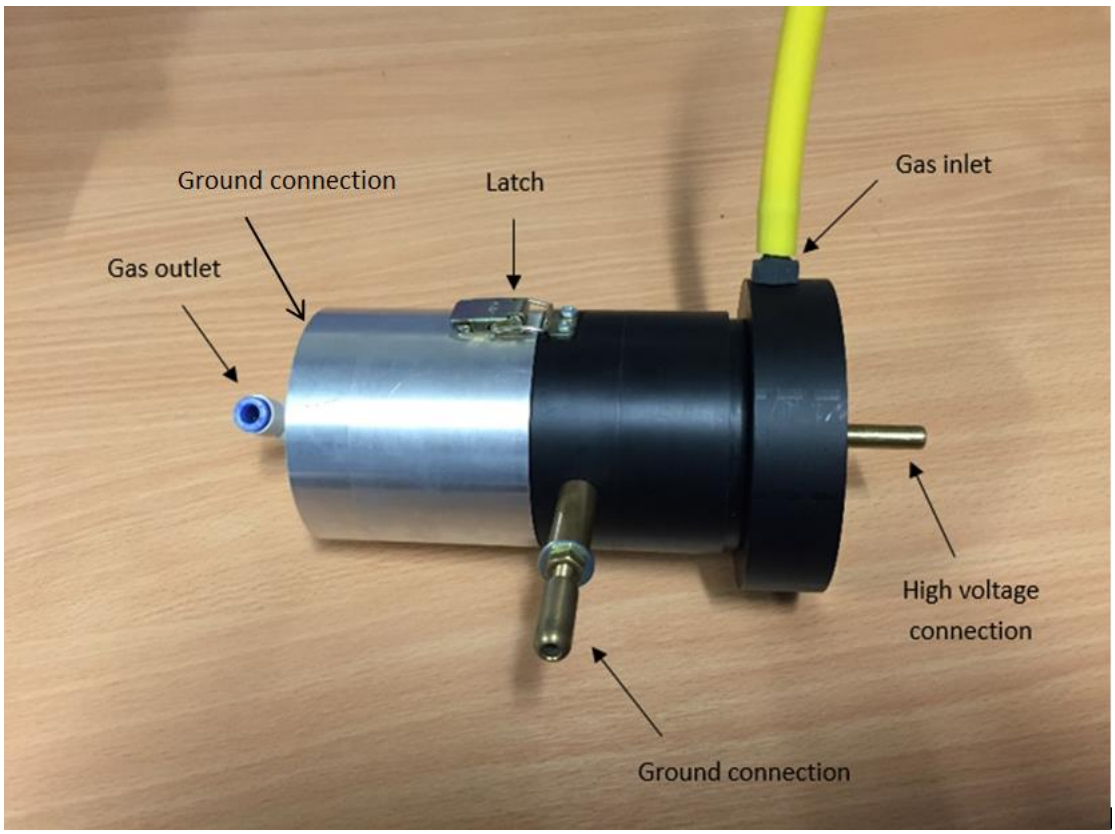

Figure 3-3. The electrostatic precipitator body

3.2.2 Electrostatic Precipitator Design Details

Figure 3-4 shows the cross section of the electrostatic precipitator developed during this study.

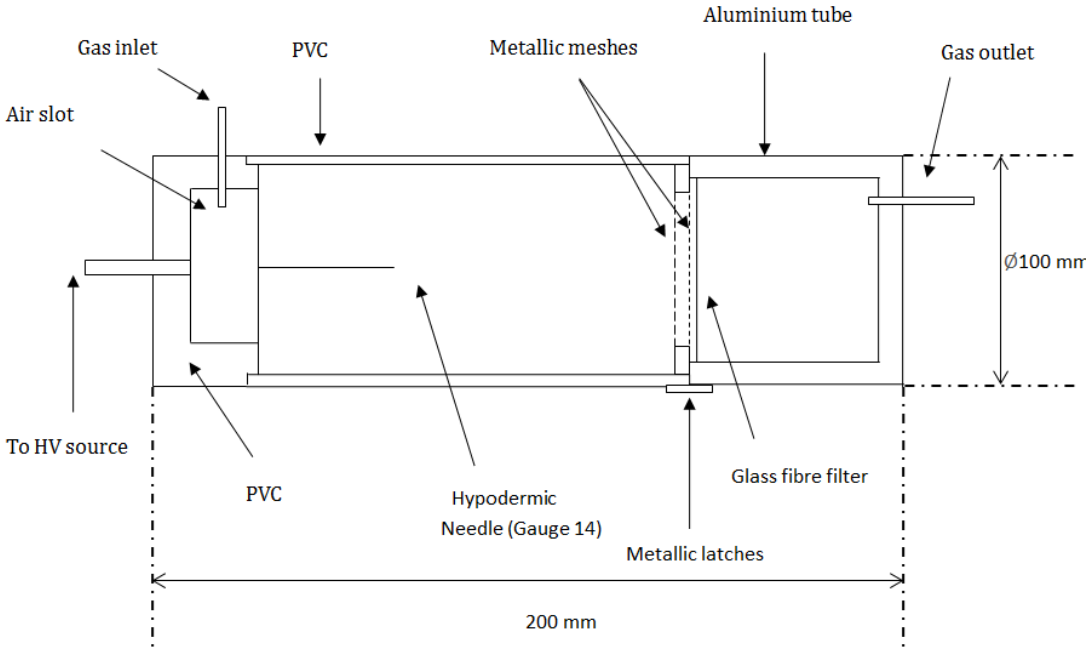

Figure 3-4. Detailed design of the electrostatic precipitator. Length of the precipitator: 200 mm. Diameter of the precipitator tube: 100 mm.

To determine the working range of the electrostatic precipitator, breakdown tests have been conducted using an ambient air flow with relative humidity of 31% and room temperature of 20 °C. The result is shown in Table 3-1 with at least five runs of the system.

Table 3-1: Working range of the electrostatic precipitator

	Corona ignition voltage (kV)	Breakdown voltage (kV)
Positive energisation	7 ± 0.3	16 ± 0.8
Negative energisation	-10 ± 0.2	-17 ± 0.5

As shown in Table 3-1, the working range of the electrostatic precipitator is +7 kV to +16 kV for positive energisation, and -10 kV to -17 kV for negative energisation.

3.3 Design of the Electrostatic Precipitation System

Figure 3-5 shows the block diagram of the designed electrostatic precipitation system.

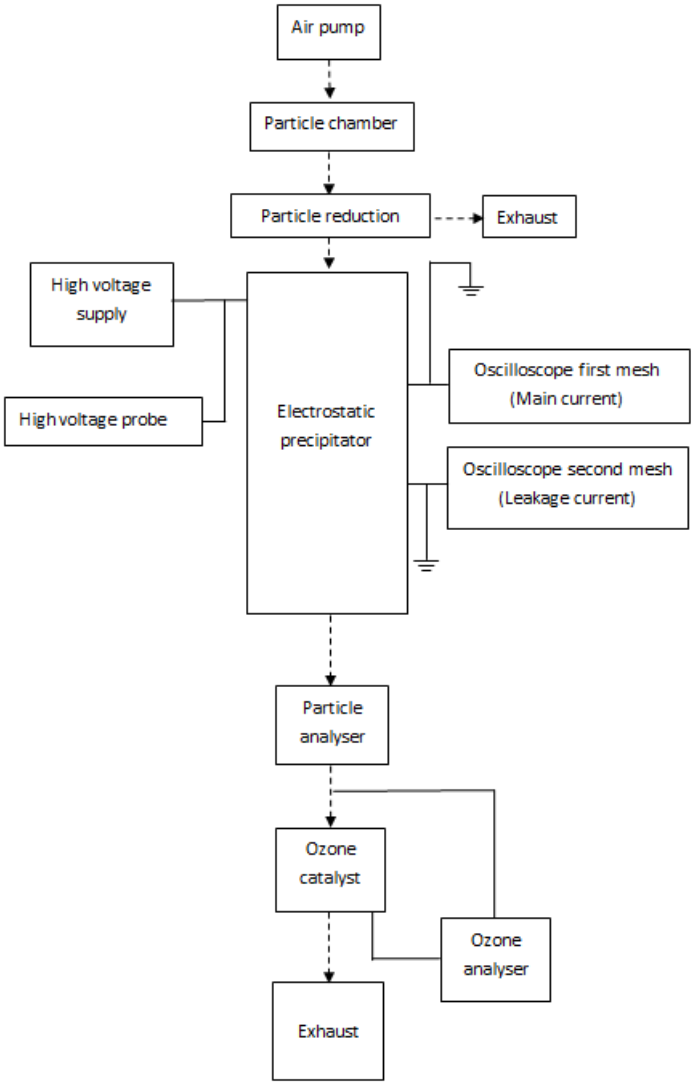

Figure 3-5. Electrostatic precipitation system design.

All components used in the system will be introduced below.

Air pump:

The air pump used in the electrostatic precipitation system was designed for aquarium tanks (AQUA AP1), and the pump produces air flow with a flow rate of 3 litres/minute. The air pump was connected to the precipitation system by a 6 mm plastic tube.

Particle chamber:

The particle chamber (Figure 3-6) was used to mix gas (air) and particles under the test. The particle chamber was made of transparent PVC to allow for visual observations. There was a gas inlet located on the bottom of the particle chamber and there were four gas outlets located on the top of the particle chamber. These four gas outlets were also used for reduction of particle concentration in airflow to prevent saturation of the particle analyser. The reduction ratios could be 1/4, 1/2, and 3/4.

There was a shelf located on the bottom of the particle chamber for burning materials to generate particles. In the research, bee wax candles and cigarettes were burnt to generate particles for precipitation tests. It was found in the tests that bee wax candles and cigarettes could be burnt during the whole process of the precipitation tests without a need to be extinguished, which proves the particle chamber provides a steady source for generating particles. It is assumed that the particles are split into the gas outlets evenly.

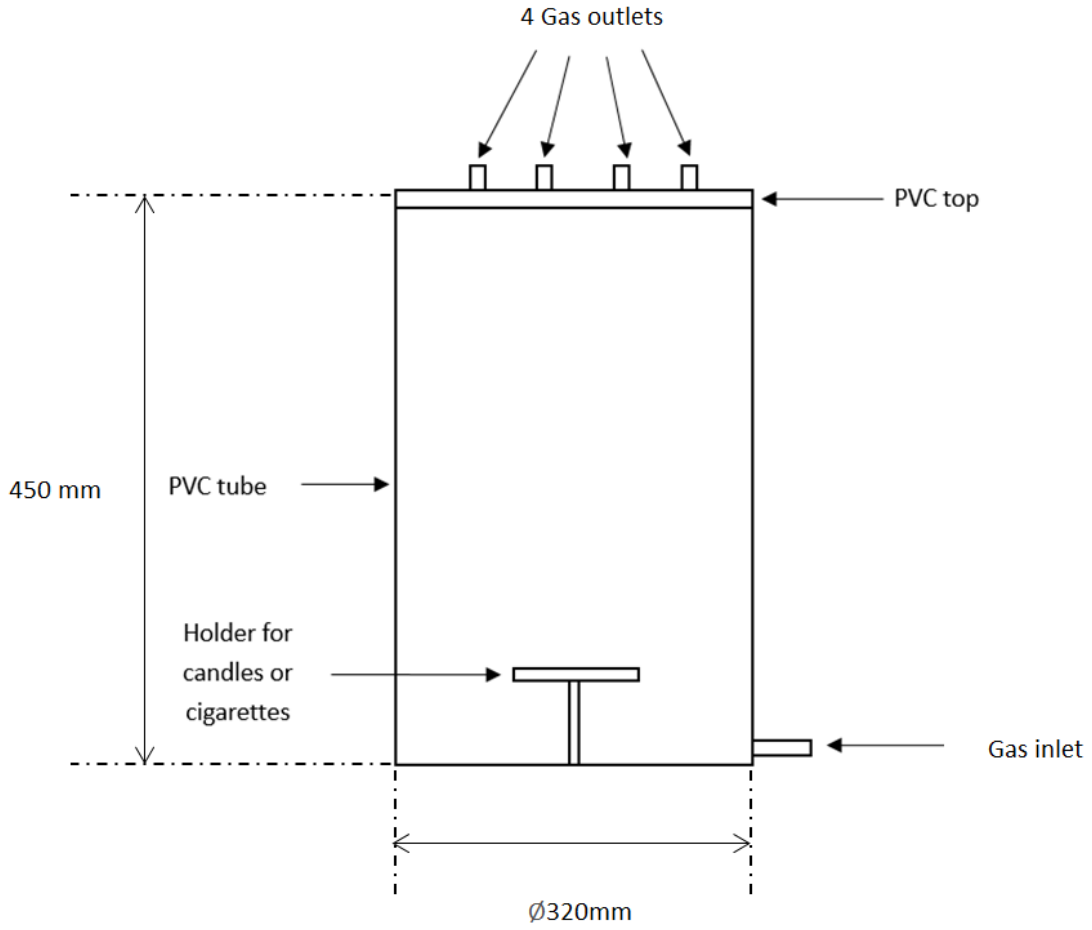

Figure 3-6. Particle chamber

Particle analyser:

A laser-based particle analyser (GRIMM Portable Aerosol Spectrometer Model 1.109), was used in the research. This analyser uses a pump to help absorb gas into the analyser with a flow rate of 2 litres/minute. The inlet of the particle analyser is a 4 mm air hose, so an adaptor (6 mm to 4 mm) was used at the outlet of the electrostatic precipitator.

This particle analyser is capable of analysing particles both from particle number and mass aspect. From the particle number aspect, the data was recorded for 31 channels in particle diameters, from 0.265 µm to 34 µm. The results were shown in counts/litre. From the

particle mass aspect, the data was recorded for PM10, PM2.5 and PM1 physically, and also recorded for inhalable, thoracic and alveolic medically. The results were shown in $\mu g/m^3$.

Ozone catalyst:

After the particle analyser, an ozone catalyst tube was connected. The reason for the ozone catalyst is that ozone might be generated when positive and negative high voltage energisations were applied in the research, and there was more ozone generated for negative energisation than positive energisation. Therefore, it is important to ensure that no ozone will be delivered into the atmosphere. The use of an ozone catalyst is to solve this problem. After the treatment of ozone catalyst, there is no ozone tested. The ozone catalyst used in the electrostatic precipitation system was MnO_2.

Ozone analyser:

An ozone analyser was connected to the electrostatic precipitation system to monitor ozone concentration during precipitation tests. The ozone analyser used in the system was BMT 964. The analyser could be connected before and after the ozone catalyst, so a comparison could be made to show the effectiveness of the ozone catalyst.

Exhaust:

The mixture of gas and particles was guided into the exhaust after the ozone catalyst. In addition, the outlet of reduction of the particles from the mixture of gas and particles were guided into the exhaust. The exhaust tube was operated using an electric fan.

High voltage DC supply:

The high voltage DC supply used in this electrostatic precipitation system was a Glassman High Voltage, INC. The high voltage supply has different modules, therefore, in the experimental tests the polarities of high voltage could be switched and different levels of

high voltage could be applied. This high voltage supply is tuneable both for current and voltage. The supply was connected to a resistor and then connected to the system to prevent too much current being applied to the system directly.

High voltage probe:

In order to show high voltage level, a high voltage probe was used. The probe used in the electrostatic precipitation system was a TES TEC HVP 40. The working limit of the high voltage probe was 40 kV for DC energisation.

Digitising Oscilloscope:

A digitising oscilloscope (Tektronix TDS 2024 digital oscilloscopes, 200 MHz bandwidth, 2 Gs/s) was used in the electrostatic precipitation system to measure current during the precipitation tests. The current can be obtained by measuring the voltage from the oscilloscope over a 1000 Ω current viewing resistor which was connected to the electrostatic precipitator. The current obtained was used for the calculation of the total delivered charge. During precipitation tests, the current through the first mesh was measured. Since most of the charge was removed by the first mesh this current was found to be relatively higher, therefore, the measurement of the charge for the first mesh was simply through the connection of BNC single shielded cable. For the second mesh, since the charge on particles was much lower than total charge in the precipitation system, the result could be easily influenced by the ambient conditions, even by moving human body parts during voltage tuning, and recording data which can affect the results. So, a double shielded cable should be used in the system to minimise the influence of an ambient environment. The current recorded on the first mesh was the main current, and the current recorded on the second mesh as leakage current.

Current viewing resistor

As mentioned, a current viewing resistor was used to measure current-time waveform. The waveform was used to measure energy consumption. The resistance of the current viewing resistor was 1000 Ω.

The overall experimental system is shown in Figure 3-7.

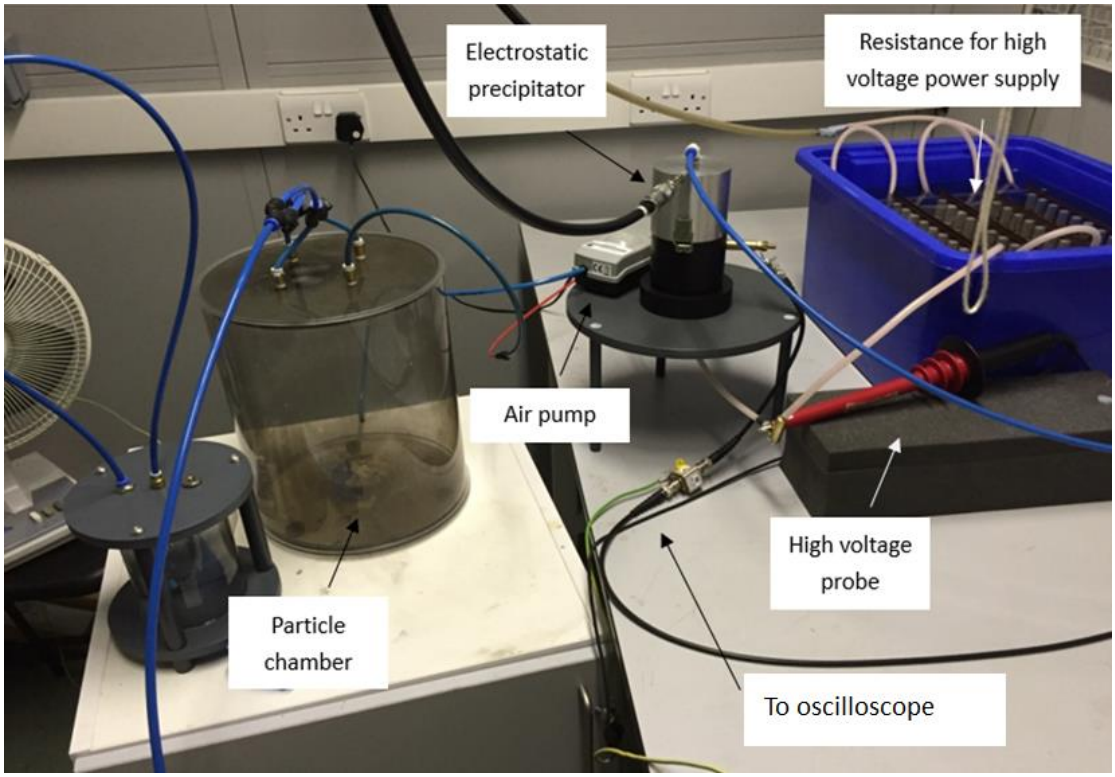

Figure 3-7. Actual electrostatic precipitation system.

3.4 Airborne Particle Types for Experiments

Four different types of airborne particles have been used in the precipitation tests. These particles are those which are present in ambient air in the laboratory, airborne particles produced by burning wax candles, cigarette smoke particles and airborne particle present in outdoor air samples collected on a Glasgow street with heavy traffic. The characteristics of these particles will be discussed in this section.

3.4.1 Indoor Particles

Indoor particles are the particles suspended in ambient air in the laboratory, and they can be easily collected and pumped into the electrostatic precipitation system. Since the laboratory air is quite clean, it was found that the untreated initial particle number of indoor particles is between 8000 and 9000 counts/litre for the smallest particle diameter channel (0.265 μm). The largest particles for ambient air in the laboratory are in the 0.750 μm channel with a concentration of ~100 counts/litre. From a particle mass aspect, the untreated initial particle mass of indoor particles for PM10, PM2.5 and PM1 are similar to the value of ~1 $\mu g/m^3$. To pump indoor particles into the electrostatic precipitation system, the pump is connected directly on to the gas inlet of the electrostatic precipitator.

3.4.2 Street Airborne Particles

To test the efficiency of the precipitation system in the case of particles present in outdoor city air, it was decided to collect samples of air from a Glasgow street with busy traffic. The street air samples will be collected in rubber balloons which will be brought into the laboratory and the street airborne particles were injected into the electrostatic precipitation system. The experimental procedure, including the air sample collection method, is discussed in this section.

3.4.2.1 Street Airborne Particles Collection System

Figure 3-8 shows the design of a balloon gas collection system. The street airborne particles are collected on the street so it is impossible to use electrical devices, hence, why a manual bicycle inflator will be used. The balloon is connected on a holder, as shown, and the balloon is fixed using a rubber band. The balloon holder is connected to a valve and, as long as the balloon is inflated, the street air is pumped into the balloon and the valve is closed.

Therefore, the inflated balloon, the balloon holder and the valve can be connected directly to the balloon gas releasing system for precipitation tests.

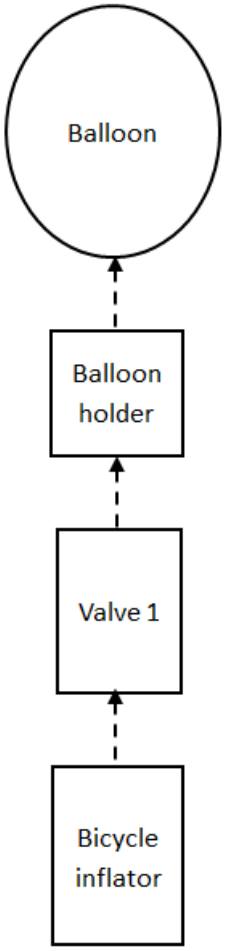

Figure 3-8. Design of balloon gas collection system.

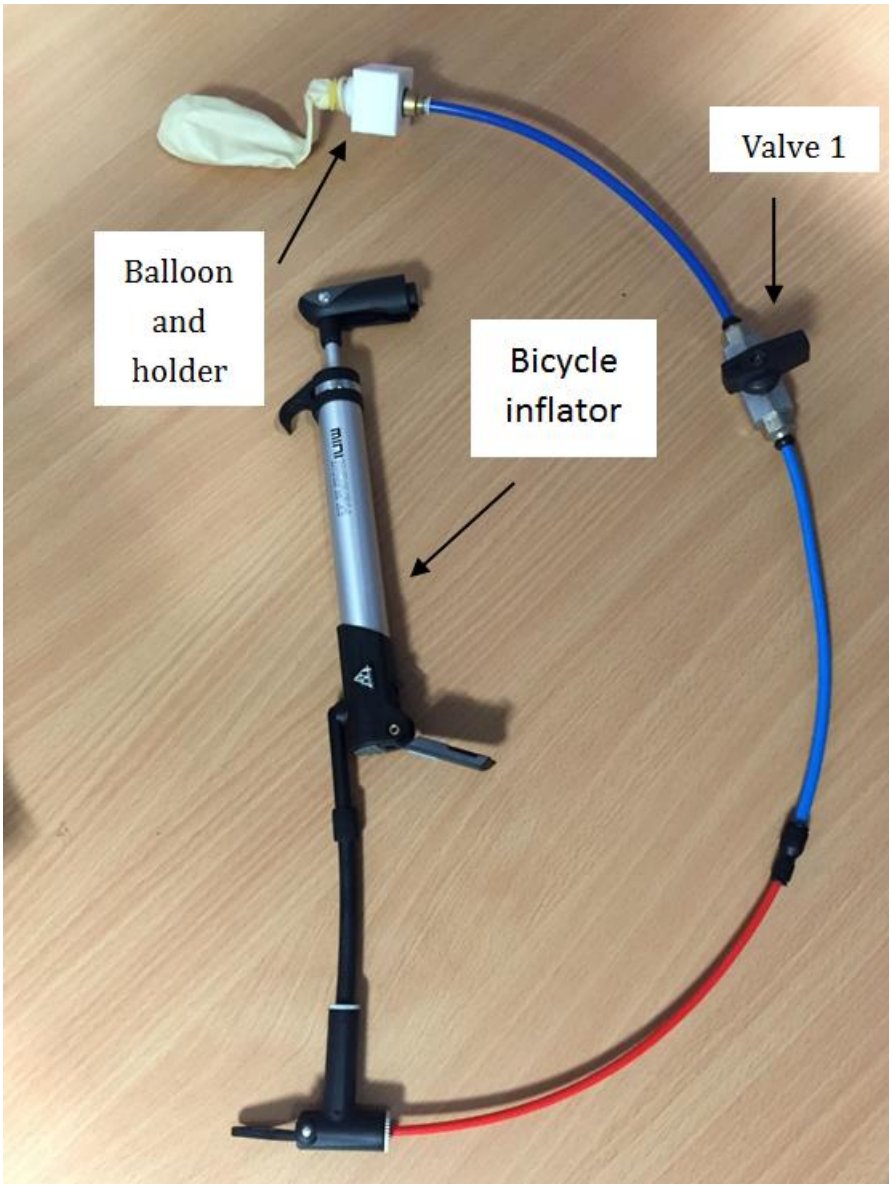

Figure 3-9. Street particle collection system

3.4.2.2 Injection of Street Airborne Particles into the Electrostatic Precipitation System

Figure 3-10 shows the design of the balloon gas injection system. In the system, three valves are used. Valve 1 is connected to the balloon and used for collecting gas on the street. Valve 2 is connected to the exhaust and is used for releasing balloon gas into the exhaust when the gas is not completely used. Valve 2 is also closed during the process of precipitation tests.

Valve 3 is used to open the flow so that gas from the balloon can enter the electrostatic precipitation system. There is a flow rate meter to monitor the gas flow rate from the balloon into the electrostatic precipitation system. A tuneable flow regulator is connected to the flow rate meter to regulate the flow rate to a certain value. In the research the flow rate is regulated to 3 litres/minute to guarantee sufficient experiment time, and the 3 litres/minute flow rate is also, correspondingly, the flow rate of the air pump. Figure 3-11 shows the physical layout of components.

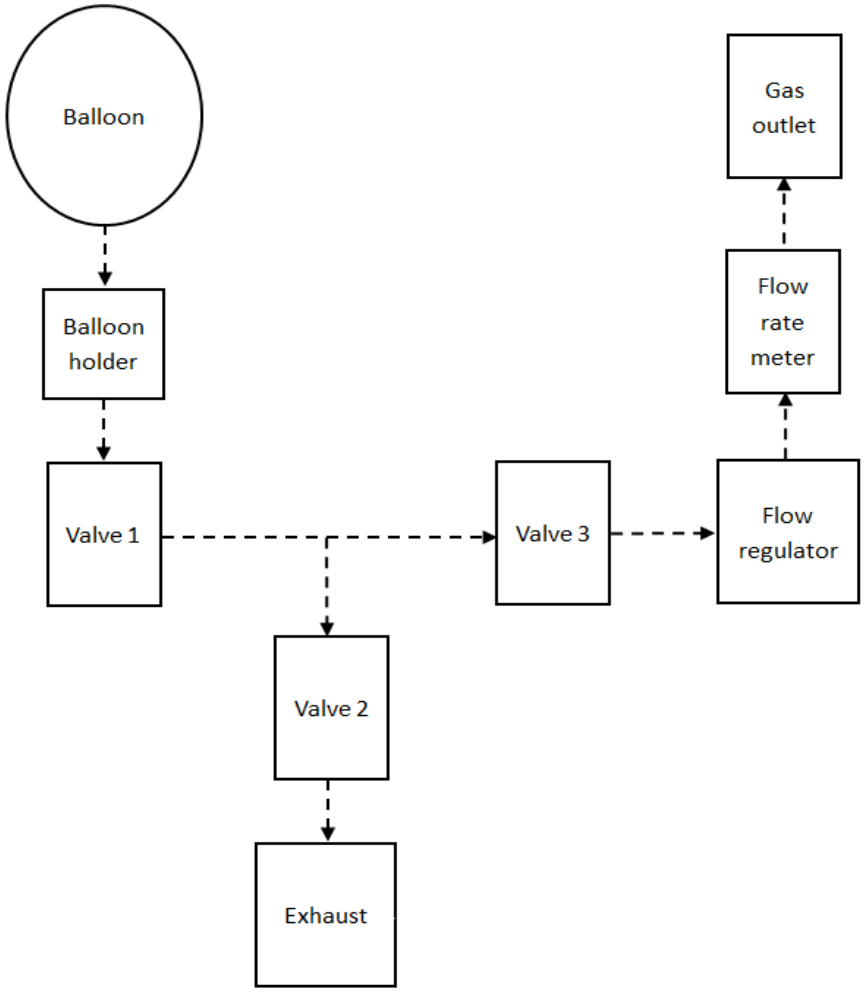

Figure 3-10. Design of balloon gas injection system.

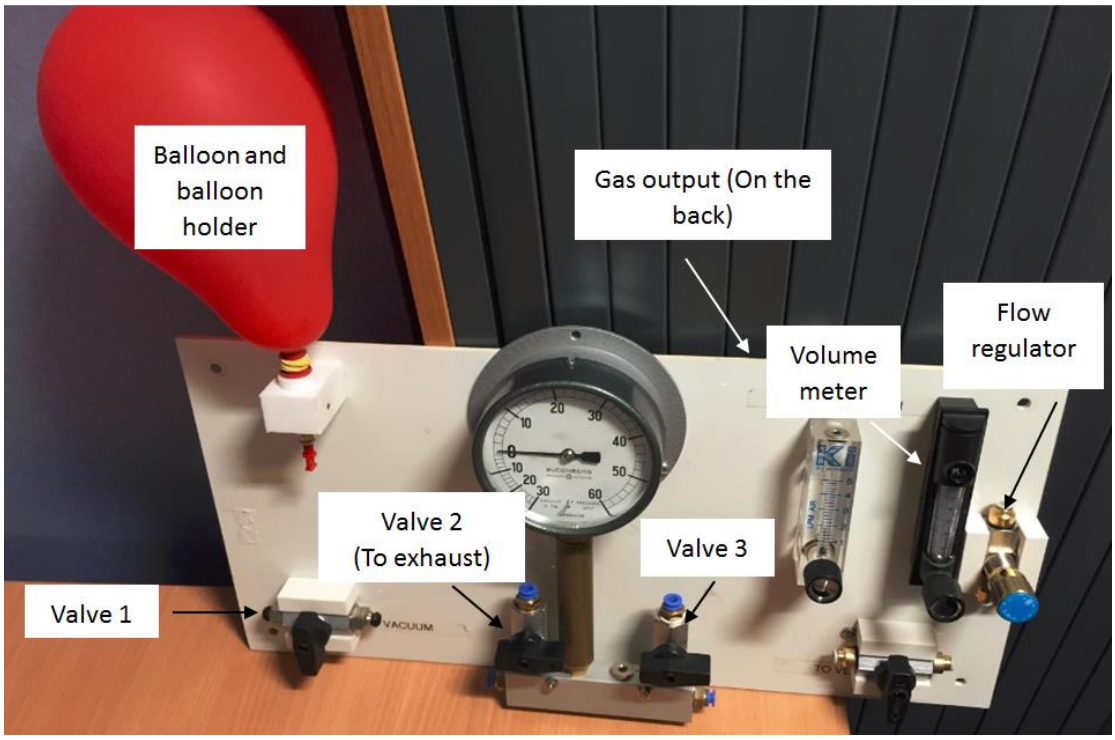

Figure 3-11. Actual balloon gas injection system used in the tests

3.4.2.3 Discussion

The air from West George Street in Glasgow city centre was collected. The collection time was between 8:00 am to 9:00 am when there is heavy traffic on the street. The collection point is at the cross of West George Street and Montrose Street. The time and location selection for gas collection is to ensure the motor vehicle exhaust level is high.

During the precipitation tests with street airborne particles collected outdoors, it was found that in the untreated air samples the particle number is ~25000 counts/litre in the smallest particle diameter channel (0.265 µm). The largest particles are in the 2.750 µm channel, and their concentration is found to be in the range from 0 to 100 counts/litre. From the particle mass aspect, the particle mass of PM10, PM2.5 and PM1 categories of particles in untreated air are similar and found to be up to 5 $\mu g/m^3$

The analysis of airborne particles in untreated air collected in Glasgow city centre demonstrates a low concentration of PM, even during the busiest time on the street with heavy traffic. The particle number and particle mass are lower than in other cities where the environmental air pollution is heavy, for example a typical PM 2.5 particle mass value commonly seen in weather reports in China is over 1000 $\mu g/m^3$

The use of the balloon proves to be an effective and useful method to collect and sample gas on the street. However, there are two main disadvantages of using a balloon.

First, balloons are restricted to the small volume themselves. The balloon used in the research could only contain 20 to 30 litres of gas. Although several balloons could be used separately to increase the total gas volume, it requires the experiment to stop while changing balloons. It not only makes the experiment more complicated but also stops the gas flow of the electrostatic precipitation system and influences the precipitation result.

Second, gas flow rate from the balloon is not stable. As the balloon deflates, its elasticity becomes lower. Since the gas flow rate is depending on the elasticity of the balloon, the gas flow rate is not stable, especially for the final 1 to 2 minutes. Therefore, it requires the experiment to be conducted within a shorter time than expected. During routine electrostatic precipitation tests with balloons, there is about 6 to 7 minutes to complete the test before the flow rate becomes unstable. The test time is sufficient for the electrostatic precipitation system designed in this research. For future work, with larger electrostatic precipitation systems, a new gas collection system needs to be designed.

Finally, during particle sample collection and particle injection, particles can attach on the inner surface of the balloon and on the air hose, it is assumed that the influence of this situation can be neglected.

3.4.3 Candle Particles

The particles generated by burning bee wax candle were used in the particle precipitation tests for the electrostatic precipitation system as developed in this chapter. Air flow laid with particles produced by burning bee wax candle was pumped into the electrostatic precipitation system to investigate the precipitation efficiency.

The main component of this type of candles is bee wax. Bee wax is a natural wax produced by honey bees of the genus Apis. Chemically, beeswax consists mainly of esters of fatty acids and various long-chain alcohols.

Bee wax candles are shown in Figure 3-12.

Figure 3-12. Bee wax candles. (length of candle: 10 cm)

When precipitation tests start, one bee wax candle is ignited inside the particle chamber. The air pump pushes air inside the particle chamber to provide air to maintain combustion. The ambient air and particles generated by the candle is mixed inside the chamber and the mixture is pumped into the electrostatic precipitator.

The initial particle number in untreated air laid with bee wax candle particles is ~20000 counts/litre for the smallest particle diameter channel (0.265 μm). The largest particles for bee wax candle are in the 0.750 μm channel, which are ~100 counts/litre. From a particle mass aspect, the initial particle mass in untreated air laid with particles generated by burning wax candles for PM10, PM2.5 and PM1 ranges is also similar with the values between 3 to 4 $\mu g/m^3$.

3.4.4 Cigarette Smoke Particles

As discussed, indoor particles, street particles and bee wax candle particles are low in both particle number and particle mass compared with practical environmental cases where heavy pollution is present. Therefore, it is important to simulate an environment with heavy particle pollution to test the effectiveness of the electrostatic precipitation system. For these tests, cigarette smoke particles have been selected.

The cigarette smoke which is used for electrostatic precipitation tests was generated using "YuXi" brand cigarettes which are manufactured in China. Before the precipitation tests, the cigarettes were ignited inside the sealed smoke chamber. The air pump pushed air inside the particle chamber to provide air to maintain combustion. The ambient laboratory air and particles generated by the cigarette are mixed inside the sealed particle chamber and then the air laid with cigarette smoke particles was pumped into the electrostatic precipitator. During the precipitation tests, the cigarette was slowly burning and was generating stable amount of smoke detected by the particle analyser.

A cigarette can generate significant amounts of particles in the closed sealed particle chamber. According to the initial measurements of untreated air samples laid with cigarette smoke particles, particle numbers in the smallest particle diameter channel (0.265 μm) could be as high as 8×10^5 to 9×10^5 counts/litre, and in the 2.750 μm channel, could be between 0

to 200 counts/litre. From the particle mass aspect, the untreated air laid with cigarette smoke for PM10, PM2.5 and PM1 ranges are similar with the value of 500 μg/m^3.

3.4.5 Summary of Different Types of Particles

The particle number and the particle mass for different types of particles are shown in Table 3-2.

Table 3-2 Summary of different types of particles.

	Particle Number (Counts/liter) (0.265 μm Channel)	Particle Number (Counts/liter) (Largest Channel)	Particle Mass for PM 10, PM 2.5 and PM 1 (μg/m^3)
Indoor Particles	8000-9000	100 (0.750 μm)	1
Street Airborne Particles	25000	0-100 (2.750 μm)	5
Candle Particles	20000	100 (0.750 μm)	3-4
Cigarette Smoke Particles	8× 10^5-9× 10^5	0-200	500

3.5 Experimental Procedures

This section will describe the methodology of the particle electrostatic precipitation test. Four types of particles (particles present in ambient laboratory air, street airborne particles,

candle particles and cigarette smoke particles), previously discussed, were used in the precipitation tests and two types of high voltage energisations (positive DC and negative DC) were used in the precipitation tests.

3.5.1 Test Arrangements

3.5.1.1 Assembly of the test system

Prior to the precipitation test the experimental system has been assembled and all necessary experimental system components have been located on the laboratory test bed and connected to each other. First a single clean glass fibre filter was inserted into the electrostatic precipitator. The DC high voltage power supply was equipped with positive or negative HV modules, thus, positive or negative energisation can be used in the precipitation tests. The output from the HV DC supply was connected to a protection resistor then the HV DC supply was connected to the HV needle electrode of the electrostatic precipitator. The electrostatic precipitator was virtually grounded through the oscilloscope connected to the first and second metallic meshes. The high voltage probe was then attached to the high voltage connection on the electrostatic precipitator body to monitor the applied voltage level. The oscilloscope was connected for monitoring the main current and the leakage current in the system.

From the gas flow aspect, the air pump was connected to the particle chamber. Subsequently, the particle chamber was connected to the electrostatic precipitator and, finally, the gas flow was injected into the particle analyser. For indoor particles, street particles and bee wax candle particles, since the particle concentration was not high, particle reduction was not used. For cigarette smoke particles, particle reduction was used to prevent the particle analyser from saturation. The reduction rate used was 75% (25% of the gas was guided into the system) which reduced a mixture of gas and particles and was guided into the exhaust with the fan switched on continuously.

3.5.1.2 Particle Preparation

In the case of indoor particle precipitation, the particle source can be all activities in the laboratory and the mechanical workshop located close to the laboratory, therefore, these airborne particles were pumped into the electrostatic precipitation system directly.

In the case of street airborne particles, the particles on the street were collected. The inflated balloon and valve 1 were connected to the balloon gas releasing system. Valve 1 was then closed before the precipitation tests.

To produce air laid with particles emitted by burning bee wax candle, a single candle was located at the centre of the particle chamber and ignited. Then, the particle chamber was closed, the air pump was switched on and air with airborne particles started to be delivered into the particle analyser. When both the number of particles in the air flow and the particle mass number reached their maximum value observed on the particle analyser, and also became stable, the precipitation tests can commence, i.e. the HV needle of the precipitator can be energised.

To generate the air flow laid with the cigarette smoke particles, similar to the case of burning candles, a single cigarette was placed at the bottom of the particle chamber and ignited. After, the particle chamber was sealed and the air pump was switched on. When both the number of particles in the air flow and the particle mass number reached their maximum value observed on the particle analyser, and also became stable, the precipitation tests can commence.

3.5.2 Precipitation Tests

During the precipitation tests, the following procedure was followed:

In the case of tests with indoor airborne, bee wax candle and cigarette smoke particles, first the air pump was switched on and then particles were introduced into the air flow.

In the case of street particles, valve 1 and valve 3 were opened and the flow regulator was tuned when the flow rate was 3 litres/minute. It was established from the tests that it takes approximately 30 seconds for the particle number and particle mass in the air flow from the balloon to be stable and maintain at the maximum value observed from the particle analyser. After that, the precipitation tests can commence.

When the particle number and particle mass values were stable at their maximum values, the high voltage electrode of the precipitator was energised with either a positive or negative high voltage DC power supply. The applied voltage level was monitored using the high voltage probe connected to the digital multimeter, and the current (the main current and leakage current) was measured using the oscilloscope.

For positive energisation, the voltage was increased in several steps after reaching the corona ignition voltage. While for negative energisation, the applied voltage was increased just above the corona ignition voltage. The selections of voltage levels for positive and negative energisation were to maximise particle precipitation efficiency and to minimise the energy losses.

During the precipitation tests the electrical parameters were recorded manually, and the obtained number of precipitated and penetrated particles, and their mass numbers, were recorded by the commercially available software supplied by GRIMM Aerosol and installed on a desktop PC connected to the GRIMM particle analyser. The raw data were then transferred into Excel for further data processing.

Following the precipitation tests, all systems were switched off. For the candle and cigarette smoke particles the air pump remained pushing gas into the exhaust for a longer time to prevent pollution in the laboratory. In the case of air tests with street particles, valve 3 was

closed and valve 2 was opened. The remaining balloon gas was pushed into the exhaust manually.

3.6 Results

This section discusses the electrostatic precipitation results. Initially the effectiveness of the use of glass fibre filter for filtration of the airborne particles has been established. After that, the electrostatic precipitation results obtained using positive and negative energisation are presented and discussed.

3.6.1 Effectiveness of the Use of the Glass Fabric Filter

Before conducting electrostatic precipitation tests it is important to establish the filtration effectiveness of the glass fibre filter. The purpose of using the glass fibre filter is to help to collect and remove particles which are collected on the second mesh, and the glass fibre filter can be replaced frequently which makes the cleaning of the system easy. A straightforward test procedure was implemented and the method and results of this test are discussed in this section.

3.6.1.1 Test Method

It requires two single tests to confirm the effectiveness of the use of glass fibre filter paper. Test 1 was conducted without the glass fibre filter paper and Test 2 was conducted with the glass fibre filter paper. The main current and leakage current of Test 1 and Test 2 were recorded since both currents are dependent on electric charge delivered into the system. According to the design, the main charge by ionisation is removed and detected by the first metallic mesh, and charge on particles is removed and detected by the second metallic mesh. The total charge is the sum of main charge and particle charge. Therefore, the main charge of Test 1 and Test 2 should be similar, although only due to the main charge being

dependent on voltage level regardless of the use of the glass fibre filter. The particle charge obtained in Test 1 should be much higher than particle charge obtained in Test 2. The aperture size of the second metallic mesh is not fine enough to block particles physically so some particles may penetrate the mesh and leave the system without being precipitated. The use of a glass fibre filter helps to block the charged particles attracted by the second metallic mesh. In Test 2, the higher current should be obtained because charge on the attracted particles are removed and recorded. Therefore, the results of current obtained should show the similarity in main current and the difference in leakage current.

Test 1 and Test 2 were conducted using particles generated by burning bee wax candles, and five tests were conducted respectively. Negative DC energisation was used in these tests at voltage level of -10 kV.

3.6.1.2 Test Results

The results of the precipitation Test 1 and Test 2 are shown in Table 3-3. This table provides the values of the main and leakage currents.

Table 3-3. Comparison of main current and leakage current of Test 1 (with filter) and Test 2 (without filter). Negative DC energisation, bee wax candle particles.

	I-main (μA)	I-leakage (nA)
Test 1 (without filter)	-15.00 ± 0.24	-0.82 ± 0.07
Test 2 (with filter)	-15.00 ± 0.23	-10.00 ± 0.15

Table 3-3 clearly shows the similarity between the main currents through the first metallic mesh in both tests, and significant difference in leakage currents through the second

metallic mesh in both tests. These results show that the use of a glass fibre filter has no influence on the main charge delivered into the precipitation system. However, the charge on particles blocked by the filter cause an increased leakage current. This means more charged particles are removed by both the second mesh and the glass fibre filter paper without further penetrating into the precipitation system. This result shows the effectiveness of the use of glass fibre filter paper in the precipitation of PM and glass fibre filters were used for particle precipitation tests for all types of particles used in this research.

3.6.2 Particle Number Reduction Ratio

In order to present the results of the operational efficiency of the electrostatic precipitation of the system the parameter of a particle number reduction ratio is used. Particle number reduction ratio is the ratio of particle number after high voltage treatment divided by the maximum particle number before treatment. The particle number reduction ratio η_r is given by

$$\eta_r = \frac{N_p}{N_{\max}} \tag{16}$$

where N_p is particle number after treatment, and N_{max} is maximum particle number before treatment.

The data for average particle number reduction ratio and particle mass after treatment were recorded by the particle analyser during the precipitation tests. The reduction ratios were obtained using at least five different individual precipitation tests and standard deviations for each data point that was calculated and was used to illustrate the performance of the system.

One important thing should be emphasised is that there are seconds of delay in the laser analyser, which means that the recorded data are always several seconds later than the

actual behaviours in the electrostatic precipitation system. For example, when voltage is applied at 10 seconds of one test, the charging and precipitation processes happen immediately inside the electrostatic precipitation system. However, the recorded data reflected that the actual process happens at 15 seconds or later depending on different types of particles and different experimental environments. This situation can be applied in the particle precipitation result discussions in Chapter 3 and Chapter 4 therefore will not be discussed repeatedly for each result.

3.6.3 Positive Energisation

Precipitation tests using positively energised HV needle were conducted following the experimental steps as discussed in 3.5.2. The results of these are discussed in this section.

The precipitation tests results are based on at least five individual tests. In order to better present the performance of the precipitation system, the particle number reduction ratio and particle mass, both as a function of time, are also included for analysis. Therefore, one typical particle number reduction ratio result and one typical particle mass result are selected and presented as a figure, and the average result is presented as a table after each figure.

3.6.3.1 Indoor Particles

Figure 3-13 shows the reduction ratio of indoor particle number as a function of time for positive energisation and for different particle sizes. The positive high voltage used in the tests was 7 kV, which is the corona ignition voltage, and the HV needle was stressed with this voltage for 30 seconds. During this time, interval particles have been injected into the system and the particle analyser was used to monitor particle numbers in various sized ranges.

It was found that the particle number decreased to ~0 in 10 seconds after the high voltage was applied and then became stable. Particle numbers for particles of different sizes followed the same tendency.

According to the particle analyser, the indoor particle number for larger particles (particle diameter > 0.475 µm) was ~0, therefore, the particle number reduction ratio for larger particles is not shown for indoor particles.

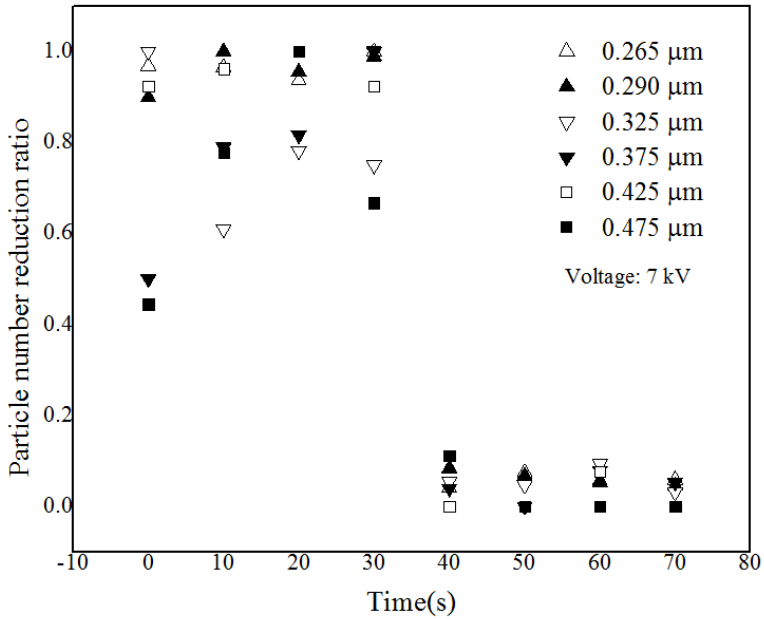

Figure 3-13. Indoor particle number reduction ratio as a function of time for positive energisation and for different particle sizes

Table 3-4 highlights the average reduction ratio of the indoor particle number for different particle sizes for positive energisation. The table shows that particle number was reduced down to ~0 after a high voltage treatment for the listed particle sizes. Particles with a diameter larger than 0.475µm were zero before and after the high voltage plasma treatment, therefore, the results are not shown in this table.

Table 3-4. Average particle number reduction ratio for different particle sizes. (Positive energisation, indoor particles).

Particle size (μm)	0.265	0.29	0.325	0.375	0.425	0.475
Average η_r	0.057 ±0.010	0.053 ±0.012	0.053 ±0.025	0.049 ±0.026	0.031 ±0.009	0

Figure 3-14 shows indoor particle mass as a function of time for positive energisation and for different particle sizes. The particle mass-time figure was recorded at the same time with the particle number reduction ratio-time figure. The figure shows that after a high voltage (7 kV) was applied at 30 seconds, the particle mass was reduced to ~0 μg/m^3 in 10 seconds. The tendency was the same from both PM and medical aspects.

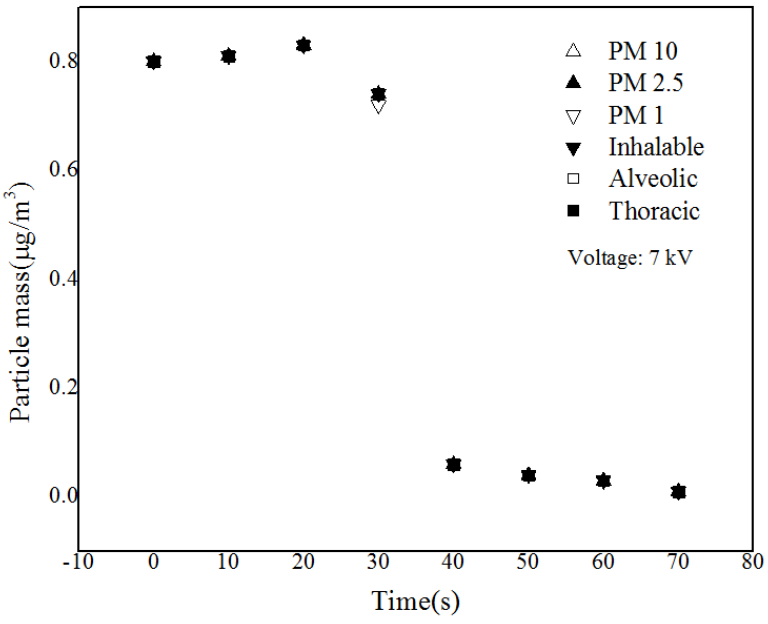

Figure 3-14. Indoor particle mass as a function of time for positive energisation and for different particle sizes.

Table 3-5 shows average indoor particle mass following treatment for different particle sizes for positive energisation. Here it can be seen that particle mass for different sizes of particles was reduced to 0 μg/m^3 after treatment.

Table 3-5. Average particle mass after treatment for different particle sizes (Positive energisation, indoor particles).

Particle size	PM10	PM2.5	PM1	Inhalable	Alveolic	Thoracic
Average particle mass after treatment (μg/m^3)	0.020 ±0.013	0.020 ±0.013	0.020 ±0.013	0.020 ±0.0103	0.020 ±0.0103	0.020 ±0.0103

3.6.3.2 Street Airborne Particles

Figure 3-15 shows the reduction ratio of street airborne particle number as a function of time for positive energisation and for different particle sizes. The positive high voltage used in the tests was 7 kV, i.e. the corona ignition voltage, and was applied at 30 seconds then maintained at 7 kV for a further 30 seconds. Similar to the indoor particle precipitation tests, the particle number decreased down to ~0 in 10 seconds then became stable. Particles of different sizes followed the same tendency.

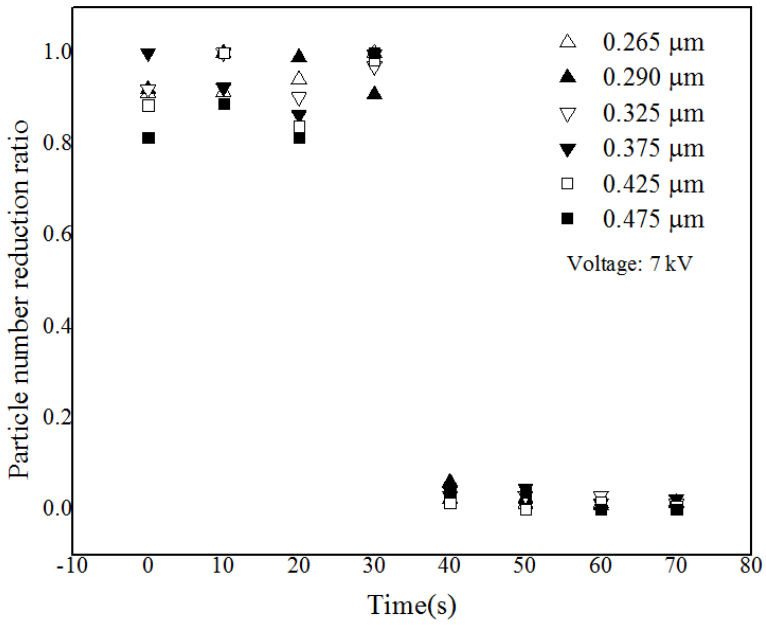

(a)

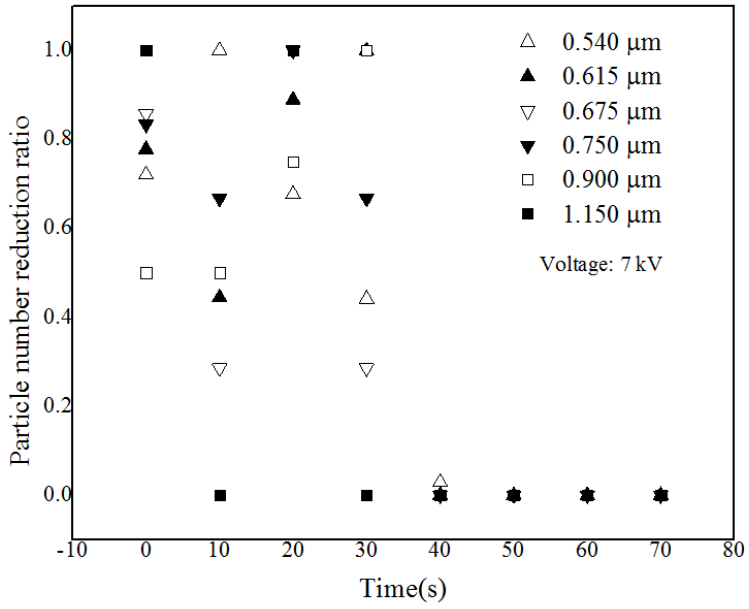

(b)

Figure 3-15. Street airborne particle number reduction ratio as a function of time for positive energisation and for different particle sizes (a) smaller size (b) larger size.

Table 3-6 shows the average reduction ratio of the street airborne particle number for different particle sizes for positive energisation. Here it can be seen that the particle number was reduced down to ~0 after a high voltage treatment for particle sizes, as listed in the table. Particles with diameter larger than 0.615 μm were completely removed after the high voltage treatment.

Table 3-6. Average particle number reduction ratio for different particle sizes. (Positive energisation, street airborne particles) (a) smaller sizes (b) larger sizes

Particle size (μm)	0.265	0.29	0.325	0.375	0.425	0.475
Average η_r	0.015 ±0.004	0.023 ±0.009	0.025 ±0.007	0.029 ±0.012	0.010 ±0.006	0.015 ±0.002

(a)

Particle size (μm)	0.54	0.615	0.675	0.75	0.9	1.15
Average η_r	0.006 ±0.001	0	0	0	0	0

(b)

Figure 3-16 shows street airborne particle mass as a function of time for positive energisation and for different particle sizes. The figure shows that after high voltage was

applied at 30 seconds, the particle mass was reduced to ~0 μg/m^3 in 10 seconds. The tendency was the same from both PM and medical aspects.

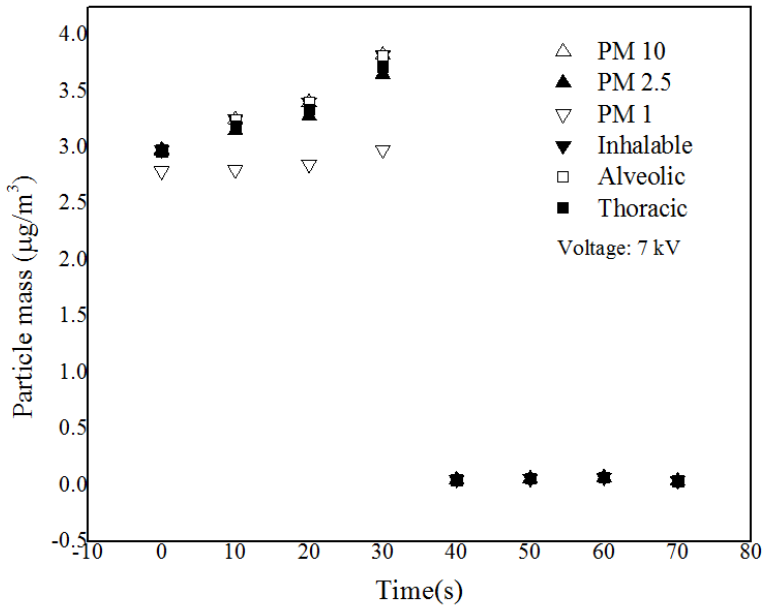

Figure 3-16. Indoor particle mass as a function of time for positive energisation and for different particle sizes

Table 3-7 shows average street airborne particle mass after treatment for different particle sizes for positive energisation. The table shows that particle mass for different sizes of particles was reduced to ~0 μg/m^3 after high voltage treatment.

Table 3-7. Average particle mass after treatment for different particle sizes. (Positive energisation, street airborne particles)

Particle size	PM10	PM2.5	PM1	Inhalable	Alveolic	Thoracic
Average particle mass after treatment ($\mu g/m^3$)	0.056 ±0.010	0.056 ±0.010	0.056 ±0.010	0.056 ±0.010	0.056 ±0.010	0.056 ±0.010

3.6.3.3 Candle Particles

Figure 3-17 shows the reduction ratio of candle particle number as a function of time for positive energisation and for different particle sizes. The positive high voltage was applied in steps to show the detailed effectiveness of increased voltage on the system. First 7.12 kV was applied, then the voltage was increased to 10.07 kV. Finally, the voltage was increased to 15.18 kV to ensure zero particle number pass through the system to be detected by the particle analyser. The figure shows that particles are removed further by the system each time the voltage was increased. Since the corona ignition voltage, which is around 7 kV, was not high enough to remove all the particles, the voltage should be increased to ensure 100% removal rate. Particle number finally decreased down to ~0 at 130 seconds then became stable. Particles of different sizes followed the same tendency.

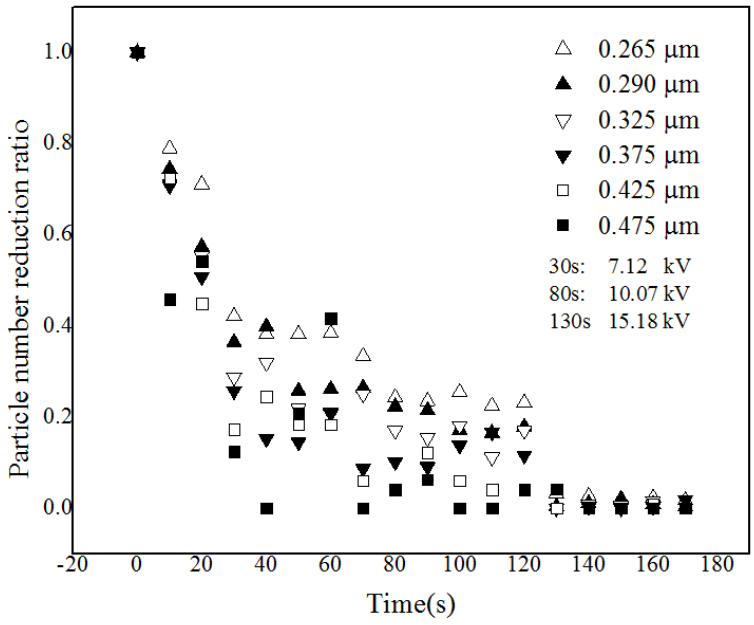
Particle number reduction ratio
Time(s)
0.265 μm
0.290 μm
0.325 μm
0.375 μm
0.425 μm
0.475 μm
30s: 7.12 kV
80s: 10.07 kV
130s 15.18 kV

(a)

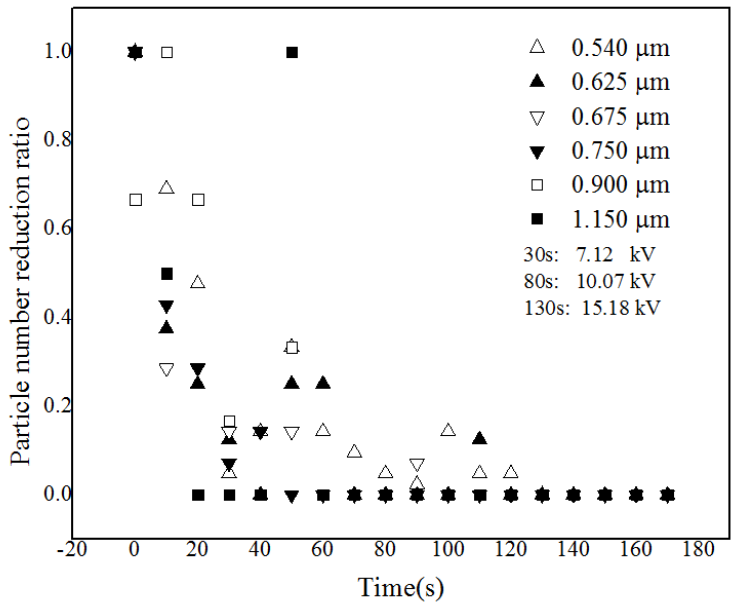
Particle number reduction ratio
Time(s)
0.540 μm
0.625 μm
0.675 μm
0.750 μm
0.900 μm
1.150 μm
30s: 7.12 kV
80s: 10.07 kV
130s: 15.18 kV

(b)

Figure 3-17. Candle particle number as a function of time for positive energisation and for different particle sizes. (a) Smaller sizes. (b) Larger sizes.

Table 3-8 shows the average reduction ratio of candle particle number for different particle sizes for positive energisation. Here it can be seen that the particle number was reduced down to ~0 after high voltage treatment for particle sizes, as listed in the table. Particles with a diameter larger than 0.615μm were completely removed after high voltage treatment.

Table 3-8. Average particle number reduction ratio for different particle sizes. (Positive energisation, candle particles) (a) smaller sizes (b) larger sizes.

Particle size (μm)	0.265	0.29	0.325	0.375	0.425	0.475
Average η_r	0.0241 ±0.006	0.009 ±0.006	0.010 ±0.007	0.005 ±0.001	0.002 ±0.001	0.008 ±0.002

(a)

Particle size (μm)	0.54	0.615	0.675	0.75	0.9	1.15
Average η_r	0.010±0.002	0	0	0	0	0

(b)

Figure 3-18 shows candle particle mass as a function of time for positive energisation and for different particle sizes. The particle mass-time figure was recorded at the same time with the particle number reduction ratio-time figure. The figure shows that after high voltage was applied and increased to 15.18 kV, the particle mass was reduced to ~0 μg/m^3 in 10 seconds and becomes stable. The tendency was the same from both PM and medical aspects.

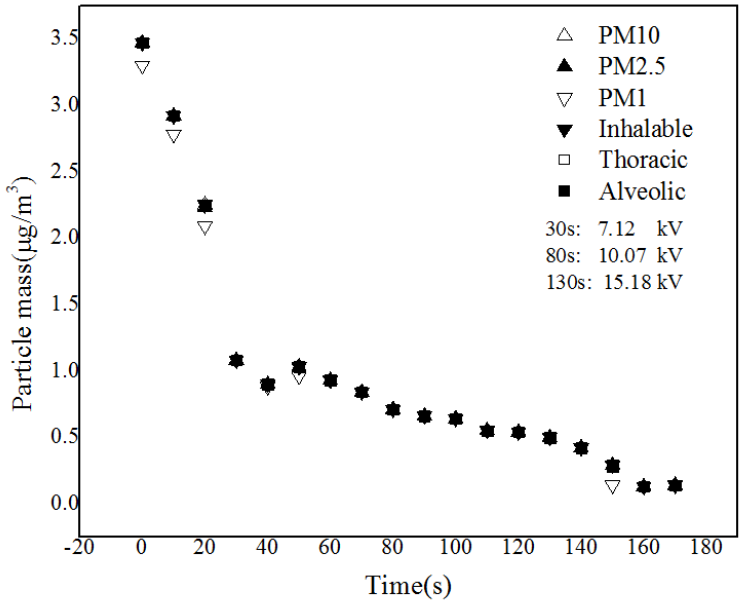

Figure 3-18. Candle particle mass as a function of time for positive energisation and for different particle sizes.

Table 3-9 shows average candle particle mass after treatment for different particle sizes for positive energisation. The table shows that particle mass for different sizes of particles was reduced to ~0 μg/m^3 after treatment.

Table 3-9. Average particle mass after treatment for different particle sizes. (Positive energisation, candle particles).

Particle size	PM10	PM2.5	PM1	Inhalable	Alveolic	Thoracic
Average particle mass after treatment(μg/m^3)	0.296 ±0.148	0.296 ±0.148	0.266 ±0.160	0.296 ±0.148	0.296 ±0.148	0.294 ±0.148

3.6.3.4 Cigarette Smoke Particles

Figure 3-19 shows the reduction ratio of cigarette smoke particle number as a function of time for positive energisation and for different particle sizes. Similar to candle particle precipitation figures, the positive high voltage was applied in steps to show the detailed effectiveness of increased voltage on the system. First 10.06 kV was applied, then the voltage was increased to 12.08 kV, then to 14.07 kV and, finally, increased to 15.20 kV to ensure ~0 particle number pass through the system. The voltage could not exceed 16 kV to prevent breakdown. The figure shows that more particles were removed from air flow as the voltage was increased. Since the corona ignition voltage, which is around 7 kV, was not high enough to remove all the particles, the voltage should be increased to ensure 100% removal. Particle number finally decreased down to ~0 at 300 seconds then became stable. Particles of different sizes followed the same tendency.

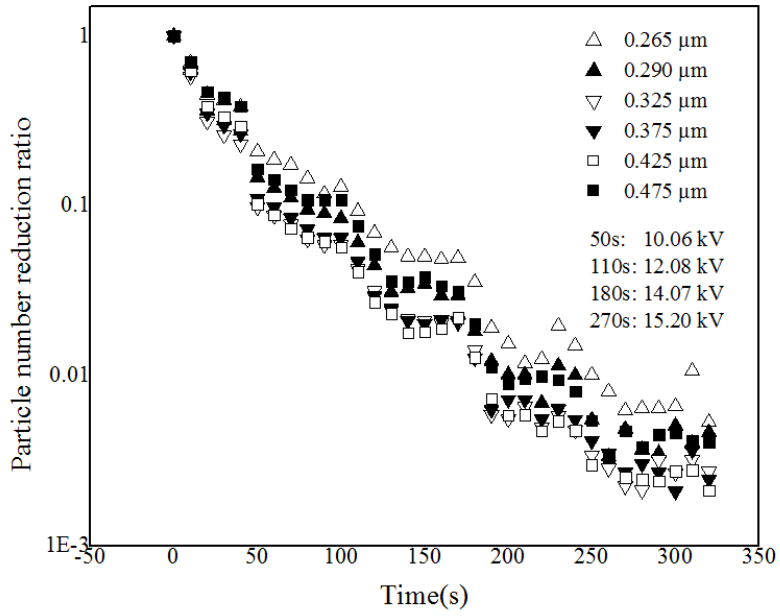

(a)

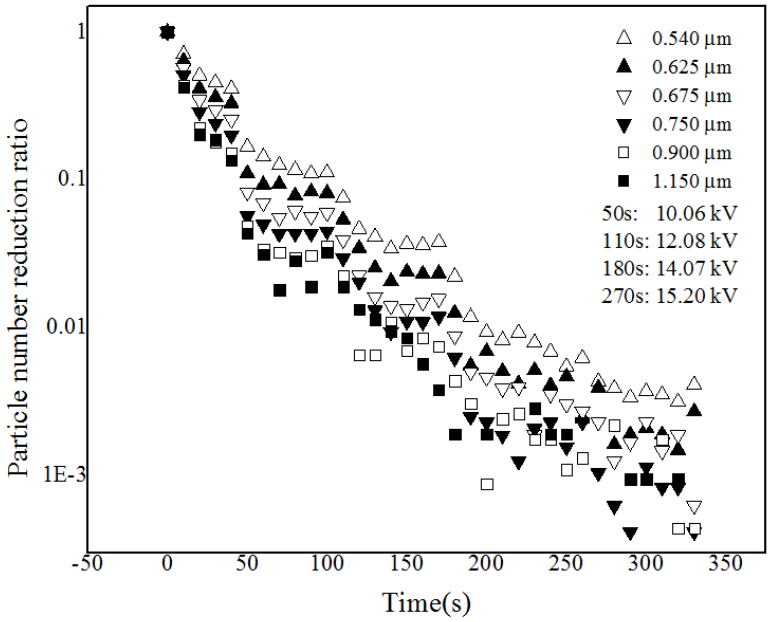

(b)

Figure 3-19. Cigarette smoke particle number reduction ratio as a function of time for positive energisation and for different particle sizes. (a) Smaller sizes. (b) Larger sizes.

Table 3-10 shows the average reduction ratio of cigarette smoke particle number for different particle sizes for positive energisation. The table shows that particle number was reduced down to ~0 after high voltage treatment for particle sizes, as listed in the table. Particles with a diameter larger than 0.615 μm were completely removed after high voltage treatment.

Table 3-10. Average particle number reduction ratio for different particle sizes. (Positive energisation, cigarette particles) (a) smaller sizes (b) larger sizes.

Particle size (μm)	0.265	0.29	0.325	0.375	0.425	0.475
Average η_r	0.007 ±0.002	0.004 ±0.001	0.003 ±0.001	0.003 ±0.001	0.003 ±0.001	0.004 ±0.001

(a)

Particle size (μm)	0.54	0.615	0.675	0.75	0.9	1.15
Average η_r	0.004±0.001	0	0	0	0	0

(b)

Figure 3-20 shows cigarette smoke particle mass as a function of time for positive energisation and for different particle sizes. The figure shows that more particles were removed from air flow as the voltage was increased, from the particle mass aspect. The figure also shows that, after high voltage was applied and increased to 15.20 kV, particle

mass was reduced to ~0 μg/m^3 in 10 seconds. The tendency was the same from both PM and medical aspects.

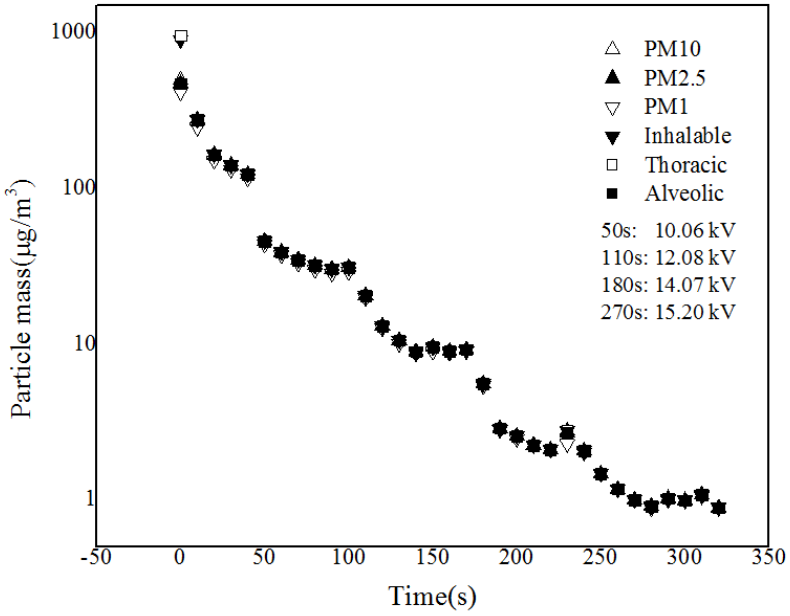

Figure 3-20. Cigarette smoke particle mass as a function of time for positive energisation and for different particle sizes.

Table 3-11 shows average cigarette smoke particle mass after treatment for different particle sizes for positive energisation. The table shows that particle mass for different sizes of particles was reduced to ~0 μg/m^3 after treatment.

Table 3-11. Average particle mass after treatment for different particle sizes. (Positive energisation, cigarette smoke particles).

Particle size	PM10	PM2.5	PM1	Inhalable	Alveolic	Thoracic
Average particle mass after treatment ($\mu g/m^3$)	0.978 ±0.071	0.978 ±0.071	0.966 ±0.066	0.978 ±0.070	0.978 ±0.070	0.978 ±0.070

3.6.4 Negative Energisation

Precipitation tests using a negatively energised HV needle were conducted following the experimental steps as discussed in 3.5.2. The results of these are discussed in this section.

Similar to the case of positive energisation, the precipitation tests results were based on at least five individual tests. In order to better present the performance of the precipitation system, the particle number reduction ratio and particle mass, both as a function of time, were included for analysis. Therefore, one typical particle number reduction ratio result and one typical particle mass result are selected and presented as a figure, and the average result is presented as a table after each figure.

3.6.4.1 Indoor Particles

Figure 3-21 shows the reduction ratio of the indoor particle number as a function of time for negative energisation and for different particle sizes. The negative high voltage used in the

tests was -10 kV, i.e. the corona ignition voltage, and was applied at 30 seconds, and the voltage level was maintained at -10 kV for a further 30 seconds. It was found that particle number decreased down to almost zero after 10 seconds then became stable. Particles of different sizes followed the same tendency. Similar to the case of positive energisation, indoor particle number for larger particles (particle diameter > 0.475 µm) was ~0. Therefore, the particle number reduction ratio for larger particles is also not shown for indoor particles in the case of negative energisation. The results of indoor particles precipitation for positive and negative energisation are similar. The only difference between positive and negative energisation in removing indoor particles from air flow is the voltage level. The voltage level for negative energisation (-10 kV) was higher than the voltage level for positive energisation (7 kV). The reason is due to the nature of energisation polarity on the same system. The corona ignition voltage is higher for negative energisation compared with positive energisation.

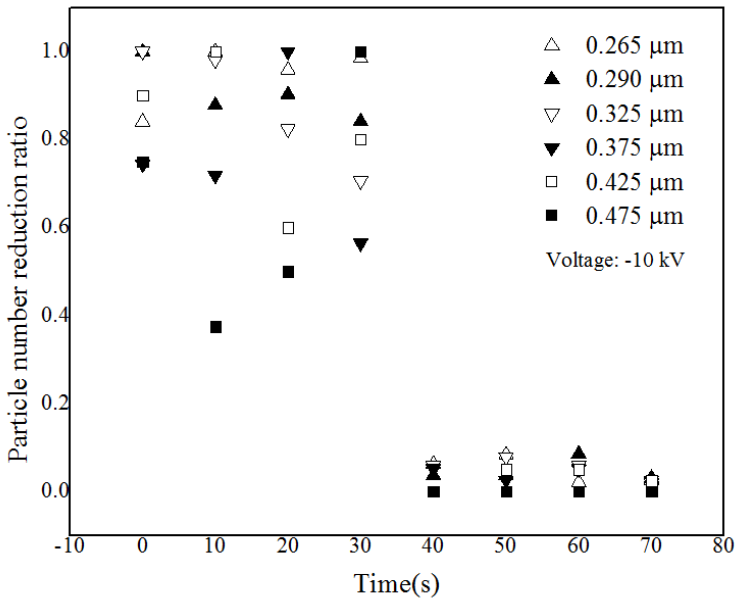

Figure 3-21. Indoor particle number reduction ratio as a function of time for negative energisation for different particle sizes.

Table 3-12 shows the average reduction ratio of indoor particle number for different particle sizes for negative energisation. Similar to the case of positive energisation, the table shows that particle number was reduced down to ~0 after high voltage treatment for particle sizes, as listed in the table. Particles with a diameter larger than 0.475 μm were zero before and after high voltage treatment and are not shown in the table.

Table 3-12. Average particle number reduction ratio for different particle sizes. (Negative energisation, indoor particles).

Particle size (μm)	0.265	0.29	0.325	0.375	0.425	0.475
Average η_r	0.046±0.024	0.045±0.020	0.048±0.022	0.034±0.015	0	0

Figure 3-22 shows indoor particle mass as a function of time for negative energisation and for different particle sizes. The particle mass-time figure was recorded at the same time with the particle number reduction ratio-time figure. The figure shows that after a high voltage was applied at 30 seconds, the particle mass was reduced to ~0 $\mu g/m^3$ in 10 seconds. The tendency was the same from both PM and medical aspects.

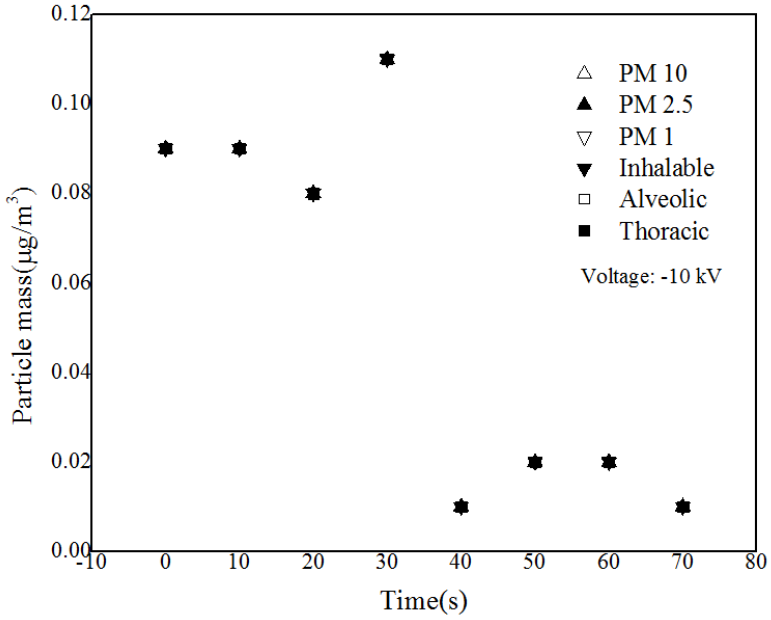

Figure 3-22. Indoor particle mass as a function of time for negative energisation for different particle sizes.

Table 3-13 shows the average indoor particle mass following treatment for different particle sizes for negative energisation. Similar to the case of positive energisation, the table shows that particle mass for different sizes of particles was reduced to ~0 μg/m^3 after treatment.

Table 3-13. Average particle mass after treatment for different particle sizes. (Negative energisation, indoor particles).

Particle size	PM10	PM2.5	PM1	Inhalable	Alveolic	Thoracic
Average particle mass after treatment ($\mu g/m^3$)	0.014 ±0.005	0.014 ±0.005	0.014 ±0.005	0.014 ±0.005	0.014 ±0.005	0.014 ±0.005

3.6.4.2 Street Airborne Particles

Figure 3-23 shows the reduction ratio of street airborne particle number as a function of time for negative energisation and for different particle sizes. The negative high voltage used in the tests was -10 kV, i.e. the corona ignition voltage, was applied at 30 seconds and the voltage level maintained at -10 kV for 30 seconds. Similar to the results of indoor particles for negative energisation, the particle number decreased down to ~0 in 10 seconds then became stable. Particles of different sizes followed the same tendency. The results of street airborne particle precipitation for positive and negative energisation are similar. The voltage level used for negative energisation was higher than the voltage level (-10 kV) for positive energisation (7 kV).

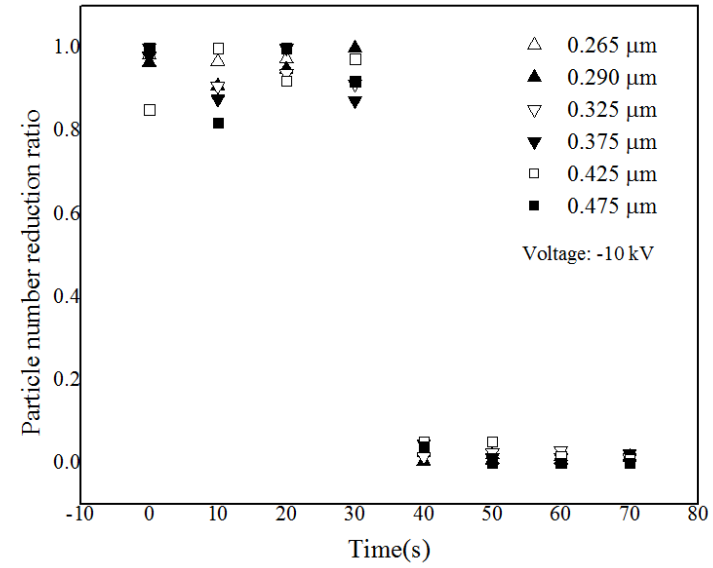

(a)

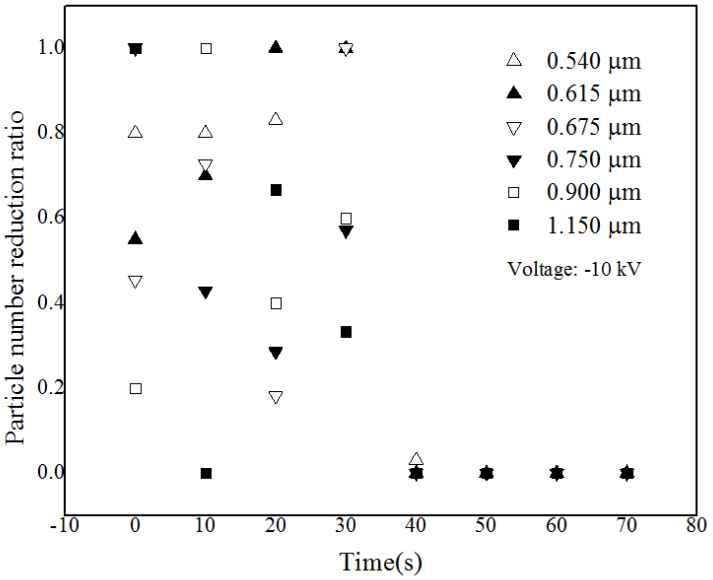

(b)

Figure 3-23. Street airborne particle number reduction ratio as a function of time for negative energisation and for different particle sizes. (a) Smaller sizes. (b) Larger sizes.

Table 3-14 shows the average reduction ratio of street airborne particle number for different particle sizes for negative energisation. The table shows that the particle number was reduced down to ~0 after high voltage treatment for particle sizes, as listed in the table. Particles with diameter larger than 0.615 μm were completely removed after high voltage treatment.

Table 3-14. Average particle number reduction ratio after treatment for different particle sizes. (Negative energisation, street airborne particles)

Particle size (μm)	0.265	0.29	0.325	0.375	0.425	0.475
Average η_r	0.015 ±0.004	0.023 ±0.002	0.025 ±0.007	0.029 ±0.012	0.010 ±0.006	0.015 ±0.002

(a)

Particle size (μm)	0.54	0.615	0.675	0.75	0.9	1.15
Average η_r	0.006±0.001	0	0	0	0	0

(b)

Figure 3-24 shows street airborne particle mass as a function of time for negative energisation and for different particle sizes. The figure shows that after high voltage was

applied at 30 seconds, the particle mass was reduced to ~0 μg/m^3 in 10 seconds. The tendency was the same from both PM and medical aspects.

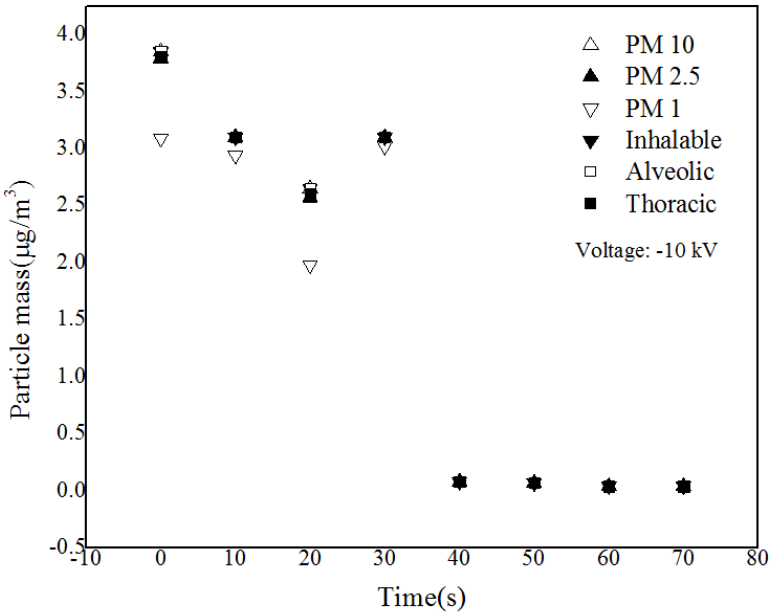

Figure 3-24. Street airborne particle mass as a function of time for negative energisation for different particle sizes.

Table 3-15 shows average street airborne particle mass after treatment for different particle sizes for negative energisation. The table shows that particle mass for different sizes of particles was reduced to ~0 μg/m^3 after treatment.

Table 3-15. Average particle mass for different particle sizes. (Negative energisation, street airborne particles).

Particle size	PM10	PM2.5	PM1	Inhalable	Alveolic	Thoracic
Average particle mass after treatment ($\mu g/m^3$)	0.054 ±0.017	0.054 ±0.017	0.054 ±0.017	0.054 ±0.017	0.054 ±0.017	0.054 ±0.017

3.6.4.3 Candle Particles

Figure 3-25 shows the reduction ratio of candle particle number as a function of time for negative energisation and for different particle sizes. The negative high voltage used in the tests was -10.36 kV and was applied at 0 seconds. The particle number decreased down to ~0 in 30 seconds then became stable. Unlike the candle particles removal for positive energisation, the voltage used for negative energisation was the corona ignition voltage and there was no need to increase the voltage further to achieve 100% precipitation efficiency. Particles of different sizes followed the same tendency.

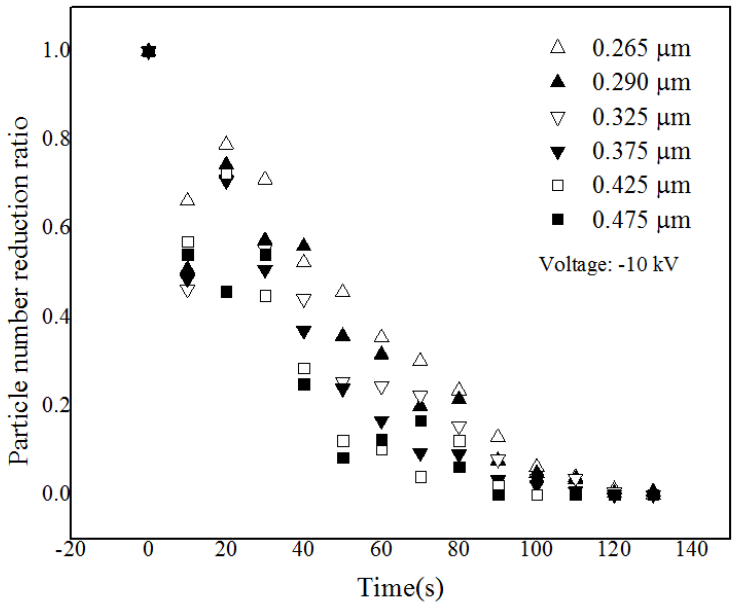

(a)

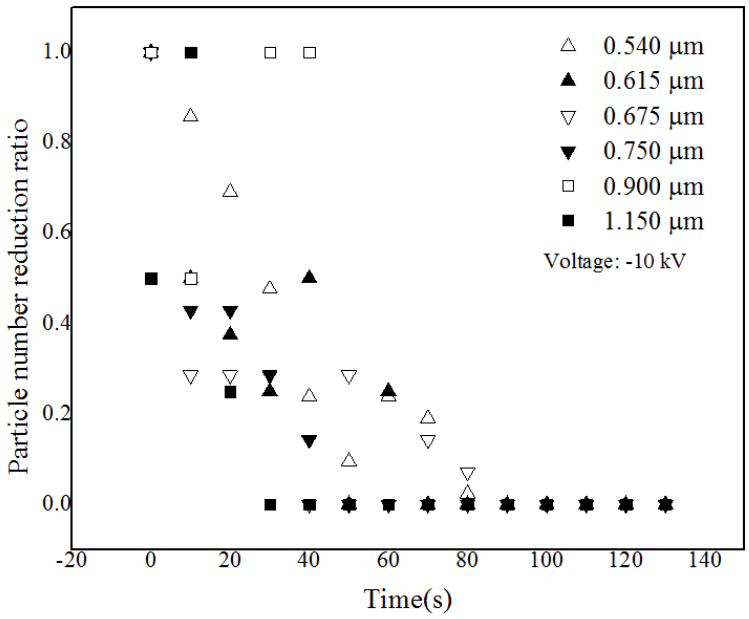

(b)

Figure 3-25. Candle particle number as a function of time for negative energisation and for different particle sizes. (a) Smaller sizes. (b) Larger sizes.

Table 3-16 shows the average reduction ratio of candle particle number for different particle sizes for negative energisation. The table shows that particle number was reduced down to ~0 after high voltage treatment for particle sizes, as listed in the table. Particles with a diameter larger than 0.540 μm were completely removed after high voltage treatment.

Table 3-16. Average particle number reduction ratio after treatment for different particle sizes. (Negative energisation, candle particles).

Particle size (μm)	0.265	0.29	0.325	0.375	0.425	0.475
Average η_r	0.047 ±0.004	0.034 ±0.021	0.032 ±0.003	0.012 ±0.001	0.004 ±0.001	0.008 ±0.002

(a)

Particle size (μm)	0.54	0.615	0.675	0.75	0.9	1.15
Average η_r	0	0	0	0	0	0

(b)

Figure 3-26 shows candle particle mass as a function of time for negative energisation and for different particle sizes. The figure shows that after high voltage was applied at 0 seconds, the particle mass was reduced to ~0 μg/m^3 in 30 seconds. The tendency was the same from both PM and medical aspects.

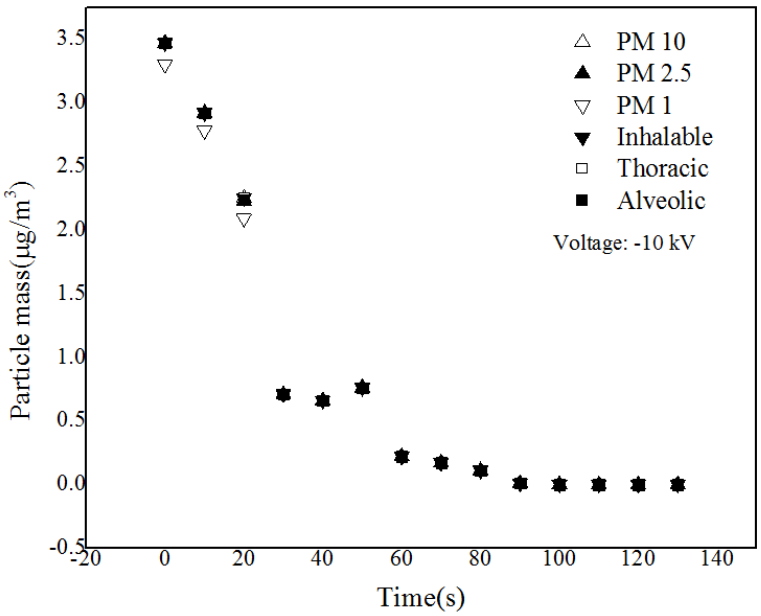

Figure 3-26. Candle particle mass as a function of time for negative energisation and for different particle sizes.

Table 3-17 shows average candle particle mass after treatment for different particle sizes for negative energisation. The table shows that particle mass for different sizes of particles was reduced to almost ~0 µg/m^3 after treatment.

Table 3-17. Average particle mass for different particle sizes. (Negative energisation, candle particles).

Particle size	PM10	PM2.5	PM1	Inhalable	Alveolic	Thoracic
Average particle mass after treatment ($\mu g/m^3$)	0.002 ±0.001	0.002 ±0.001	0.002 ±0.001	0.002 ±0.001	0.002 ±0.001	0.002 ±0.001

3.6.4.4 Cigarette Smoke Particles

Figure 3-27 shows the reduction ratio of cigarette smoke particle number as a function of time for positive energisation and for different particle sizes. The negative high voltage used in the tests was -10 kV and was applied at 50 seconds. The particle number decreased to ~0 in 50 seconds then became stable. Unlike candle particles precipitation for positive energisation, the voltage used for negative energisation was the corona ignition voltage and there was no need to increase the voltage to achieve 100% precipitation efficiency. Particles of different sizes followed the same tendency.

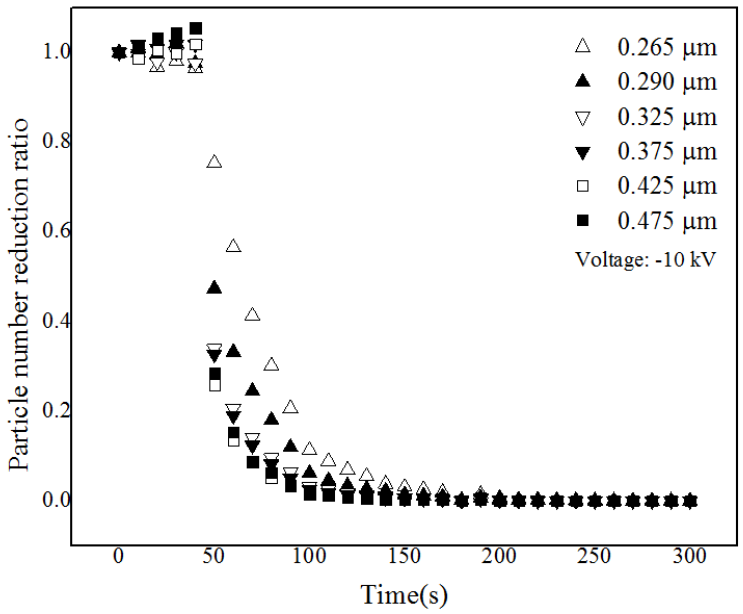

(a)

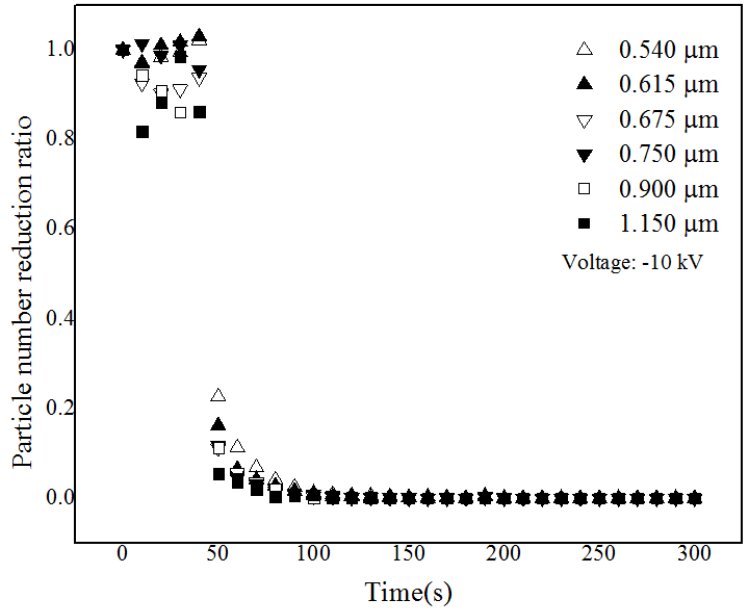

(b)

Figure 3-27. Cigarette smoke particle number as a function of time for negative energisation and for different particle sizes. (a) Smaller sizes. (b) Larger sizes.

Table 3-18 shows the average reduction ratio of cigarette smoke particle number for different particle sizes for negative energisation. The table shows that particle number was reduced down to absolutely zero after high voltage treatment for particle sizes, as listed in the table.

Table 3-18. Average particle number reduction ratio after treatment for different particle sizes. (Negative energisation, cigarette particles).

Particle size (μm)	0.265	0.29	0.325	0.375	0.425	0.475
Average η_r	0	0	0	0	0	0

(a)

Particle size (μm)	0.54	0.615	0.675	0.75	0.9	1.15
Average η_r	0	0	0	0	0	0

(b)

Figure 3-28 shows cigarette smoke particle mass as a function of time for negative energisation and for different particle sizes. The figure shows that after high voltage was applied at 50 seconds, the particle mass was reduced to 0 μg/m^3 after a further 50 seconds. The tendency was the same from both PM and medical aspects.

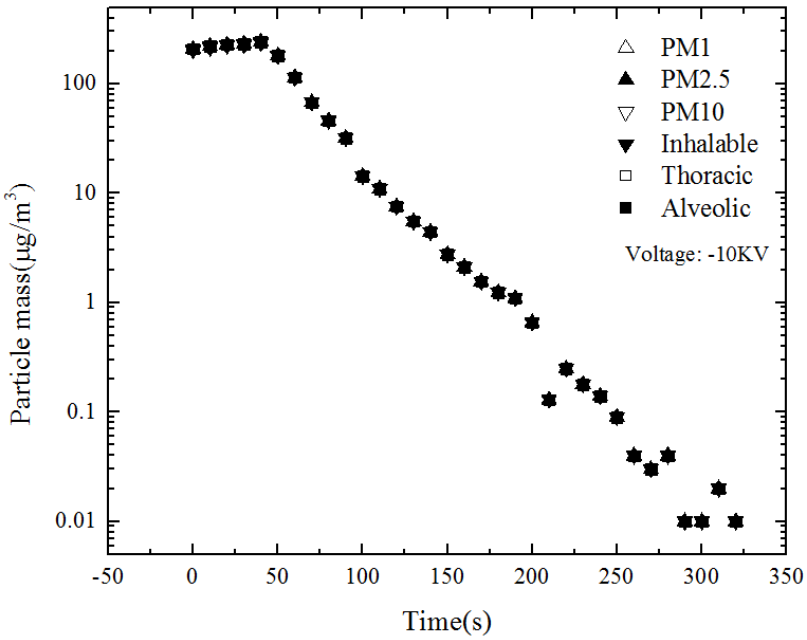

Figure 3-28. Cigarette smoke particle mass as a function of time for negative energisation and for different particle sizes.

Table 3-19 shows average cigarette smoke particle mass after treatment for different particle sizes for negative energisation. The table shows that particle mass for different sizes of particles was reduced to ~0 μg/m^3 after treatment. The reason of using log scale on particle mass axis is to show the numbers more clearly.

Table 3-19. Average particle mass for different particle sizes. (Negative energisation, cigarette smoke particles)

Particle size	PM10	PM2.5	PM1	Inhalable	Alveolic	Thoracic
Average particle mass after treatment($\mu g/m^3$)	0.016 ±0.008	0.016 ±0.008	0.016 ±0.008	0.016 ±0.008	0.016 ±0.008	0.016 ±0.008

3.7 Discussions on Particle Electrostatic Precipitation Results

3.7.1 Discussions on Particle Electrostatic Precipitation Results

The particle electrostatic precipitation results in the needle-mesh electrostatic precipitation system show that the system is very effective in particle precipitation. The unique needle-mesh topology system can provide an efficient and stable removal of particles as small as 250 nm in the precipitation tests. The achieved particle removal efficiency (~100%) was high from both particle number and particle mass point of view. The system was capable of removing almost all particles which passed through the system within a short period. Both positive and negative high voltage DC energisation can be applied to the system and both polarities work efficiently. Negative energisation has lower voltage levels to achieve 100% removal efficiency when compared with positive energisation. The small-scale feature of the system gives a high flexibility to be applied to different environments. The system is also easy to clean, which requires a simple procedure of opening the latches and replacing the glass fibre filter. When particle concentration is high (for example cigarette smoke particles), it requires the replacement of the glass fibre filter every 10-20 runs of

experiments with single experimental time of 5 minutes. The cost of the system is very low and it is easy to manufacture.

3.7.2 Ozone Concentration

Ozone concentration has been considered in this research with an ozone analyser monitoring the ozone concentration of the system (unit: ppm which means parts per million). The catalyst was used to control ozone concentration, and the catalyst used in this research was MnO_2. In the case of positive energisation, ozone concentration (7 kV with 19 ppm and 15.2 kV with 22 ppm) was decreased down to ground level (0.004 ppm). While in the case of negative energisation, ozone concentration (-10.36 kV with 26 ppm) was decreased down to ground level (0.004 ppm).

3.8 Energy Consumption Analysis

In this section, the energy consumption of the precipitation process is presented, discussed and analysed. The analysis of energy consumption is based on the transient current waveform obtained during the electrostatic precipitation process. It is important not only to maximise the precipitation efficiency but, at the same time, to minimise the energy consumption of the precipitation process. The optimal solution would be to design a system which provides high particle removal efficiency and minimum energy consumption.

3.8.1 Typical Corona Current Waveforms

Characteristics of corona current waveform are introduced in this part. Figure 3-29 shows a typical DC energised corona current-time waveform for single impulse and for positive and negative energisation. Figure 3-29 (a) shows a positive DC energised corona current for single impulse and Figure 3-29 (b) shows a negative DC energised corona current for single impulse.

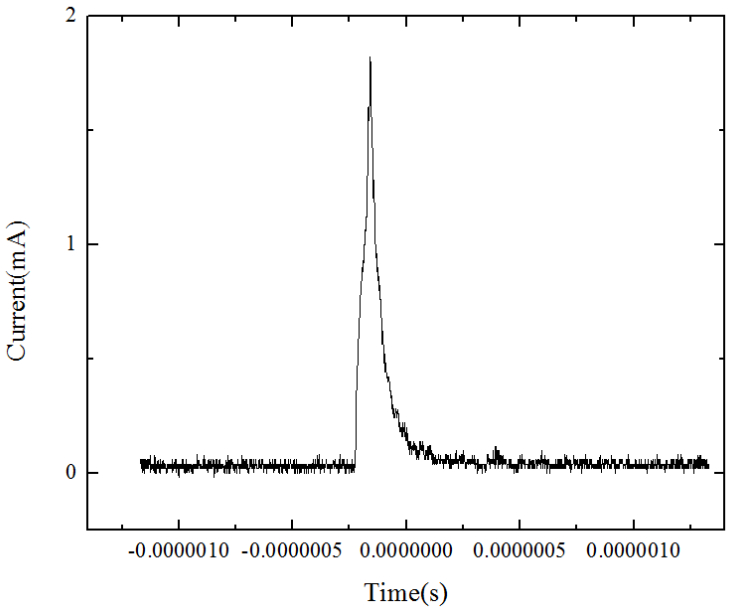

(a)

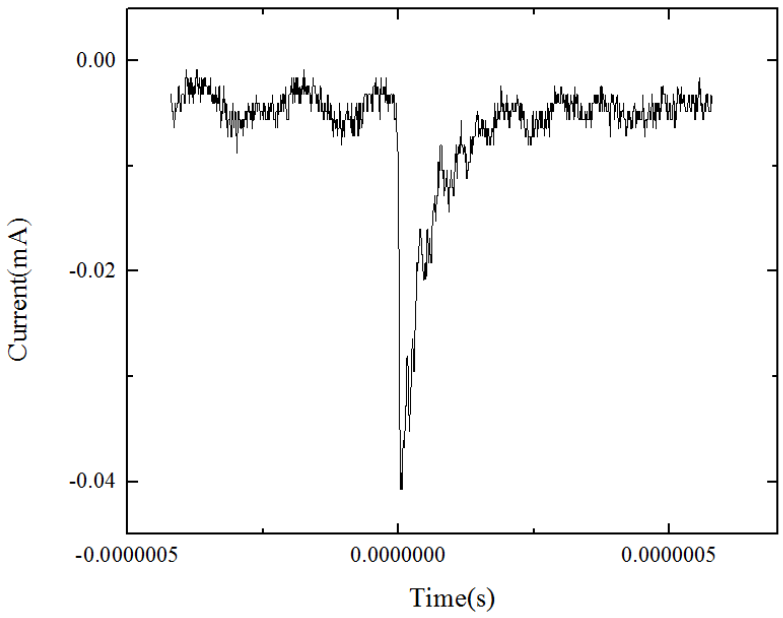

(b)

Figure 3-29. Typical DC energised corona current-time waveform for single impulse. (a) Positive DC. (b) Negative DC.

There are three characteristics of the corona current impulses:

The magnitude of a positive corona impulse is larger than that of a negative corona impulse.

The frequency of both positive and negative DC energised corona current impulses increases as the applied high voltage is increased. The impulses disappear at certain voltage levels for both energisations just before a breakdown voltage.

There is no detectable DC component for positive energisation with the increase of applied positive high voltage. The DC component for negative energisation increases as the applied negative high voltage increase until breakdown voltage.

3.8.2 Methodology of Energy Consumption Calculation

The methodology for obtaining energy consumption during the precipitation process is provided in this section.

3.8.2.1 Reasons of Using Current-time Waveform Integration

During the precipitation tests, as introduced in Section 3.5, initially experiments with two electrometers were used to evaluate the main current and the leakage current. It was found that of the leakage current is four times lower than the main current. For example, in the case of ambient air flow when the HV electrode of the precipitation test cell was energised by negative DC voltage with magnitude 10.06 kV, the main current in the test cell was 1.85×10^{-5} A, and the leakage current was 3×10^{-9} A. Therefore, in the analysis of energy consumption of the precipitation process the leakage current can be ignored.

The current in the system is transient which consists of two components: DC current component and fast impulsive component. The current measured by the Keithley analogue electrometers is not accurate as the electrometers are slow with a response time in the

milliseconds range, thus, these measurements provide an average current. Therefore, the current measured by the electrometers can be used for evaluation of the energy consumption. However, for a more accurate analysis of the energy consumed during the precipitation process the transient current components (impulsive current components) should be obtained. An accurate method of measuring the transient current impulses is introduced in this chapter which was used in the study for current and energy consumption analysis.

3.8.2.2 Methodology of Current-time Waveform analysis

The transient current impulses have been obtained using the current viewing resistor (1000 Ω).

The obtained current waveform contains two components, the DC current component and impulsive current component. These two components were separately taken into account in this analysis.

The total DC charge was obtained by the integration of I_{DC} which is the DC current component. Thus, the charged delivered by the DC component, Q_{DC} is given by

$$Q_{DC} = I_{DC} \times t \qquad (17)$$

To calculate the charge delivered by the single current impulse, the current waveform of the impulse was integrated from starting point to the impulse end point (point A to point B in Figure 3-30 (a)).

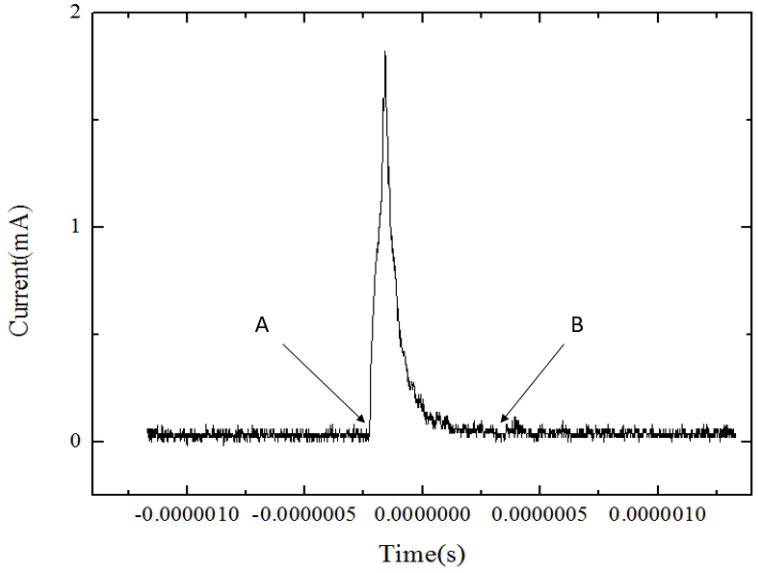

(a)

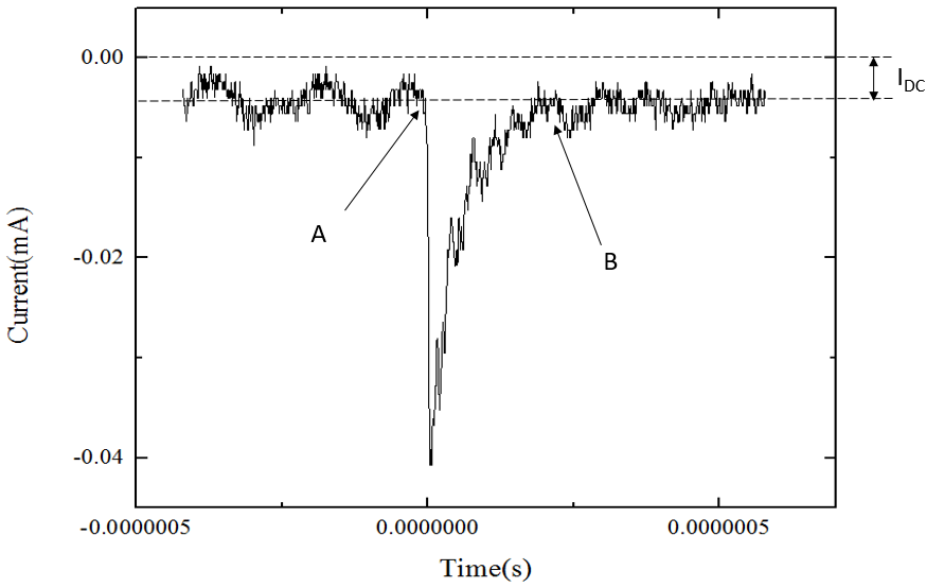

(b)

Figure 3-30. Typical DC energised corona current-time waveform for single impulse. (a) Positive DC. (b) Negative DC.

To obtain the total charge delivered by both DC and impulsive components, the DC charge was calculated by integration of the DC current from point A to point B using a straight interpolation line between these points (as shown in Figure 3-30 (b)). The charge of a single impulse only (without DC component) is obtained as a difference of the impulsive and DC parts. Mathematically, this procedure is given by

$$Q_{IMP-SINGLE} = \int_{t_A}^{t_B} I(t)dt - I_{DC} \times (t_B - t_A) \tag{18}$$

where I(t) is the impulsive current, t_A is the impulse starting point and t_B is the impulse finishing point.

Following this, the total charge delivered into the precipitation system during specific time interval, t, can be calculated by multiplying single impulsive charge by the frequency of impulses and time t. The total impulsive charge, $Q_{IMP\text{-}TOTAL}$, is given by

$$Q_{IMP-TOTAL} = Q_{IMP-SINGLE} \times frequency \times (t_B - t_A) \tag{19}$$

Finally, the total charge delivered during the electrostatic precipitation process, Q_{TOTAL}, is obtained as a sum of the total impulsive charge and the DC charge, which is given by

$$Q_{TOTAL} = Q_{IMP-TOTAL} + Q_{DC} \tag{20}$$

The average current during precipitation is the total charge divided by time

$$I_{AVERAGE} = \frac{Q_{TOTAL}}{t} \tag{21}$$

Thus, the total energy of the precipitation process is given by

$$W = U \times I_{AVERAGE} \times t \tag{22}$$

where U is the applied voltage

The energy consumption of the precipitation process is expressed as the energy consumption in the system per cubic meter of treated air. Thus, the energy consumption of the precipitation process is given by

$$E_C = \frac{W}{V_G} \tag{23}$$

where E_C is energy consumption, and V_G is volume of the treated air. V_G is given by.

$$V_G = Q_G \times t \tag{24}$$

where Q_G is gas flow rate.

Finally, energy consumption can be calculated using the following equation

$$E_C = \frac{U \times (Q_{IMP-SINGLE} \times frequency + Q_{DC})}{Q_G} \tag{25}$$

The energy consumption was obtained using data from at least five individual precipitation tests. The standard deviation for energy consumption figures has been obtained.

The equation above states that the standard deviation of the energy consumption is the product of two variables: $Q_{IMP-SINGLE}$ and frequency. Thus, the standard deviation of energy consumption was calculated using the following method.

According to [70], the standard deviation of product $\overline{w}$ of the two mean data x and y:

$$\overline{W} = \overline{X} \times \overline{Y} \tag{26}$$

with individual standard deviations σ_x and σ_y is given by

$$\sigma_{\overline{W}} = \left|C\right| \times \overline{X} \times \overline{Y} \times \sqrt{\frac{\sigma_{\overline{X}}^{2}}{\overline{X}^{2}} + \frac{\sigma_{\overline{Y}}^{2}}{\overline{Y}^{2}}} \tag{27}$$

where c is a product of constant in each component x and y and, in this case of the standard deviation calculation of energy consumption evaluation, x is $Q_{IMP\text{-}SINGLE}$ while y is frequency in Equation (25).

3.8.3 Results

The flow rate of the system is 2 litres/minute (3.3×10^{-5} m^3/s), which was used for the energy consumption calculation.

3.8.3.1 Positive Energisation

For positive energisation, 7 kV was used to remove particles with low concentration (indoor particles and street airborne particles) and 15.20 kV was used to remove particles with high concentration (candle particles and cigarette smoke particles)

For the voltage level 7 kV, the frequency of the high voltage DC energised current impulses was 2.5 kHz and for voltage level 15.20 kV, the frequency the high voltage DC energised current impulses was 5.8 kHz.

The parameters listed above were used for the calculation of energy consumption. The energy consumption of needle-mesh topology electrostatic precipitation system for positive energisation is shown in Table 3-20.

Table 3-20. Energy consumption of needle-mesh topology system for positive energisation.

Voltage (kV)	7	15.20
Frequency (kHz)	2.5±0.3	5.8±2.5
Single impulsive charge (C)	$7.33\times 10^{-11}\pm 6.04\times 10^{-12}$	$4.83\times 10^{-10}\pm 6.55\times 10^{-11}$
Energy consumption (Wh/m^3)	0.01±0.0013	0.353±0.15

3.8.3.2 Negative Energisation

For negative energisation, -10.36 kV was capable of removing all types of particles used. The frequency of the high voltage DC energised current impulses with voltage level -10.36 kV was 74 kHz. These parameters were used for the calculation of energy consumption. The energy consumption of needle-mesh topology electrostatic precipitation system for negative energisation is shown in Table 3-21.

Table 3-21. Energy consumption of needle-mesh topology system for positive energisation.

Voltage (kV)	-10.36
Frequency (kHz)	74±18
Single impulsive charge (C)	$3.19\times 10^{-11}\pm 4.13\times 10^{-12}$
DC component (A)	-5×10^{-7}
Energy consumption (Wh/m^3)	0.258±0.058

3.8.4 Discussion on Energy Consumption

The methodology for calculating the energy consumption of the electrostatic precipitation system has been presented and the energy consumption has been obtained for the needle-mesh topology electrostatic precipitation system. The obtained values have been compared with the typical energy consumption levels as found in the literature. The typical electrostatic precipitator energy consumption value found in paper [59] was between 0.1 to 0.5 Wh/m^3, with the gas velocity of 2-6 m/s and voltage level of up to 20 kV. The electrostatic precipitation system developed in paper [59] provided the energy consumption value of 0.06-0.42 Wh/m^3, with the gas velocity of 0.8 m/s and voltage level of up to 15-16 kV. Paper [71] shows that the energy efficiency of 0.44 Wh/m^3 can achieved with the gas velocity of >15-20 m/s and voltage level of 10-17 kV. Another research paper [60] shows that the energy consumption level investigated was 0.1 Wh/m^3 with voltage level of 60 kV. It has been presented in this chapter that the electrostatic precipitation system developed is with very low energy consumption for both positive (0.01 Wh/m^3 and 0.353 Wh/m^3) and negative DC energisation (0.258 Wh/m^3). This comparison shows that the energy consumptions for the needle-mesh topology electrostatic precipitation system for both positive and negative DC energisation are close to, or lower than, the typical value previously obtained which provides the system with a high particle removal efficiency and high energy usage efficiency.

3.9 Conclusions

In this chapter, a novel needle-mesh precipitation system has been designed and constructed. Unlike traditional tip-plane topology electrostatic precipitators, a gauge 14 hypodermic needle was used in the design of the electrostatic precipitator to be applied to a high voltage. The double meshes were applied to ground, so the voltage drop was formed between the needle tip and the meshes. The sharp tip of the hypodermic needle was the key factor for gas ionisation, and ions and electrons were generated in the space between the

needle tip and the two meshes. From a gas flow aspect, flue gas with particles was pumped into the electrostatic precipitator through the inlet. The combination of flue gas and particles all passed through the centre of the needle. Particles were then charged in the space between the needle tip and the first mesh. The first mesh was used both for grounding to form a voltage drop in the electrostatic precipitator and for current analysis, so the pore size of the first mesh was designed to be relatively larger to allow the particles to pass through. The second mesh and a glass fibre filter between the two meshes were designed to collect all the charged particles. The effectiveness of the glass fibre filter has been confirmed in the experiment.

To prove the feasibility of the proposed design, the electrostatic precipitation system with a needle-double-mesh topology was used in precipitation tests with different airborne particles (indoor particles, street airborne particles, bee wax candle particles and cigarette smoke particles). A particle generation system for bee wax candle particles and cigarette smoke particles has been designed and developed. There was also a balloon system designed for street particle collection and injection into the electrostatic precipitation system, which can be used for a small volume of gas transfer when the direct collection of gas is difficult. The data for particle precipitation was recorded from both a particle number and particle mass aspect. The particle number and particle mass for cigarette smoke particles were close to those as reported in heavily polluted areas in the real world. Results show that the designed electrostatic precipitation system is capable of removing almost all the particles from the heavily polluted atmosphere, and also that the performance of the system is excellent and stable. The particle precipitation efficiency for different particles can be as high as almost 100% and this high efficiency can be achieved in very short system running time (less than 30 seconds).

The precipitation operations can be conducted using both positive and negative DC high voltage energisations. It was found that the performances of both polarities of energisation are very good with almost 100% particle precipitation efficiency within a short time (less

than 30 seconds), especially when particle concentration was not high (indoor particles, airborne street particles and bee wax candle particles). When particle concentration is very high (cigarette smoke particles) the performance of the system was also good and stable. For negative energisation, the voltage level used (-10 kV) was similar to the situation when particle concentration was relatively lower, which was just above the corona ignition voltage. However, it required the increase of the voltage level for positive energisation (from 7 kV to 15 kV) to achieve 100% particle precipitation efficiency when particle concentration was high.

The energy consumption of the designed system was obtained. In this research, a method of calculating energy consumption based on the current-time waveform was developed. The energy consumption was calculated by the integration of current-time waveforms recorded during particle precipitation tests, which is close to the real situation inside the precipitator. This method provides another way to calculate energy consumption, which can be more accurate. With the developed method, energy consumptions for different situations were calculated and compared with the energy consumptions in literature and was found that the electrostatic precipitation system developed had a very low energy consumption for both positive DC energisation (0.01 Wh/m^3 and 0.353 Wh/m^3) and negative DC energisation (0.258 Wh/m^3).

The ozone concentration level has also been considered in the research where the design of the system also included an ozone concentration control section, in which a catalyst was used. The ozone level was then lowered to ground level after control which is also environmental friendly.

Particle electrostatic precipitation technologies in literature have been reviewed for comparison with the hypodermic needle-mesh system developed in this chapter, [52] [57] [72] [73] [74] [54] [75] [53].

According to [52], the research was based on a DC energised electrostatic precipitation system with conventional needle-plate configuration. The system in this literature was similar in width (190 mm) to the system shown in this chapter. The research investigated ten cases of design based on different types of filters and collection plate. The filters included glass fibre filters, polyethylene, bag filter media, polyester, polyethylene terephthalate, non-woven media and refined cotton media. The collection plates included an iron plate, iron grid and activated carbon media. Fly ash was used as the pollution source of the research. The energisation polarity used in the research was positive. The voltage level used in different cases of combination of filters and collection plates ranged from 15 kV to 20 kV for particle removal, which was higher than the voltage level used in the research shown in this chapter (7 kV to 15 kV for positive energisation and -10 kV for negative energisation), and may also result in higher energy consumption due to increased voltage level. The precipitation results for larger particles (larger than 1 μm) can be as high as 99%. However, particle precipitation efficiency for a particle's diameter smaller than 1 μm was unstable (20% to 70%), while the particle precipitation efficiency for the system shown in this chapter can be as high as 100% for particles as small as 0.265 μm.

A needle cylindrical electrostatic precipitation system [57] was also reviewed and compared with the hypodermic needle-mesh system as developed in this chapter. The needle cylindrical system was based on a central needle electrode (DC high voltage energised) and cylindrical collection plate. The design also included a soft X-ray emitter to help increase the particle precipitation efficiency. The needle cylindrical system from this paper had a low flow rate of 3 litres/minute which was similar to this research (2 litres/minute) as shown in this chapter. NaCl nanoparticles (~100 nm) were used for particle source. Both positive (9 kV) and negative energisations (-9kV) have been used for the needle cylindrical system for maximum particle precipitation efficiency. The maximum particle precipitation efficiency for nanoparticles (~100 nm) can be as high as 98% which is similar to the hypodermic needle-mesh system (100%). Although the voltage level of the needle cylindrical was slightly

lower than the hypodermic needle-mesh system (7 kV to 15 kV for positive energisation and -10 kV for negative energisation). The energy consumption for the needle cylindrical system (0.06 Wh/m^3 for positive energisation and 0.18 Wh/m^3 for negative energisation) was similar to the hypodermic needle-mesh system (0.01 Wh/m^3 and 0.353 Wh/m^3 for positive energisation, and 0.258 Wh/m^3 for negative energisation). The behaviours of the two systems were similar, however, the design of the hypodermic needle-mesh system is simple and with low cost as no soft X-ray emitter is used when compared with the needle cylindrical system in this paper. Another advantage may be the capability of the system as developed in this chapter when dealing with particles with a more complex composition, such as cigarette smoke particles.

Since the hypodermic needle-mesh system developed in this chapter aims to potentially be applied to improve indoor environment by precipitating particles suspended in the indoor ambient environment, similar approaches have been reviewed and compared. The reviewed research [54] has developed a system to improve the indoor air quality by particle collection, odour removal and sterilisation of *E.coli*. In the particle collection section, the system designed was based on multiple needle electrodes with the mesh filter. The multiple needles were located on a 55 mm diameter plate, and the needle-plate distance was 5 mm, which is similar to the size of the hypodermic needle-mesh system developed in this chapter. The high voltage supply used for the multiple needle system was negative energisation with a voltage level of -5 kV. The particle collection efficiency was about 50% with a collection time of 80 minutes. Considering the working voltage level for indoor particles for hypodermic needle-mesh system in this chapter (7 kV for positive energisation and -10 kV for negative energisation) was slightly higher than the multiple needle system from this paper, and the particle precipitation efficiency for indoor particles was 100% for particle larger than 0.265 µm, it can be expected that better performance can be achieved when the hypodermic needle-mesh system was applied in practice even for a more polluted indoor environment.

Another research [53] presented an electrostatic precipitation system based on a configuration of a single needle and a hole-punched plate. The size of the needle hole-punched plate system (length 150 mm and width 90 mm) was similar to the hypodermic needle-mesh system developed in this chapter. Carbon particles were used as the source of pollution with diameters ranging from 0.03 µm to 3 µm. A negative high voltage energisation was applied to the needle hole-punched plate system with the voltage level from -4 kV to -15 kV and the working voltage level of the hypodermic needle-mesh system developed in this chapter at -10 kV. This paper investigated the influence of the size of the hole and, therefore, different sizes of holes were used in the research. Particle precipitation efficiency in this paper for particle diameters around 0.265 µm was approximately 65% at best whereas the efficiency for different cases were all below 80%. Although particle precipitation results with particle diameters smaller than 0.265 µm were not measured for the hypodermic needle-mesh system as developed in this chapter, particle precipitation efficiency for particle diameters larger than 0.265 µm was 100%, which shows an advantage when compared with the needle hole-punched plate system in this paper.

The comparison and analysis of result in the literature and the result in this chapter show that the hypodermic needle-mesh electrostatic precipitation system shows good performance. The particle precipitation efficiency of the system is either similar to, or higher than, the particle precipitation efficiency in the literature. The energy consumption of the system is lower than the energy consumption found in literature, which shows that the system developed in this chapter is energy saving. The high particle precipitation efficiency and low energy consumption result in a very good performance for this system.

4 Development of the Coaxial Topology Electrostatic Precipitation System

4.1 Introduction

In Chapter 3, a small-scale electrostatic precipitation system with a needle-mesh topology has been developed and the precipitation performance of the system has been obtained and analysed. This needle-mesh topology system is capable of precipitating particles from gas flow with a relatively low flow rate of 2 litres/min and with a high efficiency and low energy consumption. The success of this small volume system brings the research to a further stage, which is to scale up the system to meet the demands of potential practical industrial and environmental applications. For the development of practical precipitation systems it is also important to investigate the influence of humidity of air on the particle precipitation process in the electrostatic precipitation systems. Due to limitations of the humidity tests in the small needle-mesh topology system, the full-scale investigation of humidity influence on particle precipitation was conducted using the larger scale system (coaxial topology), as discussed in this chapter.

In the framework of the present project a larger scale electrostatic precipitation system with coaxial topology has been designed and manufactured in this chapter. The key component of the electrostatic precipitation system is a coaxial topology electrostatic precipitator. The approach provides two possible solutions for improvements to the coaxial topology electrostatic precipitation system when particle concentration is high.

The first solution is to increase the number of precipitation stages, for example, by using a double stage system instead of a single stage precipitator. Theoretically the increased of number of stages should provide longer particle exposure time in plasma, which will make particle charging and particle collection more efficient.

The second solution is to provide an environment with increased humidity inside the electrostatic precipitator to achieve better performance. It is expected that the increase of humidity inside the electrostatic precipitator can provide a higher particle precipitation efficiency, and the results of these precipitation tests are presented and discussed in this chapter.

As in the case of the needle-mesh precipitation system discussed in Chapter 3, different types of airborne particles (indoor air particles, bee wax candle particles, street particles and cigarette smoke particles) have been used in the precipitation tests in the coaxial topology as presented in Chapter 4. Street airborne particles were not used in this research as the volume of the collection system based on the balloon was limited and the limited volume was not suitable for a larger scale coaxial electrostatic precipitation system. Therefore, only indoor airborne particles, bee wax candle particle and cigarette smoke particles were selected for precipitation tests in this chapter. The particle number and particle mass for cigarette smoke particles is close to those reported in heavily polluted areas in practical applications. The aim is to prove that a single stage coaxial electrostatic precipitation system designed in this research is capable of precipitating almost all the particles from air flow with relatively lower particle concentration (indoor particles and bee wax candle particles). When particle concentration is high (cigarette smoke particles), using a double stage system and increasing humidity are the two different methods to maintain system performance at a high state, as in the case of lower particle concentration.

The precipitation system was operated under both positive and negative DC energisation and the comparison of precipitation efficiency for both cases has been made. The energy consumption was also considered in this study as the design of the system aimed to be environmental friendly. Using the energy consumption calculation method developed in Chapter 3, energy consumptions for different situations were calculated.

4.2 Coaxial Topology: Main Advantages

This part of the study is focused on the investigation of efficiency of a larger scale electrostatic precipitation system which could be used in practice. The effect of increased humidity on the precipitation efficiency and the effect of increased stage of system on the precipitation efficiency are to be investigated as these two effects can be used to increase particle precipitation efficiency of electrostatic precipitation systems.

As discussed in Chapter 3, the electrostatic precipitation system with a needle-mesh topology provided high efficiency of particle precipitation efficiency, ~100%. However, there are two disadvantages of that system which makes the use of the larger scale system and increased humidity system an improved performance in practical applications.

First, since the system described in Chapter 3 was needle based, the flow rate of treated air was limited by the topology and design of hypodermic needles. The small cross section of the hypodermic needles means the total untreated gas volume over a certain time is limited, otherwise the increased flow rate will cause shorter particle exposure time in the corona reaction area. Shorter exposure time may then result in reduced charging of particles which causes lower electric force and potential penetration of particles in the system. Therefore, to address this issue an increased distance between the needle and the mesh can be used. However, the corona active area will remain the same, but a higher potential will be required to compensate for the increased distance in order to maintain a reasonable electric field which is necessary for the precipitation of particles. The increased voltage may result in an undesirable spark breakdown, increase the energy consumption of the system as well as generation of ozone.

Second, in order to investigate the influence of humidity of air on the efficiency of particle precipitation, a humidifier will be introduced in the precipitation system. Initial tests have been conducted using the needle-mesh electrostatic precipitator and was found that the

water vapour generated by the humidifier was easily formed into water droplets inside the electrostatic precipitator. Since the cross section of the hypodermic needles was small, the water droplets could easily block the needle which stops the gas circulation of the system, i.e. which makes it very difficult to increase humidity inside the needle-mesh topology electrostatic precipitation system.

Considering these two issues associated with the needle-mesh electrostatic precipitator, a new system should be designed to meet the demands of both larger scale and the possibility of using air flow with an increased humidity. Here, the classical coaxial topology is considered. The system could be scaled up by increasing the size of the electrostatic precipitator and, as long as the gas inlet and outlet are large enough, water droplets will not block the entire system. This is the reason for the use of coaxial topology in this part of the research.

4.3 Design of the Coaxial Topology Electrostatic Precipitation System

In this section, the design of the coaxial topology electrostatic system developed in the framework of this research is presented.

4.3.1 Materials

The materials used for a central HV electrode, tube and dielectric flanges are introduced in this section.

4.3.1.1 HV Central Electrode

The central electrode is one of the key components of the cylindrical electrostatic precipitator. A material with a good electrical conductivity should be used and, in this coaxial

system, copper (conductivity of copper: 58.5× 10^6 S/m, also cheap and easy to machine) was used to manufacture a 5 mm diameter rod HV electrode for the second stage and a 1 mm diameter stainless steel (conductivity of stainless steel: 1.45 × 10^6 S/m) as an HV electrode for the first energisation stage. Both the rod and the wire were 70 cm in length. The two types of electrodes were used in two stages of the electrostatic precipitator with the same topology. The reason for a two-stage system will be introduced Section 4.7. The electrode was fixed to the bottom of the electrostatic precipitator using screw connection and was fixed on to the top of the electrostatic precipitator using a banana plug.

4.3.1.2 Ground tube

The metallic grounded (external) tube is another component of the electrostatic precipitator. The metallic tube is used to collect precipitated particles in the field formed between the HV central electrode and the grounded tube. According to the design, a material with good conductivity should be used. The material should also be inexpensive in an attempt to lower the cost since it is a large electrostatic precipitator device. Also, it is better to have a material with low density to ensure a lower weight of the electrostatic precipitator will be used in different environment. Therefore, considering these requirements, aluminium (conductivity of aluminium: 36.9 × 10^6 S/m) was selected to be the material for the metallic tube. The internal diameter of the tube was 88 mm. There was also an electric connection on the tube which was used to connect to the electrometer for monitoring the current during tests. The electric connection was also used for grounding to have a potential difference between the wire and the tube to generate electric field inside the electrostatic precipitator.

4.3.1.3 Dielectric Flanges

Two dielectric flanges, situated on the top and the base of the electrostatic precipitator, were used to hold both the body of the precipitator and the wire at both ends to ensure the

wire is steady and straight to form a uniform electric field. To accomplish this aim, two PVC (relative permittivity of PVC: 3.9) cylindrical components with the same size were manufactured with one located at the base of the electrostatic precipitator, and the other located at the top. The wire was fixed on the base by a screw connection and fixed on the top by banana connection. Once the wire was fixed at both ends of the electrostatic precipitator, the top of the electrostatic precipitator was fixed using six screws. There was one gas inlet on the top of the electrostatic precipitator connected by a 12 mm push-in air hose connector, and there was one gas outlet on the base of the electrostatic precipitator connected by a 12 mm push-in air hose connector. There was also one electric connection on the top of the electrostatic precipitator which was used to connect with the high voltage supply to the wire to ensure the wire had a high electric potential.

4.3.2 Coaxial Electrostatic Precipitator Design Details

The detailed design of the electrostatic precipitator is shown in Figure 4-1.

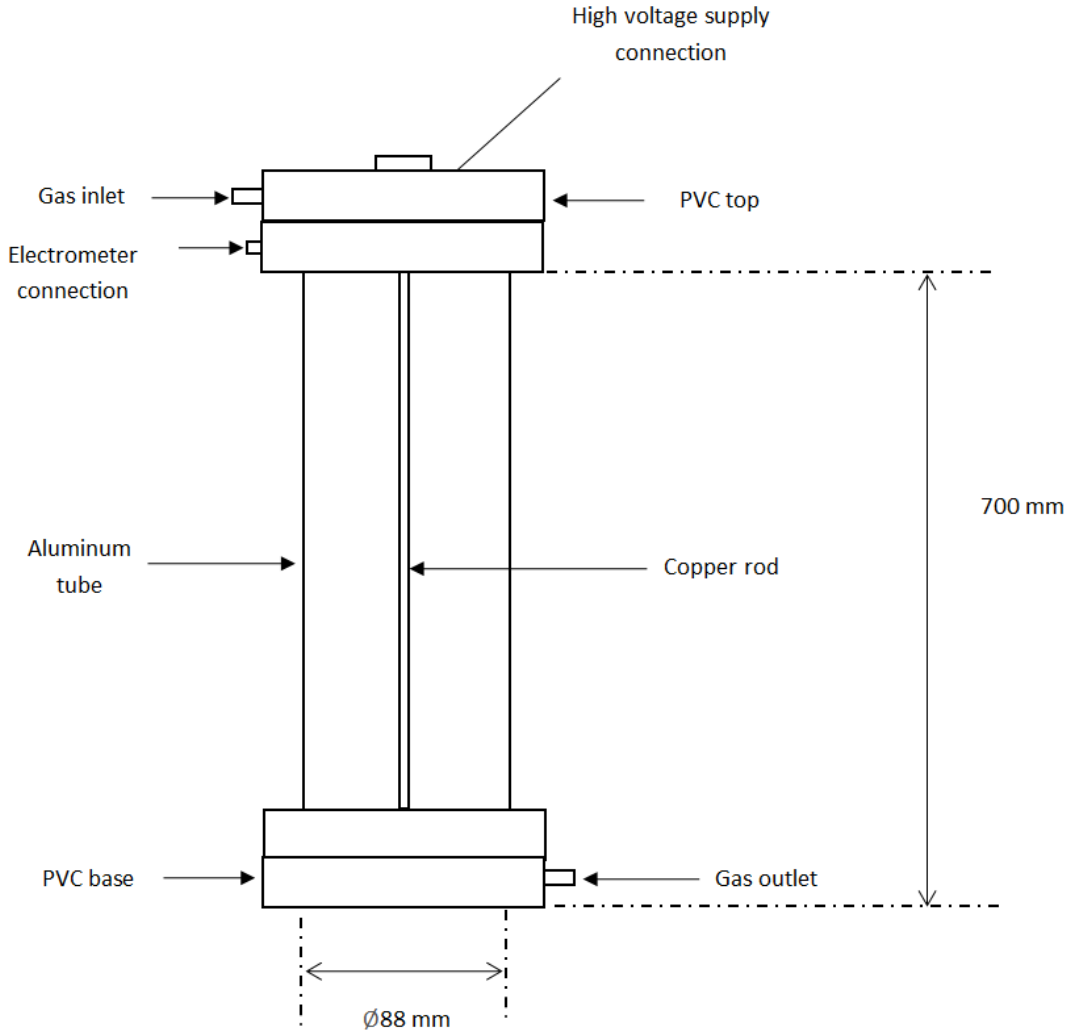

Figure 4-1. Detailed design of the coaxial electrostatic precipitator.

Figure 4-1 shows the detailed design of the coaxial electrostatic precipitator. The working range of the electrostatic precipitators with different types of electrodes has been tested by conducting straight forward breakdown tests (with indoor particles) for at least five runs of the system, with the results shown in Table 4-1.

Table 4-1. Working range of the coaxial topology electrostatic precipitator with different electrodes.

Central electrode type	Copper rod (Ø 5mm)		Stainless steel wire (Ø 1mm)	
Energisation polarity	Positive	Negative	Positive	Negative
Corona ignition voltage (kV)	20±0.4	-14±0.3	16±0.3	-9±0.1
Breakdown voltage (kV)	26±0.5	-27±0.4	22±0.4	-23±0.3

4.3.3 Humidifier

In order to investigate the influence of humidity on particle precipitation in the electrostatic precipitation system, it is important to create an environment with increased humidity. Therefore, a humidifier was used in the system to increase the humidity level. A humidifier is a device for converting water into water vapour to increase the humidity in a certain environment. The humidifier used in the system is a Challenge 3.2 Litre Ultrasonic Humidifier (as shown in Figure 4-2). This humidifier uses ultrasonic humidification to release water particles out of the humidifier. It has a quiet operation and the vapour capacity is up to 250ml per hour. The humidifier's intensity of water vapour can also be configured to suit and, in this instance, the relative humidity used for tests was 90%.

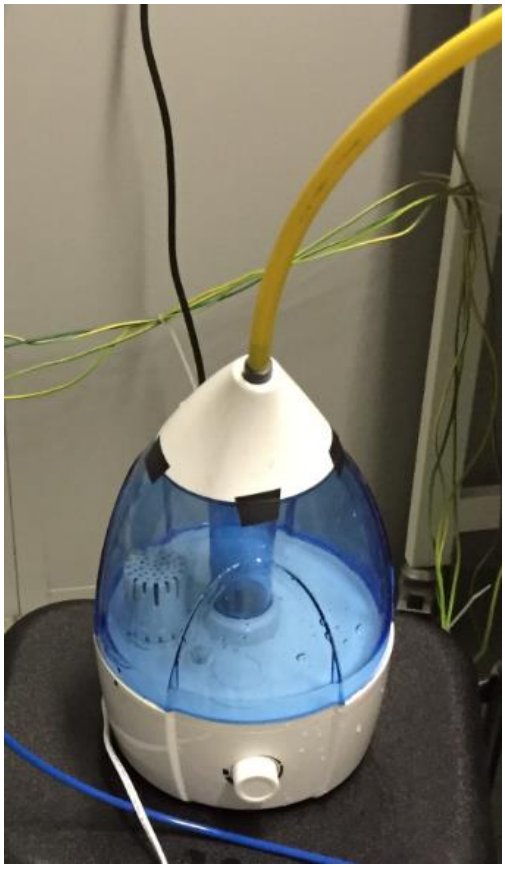

Figure 4-2. Humidifier with a hose connected to the precipitation system.

Since the humidifier is designed to be used in daily life, some changes are required to guide the water vapour into the electrostatic precipitation system while the humidifier was applied in the laboratory. Therefore, a gas adaptor was manufactured to connect the gas outlet of the humidifier and the 12 mm air hose.

4.3.4 Air Flow Mixer

The influence of the increased humidity of air on the particle precipitation efficiency was investigated by conducting precipitation tests both with and without the injection of water vapour into the air flow. In order to conduct tests with increased humidity of air, the water vapour generated by the humidifier should be mixed with the air contaminated with particles. Therefore, a mixing tube has been designed and manufactured to mix the two.

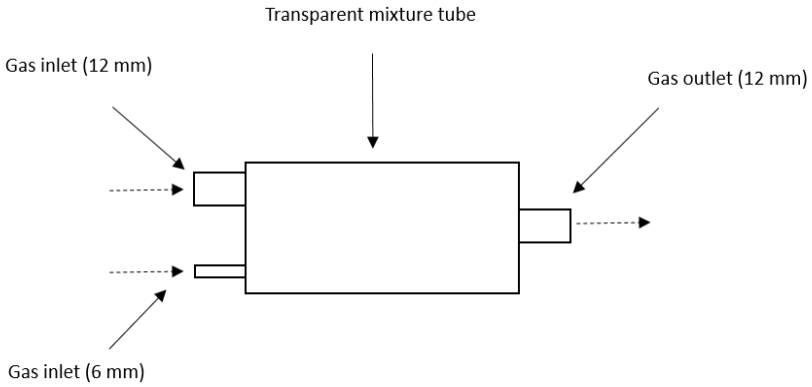

Figure 4-3. Design of mixture tube.

Figure 4-3 shows the design of the mixture tube. During tests, the water vapour was pumped into the tube through the 12 mm gas inlet and the polluted gas was pumped into the tube through the 6 mm gas inlet. The tube was made of transparent plastic, so the inside environment was visually available which makes the judgement of the existence of water vapour in the electrostatic precipitation system easier. The mixture of water vapour and pollution gas was guided out of the mixture tube by the 12 mm gas outlet.

4.4 Experimental Setup

The electrostatic precipitation experimental system for a single stage was designed and the block diagram of the precipitation system is shown in Figure 4-4.

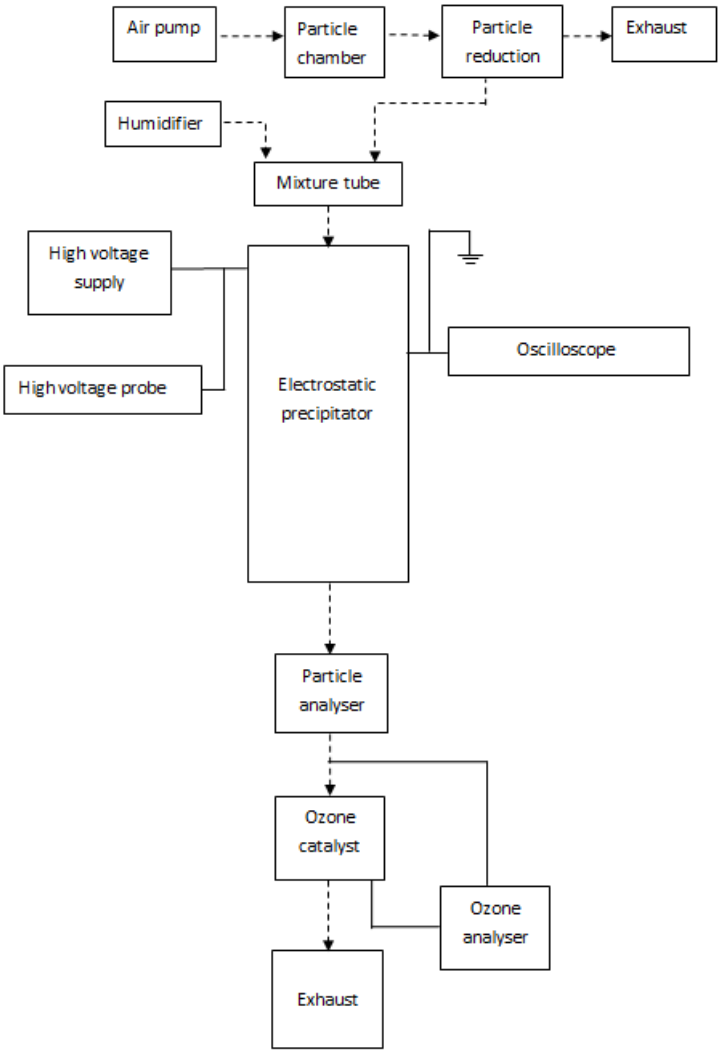

Figure 4-4. Experimental setup of coaxial electrostatic precipitation system (single stage).

Figure 4-4 shows the experimental setup of the coaxial electrostatic precipitation system for a single stage. From the gas flow aspect, similar to the needle-mesh electrostatic precipitation system developed in Chapter 3, particles were generated in the particle chamber and then pumped out of the by an air pump. The particle number can be reduced when particle concentration was high enough to cause saturation of the particle analyser. The reduction ratio can be 1/4, 1/2 or 3/4. The reduced gas was pumped into the exhaust to prevent pollution. In the instance when the humidifier was required, the gas generated by the particle chamber was guided into the mixture tube. The water vapour generated by the

humidifier was also guided into the mixture tube. The water vapour and the gas were mixed in the tube and guided into the coaxial electrostatic precipitator. The polluted gas mixture passed through the electrostatic precipitator where particle charging and particle precipitation occurred. Theoretically, particles and most water droplets can be removed and collected by the electrostatic precipitator. The remaining gas from the electrostatic precipitator was guided into the particle analyser for analysis. Ozone concentration in the air discharged from the precipitation system was monitored using the ozone analyser and there was also an ozone catalyst tube used to prevent excessive ozone being delivered into the atmosphere. After the ozone catalyst, the treated gas was guided into the exhaust.

The high voltage DC supply (Glassman HV DC supply) was connected to the HV central electrode of the coaxial electrostatic precipitator (the central copper rod of the electrostatic precipitator) through the electric connection on the electrostatic precipitator. Ionisation took place in the narrow ionisation region located around the central energised rod. The HV DC supply which was used in the tests provided both positive and negative energisation and the high voltage level was monitored by the high voltage probe, TES TEC HVP 40 (40 kV DC probe). The electrostatic precipitator was grounded through the grounding connection and the grounding provided a low potential of the outer aluminium cylindrical tube of the electrostatic precipitator. Since the central copper rod applied with high voltage was a high potential, the electric field was formed by the potential difference between the rod and the cylindrical tube. An oscilloscope (Tektronix TDS 2024) was connected to the electrostatic precipitator to monitor the current during tests. The current can be obtained by measuring the voltage from the oscilloscope over a 1000 Ω current viewing resistor which was connected to the electrostatic precipitator.

4.5 Experimental Procedures

Electrostatic precipitation tests have been conducted using the cylindrical system energised with DC high voltage of both polarities. Full experiment procedures are introduced in this section.

4.5.1 Test Preparation

4.5.1.1 Test System Components

The test system has been prepared and all components have been connected. When certain type of energisation polarity was needed for tests, the high voltage power module was switched before tests. The power supply and the ground were all connected to the electrostatic precipitation system through the high voltage connection and ground connection respectively. The voltage level was monitored by the high voltage probe (TES TEC HVP 40) connected to the digital multimeter, and the current during tests was monitored by the oscilloscope. The probe and the oscilloscope Tektronix TDS 2024 with bandwidth of 200 MHz and sampling rate of 2 GS/s were connected to the system before tests.

From a gas flow aspect, the air pump was connected to the particle chamber. Subsequently, the particle chamber was connected to the mixture tube (when increased humidity was needed) then connected to the gas inlet of the electrostatic precipitator. Finally, the gas flow was guided into the particle analyser. For indoor particles, and bee wax candle particles, since the particle concentration was not high, particle reduction was not used. For cigarette smoke particles, particle reduction was used to prevent particle analyser from saturation. The reduction ratio used in these tests was 25%. The 75% reduced gas and particles were guided into the exhaust with the fan switched on continuously.

4.5.1.2 Airborne Particles Used in the Tests

Particle preparation should be conducted before tests. Three types of particles were used for the tests of coaxial topology electrostatic precipitation system: indoor particles, bee wax candle particles and cigarette smoke particles.

For indoor particles, the particles can be taken from the ambient environment in the high voltage laboratory, so the particles were pumped into the electrostatic precipitation system directly during tests. As discussed in Chapter 3, the untreated initial particle number for indoor particles is between 8000 and 9000 counts/litre for the smallest particle diameter channel (0.265 μm). The largest particles for ambient air in the laboratory are in the 0.750 μm channel, which are around 100 counts/litre. From a particle mass aspect, the untreated initial particle mass for PM10, PM2.5 and PM1 are similar at approximately 1 $\mu g/m^3$.

For bee wax candle particles, the particles were due to the burning candle located at the centre bottom of the particle chamber and were pumped into the system by the air pump during tests. When the particle number and particle mass were stable at the maximum value observed from the particle analyser, the candle particles were ready for particle precipitation tests. As discussed in Chapter 3, the untreated initial particle number of bee wax candles is ~20,000 counts/litre for the smallest particle diameter channel (0.265 μm). The largest particles for candles in the laboratory are in the 0.750 μm channel, which are ~100 counts/litre. From a particle mass aspect, the untreated initial particle mass for PM10, PM2.5 and PM1 are also similar, at approximately between 3 to 4 $\mu g/m^3$.

For cigarette smoke particles, the particles were due to the burning cigarette located at the bottom of the particle chamber and were pumped into the system by the air pump during tests. When the particle number and particle mass were stable at the maximum value observed from the particle analyser, the cigarette smoke particles were ready for particle precipitation tests. As discussed in Chapter 3, the initial untreated particle number for

cigarette smoke particles could be recorded from the smallest particle diameter channel (0.265 µm), which is 8×10^5 to 9×10^5 counts/litre, up to the 2.75 µm channel, which is 0 to 200 counts/litre. From a particle mass aspect, the untreated initial particle mass for PM10, PM2.5 and PM1 are also similar, which can be over 500 $\mu g/m^3$.

The indoor particles, candle particles and cigarette smoke particles which have been used for electrostatic precipitation tests have been discussed and summerised in Section 3.4.5.

Street airborne particles were not used in the precipitation tests with a coaxial topology electrostatic precipitator. According to the design of particle collection and releasing system, as discussed in Section 3.2.2.1, the total volume of gas was limited to a low value due to the difficulty of collection and the limited volume of the balloon. Since the coaxial topology electrostatic precipitator aimed to be used in a larger scale system, the volume of single balloon was insufficient to meet the requirements. There was another thought to use several balloons in parallel. In this case the balloons needed to be replaced during tests, however, the results on the particle analyser will be influenced manually during the process of replacing balloons. Therefore, due to the experimental limitations, street airborne particles were not used in the tests with a coaxial topology electrostatic precipitation system.

4.5.1.3 Air Flow with Increased Humidity

During the tests with increased air humidity, the humidifier was switched on and connected to the gas inlet of the mixture tube. The intensity of the humidifier was selected in such way as to ensure that sufficient water vapour is injected into the electrostatic precipitation system to increase the relative humidity of air up to 90% and, at the same time, ensure the optimal amount of water droplets are generated to prevent the air hose from being blocked. It is assumed that the gas flow of the humidifier does not affect the gas flow rate of the system.

4.5.2 Test Procedures

During the precipitation tests, the experiments were conducted in the following procedures:

For indoor particles, bee wax candle particles and cigarette smoke particles, the air pump was switched on first, then the candles and cigarettes were ignited and the air flow was pumped through the particle chamber and injected into non-energised precipitator and the particle analyser. When particle number and particle mass were observed to be stable at their maximum values from the particle analyser, the precipitation tests could commence.

For the tests with the increased humidity, the humidifier was switched on after airborne particles were generated.

When the particle number and particle mass were stable at their maximum values, the high voltage DC supply was applied to the central electrode and the system was energised. The applied voltage and the maximum current which the HV DC system can deliver were regulated directly using the high voltage supply control panel. The high voltage level can be read on the multimeter connected to the HV DC probe, and the current which the HV DC supply delivers to the precipitation system can be obtained through the oscilloscope over the shunt.

During the precipitation tests, electrical parameters and electrostatic precipitation results were recorded by the software of the particle analyser which was transferred to Excel for data processing.

Following the precipitation tests, the precipitation system was de-energised. For candle particles and cigarette smoke particles, the air pump remained on after the tests for a few minutes to remove remaining particles in the smoke chamber into the exhaust to prevent pollution in the laboratory.

4.6 Results of Precipitation Tests: Coaxial Topology Electrostatic Precipitation System

This section discusses the results of electrostatic precipitation tests in the single stage coaxial precipitation system. The performance of the single coaxial electrostatic precipitation system is assessed by precipitation of indoor particles, bee wax candle particles and cigarette smoke particles (31% relative humidity).

Similar to the analysis of results in Chapter 3, the precipitation tests results were based on at least five individual tests. In order to present the performance of the precipitation system better, both particle number reduction ratio and particle mass as a function of time are also included for analysis (The calculation of particle reduction ratio has been discussed in Section 3.6.2.). Therefore, one typical particle number reduction ratio result and one typical particle mass result are selected and presented as a figure, and the average result is presented as a table after each figure.

4.6.1 Indoor Particles

For indoor particles, voltage levels used for both positive and negative DC energisation were just above the corona ignition voltage, which were 20.79 kV and -14.37 kV respectively.

4.6.1.1 Positive Energisation

Figure 4-5 shows the reduction ratio for indoor particles as a function of time for different particle sizes under positive energisation.

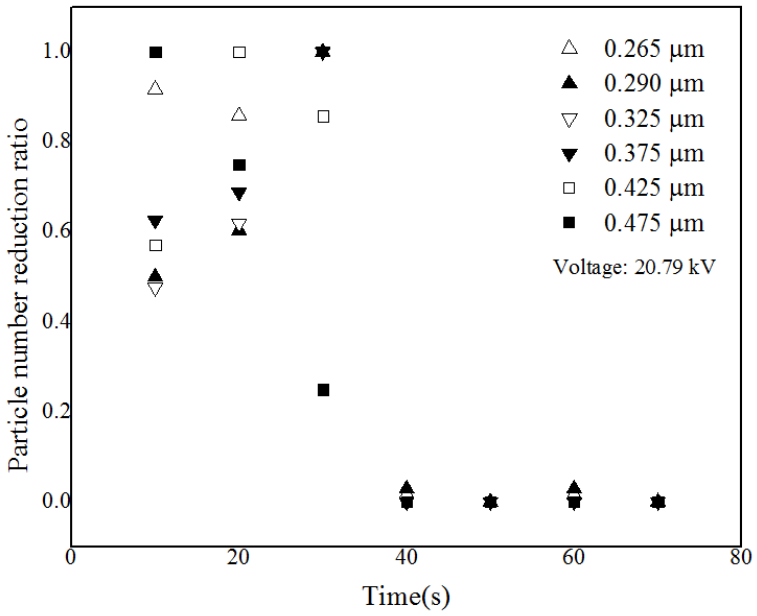

Figure 4-5. Indoor particle number reduction ratio as a function of time for different particle sizes under positive energisation.

Figure 4-5 clearly shows that the coaxial precipitation system reduces particle number to ~ 0 for all particle sizes. The particle precipitation process occurs when a high voltage was applied (at 30 seconds) at a voltage level of 20.79 kV and the process was completed within 10 seconds, then, the particle number was stabilised. Since the particle source was from ambient air which was the clean environment of a high voltage laboratory, the particle number for particles with a diameter larger than 0.475 µm was low. Therefore, only small size particle numbers are shown.

Table 4-2. Average particle number reduction ratio for different particle sizes. (Positive energisation, indoor particles)

Particle size (μm)	0.265	0.29	0.325	0.375	0.425	0.475
Average η_r	0.67± 0.28	1.18± 0.44	0	0	0	0

Table 4-2 shows the average reduction ratio for the indoor particle number for different particle sizes with positive energisation. The table shows that the particle number was reduced down to ~0 after high voltage treatment for particle sizes listed in the table. Particles with a diameter larger than 0.475μm were reduced to zero after high voltage treatment.

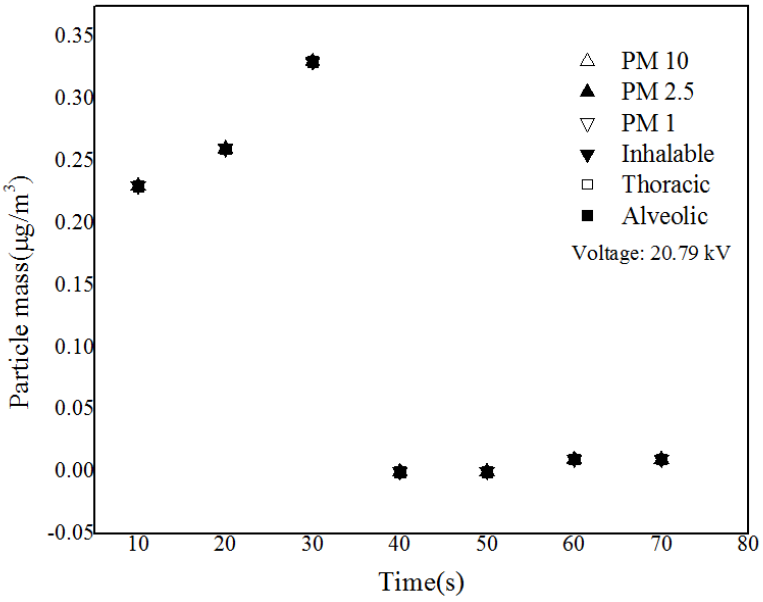

Figure 4-6. Indoor particle mass as a function of time for different particle sizes under positive energisation.

Figure 4-6 shows indoor particle mass as a function of precipitation time for different particle sizes under positive energisation. Similar to the tendency of particle number ratio, the indoor particle mass was reduced when a high voltage is applied. The particle precipitation process was completed within 10 seconds then the particle number stabilised. The result shows that ~0 μg/m^3 particles were detected at the outlet of the precipitator by the particle analyser.

The particle number reduction ratio figure and particle mass figure show that the coaxial topology electrostatic precipitation system was capable of efficiently precipitating ambient airborne particles in indoor environment.

Table 4-3. Average particle mass after treatment for different particle sizes. (Positive energisation, indoor particles)

Particle size	PM10	PM2.5	PM1	Inhalable	Alveolic	Thoracic
Average particle mass after treatment (μg/m^3)	4×10^{-3} $\pm4.9\times10^{-4}$	4×10^{-3} $\pm4.9\times10^{-4}$	4×10^{-3} $\pm4.9\times10^{-4}$	4×10^{-3} $\pm4.9\times10^{-4}$	4×10^{-3} $\pm4.9\times10^{-4}$	4×10^{-3} $\pm4.9\times10^{-4}$

Table 4-3 shows the average indoor particle mass following the HV treatment and electric field treatment for different particle sizes for positive energisation. The table shows that particle mass for different sized particles was reduced to 0μg/m^3 after the HV treatment.

4.6.1.2 Negative Energisation

Figure 4-7 shows the reduction ratio of indoor particle number as a function of time for different particle sizes under negative energisation.

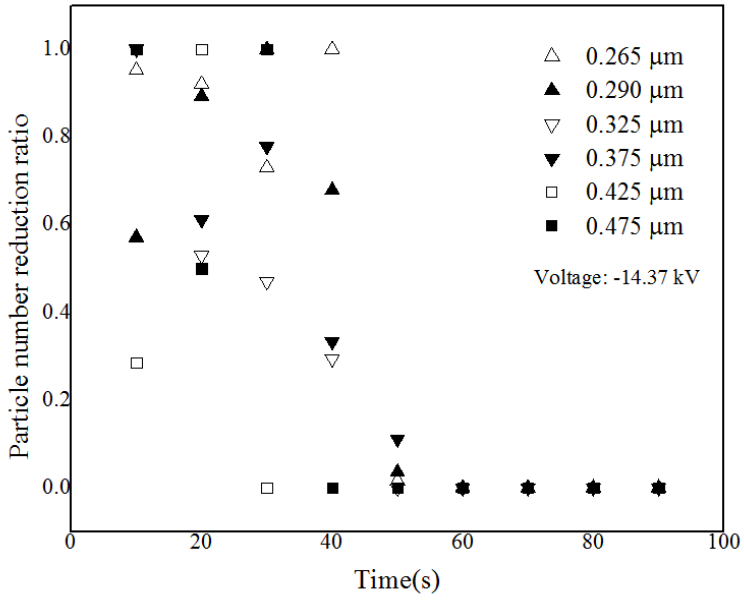

Figure 4-7. Indoor particle number reduction ratio as a function of time for different particle sizes under negative energisation.

Similar to the case of positive energisation, from Figure 4-7, it is clear that the particle number was reduced to ~0 for particles of different sizes. The particle precipitation process happens when high voltage was applied (40 seconds) at a voltage level of -14.37 kV. The process was then stabilised within 20 seconds.

Table 4-4. Average particle number reduction ratio for different particle sizes. (Negative energisation, indoor particles)

Particle size (µm)	0.265	0.29	0.325	0.375	0.425	0.475
Average η_r	0.32±0.03	0.71±0.43	0	0	0	0

Table 4-4 shows the average reduction ratio of indoor particle numbers for different particle sizes under negative energisation. The table shows that particle number was reduced down to ~0 following high voltage treatment for particle sizes, as listed in the table. Particles with a diameter larger than 0.475µm were reduced to zero following high voltage treatment, however, the result is not shown in the table.

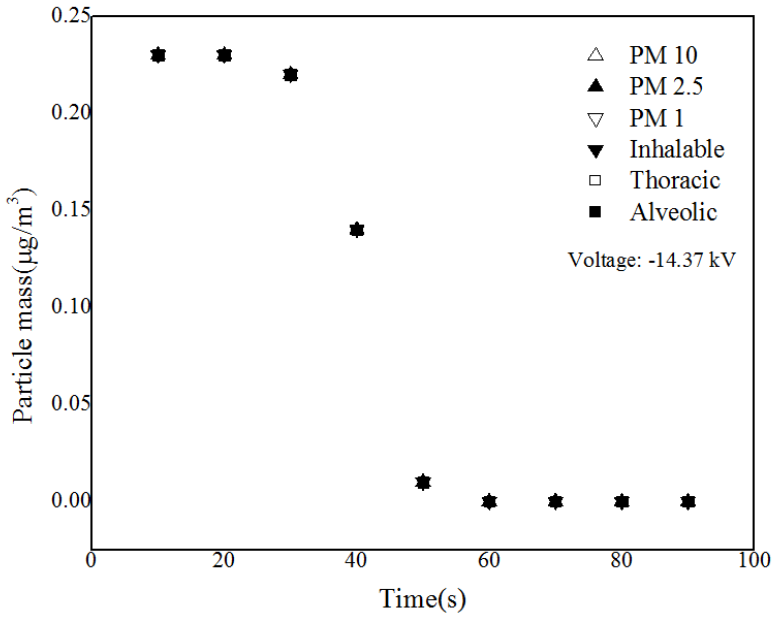

Figure 4-8. Indoor particle mass as a function of time for different particle sizes under negative energisation.

Figure 4-8 shows indoor particle mass as a function of time for different particle sizes under negative energisation. Similar to the tendency of particle mass figure under positive energisation, indoor particle mass was reduced when a high voltage was applied. The particle precipitation process was completed within 20 seconds. The result shows that ~0 $\mu g/m^3$ particles were detected by the particle analyser, which means that almost all the particles which were pumped into the system were precipitated by the system.

Table 4-5. Average particle mass after treatment for different particle sizes. (Negative energisation, indoor particles)

Particle size	PM10	PM2.5	PM1	Inhalable	Alveolic	Thoracic
Average particle mass after treatment ($\mu g/m^3$)	2×10^{-3} $\pm4\times10^{-4}$	2×10^{-3} $\pm4\times10^{-4}$	2×10^{-3} $\pm4\times10^{-4}$	2×10^{-3} $\pm4\times10^{-4}$	2×10^{-3} $\pm4\times10^{-4}$	2×10^{-3} $\pm4\times10^{-4}$

Table 4-5 shows the average indoor particle mass following HV treatment for different particle sizes for negative energisation. The table shows that particle mass for different sized of particles was reduced to ~0 $\mu g/m^3$ following high voltage treatment.

4.6.2 Candle Particles

For candle particles, the voltage used for both positive and negative DC energisation were just above the corona ignition voltage, which were 20.79 kV and -14.37 kV respectively.

4.6.2.1 Positive Energisation

Figure 4-9 shows the reduction ratio of candle particle number as a function of time for different particle sizes under positive energisation.

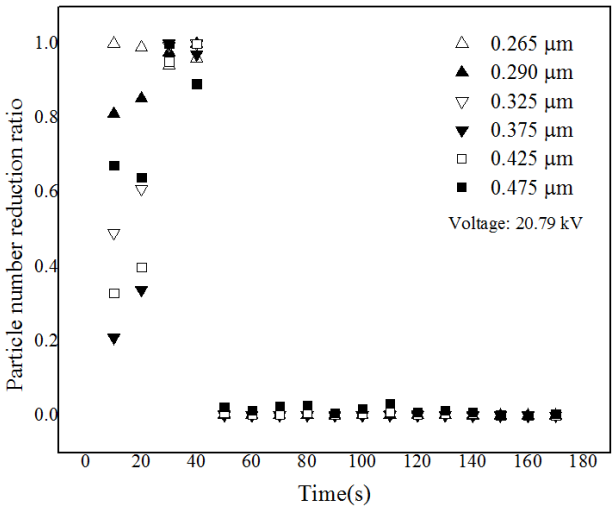

(a)

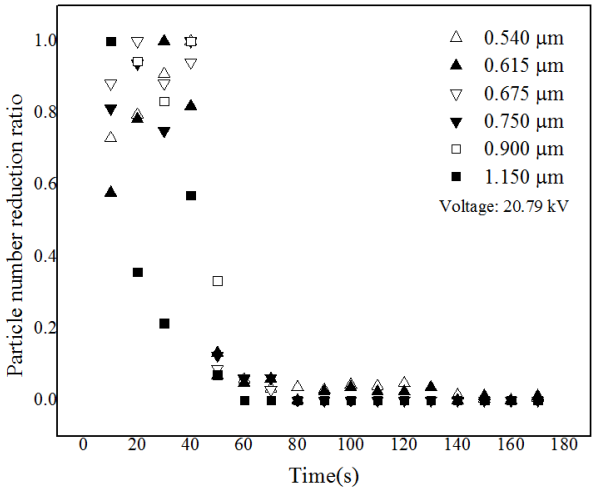

(b)

Figure 4-9. Candle particle number reduction ratio as a function of time for different particle sizes under positive energisation. (a) Smaller sizes (b)Larger sizes.

Figure 4-9 shows that the candle particle number for different sizes of particles was reduced to ~0. The particle precipitation process occurs when a high voltage was applied (40 seconds) at a voltage level of 20.79 kV. The process was stabilised within 20 seconds.

Table 4-6. Average particle number reduction ratio for different particle sizes. (Positive energisation, candle particles) (a) smaller sizes (b) larger sizes.

Particle size (μm)	0.265	0.29	0.325	0.375	0.425	0.475
Average η_r	0.05±0.03	0.03±0.02	0.03±0.02	0.06±0.05	0.26±0.22	0.06±0.05

(a)

Particle size (μm)	0.54	0.615	0.675	0.75	0.9	1.15
Average η_r	0.12±0.03	0	0	0	0	0

(b)

Table 4-6 shows the average reduction ratio of indoor particle numbers for different particle sizes under positive energisation. The table shows that particle number was reduced down to ~0 following high voltage treatment for particle sizes, as listed in the table. Particles with a diameter larger than 0.615 μm were reduced to zero following high voltage treatment.

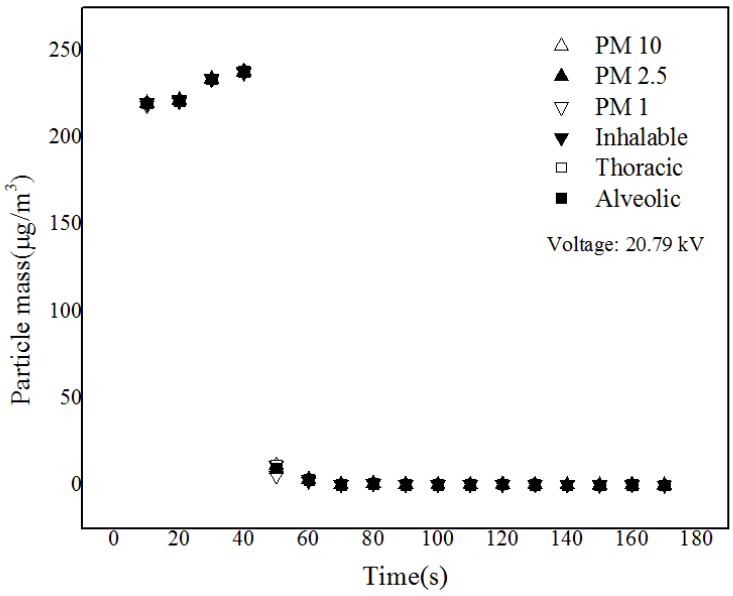

Figure 4-10. Candle particle mass as a function of time for different particle sizes under positive energisation.

Figure 4-10 shows candle particle mass as a function of time for different particle sizes under positive energisation. The figure shows that candle particle mass was reduced dramatically when high voltage was applied, and the particle precipitation process was completed within 20 seconds. The result shows that ~0 μg/m^3 particles were detected by the particle analyser.

Table 4-7. Average particle mass after treatment for different particle sizes. (Positive energisation, candle particles).

Particle size	PM10	PM2.5	PM1	Inhalable	Alveolic	Thoracic
Average particle mass after treatment (μg/m^3)	0.19 ±0.01	0.19 ±0.01	0.19 ±0.01	0.19 ±0.01	0.19 ±0.01	0.19 ±0.01

Table 4-7 shows the average candle particle mass following treatment for different particle sizes under positive energisation. The table shows that particle mass for different sizes of particles was reduced to ~0μg/m^3 following high voltage treatment.

4.6.2.2 Negative Energisation

Figure 4-11 shows the reduction ratio of candle particle number as a function of time for different particle sizes under negative energisation.

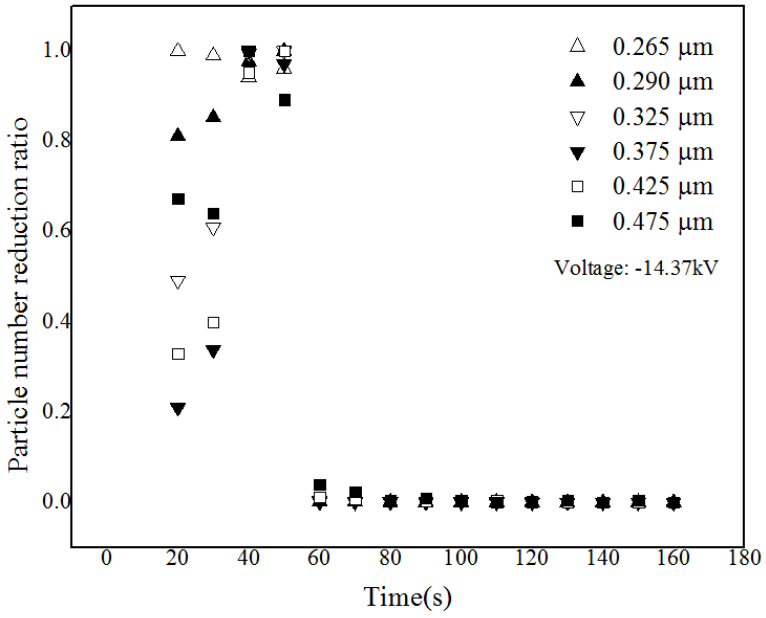

(a)

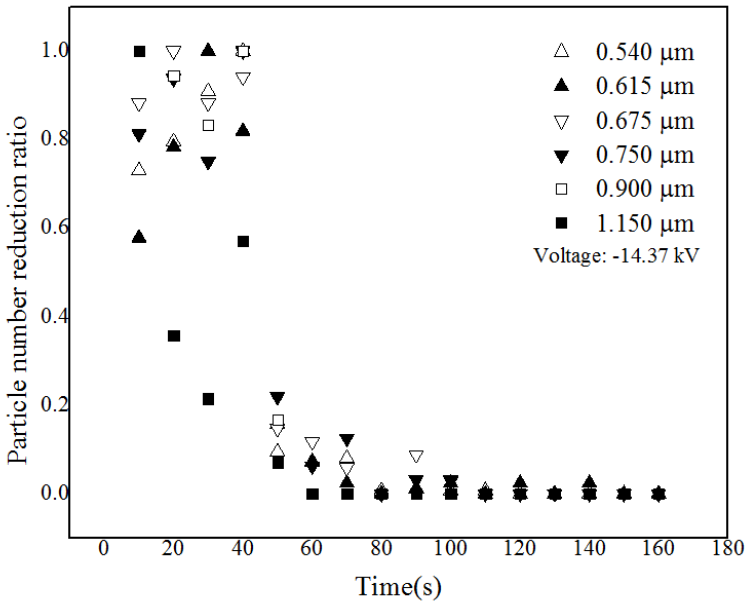

(b)

Figure 4-11. Candle particle number reduction ratio as a function of time for different particle sizes under negative energisation. (a) Smaller particles (b) Larger particles.

Figure 4-11 shows the candle particle number was reduced to ~0 for particles of different sizes. The particle precipitation process occurred when a high voltage was applied (40 seconds) at a voltage level of -14.37 kV. The process was stabilised within 30 seconds.

Table 4-8. Average particle number reduction ratio for different particle sizes. (Negative energisation, candle particles) (a) smaller sizes (b) larger sizes.

Particle size (μm)	0.265	0.29	0.325	0.375	0.425	0.475
Average η_r	6×10^{-3} $\pm5\times10^{-3}$	3×10^{-3} $\pm2\times10^{-3}$	4×10^{-3} $\pm2\times10^{-3}$	4×10^{-3} $\pm3\times10^{-3}$	6×10^{-2} $\pm2\times10^{-3}$	0

(a)

Particle size (μm)	0.54	0.615	0.675	0.75	0.9	1.15
Average η_r	0	0	0	0	0	0

(b)

Table 4-8 shows the average reduction ratio of the indoor particle number for different particle sizes under negative energisation. The table shows that the particle number was reduced down to ~0 following high voltage treatment for particle sizes, as listed in the table. Particles with diameter larger than 0.475 μm were reduced to zero following high voltage treatment.

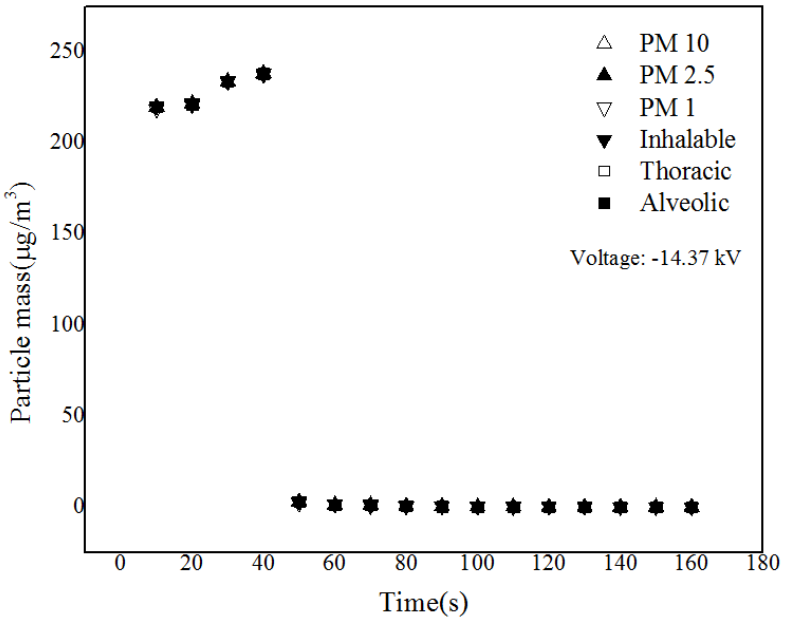

Figure 4-12. Candle particle mass as a function of time for different particle sizes under negative energisation.

Figure 4-12 shows candle particle mass as a function of time for different particle sizes under negative energisation. The figure shows that candle particle mass was reduced dramatically when a high voltage was applied, and the particle precipitation process was stabilised within 10 seconds. The result shows that ~0 μg/m^3 particles were detected by the particle analyser.

Table 4-9. Average particle mass after treatment for different particle sizes. (Negative energisation, candle particles)

Particle size	PM10	PM2.5	PM1	Inhalable	Alveolic	Thoracic
Average particle mass after treatment (μg/m^3)	0.06 ±0.05	0.06 ±0.05	0.06 ±0.05	0.06 ±0.05	0.06 ±0.05	0.06 ±0.05

Table 4-9 shows average candle particle mass following treatment for different particle sizes for negative energisation. The table shows that particle mass for different sized particles was reduced to ~0μg/m^3 following high voltage treatment.

4.6.3 Cigarette Smoke Particles

For cigarette smoke particles, the particle number and particle mass were much higher than the ambient particles and candle particles. From a particle precipitation point of view, the voltage level just above the ignition voltage was not as efficient as in the case of indoor particles and candle particles. Therefore, in order to achieve almost 100% precipitation efficiency, the voltage applied was increased up to the breakdown voltage of the electrostatic precipitator. For positive DC energisation the voltage used was 25 kV, and for negative DC energisation the voltage used was -26 kV.

4.6.3.1 Positive Energisation with Ambient Humidity

The precipitation tests were conducted using cigarette particles in air with ambient humidity (~31%). Figure 4-13 shows the results of these tests as a reduction ratio of the particle number for positive energisation of the precipitation system.

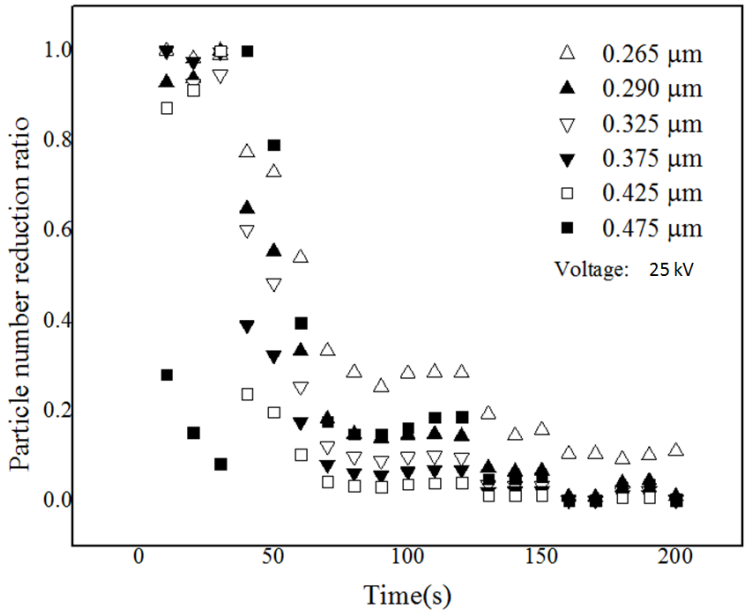

(a)

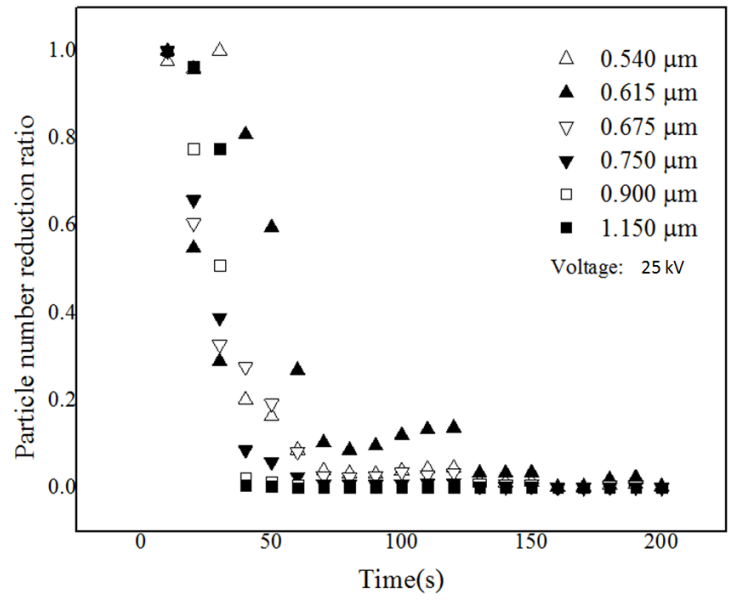

(b)

Figure 4-13. Cigarette smoke number reduction ratio as a function of time for different particle sizes under positive energisation with ambient humidity. (a) Smaller particles (b) Larger particles.

Figure 4-13 shows the reduction ratio of cigarette smoke particle number as a function of time for different particle sizes under positive energisation. The reduction ratio for particle with larger dimensions, as shown in (b), was satisfactory as ~100% removal efficiency can still be achieved. The precipitation process started at 40 seconds at a voltage level of 25 kV and took ~80 seconds to remove almost all the particles.

However, the result was different in the case of smaller particles, as shown in (a). Although the particle number was significantly reduced when a high voltage was applied, there was still ~10% of particles which cannot be precipitated by the electrostatic precipitation system. Since the voltage level used (25 kV) was just below the breakdown voltage, it was not possible to increase the precipitation efficiency further by increasing the working voltage level.

Table 4-10. Average particle number reduction ratio for different particle sizes. (Positive energisation, cigarette smoke particles) (a) smaller sizes (b) larger sizes

Particle size (μm)	0.265	0.29	0.325	0.375	0.425	0.475
Average η_r	10.29±0.60	2.29±1.62	1.04±0.94	0.60±0.57	0.35±0.33	1.56±1.54

(a)

Particle size (μm)	0.54	0.615	0.675	0.75	0.9	1.15
Average η_r	0.35±0.33	1.03±0.94	0.28±0.24	0.08±0.06	0.01±0.005	0.01±0.004

(b)

Table 4-10 shows the average cigarette smoke particle number reduction ratio for different particle sizes for positive energisation. The table shows that although the particle number was reduced significantly after high voltage treatment for particle sizes listed in the table, there were still particles which cannot be precipitated by the system, especially for smaller particles.

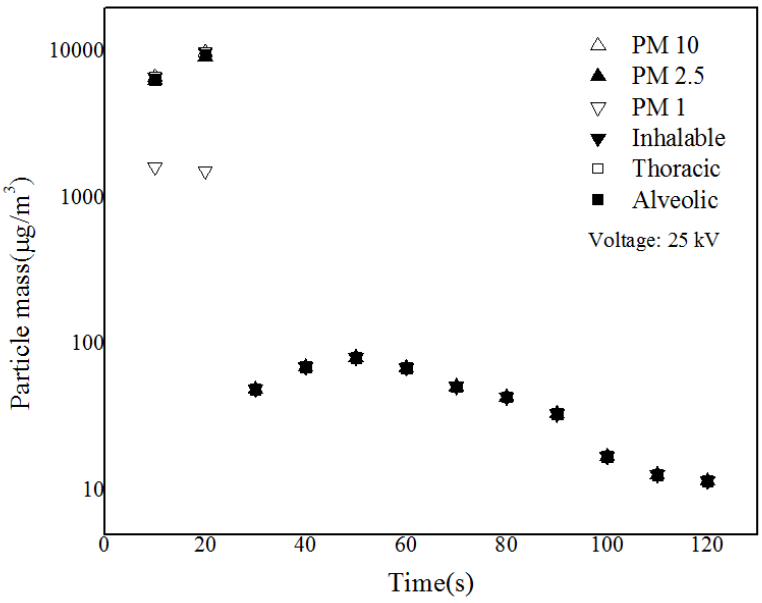

Figure 4-14. Cigarette smoke particle mass as a function of time for different particle sizes under positive energisation with ambient humidity.

Figure 4-14 shows the cigarette smoke particle mass as a function of time for different particle sizes under positive energisation. The figure shows that there was still a certain amount of particles that remained following high voltage treatment. The reason of using log scale on particle mass axis is to show the relative numbers more clearly.

Table 4-11. Average particle mass after treatment for different particle sizes. (Positive energisation, cigarette smoke particles).

Particle size	PM10	PM2.5	PM1	Inhalable	Alveolic	Thoracic
Average particle mass after treatment ($\mu g/m^3$)	14.15 ±1.94	14.15 ±1.94	14.13 ±1.94	14.15 ±1.94	14.15 ±1.94	14.15 ±1.94

Table 4-11 shows the average cigarette smoke particle mass following high voltage treatment for different particle sizes under positive energisation. The table shows that the particle precipitation result was not satisfactory since there were still particles remaining after the high voltage treatment from a particle mass aspect.

4.6.3.2 Positive Energisation with Increased Humidity

As was shown in the previous sections, in the case of air laid with particles in high concentrations (for example air with cigarette smoke particles), the single stage precipitation system did not remove 100% of particles and particle penetration has taken place. Particle penetration signifies that the smoke particles pass through the coaxial energised cylinder system without being participated. Particle penetration reflects the decrease in particle precipitation efficiency, so the system performance can be unsatisfactory. In order to prevent particle penetration in the electrostatic precipitation system and to improve the performance of the system, an increased humidity of air injected into the precipitator is considered and investigated. The relative humidity used in these tests was 90%.

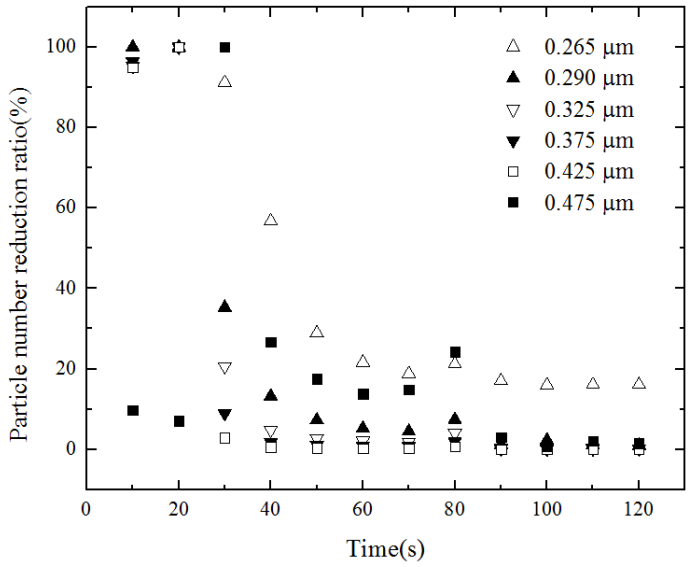

(a)

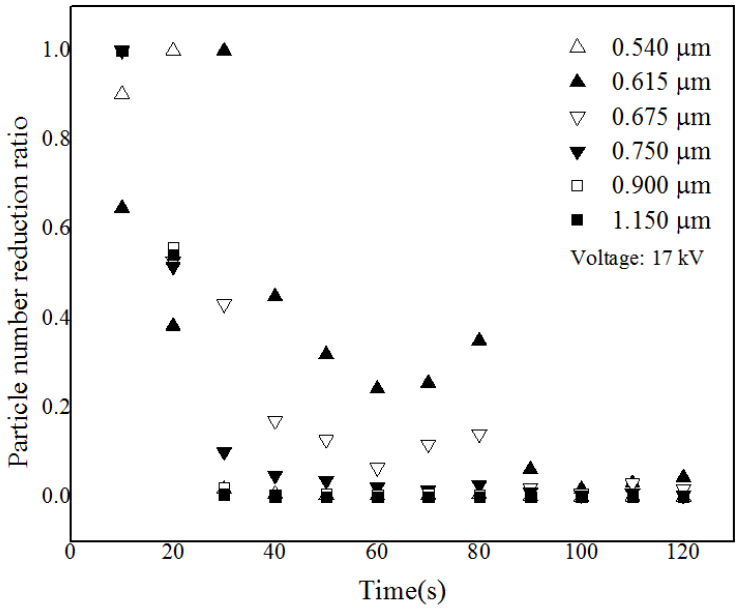

(b)

Figure 4-15. Cigarette smoke particle number reduction ratio with increased humidity as a function of time for different particle sizes under positive energisation. (a) Smaller particles (b) Larger particles.

Figure 4-15 shows the reduction ratio of the cigarette smoke particles in humid air as a function of time for different particle sizes under positive energisation. Similar to the results in air with the ambient relative humidity (rh = 31%), it was established that the electrostatic precipitation system was capable of removing almost all particles with diameters above 0.75μm within 50 seconds after application of high voltage. However, although the particle number was significantly reduced when the high voltage was applied, there was still particle penetration of the electrostatic precipitation system, as shown in the figure. The result shows that the increased humidity of air alone did not improve the precipitation efficiency when compared with precipitation tests for air without a humidifier under positive energisation. The issues of the precipitation system operation with air and increased humidity under positive energisation will be discussed in Section 4.6.3.3.

Table 4-12. Average particle number reduction ratio for different particle sizes. (Positive energisation, cigarette smoke particles, increased humidity) (a) smaller sizes (b) larger sizes.

Particle size (μm)	0.265	0.29	0.325	0.375	0.425	0.475
Average η_r	17.28±2.00	2.60±2.48	1.07±0.49	0.47±0.22	0.19±0.08	2.33±1.18

(a)

Particle size (μm)	0.54	0.615	0.675	0.75	0.9	1.15
Average η_r	0.17±0.02	3.689±1.50	2.32±1.13	1.038±0.84	0.11±0.03	0.02±0.01

(b)

Table 4-12 shows the average reduction ratio of the cigarette smoke particle number for different particle sizes in the case of air with the increased humidity under positive energisation. The table shows that although particle number was reduced significantly after high voltage treatment for all particle sizes listed in the table, there were still particles penetrating from the system, this was especially notable for smaller particles (particle diameter around 0.265µm).

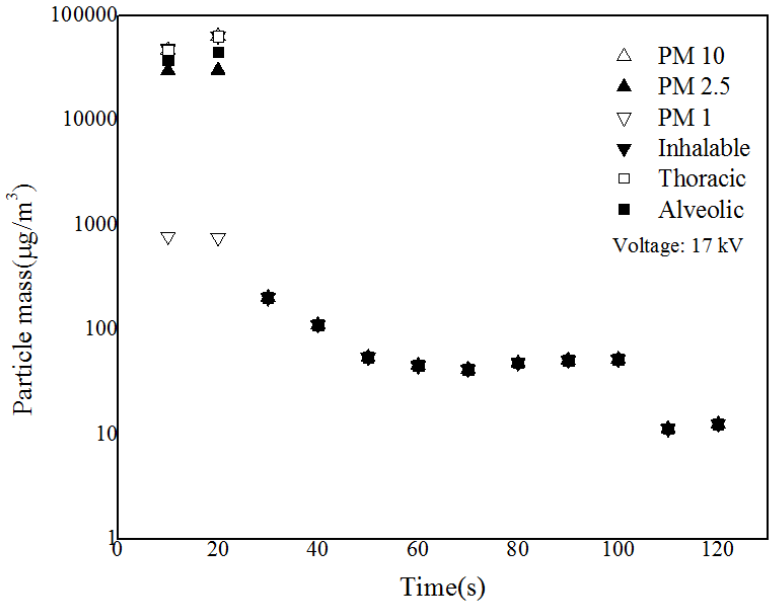

Figure 4-16. Cigarette smoke particle mass with increased humidity as a function of time for different particle sizes under positive energisation.

From a particle mass aspect, as shown in Figure 4-16, the result was similar those without a humidifier. There was still some remaining particle mass after the precipitation process, therefore, the increased humidity likewise did not improve particle mass reduction. The reason of using log scale on particle mass axis is to show the numbers more clearly.

Table 4-13. Average particle mass after treatment for different particle sizes. (Positive energisation, cigarette smoke particles, increased humidity).

Particle size	PM10	PM2.5	PM1	Inhalable	Alveolic	Thoracic
Average particle mass after treatment ($\mu g/m^3$)	11.48 ±0.80	11.48 ±0.80	11.46 ±0.80	11.48 ±0.80	11.48 ±0.80	11.48 ±0.80

Table 4-13 shows average cigarette smoke particle mass after treatment for different particle sizes for increased humidity under positive energisation. The table shows that there were still particles remaining following high voltage treatment for increased humidity under positive energisation from a particle mass aspect. The remaining particle mass without a humidifier was around 14$\mu g/m^3$ and the remaining particle mass with a humidifier was around 11$\mu g/m^3$. Therefore, it can be said that the increase of humidity did not improve particle precipitation efficiency.

4.6.3.3 Disadvantages of Positive Energisation with Increased Humidity

During the precipitation tests, some issues associated with the use of air with increased humidity in combination with positive high voltage DC energisation have been identified. These issues can influence the performance of the precipitation system to a significant degree.

First, it was found that humid air inside the electrostatic precipitator was prone to causing electrical issues (to cause undesirable spark discharge inside the precipitator) and makes it

very difficult to achieve a stable precipitation regime. When a spark breakdown occurred, the precipitation results were not satisfactory as plasma discharge is concentrated in a narrow breakdown channel and collected particles could be re-introduced into the air flow due to the shock impact caused by spark discharges.

Second, although the voltage level could be maintained at a certain value below the spark breakdown threshold, this voltage was relatively low. The low working voltage level has resulted in a lower precipitation efficiency as shown in Section 4.6.3.2.

Third, the current-time waveform was very unstable within the working voltage level range and was not able to be used for data processing. This subsequently means that the particle charging process within the precipitator was not stable which, again, could cause the reduced efficiency of precipitation.

Considering these issues associated with air with increased humidity in combination with positive energisation, this approach was abandoned in this study.

4.6.3.4 Negative Energisation with Ambient Humidity

The performance of the coaxial electrostatic precipitation system with ambient humidity of 31% was studied and the obtained results are shown in this section.

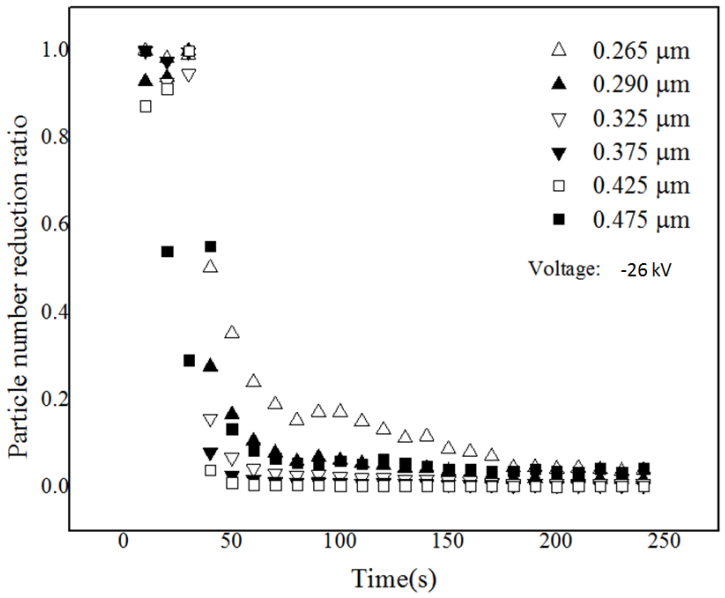

(a)

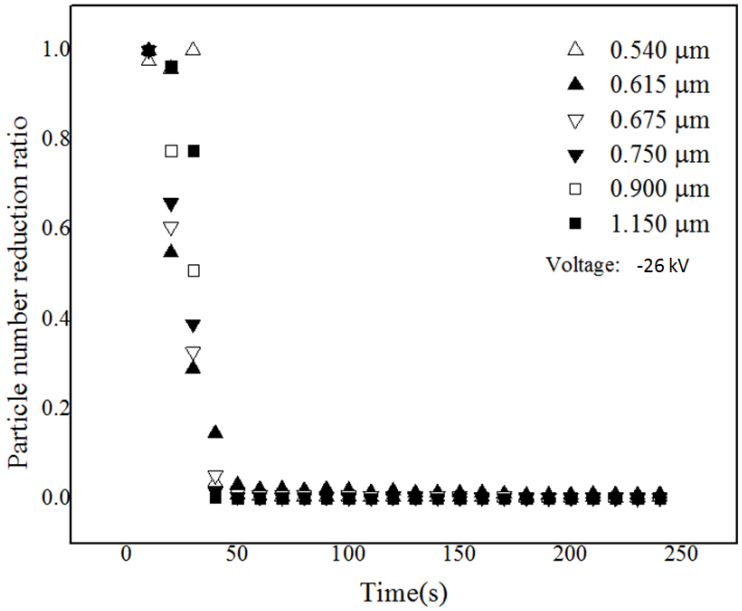

(b)

Figure 4-17. Cigarette smoke particle number reduction ratio as a function of time for larger particles under negative energisation with ambient humidity. (a) Smaller sizes (b) Larger sizes.

Figure 4-17 shows the reduction ratio of cigarette smoke particle number as a function of time for different particle sizes under negative energisation with ambient humidity (31%). From the figure, it is clear that the coaxial electrostatic precipitation system was efficient in removing large particles when a high voltage (-26 kV) was applied. The process was stabilised within 120 seconds.

However, the precipitation result for smaller particles was not satisfactory. As shown in (a), the precipitation process was slow and there was still particle penetration of the electrostatic precipitation system detected by the particle analyser.

Table 4-14. Average particle number reduction ratio for different particle sizes. (Negative energisation, cigarette smoke particles) (a) smaller sizes (b) larger sizes.

Particle size (μm)	0.265	0.29	0.325	0.375	0.425	0.475
Average η_r	4.10±0.24	1.90±0.14	0.89±0.02	0.45±0.03	0.24±0.02	3.80±0.44

(a)

Particle size (μm)	0.54	0.615	0.675	0.75	0.9	1.15
Average η_r	0.29±0.06	0.95±0.07	0.34±0.07	0.13±0.04	0.06±0.03	0.03±0.01

(b)

Table 4-14 shows the average reduction ratio of the cigarette smoke particle number for different particle sizes with negative energisation. The table shows that although particle

number was reduced significantly following high voltage treatment for particle sizes listed in the table, there were still particles penetrating from the system, especially for smaller particles.

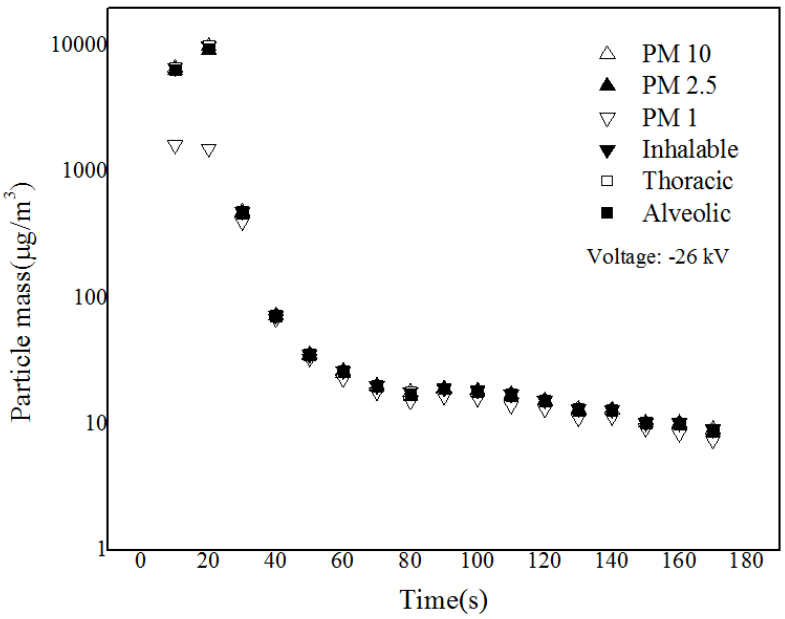

Figure 4-18. Cigarette smoke particle mass as a function of time for different particle sizes under negative energisation with ambient humidity.

From a particle mass aspect, it was clear that there was still remaining particle mass after precipitation. Since the voltage used was just below the breakdown voltage, it was impossible to increase the precipitation efficiency by increasing working voltage. The reason of using log scale on particle mass axis is to show the relative numbers more clearly.

Table 4-15. Average particle mass after treatment for different particle sizes. (Negative energisation, cigarette smoke particles)

Particle size	PM10	PM2.5	PM1	Inhalable	Alveolic	Thoracic
Average particle mass after treatment ($\mu g/m^3$)	11.14 ±1.64	10.90 ±1.67	9.55 ±1.55	11.14 ±1.64	11.14 ±1.64	11 ±1.65

Table 4-15 shows the average cigarette smoke particle mass following high voltage treatment for different particle sizes under negative energisation with ambient humidity (31%). The table shows that when particle concentration was high, there were still particles penetrating the system.

4.6.3.5 Negative Energisation with Increased Humidity

The influence of the increased humidity of air (relative humidity of 90%) on the precipitation process was investigated under negative DC energisation. The results of this study are shown in this section.

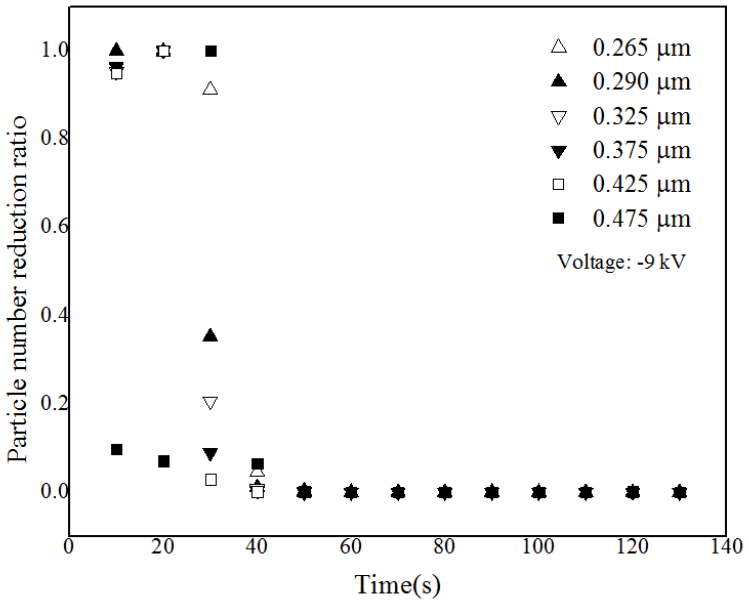

(a)

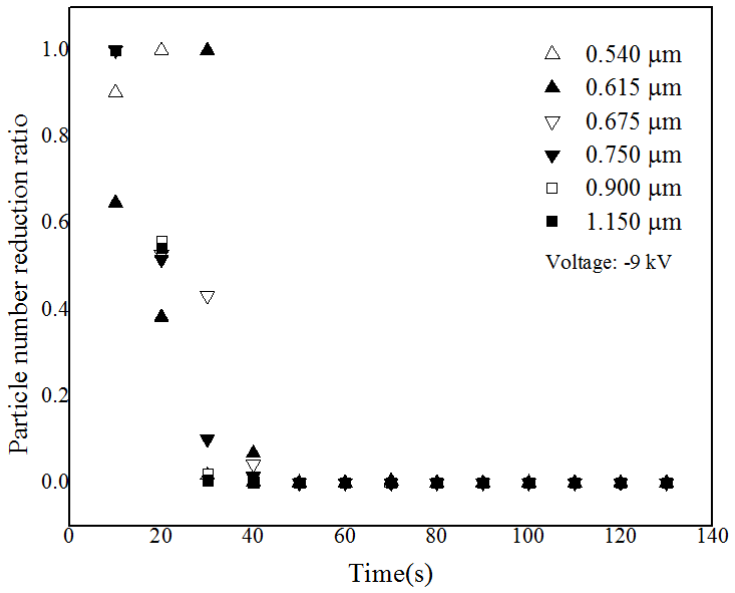

(b)

Figure 4-19. Cigarette smoke particle number reduction ratio with increased humidity as a function of time for different particle sizes under negative energisation with increased humidity. (a) Smaller particles (b) Larger particles.

Figure 4-19 shows the reduction ratio cigarette of smoke particle number with increased humidity as a function of time for different particle sizes under negative energisation. Figure (b) clearly shows that increased humidity in the electrostatic precipitation system was efficient in particle precipitation for larger particles. For smaller particles, the precipitation results improved when compared with the case of air with ambient humidity (rh 31%). Figure (a) shows the reduction ratio of cigarette smoke particles in humid air (rh 90%) as a function of time for smaller particles under negative energisation. The figure shows that the increased humidity can help remove almost all the particles and to reduce particle number down to 0% following the precipitation process. It is also worth noting that the time of the precipitation process was shortened and completed within 20 seconds. Compared with the case of air with an ambient humidity, it is clear that the increased humidity helped to significantly improve the precipitation efficiency.

Table 4-16. Average particle number reduction ratio for different particle sizes. (Negative energisation, cigarette smoke particles, increased humidity) (a) smaller sizes (b) larger sizes.

Particle size (μm)	0.265	0.29	0.325	0.375	0.425	0.475
Average η_r	0.03 ±0.02	0.01 ±0.003	0.002 ±0.001	0.001 ±0.001	0.001 ±0.001	0.05 ±0.001

(a)

Particle size (μm)	0.54	0.615	0.675	0.75	0.9	1.15
Average η_r	0.001±0.001	0	0	0	0	0

(b)

Table 4-16 shows the average reduction ratio of the cigarette smoke particle number for different particle sizes for increased humidity with negative energisation. The table shows that a ~100% reduction ratio was achieved for particles with different sizes with increased humidity.

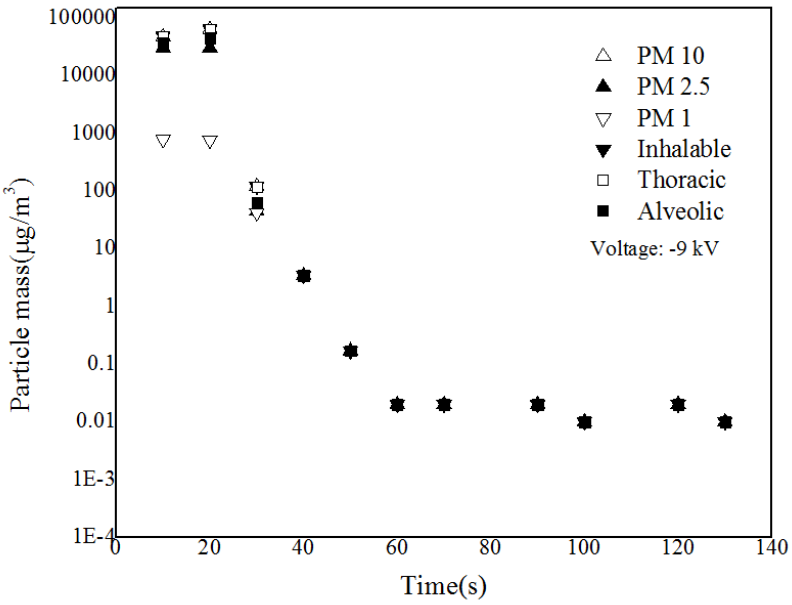

Figure 4-20. Cigarette smoke particle mass with increased humidity as a function of time for different particle sizes under negative energisation.

Figure 4-20 shows cigarette smoke particle mass with increased humidity as a function of time for different particle sizes under negative energisation. From a particle mass aspect, the result also shows that almost all particles were removed by the electrostatic precipitation system with increased humidity. It shows that increased humidity has significantly improved the precipitation efficiency. The reason of using log scale on particle mass axis is to show the relative numbers more clearly.

Table 4-17. Average particle mass after treatment for different particle sizes. (Negative energisation, cigarette smoke particles, increased humidity)

Particle size	PM10	PM2.5	PM1	Inhalable	Alveolic	Thoracic
Average particle mass after treatment ($\mu g/m^3$)	0.01 ±0.007	0.01 ±0.007	0.01 ±0.007	0.01 ±0.007	0.01 ±0.007	0.01 ±0.007

Table 4-17 shows average cigarette smoke particle mass after treatment for different particle sizes and increased humidity under negative energisation. The table shows that the system was efficient in particle precipitation for particles with different sizes.

4.6.3.6 Performance of Negative Energisation with Increased Humidity

Contrary to the case of positive energisation, it was found that the performance of the electrostatic precipitator energised with negative high voltage in combination with increased humidity of air has been improved when compared to air with ambient humidity. It was shown that 100% precipitation efficiency can be achieved for air laid with cigarette smoke particles in the case of air with increased humidity. The voltage level which was required to achieve such high precipitation performance (~100%) was much lower when compared to air with ambient humidity, -9 kV and -26 kV respectively.

It was found that, in the case of air with increased humidity, the energisation level was equal to the corona ignition voltage and was sufficient to achieve 100% precipitation efficiency. It was observed that, in this case, the current-time waveform was stable which makes the particle charging process stable and efficient (this was reflected by the high value of the

precipitation efficiency). Also, it was found that the frequency of negative high voltage DC energised current impulses in environments with an increased humidity was significantly higher when compared with the frequency of current impulses in the air with ambient humidity. The frequency of the impulses was ~5.2 kHz for -14 kV and ~13 kHz for -26 kV for discharges in air with the ambient humidity (31%), and the frequency of the impulses was ~70 kHz to -9 kV for discharges in air with the increased humidity (90%). The increased frequency of negative high voltage DC energised impulses can result in a higher delivered charge to airborne particles and to more efficient charging of the PM in air flow.

4.6.3.7 Influence of Increased Humidity on Performance of Electrostatic Precipitation

The precipitation results obtained using air with increased humidity have been presented in Section 4.6.3.3 and Section 4.6.3.6. The influence of increased humidity of air flow on the precipitation process is summarised below:

Positive energisation:

a) The magnitude of a corona ignition voltage is lowered from 20.8 kV (±0.4 kV) to 16 kV (±0.1 kV) by the influence of the increased humidity.

b) The magnitude of the breakdown voltage is lowered from 26 kV (± 0.5 KV) to 24 kV (± 0.5 kV) by the influence of the increased humidity.. At times, the breakdown voltage which was lower than 24 kV has been observed.

c) The frequency of the positive corona impulses is unstable and is very difficult for measurement.

d) The frequency of the corona current for increased humidity is significantly more intensive (increased frequency) when compared with the frequency of a corona current for ambient

humidity. This phenomenon can only be obtained visually as the frequency of positive corona impulses is unstable and very difficult to measure since it was very difficult to capture the current waveform on the oscilloscope.

e) The performance of the electrostatic precipitation system is not improved by the use of air flow with increased humidity.

Negative energisation:

a) The magnitude of the corona ignition voltage is lowered from -14.4 kV (± 0.3 kV) to -9 kV (± 0.2 kV) by the influence of the increased humidity.

b) The magnitude of the breakdown voltage is lowered from -27 kV (± 0.4 kV) to -23 kV (± 0.4 kV) by the influence of the increased humidity. The breakdown voltage for the increased humidity environment is stable.

c) The frequency of the corona current is much higher for increased humidity when compared with the frequency of the corona current for ambient humidity. For the corona ignition voltage, the frequency increases from 5.2 kHz (± 2.5 kHz) (-14.4 kV normal humidity) to 66 kHz (± 20 kHz) (-9 kV increased humidity). Compared to the case of increased humidity with positive energisation when current waveform was not measureable, this 20 kHz standard deviation was acceptable.

d) The performance of the electrostatic precipitation system is improved by the use of air flow with increased humidity. In the case of air with increased humidity, 100% precipitation efficiency has been achieved for all types of particles. The applied voltage level is -9 kV which is much lower than -14.37 kV that is required to achieve 100% precipitation efficiency using air flow with ambient humidity for cigarette smoke particles i.e. the particle with the highest particle concentration.

4.7 Double Stage Electrostatic Precipitation System

4.7.1 Motivations of the development of the Double Stage Electrostatic Precipitation System

The precipitation results obtained with the single coaxial stage electrostatic precipitation system were satisfactory when particle concentration was not high. When the particle concentration was high, the precipitation efficiency reduced significantly. The increased humidity has been proven to be an effective way to increase the precipitation efficiency under negative energisation. However, in the environment where such increased humidity of air (or other gas) is unachievable or not allowed, the precipitation system should be improved to meet the practical demands on precipitation efficiency. One of the potential improvements could be the introduction of an additional precipitation stage i.e. the development of a double stage electrostatic precipitation system.

4.7.2 Design of the Double Stage Electrostatic Precipitation System

The double stage electrostatic precipitation system is two coaxial electrostatic precipitators connected in series. The detailed design of the system is shown in Figure 4-21.

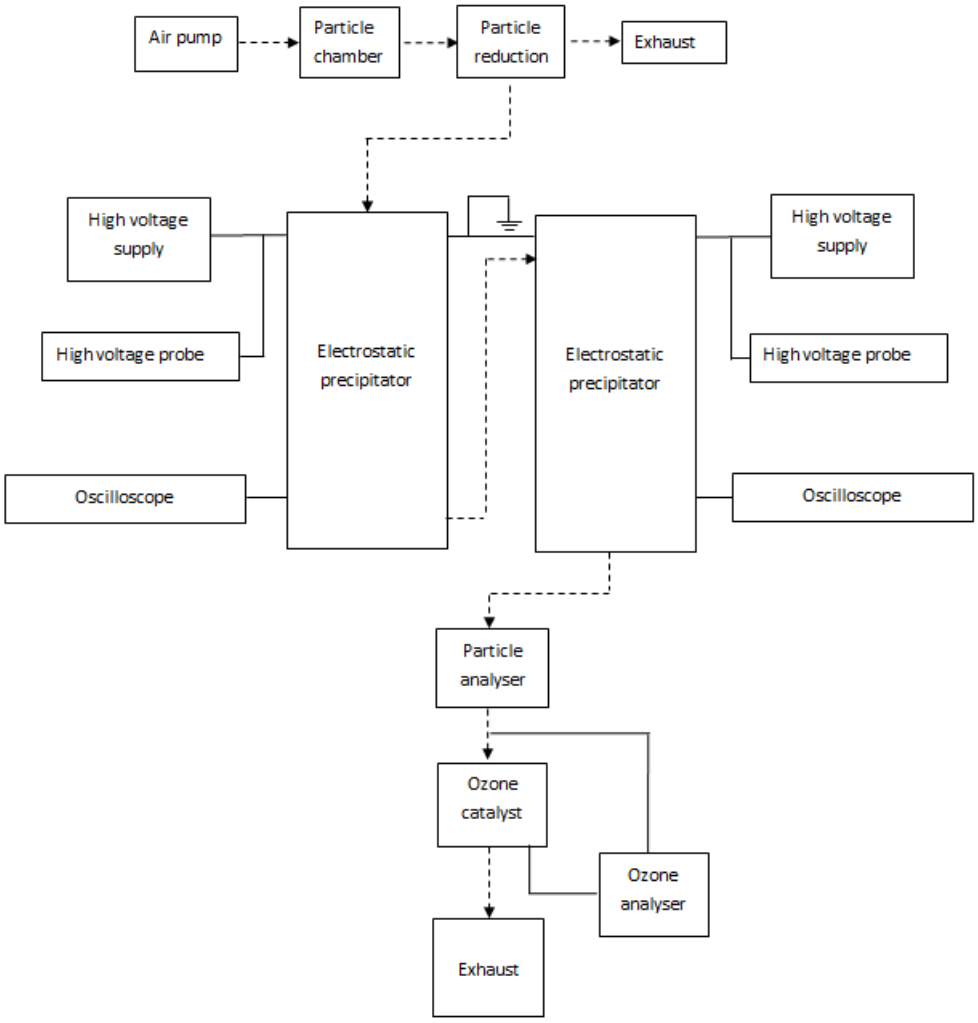

Figure 4-21. Detailed design of the double stage electrostatic precipitation system.

Figure 4-21 shows the detailed design of the double stage electrostatic precipitation system. The design of each stage of this system was the same as the design of the single stage coaxial electrostatic precipitation used in Section 4.3.2. Each stage was composed of one coaxial cylindrical precipitator, where the first stage was identical in dimensions to the single stage described in Section 4.3.2, Figure 4-1. However, the HV electrode in the second stage was made of stainless steel wire with a diameter of 1 mm instead of the copper rod with a diameter of 5 mm used as in the first stage.

The air flow laid with aerosol particles was pumped into the system and was delivered into the first precipitation stage through the gas inlet. Then, after charging and initial precipitation, the air flow with residual airborne particles is delivered into the second stage of the precipitation system where the precipitation process can continue to occur under the action of the electric field in this second stage. Particle precipitation can take place at both electrostatic precipitators.

High voltage DC supplies (Glassman) were connected to both high voltage electrodes in the first and second stages of the precipitator system. The high voltage was applied to the central HV electrodes of both stages (copper rod and wire). As in the case of the single stage, ionisation can take place in the area around the central HV electrodes. The high voltage level was monitored with the high voltage probe (TES TEK HVP-40) and a digital multimeter. The external cylinders of both stages were connected to oscilloscope (Tektronix TDS 2024) which can provide a virtual ground and allow current monitoring for both stages of the precipitation system. The current can be obtained by measuring the voltage from the oscilloscope over a 1000 Ω current viewing resistor which was connected to the electrostatic precipitator.

4.7.3 Experimental Procedures

The conducted precipitation tests using the double stage system followed the experimental procedures as described in Section 4.5 for the single stage precipitation system, with only one difference; the humidifier was not used in these experiments with the double stage system. Thus, the results obtained using the double stage system will be compared with the precipitation results obtained in the single stage using air with ambient humidity rh 31%).

During the tests, the working voltage was selected to be above the voltage of both stages of electrostatic precipitators to provide the corona ignition voltage for both precipitators. The working range of the electrostatic precipitators has been discussed in Section 4.3.2. The

working range of the first stage precipitator was from 20 kV (±0.4 kV) to 26 kV (±0.5 kV) for positive energisation and -14 kV (±0.3 kV) to -27 kV (±0.4 kV) for negative energisation. The working range of the second stage precipitator was from 16 kV (±0.3 kV) to 22 kV (±0.4 kV) for positive energisation and -9 kV (±0.1 kV) to -23 kV (±0.3 kV) for negative energisation. The experiments were conducted using both positive and negative DC high voltage energisations.

4.7.4 Results of the Double Stage Electrostatic Precipitation System

The particle precipitation results for a double stage system are discussed in this section. Previous results show that the indoor particles and bee wax candle particles can be perfectly precipitated by the single stage system with 100% precipitation efficiency. The particle precipitation efficiency for cigarette smoke particles cannot reach 100% due to the high concentration of cigarette smoke particles. Therefore, the design of double stage system aims to improve the performance of the system for cigarette smoke particle precipitation. In this section, the particle precipitation results of double stage system are compared with single stage system for cigarette smoke particles with both positive energisation and negative energisation.

4.7.4.1 Positive Energisation

For positive energisation with a double stage system, the voltage level applied to the system was 20.29 kV. This voltage level was above the corona ignition voltage for both first and second stage.

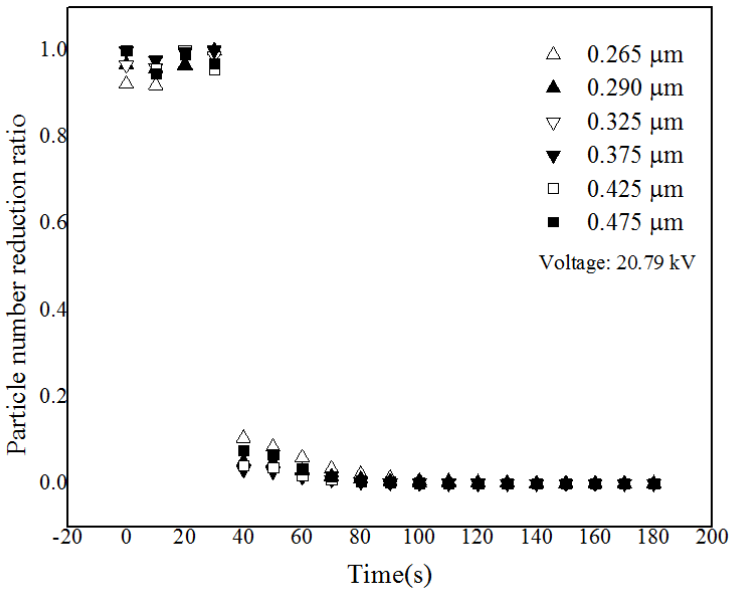

(a)

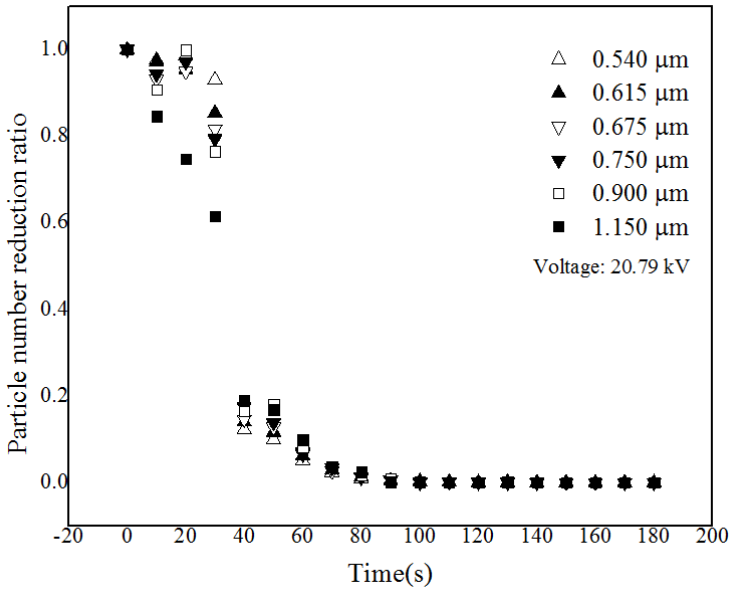

(b)

Figure 4-22. Cigarette smoke particle number reduction ratio as a function of time for different particle sizes under positive energisation for double stage system (a) smaller sizes (b) larger sizes.

Figure 4-22 shows the reduction ratio of particle number as a function of time for different particle sizes under positive DC energisation for a double stage system. The results show that particle number can be reduced significantly when a high voltage was applied at 30 seconds and, finally, the particle number was reduced to 0 within 70 seconds. This shows a great improvement compared to single stage electrostatic precipitation system under positive DC energisation.

Table 4-18. Average particle number reduction ratio for different particle sizes. (positive energisation, double stage system, cigarette smoke particles) (a) smaller sizes (b) larger sizes.

Particle size (μm)	0.265	0.29	0.325	0.375	0.425	0.475
Average η_r	0.05 ±0.0002	0.02 ±0.0002	0.01 ±0.0001	0.001 ±0.0001	0.003 ±0.0001	0.003 ±0.0001

(a)

Particle size (μm)	0.54	0.615	0.675	0.75	0.9	1.15
Average η_r	0.01±0.001	0	0	0	0	0

(b)

Table 4-18 shows the average reduction ratio of cigarette smoke particle number for different particle sizes for double stage system with positive energisation. The table shows that ~100% reduction ratio was achieved for particle with different sizes with double stage system from particle number aspect.

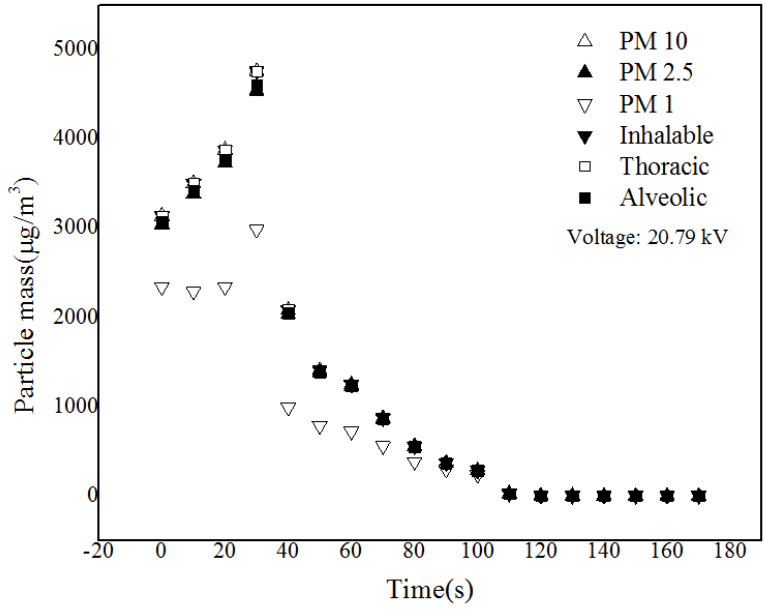

Figure 4-23. Cigarette smoke particle mass as a function of time for different particle sizes under positive energisation for double stage system.

Figure 4-23 shows cigarette particle mass as a function of time for different particle sizes under positive DC energisation for a double stage system. Similar to particle number reduction result, particle mass can be reduced to 0 μg/m^3 within 70 seconds. The result was also better than single stage particle mass reduction result under positive DC energisation.

Table 4-19. Average particle mass after treatment for different particle sizes. (Positive energisation, double stage system, cigarette smoke particles)

Particle size	PM10	PM2.5	PM1	Inhalable	Alveolic	Thoracic
Average particle mass after treatment ($\mu g/m^3$)	0.09 ±0.01	0.09 ±0.01	0.09 ±0.01	0.09 ±0.01	0.09 ±0.01	0.09 ±0.01

Table 4-19 shows average cigarette smoke particle mass following high voltage treatment for different particle sizes for a double stage system under positive energisation. The table shows that the system was efficient in particle precipitation for particles with different sizes from a particle mass aspect.

4.7.4.2 Negative Energisation

For negative energisation with a double stage system, the voltage level applied to the system was -14.37 kV. This voltage level can provide both first stage and stage with corona currents.

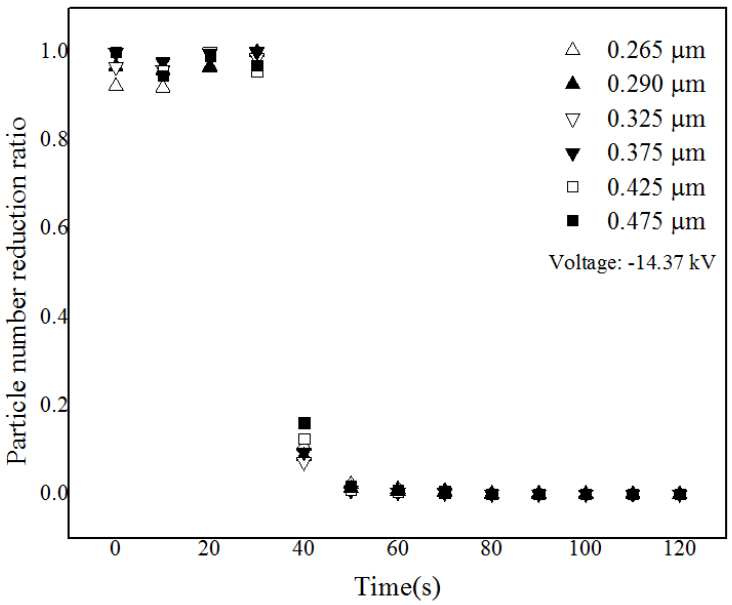

(a)

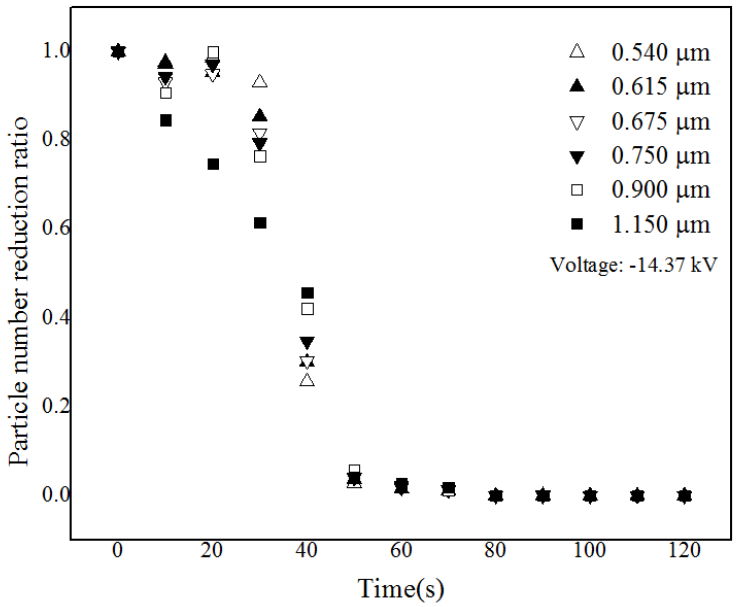

(b)

Figure 4-24. Cigarette smoke particle number reduction ratio as a function of time for different particle sizes under negative energisation for a double stage system.

Figure 4-24 shows the reduction ratio of cigarette particle number as a function of time for different particle sizes under negative DC energisation for a double stage system. The results show that particle number can be reduced significantly when a high voltage was applied at 30 seconds and was reduced down to 0 within 20 seconds, which was a great improvement when compared with single stage electrostatic precipitation system under negative DC energisation.

Table 4-20. Average particle number reduction ratio for different particle sizes. (Negative energisation, double stage system, cigarette smoke particles) (a) smaller sizes (b) larger sizes.

Particle size (μm)	0.265	0.29	0.325	0.375	0.425	0.475
Average η_r	0.07 ±0.004	0.01 ±0.002	0.01 ±0.001	0.001 ±0.001	0.001 ±0.001	0.009 ±0.002

(a)

Particle size (μm)	0.54	0.615	0.675	0.75	0.9	1.15
Average η_r	0	0	0	0	0	0

(b)

Table 4-20 shows the average reduction ratio of cigarette smoke particle number for different particle sizes in a double stage system under negative energisation. The table

shows that ~100% reduction ratio was achieved for particles with different sizes and with a double stage system under negative energisation from a particle number aspect.

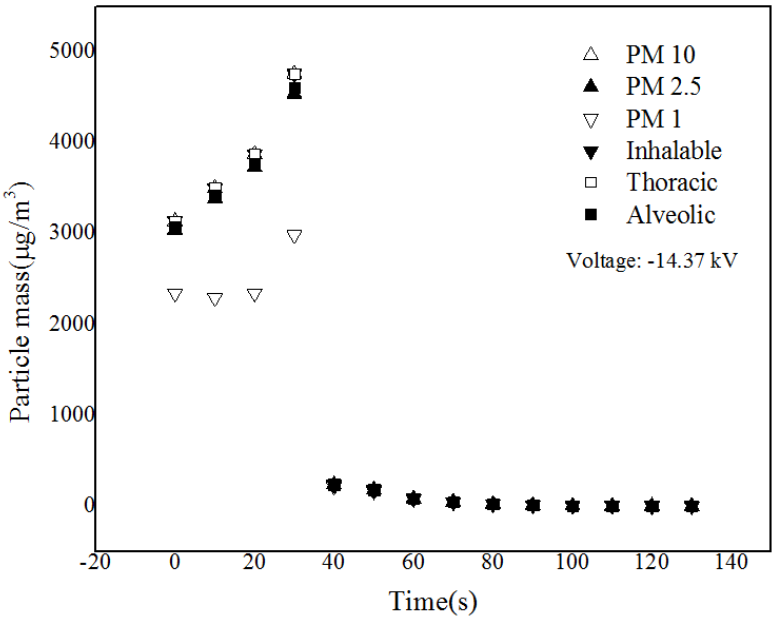

Figure 4-25. Cigarette smoke particle mass as a function of time for different particle sizes under negative energisation for double stage system.

Figure 4-25 shows cigarette smoke particle mass as a function of time for different particle sizes under negative DC energisation for a double stage system. Similar to the particle number reduction result, particle mass can be reduced to 0 μg/m^3 within 20 seconds. The result was also better than the single stage particle mass reduction result under negative DC energisation.

Table 4-21. Average particle mass after treatment for different particle sizes. (Negative energisation, double stage system, cigarette smoke particles).

Particle size	PM10	PM2.5	PM1	Inhalable	Alveolic	Thoracic
Average particle mass after treatment ($\mu g/m^3$)	0.21 ±0.04	0.21 ±0.04	0.21 ±0.04	0.21 ±0.04	0.21 ±0.04	0.21 ±0.04

Table 4-21 shows average cigarette smoke particle mass following treatment for different particle sizes for a double stage system under negative energisation. The table shows that the system was efficient in particle precipitation for particles with different sizes.

4.8 Discussions on Particle Electrostatic Precipitation Results

4.8.1 Discussions on Particle Electrostatic Precipitation Results

The particle electrostatic precipitation results obtained using the coaxial topology electrostatic precipitation system show that this system provided a high efficiency of PM removal from air. The system worked very well and was stable in routine tests. Particle removal efficiency was very high from both a particle number aspect (~100% particle number reduction ratio) and particle mass aspect (particle mass reduced down to ~0 $\mu g/m^3$). The system was capable of removing almost everything which passed through the system within a very short period (tens of seconds). Both positive and negative high voltage DC energisation can be applied to the system and both polarities works efficiently. As previously

discussed, negative energisation has a lower voltage level to achieve 100% removal efficiency when compared with positive energisation (For example, -14.4 kV and 20.8 kV were applied respectively to achieve 100% removal efficiency for candle particles).

For particles with low concentration (indoor particles and bee wax candle particles), a one stage coaxial system was capable of removing particles with 100% precipitation efficiency for both positive and negative DC energisation. For particles with high concentration (cigarette smoke particles), the 100% particle precipitation efficiency can be achieved through two methods: (a) increasing humidity in the system for negative DC energisation and (b) using an extra stage of coaxial topology electrostatic precipitator. The performances of both methods were very good and efficient.

4.8.2 Ozone Concentration

Similar to the research in Chapter 3, ozone concentration has been considered in this research with an ozone analyser monitoring the ozone concentration of the system. The catalyst was used to control ozone concentration, and the catalyst used in this research was MnO_2. In the case of single stage system for positive energisation, ozone concentration (20.79 kV with 23 ppm) was decreased down to ground level (~0.004 ppm). While in the case of single stage system with negative energisation, ozone concentration (-14.37 kV with 35 ppm) was decreased down to ground level (~0.004 ppm). In the case of double stage system for positive energisation, ozone concentration (20.79 kV with 40 ppm) was decreased down to ground level (~0.004 ppm). While in the case of single stage system with negative energisation, ozone concentration (-14.37 kV with 50 ppm) was decreased down to ground level (~0.004 ppm). Finally, in the case of increased humidity system with negative energisation, ozone concentration (-9 kV with 20 ppm) was decreased down to ground level (~0.004 ppm).

4.9 Energy Consumption Analysis

In this section, the energy consumption for coaxial topology electrostatic precipitation system is obtained. Similar to the energy consumption calculation for the needle-mesh topology system, the energy consumption evaluation calculation for a coaxial topology system was based on the current-time waveform obtained during the electrostatic precipitation process. The reason for the energy consumption evaluation is that the efficiency of energy usage is important. The ideal situation is to build a precipitation system with high particle removal efficiency and with low energy consumption.

Figure 4-26 shows the typical DC energised corona current-time waveform of coaxial topology electrostatic precipitation system for a single impulse for both positive energisation and negative energisation. The characteristics of the current-time waveform obtained during the electrostatic precipitation process of the coaxial topology system were similar to the current-time waveform of the needle-mesh topology system discussed in Section 3.8.1. There is no detectable DC component for positive energisation with the increase of applied positive high voltage. The frequency of both positive and negative DC energised corona current impulses increases as the applied high voltage is also increased. The impulses disappear at certain voltage levels for both energisations just before the breakdown voltage. The DC component for negative energisation increases as the applied negative high voltage increase until the breakdown voltage.

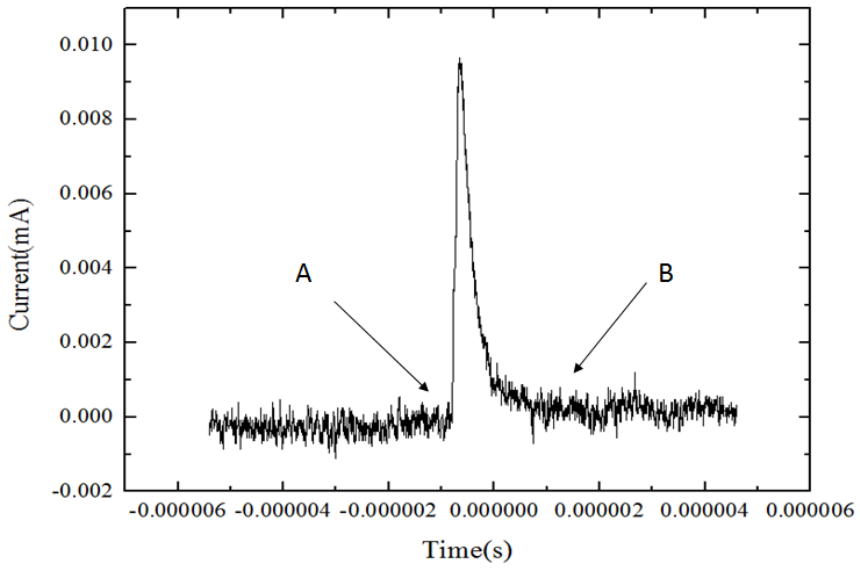

(a)

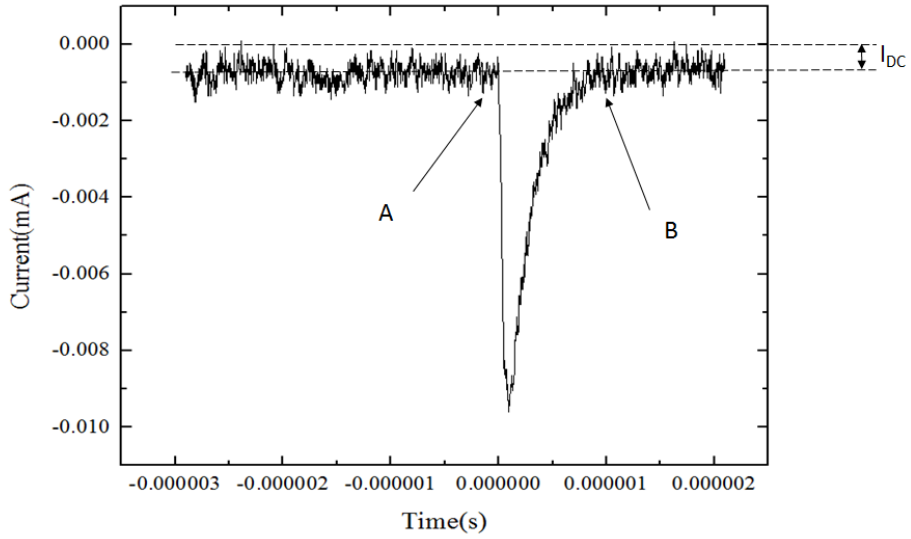

(b)

Figure 4-26 Typical DC energised corona current-time waveform of coaxial topology electrostatic precipitation system for single impulse. (a) Positive DC. (b) Negative DC.

The methodology for the energy consumption evaluation calculation for coaxial topology system was exactly the same as the needle-mesh system, as discussed in Chapter 3. The detailed methodology has been discussed and illustrated in Section 3.8.2, therefore, the energy consumption can be calculated.

4.9.1 Results

The flow rate of the system is 2 litres/minute (3.3×10^{-5} m^3/s), which was used for the energy consumption calculation.

4.9.1.1 Positive Energisation

For positive energisation, both single stage and double stage topologies have been used.

For a single stage system (copper rod stage), 20.79 kV (corona ignition voltage) was used to remove indoor particles and candle particles. 25 kV was used to remove particles with high concentration (cigarette smoke particles).

In the case of the double stage system, for the first stage (copper rod stage), when the voltage level was 20.79 kV the frequency of the current impulses was 2.8 kHz. For a voltage level of 25 kV, the frequency was 8.3 kHz. For second stage (copper wire stage), when voltage level was 20.79 kV the frequency of the current impulses was 30 kHz.

The parameters listed above were used for the calculation of energy consumption. The result of the energy consumption calculation for positive energisation is shown in Table 4-22 and the energy consumption for different types of particles with positive energisation is shown in Table 4-23.

Table 4-22. Energy consumption evaluation calculation result for positive energisation.

	First stage		Second stage
Voltage (kV)	20.79	25	20.79
Frequency (kHz)	2.8±1.5	8.3±2.9	30±10
Single impulsive charge (C)	3.01×10^{-10} $\pm3.34\times10^{-11}$	1.96×10^{-10} $\pm1.02\times10^{-13}$	2.88×10^{-10} $\pm1.79\times 10^{-11}$
Energy consumption(Wh/m^3)	0.145±0.078	0.343±0.12	1.52±0.538

Table 4-23. Energy consumption for different types of particles.

Particle type	Energy consumption(Wh/m^3)
Indoor particles	0.145±0.078
Candle particles	0.145±0.078
Cigarette particles (Single stage with high voltage level 25 kV)	0.343±0.12
Cigarette particles (Double stage with low voltage level 20.79 kV for both stages)	1.665±0.543

4.9.1.2 Negative Energisation

For negative energisation, both single stage and double stage topologies have been used.

For a single stage system (copper rod stage), a -14.37 kV (corona ignition voltage) was used to remove indoor particles and candle particles. -20.29 kV was used to remove particles with high concentration (cigarette smoke particles).

In the case of the double stage system, for first stage (copper rod stage), when the voltage level was -14.37 kV, the frequency of the current impulses was 5.2 kHz. For the voltage level was -20.29 kV, the frequency was 9.8 kHz. For the second stage (copper wire stage), when voltage level was -14.37 kV, the frequency of the current impulses was 37 kHz.

The parameters listed above were used for the calculation of energy consumption. The result of the energy consumption calculation for negative energisation is shown in Table 4-24 and the energy consumption for different types of particles with negative energisation is shown in Table 4-25.

Table 4-24. Energy consumption evaluation calculation result for negative energisation.

	First stage		Second stage
Voltage (kV)	-14.37	-20.29	-14.37
Frequency (kHz)	5.2±2.5	9.8±2.8	37±15
Single impulsive charge (C)	2.65×10^{-10} $\pm5.51\times10^{-11}$	3.24×10^{-10} $\pm1.69\times10^{-11}$	1.96×10^{-10} $\pm1.55\times10^{-11}$
DC current component (A)	-2×10^{-7}	-4×10^{-7}	-8×10^{-7}
Energy consumption (Wh/m^3)	0.19±0.088	0.605±0.155	0.978±0.353

Table 4-25. Energy consumption for different types of particles.

Particle type	Energy consumption (Wh/m^3)
Indoor particles	0.19±0.088
Candle particles	0.19±0.088
Cigarette particles (Single stage with high voltage level -20.29 kV)	0.978±0.353
Cigarette particles (Double stage with low voltage level -14.37 kV for both stages)	1.168±0.363

4.9.1.3 Increased Humidity

For negative energisation with increased humidity (rh 90%), only one single stage system was used.

For a single stage, -9 kV (corona ignition voltage) was used to remove particles with high concentration (cigarette smoke particles). When the voltage level was -9 kV, the frequency of the high voltage DC energised current impulses was 66 kHz. These parameters were used for the calculation of energy consumption. The result of the energy consumption calculation for negative energisation is shown in Table 4-26.

Table 4-26. Energy consumption evaluation calculation results for increased humidity.

Voltage (kV)	-9
Frequency (kHz)	66±20
Single impulsive charge (C)	$5.38\times 10^{-10}\pm 1.63\times 10^{-11}$
DC current component (A)	-5×10^{-7}
Energy consumption (Wh/m^3)	2.703±0.855

4.9.2 Discussion on Energy Consumption Analysis

The energy consumption for the electrostatic precipitation system has been obtained and the energy consumption results for the coaxial topology electrostatic precipitation system have been presented and discussed. The results have been compared with the typical energy consumption levels found in the literature. The typical electrostatic precipitator energy consumption value found in paper [59] was from 0.1 to 0.5 Wh/m^3, with the gas velocity between 2-6 m/s and the voltage level up to 20 kV. The electrostatic precipitation system developed in paper [59] provided the energy consumption value of 0.06-0.42 Wh/m^3, with the gas velocity of 0.8 m/s and the voltage level of up to 15-16 kV. Paper [71] shows that the energy efficiency of 0.44 Wh/m^3 can achieved when the gas velocity is >15-20 m/s and the voltage level is between 10-17 kV. Another research paper [60] shows that the energy

consumption level investigated was 0.1 Wh/m^3 with a voltage level of 60 kV. The results are compared with the energy consumption values calculated in this research. In the research presented in this chapter, for positive energisation (100% particle precipitation efficiency), the energy consumption for indoor particles and candle particles are both 0.145 Wh/m^3, and the energy consumption for cigarette smoke particles is 1.665 Wh/m^3 (double stage system). For negative energisation (100% particle precipitation efficiency), the energy consumption for indoor particles and candle particles were both 0.19 Wh/m^3, and the energy consumption for cigarette smoke particles was 1.168 Wh/m^3 (double stage system) and 2.703 Wh/m^3 (increased humidity). The comparison shows that the energy consumptions for the coaxial topology electrostatic precipitation system for both positive and negative DC energisation are close to, or lower than, the typical value in researches. The energy consumptions for double stage system and for increased humidity are similar to the single stage system. Therefore, the results on the energy consumption calculation provide the system with both a high particle removal and high energy using efficiency.

4.10 Conclusions

In this chapter, two suggestions on the improvement of electrostatic precipitation performance were made and explored. Since coaxial topology of electrostatic precipitators is widely used in industry, the suggestions which are made based on this type of design and are aimed at the resolution of typical problems attributed to traditional electrostatic precipitation systems. The electrostatic precipitation system with coaxial topology designed in this project had a central HV electrode which was made of copper wire or copper rod. This central HV electrode was energised with high voltage above the corona ignition level. The outer aluminium cylinder of the coaxial system was grounded and served as a collection electrode for precipitated particles. Following the application of high voltage to the central electrode gas laid with airborne particles, it was ionised in the region close to the central HV electrode (ionisation zone) and produced ions that moved towards the grounded outer

electrode under the action of the electric field in the coaxial system. These ions collided with and charged these airborne particles. Thus, the charged airborne particles also moved towards the grounded electrode which served as a particle collection electrode. From the gas flow aspect, gas/air laid with airborne particles was pumped into the inlet of the coaxial topology electrostatic precipitator. As discussed airborne particles were charged in the electrostatic precipitation system and were removed from the gas flow, then, the purified gas was guided out of the system from the gas outlet of the electrostatic precipitator. The coaxial topology system was larger than the needle-mesh system as developed in Chapter 3, which means that larger volume of gas can be treated which may be required for certain situations.

Precipitation tests were conducted to obtain the performance of the developed systems. Different types of particles (indoor particles, bee wax candle particles and cigarette smoke particles) were used in the conducted precipitation tests.

The particle generation system designed and developed in Chapter 3 was used in the present tests to air flow laid with bee wax candle and cigarette smoke particles. Both the particle number aspect and particle mass were recorded during the precipitation tests. The particle number and particle mass for cigarette smoke particles is close to those are reported in weather reports of heavily polluted area in practical cases.

Results show that the designed electrostatic precipitation system was capable of removing almost all the particles from atmosphere with relatively lower particle concentration (indoor particles and bee wax candle particles). The particle precipitation test results show that the performance of the system was excellent and stable. The particle precipitation efficiency for indoor particles and bee wax candle particles can be as high as ~100% and the high efficiency can be achieved in very short system running time (tens of seconds).

The system can be conducted using both positive and negative DC high voltage energisation. Similar to the needle-mesh system developed in Chapter 3, it was found that the performances of both polarities of energisation are very good, especially when particle concentration is not high (indoor particles and bee wax candle particles). The difference was that the voltage level for positive energisation (20.79 kV) was higher than the voltage level for negative energisation (-14.37 kV) to achieve 100% particle precipitation efficiency. For negative energisation, the voltage level used was just above the corona ignition voltage. However, it required the increase of the voltage level for positive energisation to achieve almost 100% particle precipitation efficiency.

The precipitation performance of the system was unsatisfactory when the particle concentration was high, as in the case of cigarette smoke particles. In the worst case there was a >10% particle penetration. Although 90% of precipitation efficiency was a reasonable result for the electrostatic precipitation system, the aim of this investigation was to develop the system which will provide maximum, ideally 100%, precipitation efficiency. Therefore, further steps were made in this research project to improve the electrostatic precipitation efficiency.

One improvement which was implemented in this research project was an additional precipitation stage in the electrostatic precipitation system. Thus, the double stage system was designed and developed. The precipitation results obtained using this double stage system were compared with the precipitation efficiency of the single stage precipitator. The double stage design aims at increasing the particle exposure time to ion flux and electric field in the electrostatic precipitation system, thus, the second stage can be used to precipitate particles which penetrate the first stage of the electrostatic precipitator.

In order to increase the extra stage of the system, a similar coaxial topology electrostatic precipitator was designed and developed. Experiments have been conducted to compare the performance of the single stage system and the double stage system on particle

precipitation when particle concentration was high. The results show that the increase of the stage has provided the system with better performance (increase of particle precipitation efficiency). The particle precipitation efficiency, with the double stage system, increased to ~100% when particle concentration was high (cigarette smoke particles), which achieved the destination of the research. The improved performance can also be reflected from a voltage level aspect. The increase of stage of the system can decrease the voltage level needed for the system to have 100% particle precipitation efficiency (positive: 25 kV to 20.79 kV. negative: -20.29 kV to -14.37 kV). With the two stages of the system, the voltage levels for both positive and negative energisation were both just above the corona ignition voltage (20.79 kV for positive energisation and -14.37 kV for negative energisation), which can broaden the usage of the system in certain situations. For example, when there is a limitation in power supply to reach a higher voltage level and there is a need for particle precipitation efficiency, it can be suggested to use a double stage system.

Another improvement was the increase in humidity inside the electrostatic precipitator to achieve better performance of the system. The design of this improvement aimed to use the effect of increased humidity to increase the particle precipitation efficiency. Initially the effect of increased humidity on particle precipitation efficiency of electrostatic precipitators was to be investigated to understand the influence of increased humidity on particle precipitation. A humidifier system which can provide the electrostatic precipitator with increased humidity has, therefore, been designed. The inlet air contaminated with PM (cigarette smoke particles) was mixed with water mist before the mixture was pumped into the electrostatic precipitator.

The investigation of the precipitation performance of air flow with increased humidity provided the following results: (1) the magnitude of the corona ignition voltage was lowered for both positive and negative energisation (positive energisation from 20.79 kV to 16 kV, and negative energisation from -14.37 kV to -9 KV). (2) The magnitude of breakdown voltage was lowered for both positive and negative energisation (Positive energisation from 26 kV to

24 kV and negative energisation from -27 kV to -23 kV). (3) The frequency of the corona current was significantly more intensive when observed for both positive and negative energisation. However, there were some differences between positive and negative energisation: (1) in the case of positive energisation, the corona current was quite unstable. It was observed frequently in the tests that there was a variation in current level for certain value of voltage level which was difficult for measurement. There were also frequent spark breakdowns during the precipitation tests for positive energisation. For negative energisation, the corona current was stable, and the measurement of current was easy. The breakdown voltage level was also stable. The system worked well as long as the voltage level was kept within the working range (from corona ignition voltage to breakdown voltage). (2) For positive energisation, the performance of the electrostatic precipitation system was not improved when air flow with an increased humidity was used. While for negative energisation, the performance of the electrostatic precipitation system was improved with the increase of humidity (rh 90%). The particle precipitation efficiency was increased to 100% when particle concentration is high (cigarette smoke particles). The voltage level used for increased humidity with 100% precipitation efficiency was lower than the corona ignition voltage in normal humidity with a relative humidity of 31% (-9 kV as compared to -14 kV).

With the results of the investigation, the second suggestion on designing electrostatic precipitators to improve the performance can be made. For a negative DC energised electrostatic precipitation system, the increase of humidity can improve the performance of the system and the applied voltage level can be lowered.

The energy consumption of the precipitation process was also obtained in this research. With the developed method of energy consumption detailed in Chapter 3, the energy consumption for different situations were calculated and compared with the energy consumptions based on literature. It was found that the electrostatic precipitation system developed is with very low energy consumption for both positive and negative DC energisation. The system with improvements of double stage and increased humidity also

had a very low energy consumption. For positive energisation (100% particle precipitation efficiency), the energy consumption for indoor particles and candle particles were both 0.145 Wh/m^3, and the energy consumption for cigarette smoke particles was 1.665 Wh/m^3 (double stage system). For negative energisation (100% particle precipitation efficiency), the energy consumption for indoor particles and candle particles ere both 0.19 Wh/m^3, and the energy consumption for cigarette smoke particles was 1.168 Wh/m^3 (double stage system) and 2.703 Wh/m^3 (increased humidity).

The ozone concentration level was also measured in the research. The design of the system has also included an ozone concentration control section, in which a catalyst was used. The ozone level was lowered to ground level after control which is also environmental friendly.

Particle electrostatic precipitation technologies described in the literature have been reviewed for comparison with the system developed in this chapter. As in the present chapter the increased humidity of air and the double stage ESP design were used to improve precipitation efficiency of the ESP system, especially in the case of higher concentration of airborne particles of similar ESP systems with multiple stages and systems with an increased humidity are reviewed and compared, [55] [76] [71] [56] [77] [78] [79].

The research in [55] shows the approach of electrostatic precipitation with a multiple stage approach. The multiple stage system in the research consisted of three stages: a streamer corona reactor (AC/DC energisation), a bipolar charging reactor (negative DC energisation) and an electrostatic precipitator (positive/negative DC energisation). The streamer corona reactor had a coaxial configuration similar to the electrostatic precipitation system developed in this chapter. The bipolar charging reactor and the electrostatic precipitator in the literature were based on a wire-plate configuration. The particle source in the literature was styrene and particle diameter ranged from 0.01 μm to 1 μm, which was similar to the smallest particle size in the research in this chapter (as small as 0.265 μm). The working voltage for the bipolar charging reactor stage was -17 kV, and for the electrostatic

precipitator stage was 29 kV for positive energisation and -32 kV for negative energisation. For comparison, the working voltage for the system developed in this chapter was 20.79 kV for positive energisation and -14.37 kV for negative energisation when dealing with particles with high concentration (cigarette smoke particles), where the voltage level was much lower than the level used in the literature. The research in this paper investigated different voltage combinations with different voltage levels and voltage polarities. The best particle precipitation efficiency of the literature is around 80%, which was much lower than the particle precipitation efficiency of the double stage system developed in this chapter (100%). Energy consumption was also evaluated in this paper at 3.33 Wh/m^3, which was much higher when compared with the energy consumption of the double stage system developed in this chapter (1.665 Wh/m^3 and 1.168 Wh/m^3). Another investigation of this paper was that negative energisation can make the system more effective in particle precipitation. In this chapter, similar behaviours of the particle precipitation system have also been obtained.

Similar approaches with multiple stage system were also conducted by other researches. The approach in paper [76] investigated the behaviour of double stage particle precipitation system with a co-flow particle pre-charger and a parallel plate collection stage. The particle diameter in this paper ranged from 0.2 μm to 4 μm, which was similar to the smallest particle size channel in this chapter (as small as 0.265 μm). The co-flow particle pre-charger was energised with negative DC energisation and the working voltage levels were -12 kV and -16 kV. The parallel plate collection stage was energised with positive DC energisation and the working voltage level was 20 kV. The working voltage level for the system developed in this chapter was similar to the value in the paper, which were 20.79 kV for both stages of positive energisation and -14.37 kV for both stages of negative energisation. The system developed in this paper can also be energised with impulsive energisation to the co-flow particle pre-charger. However, the particle precipitation efficiency for impulsive energisation was lower than the particle precipitation efficiency for the DC energisation case. Different voltage level combinations have been applied to the system for competition. The particle

precipitation results in this paper show that the system was with highest particle precipitation when -16 kV and 20 kV were applied to the pre-charger and the collection plate respectively. The highest particle precipitation efficiency for particles larger than 1 μm can be as high as 100%. However, particle precipitation efficiency for particles smaller than 1 μm was below 100% and approximately 80% when the particle diameter was around 0.2 μm. In other cases, particle precipitation efficiency was around 80% or below 80%. While in this chapter, the particle precipitation efficiency for the developed double stage system was much higher with 100% precipitation efficiency for particles as small as 0.265 μm.

Researches on electrostatic precipitation with increased humidity have also been reviewed and compared with the system with increased humidity as developed in this chapter. There is an approach [56] based on an electrostatic precipitator with discharge electrodes consisting of seven circular discs with zigzag-shaped edges for particle charging and removal. The particle sources used for this paper were oleic acid, Al_2O_3 and SiO_2 particles. The particle size ranged around the hundreds of nanometres and below 1 μm. Similar to the system developed in this chapter, water mist was used to increase humidity in the system. It was found in this paper that increased humidity can improve the performance of the electrostatic precipitation system by increasing particle precipitation efficiency for the three types of particles, which was a good agreement to the conclusion of this chapter. The voltage levels used for in this paper were 21 kV for oleic acid particles and Al_2O_3 particles, and 18 kV for SiO_2. The voltage level used for the system with increased humidity developed in this chapter was -9 kV and was much lower than in this paper, which potentially can result in a much lower energy consumption. The particle precipitation efficiency in this paper for increased humidity was very high at >90%. However, the particle precipitation efficiency for particles smaller than 300 μm dropped below 90%. The particle precipitation efficiency for the system with increased humidity developed in this chapter can be as high as 100% for particles as small as 0.265 μm, which means a higher particle precipitation efficiency compared with the research in this paper.

Since it is noticed that the water mist in the electrostatic precipitator developed in this chapter can form a thin wet membrane on the collection plate, a similar approach [77] has been reviewed and compared with the performance of the system developed in this chapter. The system in this paper uses a coaxial configuration electrostatic precipitator which was similar to the system in this chapter. The particles used in this paper were PM 2.5 particles (particle diameter less than 2.5 μm). The paper compared particle precipitation efficiency of the metal collection plate and the collection plate with a wet membrane (relative humidity 45%). It was found that the particle precipitation efficiency with wet membrane is much higher than the case of metal collection plate, which shows similar conclusions in this chapter. The voltage level used in this paper ranged from 30 kV to 55 kV with both positive and negative energisation. The best result of particle precipitation efficiency was around 70% with a 55 kV voltage level, and other cases were all below 70%. Compared with this paper, the particle precipitation efficiency for the system with increased humidity developed in this chapter can be as high as 100% with lower voltage level used (-9 kV). The higher particle precipitation efficiency shows better system performance, and lower voltage level shows lower energy consumption.

The comparison and analysis of result in the literature and this chapter show good agreements of conclusions on increased electrostatic precipitator stage and increased humidity to the system. The particle precipitation efficiency for the cases of double stage system and increased humidity system is either similar to, or higher than, the particle precipitation efficiency in the literature. The energy consumptions of the double stage system and increased humidity system are all lower than those found in literature, which shows that the two systems developed in this chapter are both energy saving. The high particle precipitation efficiency and low energy consumption result in a very good performance for both systems.

5 Biological Decontamination of the Electrostatic Precipitation System

5.1 Introduction

Chapter 3 and Chapter 4 were focused on the development of plasma charging and electrostatic particle precipitation systems with a high efficiency of the removal of airborne particles from air flow. The obtained results show that the developed systems provided excellent precipitation performance and were with low energy consumption. However, in many practical applications, it is important not only to remove aerosol particles from air but also to kill the pathogenic microorganisms which can be present on these particles or in water droplets. These fine and ultrafine aerosol particles contaminated with pathogenic microorganisms pose a significant health risk, especially in the case of vulnerable people such as patients of hospitals, people with a reduced immune defence, etc. Higher concentrations of bio-contaminated aerosols can be found in multiple indoor environments, such as schools, hospitals, public transport and other places. In many cases it is very difficult to control such aerosols and efficient methods of aerosol removal and bio-decontamination are urgently required.

The present research project also focuses on potential bio-decontamination capabilities of the developed plasma precipitation systems. It will be a critical advantage of such plasma systems – their ability to combine both actions: aerosol removal from air flow and bio-decontamination of the precipitated aerosol particles. Thus, the present chapter bio-decontamination efficiency of the developed plasma precipitation systems has been investigated.

The main aim of the study presented in this chapter is to demonstrate that plasma is not only effective for charging airborne particles and their precipitation, but can also provide

biological decontamination of microorganisms. The successful outcome of this research will provide a background for the use of developed plasma electrostatic precipitation systems in a wider range of practical applications which require cleaning and bio-decontamination.

This chapter presents the results of the biological decontamination study of corona discharges. In this chapter, the effect of a corona discharge on microorganisms was investigated to show the biological decontamination effectiveness of corona discharges developed in the precipitation systems.

To investigate this bio-decontamination effect the needle-mesh electrostatic precipitation was altered, as detailed in Chapter 3, to build a biological decontamination system. An air flow delivery system was designed to deliver air with biologically contaminated airborne particles in the plasma reactor to meet the needs of the experiments. The degree of biological decontamination was monitored by calculating colony forming units on agar dishes obtained for air flows with and without biologically contaminated aerosols. A microorganism collection system was designed and developed, and a microorganism cultivation method was also developed to monitor bio-decontamination efficiency. The model microorganisms selected for this study were the unidentified microorganisms growing on mouldy bread which provide a direct source of the bio-decontaminated aerosol.

In previous particle precipitation tests, it was found that negative DC energisation is with stable and high precipitation efficiency. Therefore, negative DC energisation has been used in the biological decontamination tests with different high voltage levels. Different gas flow rates were also used for comparison. The results show that plasma is effective on biological decontamination. Energy consumption was also considered in this research due to the design of the system also aims to be environmental friendly. Using the energy consumption calculation method developed in Chapter 3, energy consumptions for different situations were calculated.

5.2 Methodology of the Bio-decontamination Tests

To investigate the effect of corona discharges on microorganisms, a needle-mesh corona reactor was used to generate corona discharges and ions in air flow with bio-aerosols. The bio-decontamination experimental system includes the corona reactor, a microorganism source generating system and a microorganism collecting system. In these bio-decontamination tests microorganisms were introduced in air flow (ambient laboratory air with relative humidity of 31%rh), then, this air flow with the bio-aerosol was injected in the corona reactor and stressed with a negative high voltage.

The exhaust air flow was pumped through the microorganism collection chamber. The results of bio-decontamination were compared for two cases: when the corona reactor was energised with high voltage and when there was no voltage applied to the needle corona electrode.

The bio-aerosol passed through the collection chamber and microorganisms, if in this air flow after the corona reactor, were attached to the nutrition agar plate located in the collection chamber. Subsequently, these microorganisms were grown in the bio-incubator and the colony number units have been counted. It was expected that corona discharges can result in decontamination of bio-aerosol present in the air flow.

5.3 Design of the Corona Bio-decontamination System

The design of the corona biological decontamination system is shown in this section. The system consists of four parts: corona reactor, bio-aerosol generation system, microorganism collection system and the incubation system. The detailed design of the corona biological decontamination system is introduced as follows.

5.3.1 Corona Reactor

The corona reactor used in the system has been discussed in Section 3.2. In the case of biological decontamination, microorganisms were pumped into the corona reactor from the gas inlet during tests. Microorganisms passed through the hypodermic needle then passed through the two metallic meshes and exited the corona reactor through the gas outlet. The difference was that no glass fibre filters were used in the case of biological decontamination. The reason being is that the pore size of the glass fibre filter is larger than certain types of microorganisms and these microorganisms might be blocked by the glass fibre filter without being able to enter the microorganism collection system. The block of the glass fibre filter might influence the experimental results as it is difficult to identify whether the microorganisms are inactivated or physically blocked, so the results are not persuasive. Another reason for the removal of the glass fibre filter is that the microorganism source contains high moisture, and the moisture might be absorbed by the glass fibre filter to block the pores which enhances the effect of blocking. Therefore, the glass fibre filter is removed for biological decontamination tests.

The corona reactor is shown in Figure 5-1.

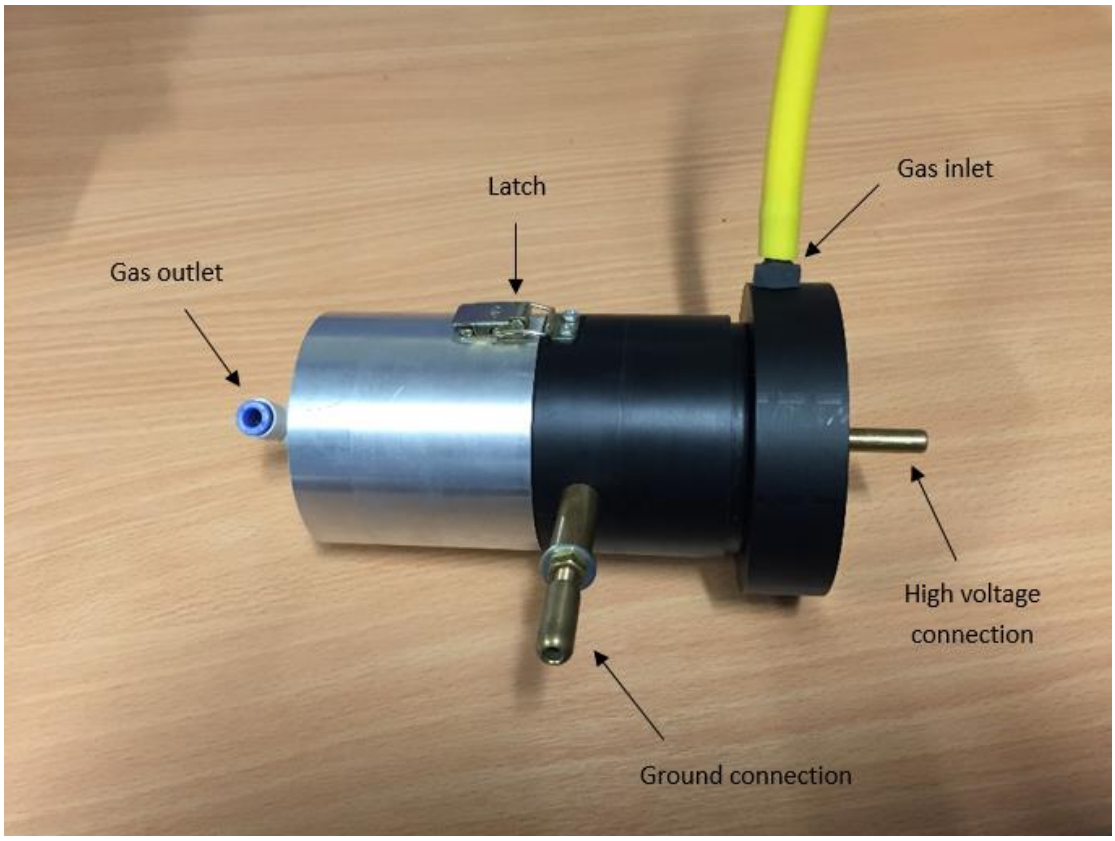

Figure 5-1. Corona reactor.

5.3.2 Bio-aerosol Generation System

The design of the bio aerosol generation system is shown in Figure 5-2.

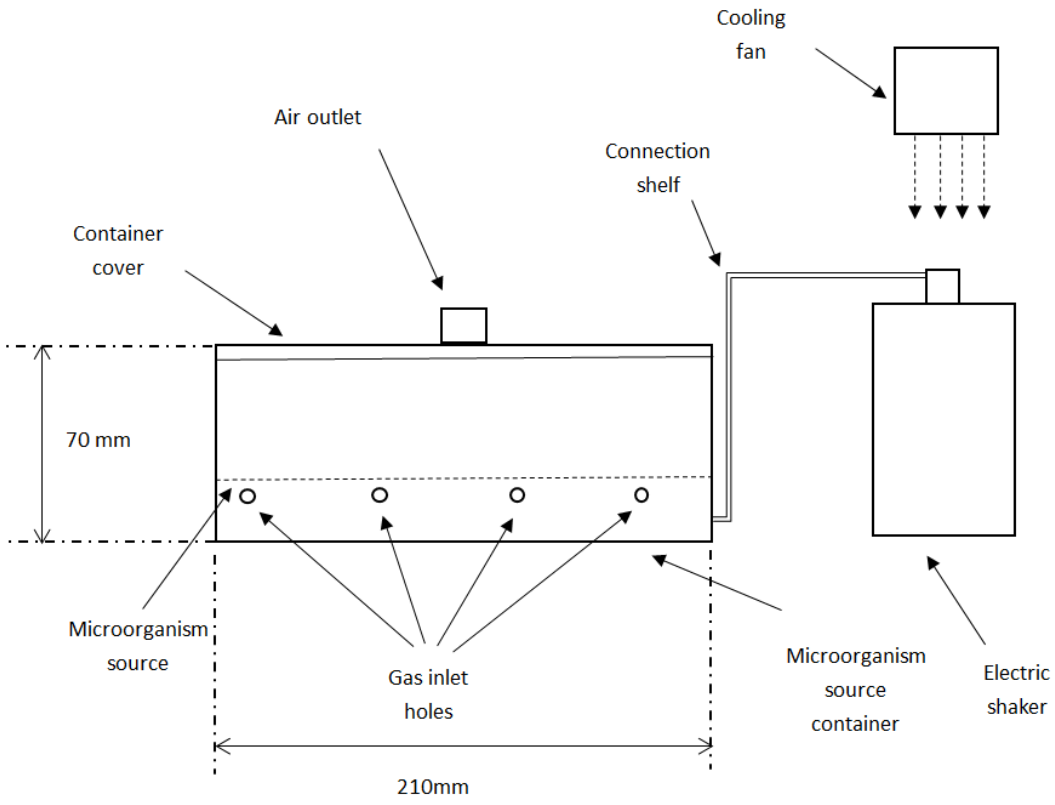

Figure 5-2. Design of bio aerosol generation system.

Bio-aerosol was generated by the system shown in Figure 5-2. The sealed container was filled with mouldy bread which was used as a source of a model microorganism (unidentified microorganisms). The container was modified from Tesco plastic food container which can be locked and sealed by the cover. The mouldy bread was cut into small pieces and placed into the container which had eight holes in the body for the air inlet. The purpose of this design is to introduce unidentified microorganisms into the air flow while air passes through the container. The bio-aerosol was injected into the corona reactor through the gas outlet which was connected with a 12 mm air hose. The increased cross section of the air hose was designed to carry a large flow rate of bio-aerosol into the plasma treatment system.

The plastic container was attached to an electric shaker with a solid connector made of plastic. The connector was fixed at the bottom of the container on one side and fixed to the top of the electric shaker on the other. There was a rotating metallic rod on the top of the

electric shaker, so the connection of the container to the shaker can transfer the rotating movement of the rod into the shaking movement of the container back and forth. The electric shaker was tuneable with different rotating frequencies which were used in the tests to establish the best frequency for shaking. It was found that the best frequency is half of the maximum frequency which was fast enough to mix the microorganisms with air but not to cause the issues with overheating. The overheating problem of the electric shaker was due to long time period of tests. A single test lasted ~30 minutes and in order to maintain the same conditions in all tests, several tests have been conducted in series. Therefore, the shaker was working continuously which may potentially cause the issue of overheating on the electric shaker body. As a result, an electric fan was used for cooling. In the tests, it was found that the use of the cooling fan helped solve the problem of overheating.

The developed bio-aerosol generating system is shown in Figure 5-3.

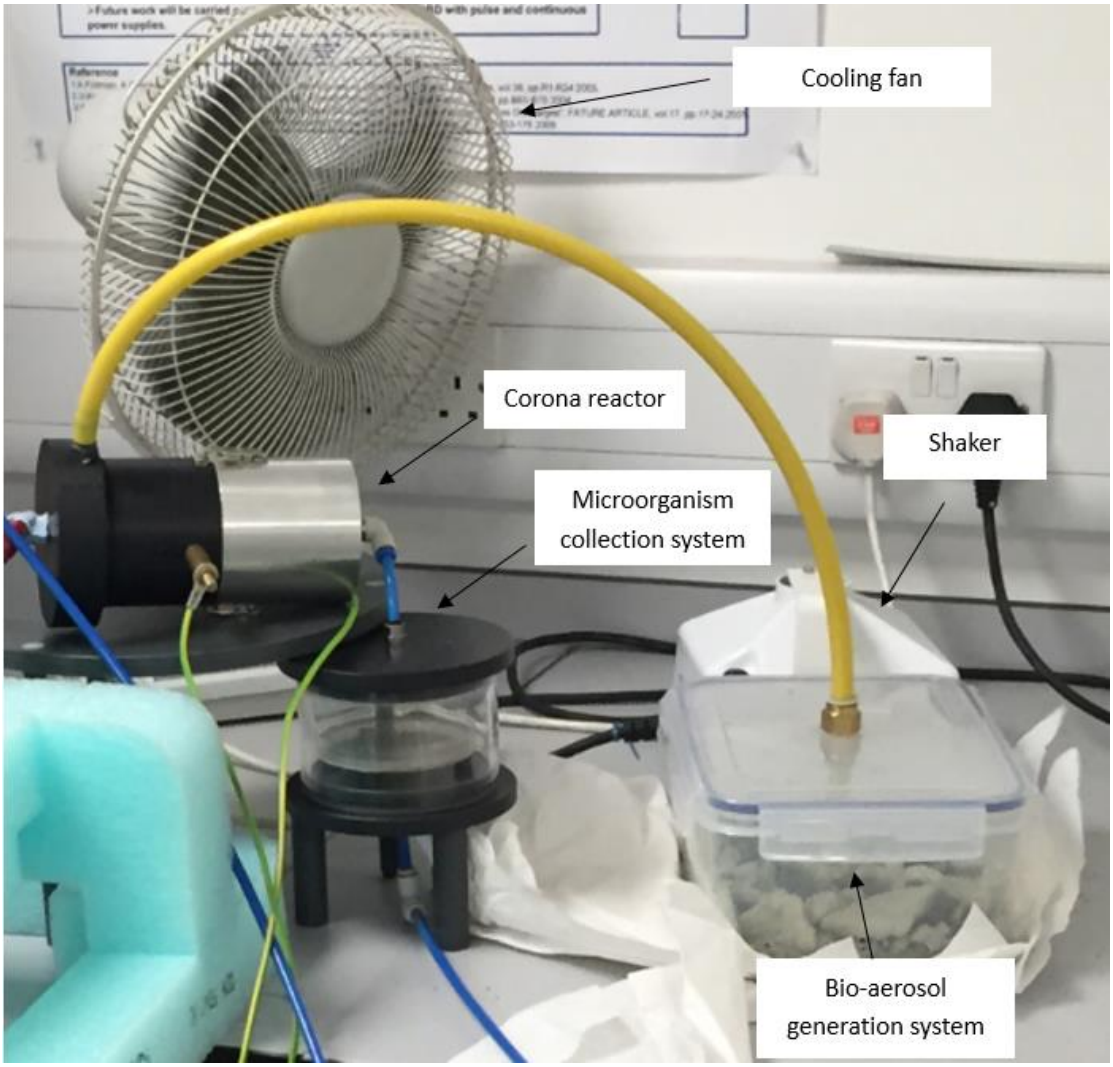

Figure 5-3. Microorganism source generation system.

5.3.3 Microorganism Collection System

The design of the microorganism collection system is shown in Figure 5-4.

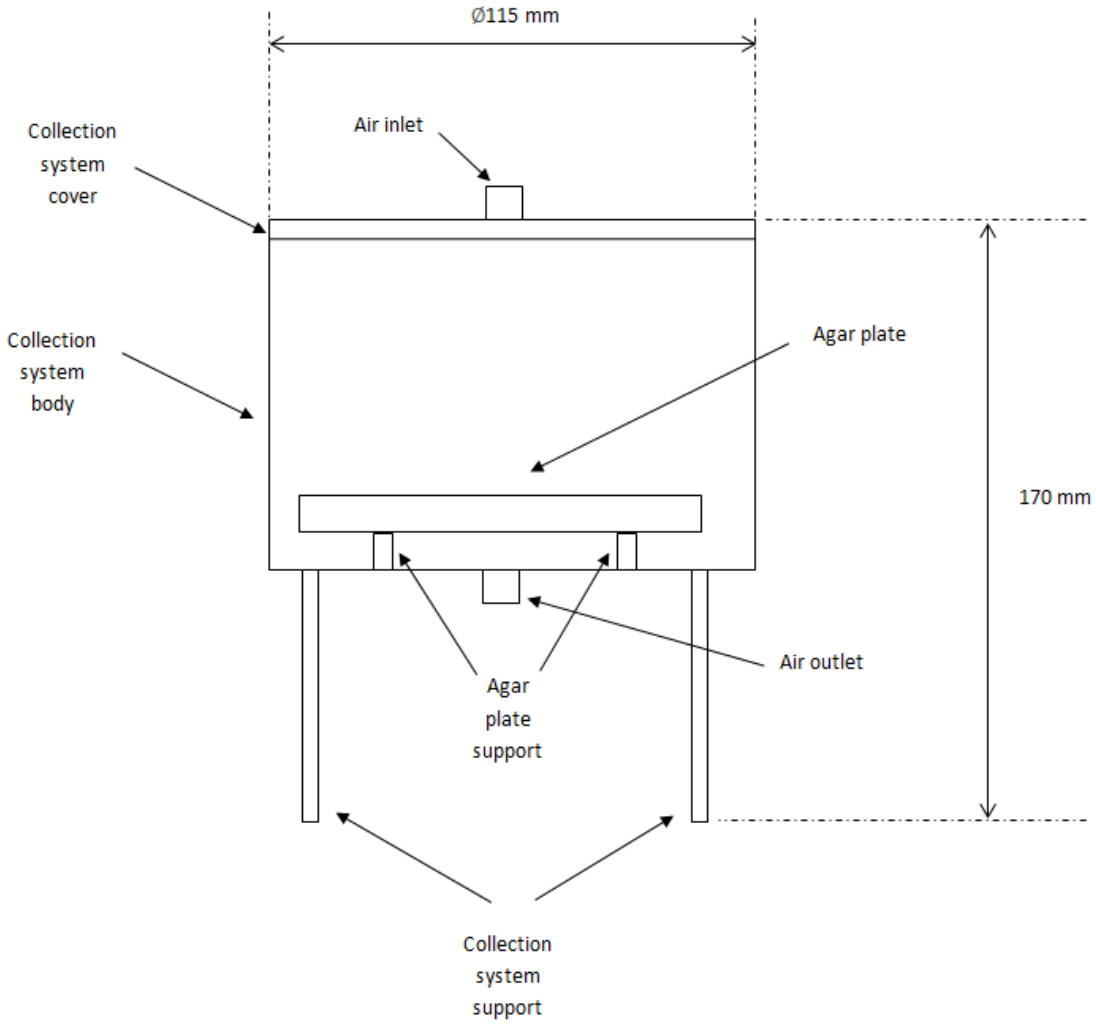

Figure 5-4. Design of microorganism collection system.

As shown in Figure 5-4, the microorganism collection system was made of transparent PVC tube. There was a cover on the top of the PVC collection system body and was sealed with a rubber O-ring. The gas inlet was located on the cover of the PVC tube.

There were three plastic supports on the bottom of the collection system body which were used to support the agar plate. The particular reason for this was to simulate air samplers which are used for biological tests.

Figure 5-5. Typical air sampler.

Figure 5-5 shows a typical air sampler which holds the agar plates. After the agar plates, there is space for air to pass through, therefore, the air sampler can suck air from the outside environment. Air flow passes through the agar plate and the space after the agar plate. Air samples are taken on this principle.

The microorganism collection system was designed following the working principle of air samplers. Air was sucked from the gas outlet at the bottom of the collection system so air flow from the gas inlet can pass through the surface of the agar plate. The design enabled the best contact of microorganism to the agar plate to ensure as many microorganisms to be collected as possible. The three plastic supports at the bottom of the collection system body were used to support the system and to give enough space for a 6 mm air hose to be connected. The microorganism collection system is shown in Figure 5-6.

Figure 5-6. Microorganism collection system.

5.3.4 Microorganism Incubation System

The nutritious agar plates with microorganisms following the tests should be incubated. The incubation process was to provide a nutritious environment with a suitable moisture

concentration and temperature for microorganisms to grow. The growth of microorganisms was for observation and for data analysis.

5.4 Experimental Setup

The experimental setup is shown in Figure 5-7.

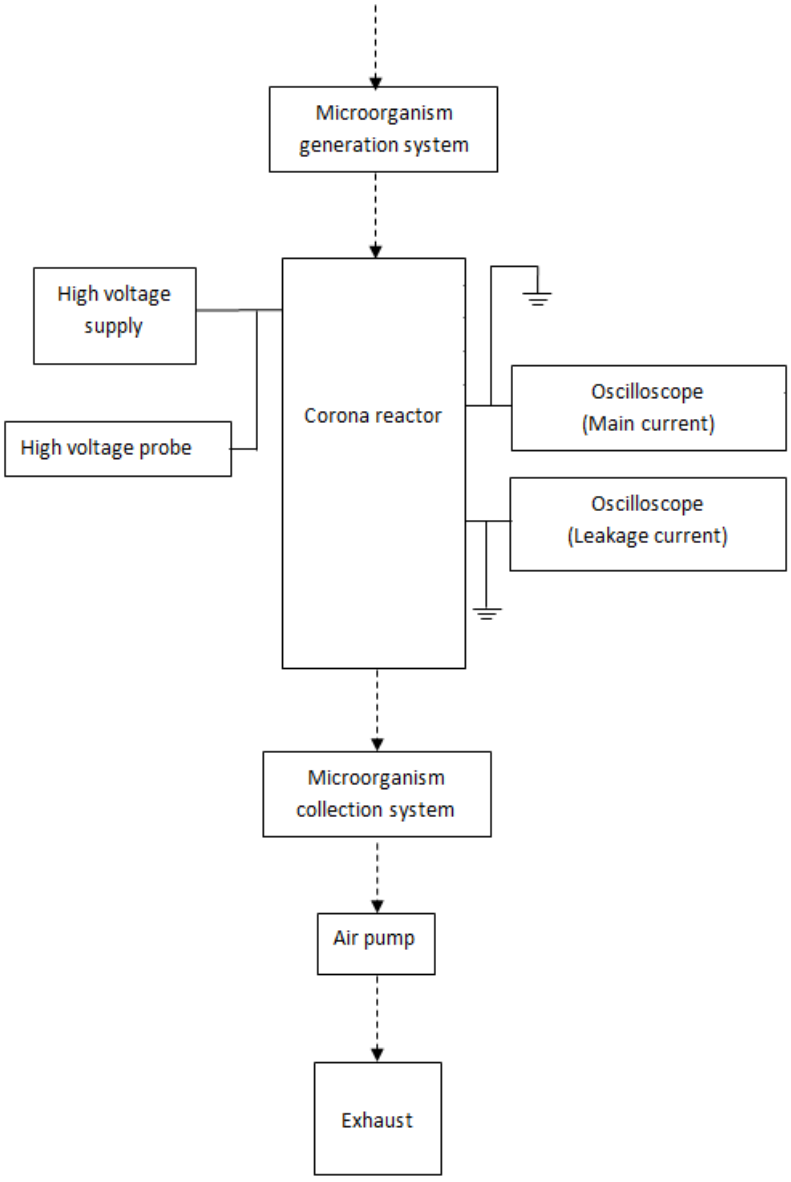

Figure 5-7. Experimental setup for biological decontamination system.

Figure 5-7 shows the experimental setup for biological decontamination system. The corona reactor, the microorganism generation system and the microorganism collection system were introduced previously in this chapter. The other components (high voltage supply, high voltage probe and the oscilloscope) have been introduced in Chapter 3, Section 3.3. The only difference is the use of a different air pump.

Air pump:

The air pump used in the biological decontamination system was the KnF VP series and was different from the air pump used in the electrostatic precipitation system. In order to follow the working principle of air samplers to collect microorganisms on agar plates, the air pump should be sucking air through the system instead of pushing it through the system. In this case, the aquarium pump was replaced by a different pump. This air pump was capable of both pushing and sucking air from the system with a flow rate of 16 litres/minute. In the research of biological decontamination, the gas inlet was connected to the air outlet at the bottom of the microorganism collection system. The gas outlet was connected to the exhaust system.

Air flow can go into the microorganism generation system first, where microorganisms were mixed with air flow. Then, the mixture goes into the corona reactor where the biological decontamination process was conducted. Subsequently, the decontaminated air flow went into the microorganism collection system to be collected by the nutritious agar. Finally, the decontaminated air flow went into the exhaust system.

Flow regulation:

As mentioned, the flow rate of the air pump was 16 litres/minute. In order to maintain the same gas flow rate as in the electrostatic precipitation, and to investigate the influence of flow rate on the efficiency of biological decontamination, a flow regulator was used. Following the comparison of different flow rates which will be discussed later in this chapter,

the flow rate was regulated to 5 litres/minute by the flow regulator to have the best biological decontamination efficiency and to maintain similar gas flow rate as in the electrostatic precipitation system.

Exhaust:

The exhaust from the plasma precipitation and bio-aerosol decontamination system has been introduced into the biological safety cabinet LABCAIRE to prevent potential contamination to the environment in the laboratory. The LABCAIRE cabinet was switched on during the entire process of the biological decontamination and was kept working for at least 30 minutes to lower the possibility of further contamination to a minimum.

Colony forming unit counter:

The colony forming unit counter used in the biological decontamination tests is BioCote. The device counts the colony forming unit number for data analysis. The agar plate was placed in the counting position. The light under the agar plate showed the colony positions clearly. Before counting, the reset button should be pressed to reset the number. A marker pen was used to press the agar plate plastic cover at each colony spot for marking.

5.5 Experimental Procedures

The biological decontamination experiment procedures are illustrated in this section.

5.5.1 Pre-test Procedures

Microorganism source and nutritious agar plates should be prepared before tests, and the biological decontamination system should be set and connected for tests.

5.5.1.1 Microorganisms Preparation

Before the tests, the microorganisms should be prepared. In this study, white bread was bought from supermarket and left to become mouldy, and the mouldy bread was used as source of model microorganisms (unidentified microorganisms). These unidentified microorganisms growing on the mouldy bread are the microorganisms that have been used to develop a bio-aerosol. During the preparation of the microorganisms, the bread bag was fastened to prevent moisture from evaporating. When the bread was mouldy and became visibly “greenish”, the microorganisms were ready for the experiments. Figure 5-8 shows the prepared mouldy bread as ready for the tests.

Figure 5-8. Mouldy bread.

5.5.1.2 Nutritious Agar Plates Preparation

Nutritious agar plates were prepared when the microorganisms were ready to be used. The agar used for the growth of microorganisms on mouldy bread was CM0139 potato dextrose agar. The agar plates were prepared in the following steps:

First, dissolve the potato dextrose agar powder into still water in a glass bottle. For each 500 ml of water add 19 g of agar powder. The mixture in the bottle was shaken well to ensure the solution was uniform.

Second, use an autoclave to sterilise the agar solution. The autoclave is a pressure chamber which has a high-temperature and pressure used for the sterilisation process. The autoclave used in the research was DIXSONS. Following the sterilisation process in the autoclave, the agar bottle was placed in 40°C water to cool down. When the temperature was reduced to 40°C, the agar plates were ready to be made.

Third, the agar plates were made inside the ventilation chamber which was already sterilised. Empty plates were prepared first, and then separately filled with the agar solution in the bottle. After the temperature of the agar in the plates decreased to room temperature and the liquid agar became jelly-like the agar plates were inverted and put into the incubator for 12 hours. The incubator is a device used to grow and maintain microbiological cultures. The incubator can maintain optimal temperature, humidity and other conditions of the internal atmosphere. The incubator maintained a temperature of 37°C. The reason to use the incubator was to select uncontaminated agar plates in the tests. Colonies will be observed on the contaminated agar plates which should not be used in the tests. After these three steps, the agar plates were successfully prepared.

5.5.1.3 Electrical Components Connection

Similar to the electrostatic precipitation tests in Section 3.5.1.1, a high voltage power supply was changed to a negative module. The supply was connected to a protection resistor then connected to the corona reactor that was grounded from the first and second metallic meshes. The high voltage probe was attached to the high voltage connection on the electrostatic precipitator to monitor the voltage level. The oscilloscope was connected to the corona reactor through the shunt resistor to monitor current during tests.

From an air flow perspective, the bio-aerosol generation system was connected to the corona reactor through a 12 mm air hose. Subsequently, the corona reactor was connected to the microorganism collection system. Then, the microorganism collection system was connected to the air pump. Finally, the air flow was guided into the exhaust through a 6 mm air hose.

The entire microorganism decontamination system is shown in Figure 5-9.

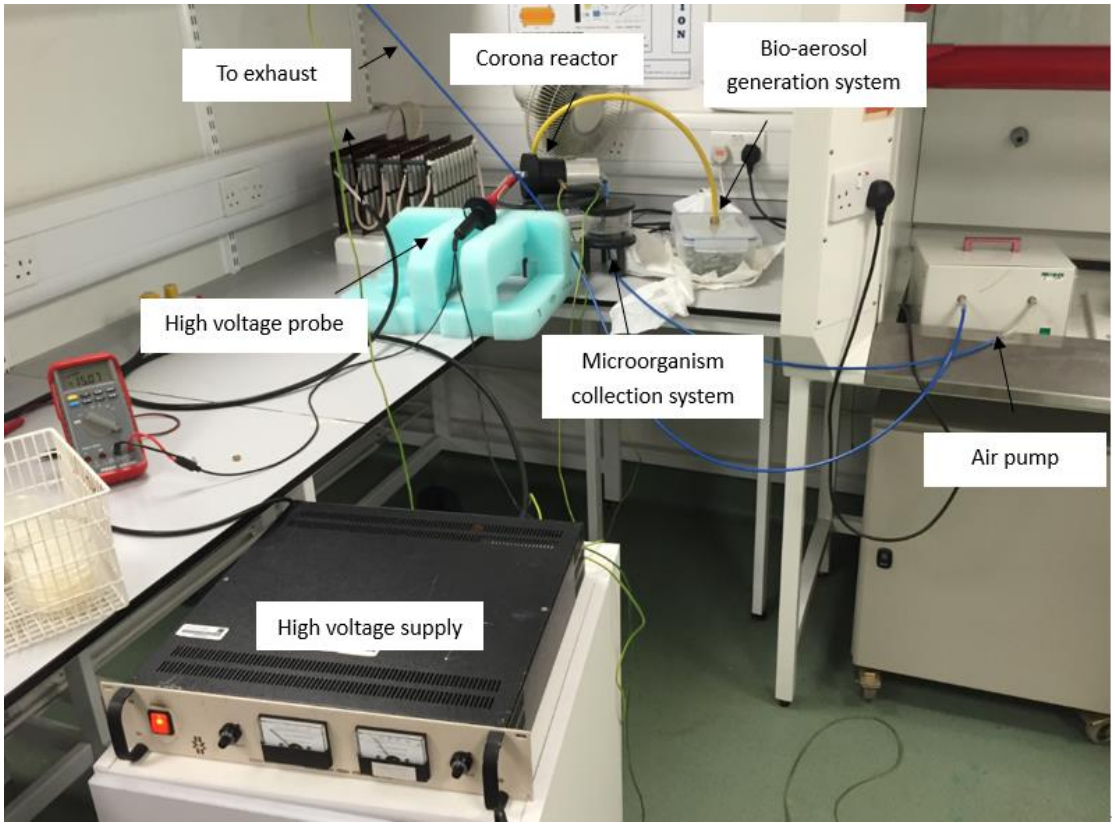

Figure 5-9. Microorganism decontamination system.

5.5.2 Bio-aerosol Decontamination Tests

The biological decontamination tests were conducted in two groups. Group 1 was to sample air with microorganisms through the system without plasma treatment, and microorganisms were collected on five agar plates respectively. Group 2 was to take the mixture of air and

microorganisms into the system with high voltage, and microorganisms were collected on another five agar plates. The results were then compared. The flow rate of the system was regulated to 5 litres/minute and the single test time period was designed to be 20 minutes to guarantee at least 100 litres of gas to pass through the system. The microorganism colony number was stable for this volume of air. The experimental procedures of each group are introduced in the following.

All the tests are conducted in biological laboratory, using gloves and biological coats to minimise any other possibilities of microorganism contaminations.

5.5.2.1 Sampling of Microorganisms

Step 1. Mouldy bread with unidentified microorganisms was separated into pieces and placed into the microorganism generation system. The generation system was then locked and sealed.

Step 2. A sterilised agar plate was placed in the microorganism collection system. The collection system covers were then closed.

Step 3. The shaker and the cooling fan were switched on.

Step 4. The air pump was switched on and after 20 minutes the agar plate is ready for incubation. The agar plate is marked and at least 5 agar plates are used for microorganism sampling.

5.5.2.2 Experiments with Plasma Discharges

Step 1. The mouldy bread was separated into pieces and placed into the contained bio-aerosol generation system. The generation system covers were then locked and sealed

Step 2. A sterilised agar plate was placed in the microorganism collection system. The cover of the collection system was closed.

Step 3. The shaker and the cooling fan were switched on.

Step 4. A negative high voltage DC was applied. The voltage level was increased to -16 kV (the reason for this voltage level will be discussed later in this chapter.)

Step 5. The air pump was switched on and after 20 minutes and the agar plate was ready for incubation. The agar plate is marked and at least 5 agar plates are used for high voltage microorganism treatment (prior to this, electrical safety procedures were conducted).

5.5.3 Post-test Procedures

Following the plasma biological decontamination tests, all devices (not including the exhaust) were switched off. The exhaust was kept working for at least 30 minutes to lower the possibility of further contamination to a minimum. After 30 minutes, the corona reactor and the microorganism collection system were cleaned for the next round of tests. Mouldy bread was then removed from the system and safely disposed. The generation system was also cleaned after the use.

The agar plates with microorganisms were numbered and marked. These agar plates were kept in the incubator for 72 hours which is a reasonable incubation time for growth of unidentified microorganisms colonies as these colonies were large enough for observation and for data analysis after this period.

5.6 Experimental Results

5.6.1 Biological Decontamination Efficiency

The experimental results of the biological decontamination tests included decontamination efficiency, η_b. The decontamination efficiency was calculated using the experimental data as

$$\eta_b = \frac{\bar{N}_s - N_p}{N_p} \times 100\% \quad (28)$$

where $\bar{N}_s$ is average colony forming unit number of microorganisms sampling and is used as the base sample number. N_p is one single colony forming unit number of microorganisms after plasma treatment. So the result of one single colony forming unit number minus the average sample number divided by the colony forming unit of this single run of experiment gives the microorganism number reduction of each experiment. The final result is based on at least 5 runs of experiments.

5.6.2 Working High Voltage Levels

As mentioned, prior to bio-aerosol decontamination, the effective working voltage level was established. To establish the required voltage level, several tests have been conducted using different voltage levels. At each voltage level above the corona ignition voltage (~10 kV), microorganisms following the plasma treatment were collected. After 72 hours in the incubator, the number of colony forming units (CFUs), N_p, was counted. Therefore, the efficiency of bio-aerosol decontamination can be calculated using the method introduced in 5.6.1 for each high voltage level, with the results of these tests shown in Figure 5-10. Each point is the mean value of at least 5 independent bio-inactivation tests and the error bars show values of standard deviation. The temperature was room temperature with relative humidity of ~30%.

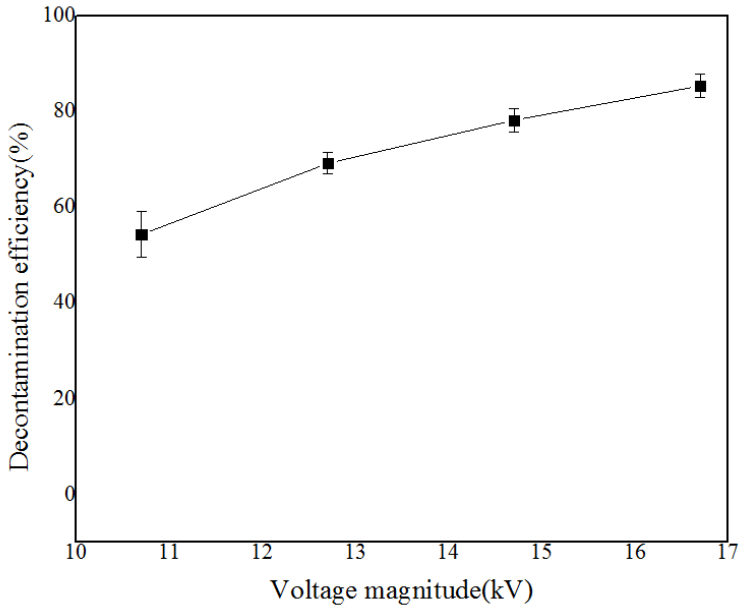

Figure 5-10. Biological decontamination efficiency as a function of voltage level.

Figure 5-10 shows the tendency of biological decontamination efficiency as a function of voltage. The initial data was the average microorganism colony forming units of sampling, which was 1330 ± 34 CFUs on the agar plate. The biological decontamination efficiencies were 54%, 69%, 78%, and 85% for -10.7 kV, -12.7 kV, -14.7 kV and -16.7 kV, respectively. The figure shows that higher voltage level can result in a higher decontamination efficiency. Voltage level higher than -16.7 kV could not be applied in the tests as several breakdowns occurred and, as such, beyond the working range of the biological decontamination system. Therefore, -16.7 kV was selected to be the optimal working voltage of the biological decontamination system.

5.6.3 Working Air Flow Rate

As discussed in Section 5.5, the flow rate of the system was regulated to 5 litres/minute. One reason for the regulation was to ensure the biological decontamination system has the same flow rate as the needle-mesh electrostatic precipitation system. Another reason was to

compare the influence of different flow rates on the efficiency of decontamination during tests to find a better flow rate for higher efficiency.

The system was first conducted with a 16 litres/minute pump. After the connection of different components through air hoses, the final flow rate through the system was tested to be 12 litres/minute. With the flow regulation, the flow rate was 5 litres/minute. Two groups of tests have been conducted in one day with the same microorganism source. Group 1 was a high voltage treatment with 12 litres/minute flow rate. The system running time for Group 1 tests was 8 minutes 20 seconds (100 litres of air). Group 2 was treated with a 5 litres/minute flow rate. The system running time for Group 2 tests was 20 minutes (100 litres of air). For the 100 litres of gas for each treatment, the high voltage level applied to the system for Group 1 and Group 2 was both -16.7 kV. The only difference of the two groups of tests was the flow rate. The result is shown in Table 5-1. The temperature was room temperature and relative humidity was ~30%.

Table 5-1. Comparison of results with different flow rates.

	12 litres/minute	5 litres/minute
Before tests (CFU)	1329±33	1329±33
After tests (CFU)	418±37	195±33
Biological decontamination efficiency	69%±2.8%	85%±2.5%

From Table 5-1 it was found that, for the same microorganism source, the biological decontamination efficiency was dissimilar for different flow rates. The biological decontamination efficiency was higher for a lower flow rate bio-aerosol. The reason for a

lower flow rate can provide microorganisms with longer exposure times in plasma, and the longer exposure time can support the process of inactivating microorganisms so that higher biological decontamination efficiency can be achieved. Indeed, the flow rate could be regulated to a lower one (less than 5 litres/minute), however, a lower flow rate also increases the experimental time and, therefore, energy consumption might be higher. Therefore, the balance between efficiency and flow rate should be considered. Since the system was altered from the needle-mesh electrostatic precipitation system, it was ideal that microorganisms were decontaminated while particles are precipitated. Therefore, the same flow rate (5 litres/minute) was used for the biological decontamination tests.

5.6.4 Results of Bio-aerosol Decontamination by Plasma

The bio-aerosol decontamination results are shown and discussed in this section.

5.6.4.1 Typical Examples of Bio-decontamination Tests

Microorganisms (unidentified microorganisms) formed colonies on agar plates with and without plasma treatment are shown both in Figure 5-11 and Figure 5-12 with 5 l/min gas flow rate. The temperature was room temperature and relative humidity was ~30%. These colonies have been formed during 72 hours in the incubator.

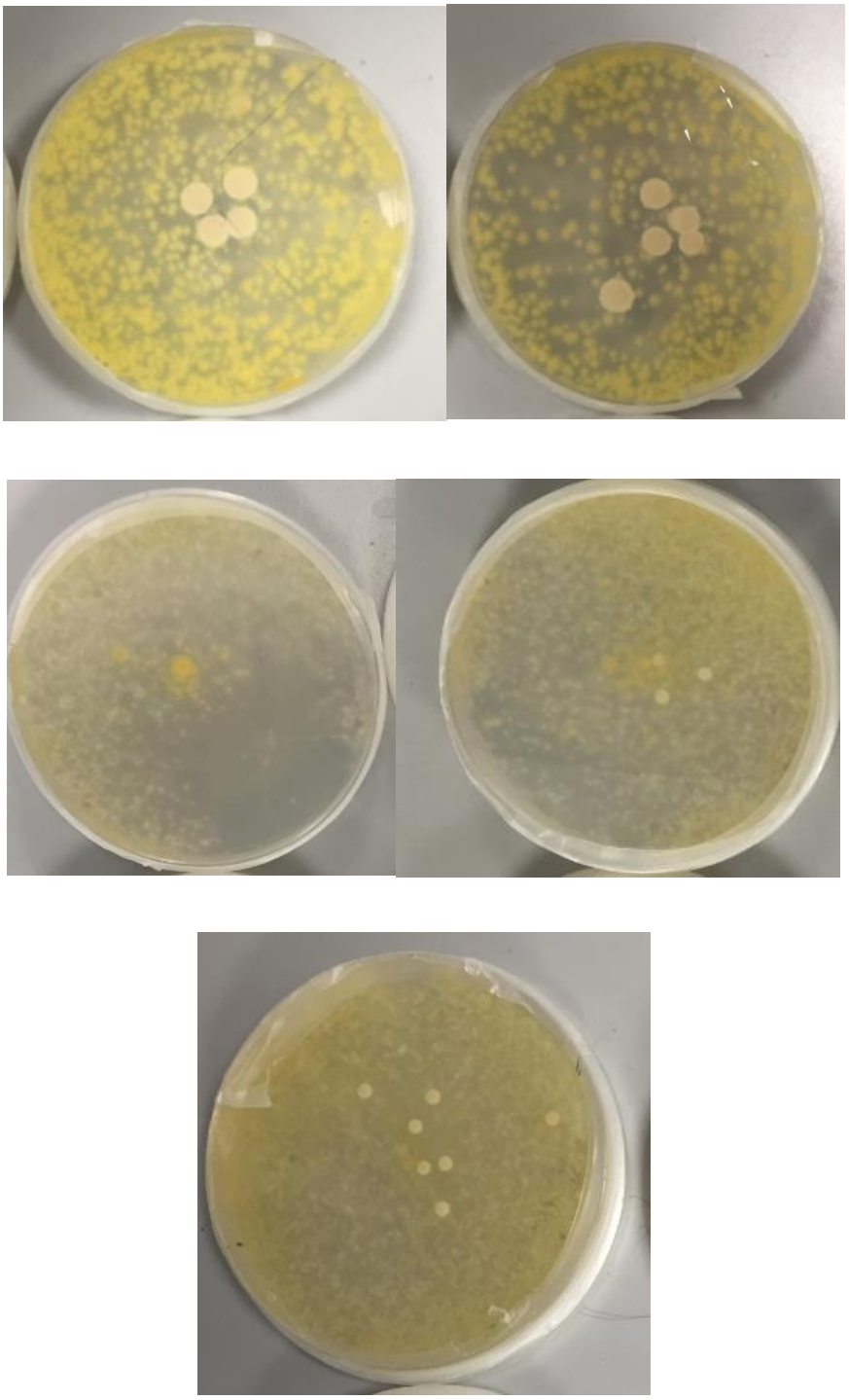

Figure 5-11. Examples of the agar plate with microorganism sample without plasma treatment with 5 l/min gas flow rate. (5 agar plates)

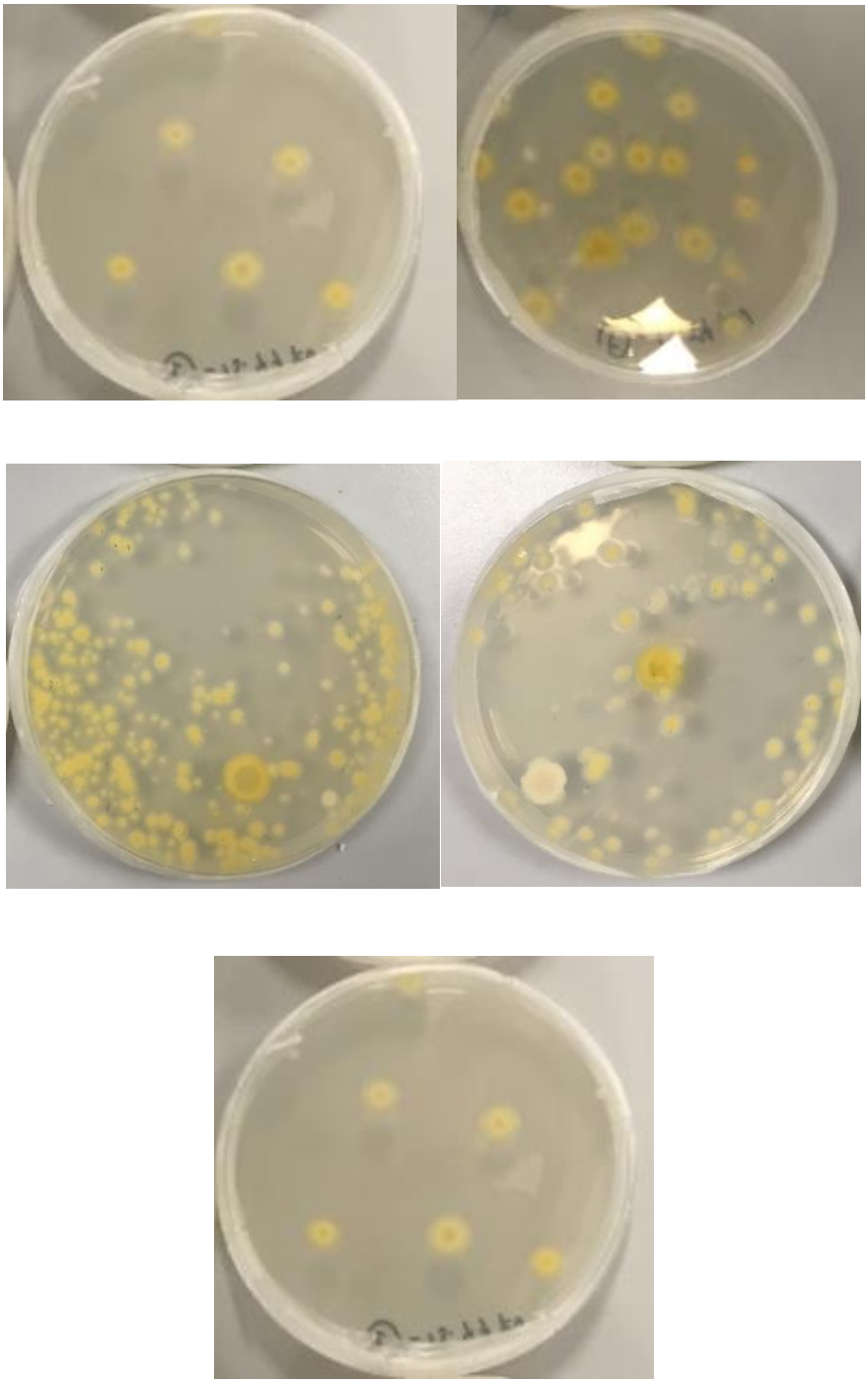

Figure 5-12. Examples of agar plates with microorganism's after plasma treatment with 5 l/min gas flow rate. (5 agar plates)

Figure 5-11 and Figure 5-12 show a typical test result. Figure 5-11 shows the five agar plates of microorganism samples without plasma treatment, and Figure 5-12 shows five agar plates of microorganism with plasma treatment. Visually, the example clearly shows the difference in number of CFUs between samples with and without plasma. The microorganisms were collected on agar plates within 7 hours with the same mouldy bread pieces. The difference between the two groups of tests was the plasma treatment of air flow contaminated with microorganisms. Therefore, the results show clearly the effect of plasma on biological decontamination.

5.6.4.2 Experimental Results

The effect of corona discharge on microorganisms was confirmed and the test results in numbers are shown in this section.

Biological test results can vary within relatively wide limits. In fact, these results were easier to be influenced by outer environment than particle electrostatic precipitation tests. The results could be influenced by humidity, temperature, gas component, gas concentration, etc. The unstable number and living condition of microorganisms from the mouldy bread was also a key factor causing the variation. Therefore, routine tests were conducted in a two-month period in different groups of experiments to establish the best and worst results of biological decontamination efficiency for this system. The results are shown in Table 5-2.

Table 5-2. Best and worst experimental result of biological decontamination.

	Best	Worst
Before treatment (CFU)	1034±139	618±101
After treatment (CFU)	72±18	166±17
Decontamination efficiency with plasma	93%±1.8%	73%±2.7%

5.6.4.3 Discussion on Biological Decontamination Results

The results of biological decontamination tests show that the corona discharge was effective in biological decontamination. It was established that negative DC energised corona was efficient in biological decontamination. The biological decontamination efficiency was high when the corona ignition voltage was achieved. The efficiency increased with the increase of a working voltage applied to the system and the efficiency could be as high as 93% when a voltage level (-16.07 kV) was just below breakdown voltage. The flow rate of the biological decontamination system was kept the same as the flow rate of needle-mesh electrostatic precipitation system in Chapter 3, therefore, the entire system could potentially be applied to the environment where high concentration of particles need to be removed and microorganisms need to be inactivated simultaneously.

5.7 Energy Consumption Analysis

The energy consumption was evaluated in the biological decontamination system. As with energy consumption evaluation calculation for needle-mesh topology particle precipitation system, the energy consumption evaluation calculation for biological decontamination

system was based on the current-time waveform during the biological decontamination process recorded by the oscilloscope over the shunt resistor. The reason for the energy consumption evaluation calculation was that the efficiency of energy used was also important. The ideal situation is to build a system with high biological decontamination efficiency and with low energy consumption.

Since the key component of the biological decontamination system and the key component of the needle-mesh electrostatic precipitation system were the same, the characteristics of the current-time waveform obtained during electrostatic precipitation process of the coaxial topology system was similar to the current-time waveform of the needle-mesh topology system as discussed in Section 3.8.1.

5.7.1 Methodology of Energy Consumption Analysis

The methodology of energy consumption evaluation calculation for coaxial topology system was exactly the same as the needle-mesh system which has been discussed in Chapter 3. The detailed methodology has been discussed and illustrated in Section 3.8.2. Therefore, the energy consumption can be calculated.

5.7.2 Energy Consumption Results

The flow rate of the system was 5 litres/minute (8.3×10^{-5} m^3/s), which was used for the energy consumption calculation. The calculation result of energy consumption of the biological decontamination system is shown in Table 5-3.

Table 5-3. Energy consumption for biological decontamination system for different voltage levels.

Voltage (kV)	-10.7	-12.7	-14.7	-16.7
Biological decontamination efficiency	54%	69%	78%	85%
Frequency (kHz)	740±18	260±100	360±120	450±110
Single impulsive charge (C)	3.19×10^{-11} $\pm4.13\times10^{-12}$	3.08×10^{-11} $\pm2.25\times10^{-12}$	2.87×10^{-11} $\pm1.49\times10^{-12}$	2.44×10^{-11} $\pm5.44\times10^{-12}$
DC current component (A)	-5×10^{-7}	-6×10^{-7}	-8×10^{-7}	-10×10^{-7}
Energy consumption (Wh/m^3)	0.102±0.023	0.357±0.138	0.521±0.166	0.639±0.198

5.7.3 Discussions on Energy Consumption

The calculation of energy consumption for the biological decontamination system has been discussed and the energy consumption results for the system have been shown. The results were compared with the typical energy consumption levels found in researches in energy consumption investigations. Since the aim of the biological decontamination system was designed to be applied to the environment where high concentration of particles need to be

removed and microorganisms need to be inactivated at the same time, the energy consumption results were compared with typical electrostatic precipitator energy consumption values. As mentioned in Chapter 3, the typical electrostatic precipitator energy consumption value found in paper [59] ranged from 0.1 to 0.5 Wh/m^3, with the gas velocity of 2-6 m/s and a voltage level of up to 20 kV. The electrostatic precipitation system developed in paper [59] provided the energy consumption value of 0.06-0.42 Wh/m^3, with the gas velocity of 0.8 m/s and a voltage level of up to 15-16 kV. Paper [71] shows that the energy efficiency of 0.44 Wh/m^3 can achieved with the gas velocity of >15-20 m/s and a voltage level of 10-17 kV. Another research paper [60] shows that the energy consumption level investigated was 0.1 Wh/m^3 with a voltage level of 60 kV. The results are compared with the energy consumption values as calculated in this research. In the research presented in this chapter, for negative energisation, the energy consumption for -10.7 kV voltage level was 0.102 Wh/m^3 with the biological decontamination efficiency of 54%, the energy consumption for -12.7 kV voltage level was 0.357 Wh/m^3 with the biological decontamination efficiency of 69%, the energy consumption for -14.7 kV voltage level was 0.521 Wh/m^3 with the biological decontamination efficiency of 78% and the energy consumption for -16.7 kV voltage level was 0.639 Wh/m^3 with the biological decontamination efficiency of 85%. The comparison shows that the energy consumption for the biological decontamination system are close to, or lower than, the typical value in researches in literature. Therefore, the results on energy consumption calculation provide the system with high biological decontamination efficiency and low energy consumption.

5.8 Conclusions

In this chapter, the effect of high voltage plasma on biological decontamination was investigated. The aim of this research was to prove the possibility of biological decontamination in atmosphere air by corona discharge. The confirmation of the result can provide a wider usage of corona discharge in research and industry. The biological

decontamination system developed for the investigation can be a suggestion of design for biological decontamination by corona discharge, especially for small volumes of gas.

To investigate the feasibility of biological decontamination in atmosphere air by corona discharge, a biological decontamination system was designed and developed. The system was altered from the electrostatic precipitation system developed in Chapter 3, i.e. a needle-mesh topology system. The core component of the biological decontamination system was the needle-mesh corona reactor and a new gas flow system was designed to meet the demands of experiments. Instead of being pumped into the system, air flow was sucked into the system to investigate biological decontamination to simulate the behaviour of air sampling machines which was easier for microorganism to be collected to test the effect of corona discharge on microorganisms. A microorganism collection system was designed to hold the nutritious agar plate. The source of microorganisms used for tests was unidentified microorganisms on mouldy bread. The source was simple, and microorganisms were easy to grow. A microorganism generation system with an electric shaker was designed and developed and the microorganism generation system aimed to shake the mouldy bread pieces, and the air flow that passed through the bread pieces can bring unidentified microorganisms into the corona reactor with a more uniform distribution in concentration. Air flow was initially mixed with microorganisms, and then sucked into the corona reactor. The biological decontamination occurred inside the corona reactor then the purified air flow was sucked out of the corona reactor and guided directly into the microorganism collection system, in which the microorganisms landed on nutritious agar plate for incubation to observe the status of microorganisms. After the microorganism collection system, the purified air flow was guided into the exhaust which is treated professionally to prevent any contamination to the laboratory.

The experiments were conducted in two groups for comparison. The first group of experiments were conducted without corona discharge, which was direct microorganism collection through the corona reactor. The results of the first group of experiments were

used as the baseline samples for comparison. The second group of experiments were conducted with a corona discharge, which was the corona treatment on microorganisms through the corona reactor. The two groups of experiments were conducted in the same day so the results for both the first and second group were assumed to be the same to make the experimental results accurate. The experimental results were recorded as the colony forming unit (CFU). Therefore, the reduction ratio of microorganisms with and without corona discharge can be calculated using the average CFU of the first group data and the average CFU of the second group data. The microorganisms for the two groups were incubated for 72 hours for best observation.

The experiments were conducted using negative DC energisation. The results show that the corona discharge is effective and apparent in biological decontamination of microorganisms, with an efficiency capable of being over 90%. As discussed in Chapter 3, the corona reactor was also very efficient in particle precipitation. The investigation of biological decontamination has provided corona discharge with a potentially wider usage. The system can be used not only to control particles in flue gas, but also to control microorganisms which can be treated by high voltage energised corona discharge. If there are requirements for both particles and microorganisms control, the system developed in this chapter is a suggestion of design to meet both demands.

Two parameters were controlled to investigate the influence on biological decontamination efficiency: gas flow rate and high voltage level. Different gas flow rates and high voltage levels were used for comparison. The experimental results show that the biological decontamination efficiency was increased as decreased gas flow rate can increase the exposure time of microorganisms under corona discharge. From a voltage level aspect, the increased high voltage level causes the increase of biological decontamination efficiency.

Energy consumption is also considered in this research as the design of the system also aims to be environmental friendly. With the developed method of energy consumption in Chapter

3, energy consumptions for different situations were calculated and compared with the energy consumptions in literature. It was found that the biological decontamination system developed is with very low energy consumption.

Since the system developed in this chapter was the investigation of the effect of plasma on biological decontamination, similar approaches in literature have been reviewed and compared with the results in this chapter, [54] [69] [68] [80] [81] [82] [83] [84] [85] [86].

The approaches in these papers show similar conclusions, as discussed in this chapter, where plasma is effective in biological decontamination and its respective effect for different types of microorganisms has been investigated. For example, in paper [80], microorganisms, such as *Pseudomonas fluorescens* vegetative cells, *Bacillus subtilis* var. *niger* endospores and *Penicillium brevicompactum* fungal spores, can be decontaminated by plasma with an efficiency over 70%. Paper [69] has shown that airborne pathogens, such as *Escherichia coli*, *Pseudomonas alcaligenes* and *Staphylococcus epidermidis,* can also be inactivated by plasma with an efficiency ranging from 20% to 70% with negative high voltage energisation i.e. the same energisation polarity as has been used in this chapter. This paper also shows similar conclusions as discussed in this chapter that an increased voltage level can result in increased decontamination efficiency.

Since the aim of the biological decontamination system developed in this chapter was to inactivate or remove microorganisms when the particle precipitation process was conducted at the same time, a similar approach in paper [54] was reviewed and compared with the results in this chapter. The study in this paper has presented a system to improve the indoor air quality by particle collection, odour removal and sterilisation of *E.coli*. The system developed for the sterilisation of *E.coli* was based on the topology of two perforated metals used for the generation of plasma where the system is energised with AC high voltage. The experimental results for *E.coli* sterilisation in this paper and the experimental results for microorganism decontamination discussed in this chapter have shown the same tendency

that plasma is effective in biological decontamination. The experimental results also have shown the same tendency that an increased voltage level can result in increased biological decontamination efficiency. The biological decontamination efficiency in this paper can be over 90% for the best case, while in this chapter, the biological decontamination efficiency can be also as high as 90% for the best case. However, in this paper, the system developed for particle precipitation and the system developed for *E.coli* sterilisation were with two different systems. The particle precipitation system was based on multiple needle-plate topology with DC energisation and the *E.coli* sterilisation system was based on double perforated metal topology with AC energisation. While in this chapter, particle precipitation and microorganism decontamination processes can be conducted using one system based on hypodermic needle-mesh topology only, which can give the system more flexibility when the system is applied in practice. Since the energisation types of the system for particle precipitation destination and for microorganism decontamination destination are both DC high voltage energisation, the system was easier to operate. The particle precipitation efficiency for the system developed in this paper and the system developed in Chapter 3 has been compared and discussed in Section 3.9. The result has shown that particle precipitation efficiency for the hypodermic needle-mesh system was much higher (100% for particles as small as 0.265 μm) than the particle precipitation system developed in this paper (50%). The combined performance for the system developed in this chapter was better than the system developed in the paper on both particle precipitation and biological decontamination.

The review of approaches of biological decontamination by plasma and the research in this chapter show that plasma is effective in biological decontamination. The comparison of these approaches with the research in this chapter show that the biological decontamination system developed in this chapter is with high decontamination efficiency. Since the system is also with very high particle precipitation efficiency, as discussed in Chapter 3, and with very low energy consumption, the performance of the system on biological decontamination will

broaden the use of this electrostatic precipitation system when a biological decontamination is required in addition to particulate matter emission control.

6 Modelling of Particle Charging and Removal Efficiency

6.1 Introduction

In order to improve and to investigate the performance of electrostatic precipitators, an electrostatic precipitator with a novel needle-mesh topology has been designed and discussed in Chapter 3. Improvements have been made to increase the performance of the electrostatic precipitators with coaxial topology, as discussed in Chapter 4. The performance of electrostatic precipitators was increased by optimising its topology (Chapter 3), by optimising the particle precipitation processes and by changing the charging environment (Chapter 4). Further performance improvements of the electrostatic precipitation system require understanding the influence of specific parameters on the electrostatic precipitator. In order to investigate the influence of these parameters, it is important to understand the dynamics of particles in electrostatic precipitators as particle velocity is one of the crucial factors which can influence the particle collection efficiency, according to the Deutsch-Anderson equation as discussed in Chapter 2. Particle displacement helps to understand the behaviours of particles inside electrostatic precipitators, therefore, a model which simulates particle dynamics and particle collection efficiency was designed for the investigation of influence on different parameters. The understanding of the influence on different parameters can help the optimisation of the design of electrostatic precipitators.

In this chapter, a model of particle charging, particle dynamics and particle collection efficiency for fine and ultrafine particles under DC energisation has been developed. The model was implemented using Simulink /Matlab software environment. Using this model, the particle dynamics in electrostatic precipitators was simulated and particle removal efficiency was obtained for particles with different permittivities, conductivities and

different dimensions. The model was applied to the topology of the coaxial electrostatic precipitator developed in Chapter 4. The model simulated dynamics of the single particle inside the electrostatic precipitator where the dynamics of the airborne particle included its velocity and displacement depending on electrical and geometrical parameters of the particles. The total charge accumulated by each particle in the electrostatic precipitator has been obtained and used to establish the electrostatic force acting on the particle. Based on the equation of motion which considers the gravity force, the electrostatic force and force of friction in the air, the particle dynamics can be obtained for different energisation levels and different particles.

One of the important components of the model was the charge of the particles. In electrostatic precipitation theory, particles were charged by plasma and subjected to an electric force which made the particle move towards the collection plate of the electrostatic precipitator. Therefore, the equation for the total charge on particles was used in the model. For the charging mechanisms both field charging and diffusion charging have been considered. There were some limitations in traditional charging equations as the only electric parameter in the traditional equation for field charge on particles considered was the relative permittivity of particles [62] [51]. However, in fact, the electric parameters included conductivity of particles, relative permittivity of particles, conductivity of medium and relative permittivity of medium. Field charging is very important in particle charging theory and the field charge dominant particle with radius larger than 1 μm. Therefore, the field charge equation with the consideration of conductivity and relative permittivity of both particles and media was derived and has been used for the field charge on particles in the model. The influence of space charge was also considered in this model. The electric field in the model was also dependent on distance between electrodes which made the model more accurate and the simulation results closer to practical cases.

In the development of this novel model a critically important parameter, the ion mobility, was required for the analysis of diffusion charging and in a space charge influenced electric

field. The influence of ion mobility was also important in designing electrostatic precipitators as can influence the dynamics of particles and the performance of electrostatic precipitators in precipitation efficiency, which will be discussed in detail in this chapter. Since the ion mobility for positive and negative energisations were different, it can reflect the influence of energisation polarity. The ion mobility is one of the most important parameters in this model which is normally difficult to obtain. The measurement in this chapter was conducted by an I-V curve fitting of both experimental and theoretical data curves. The measurement of ion mobility will be discussed in this chapter. The experimental data curve was measured using a needle-plane topology test cell which has been developed for the measurement of the ion mobility. Both positive and negative DC energisations have been considered for the ion mobility measurement, and the influence of increased humidity was also considered in this chapter.

The simulation of the particle dynamics and particle collection efficiency were conducted using practical electrical parameters of particles which could be found in practical applications. These particles included soot particles, salt particles, condensable organic compounds particles and water particles. The influence of different factors which may affect precipitation performance and particle collection efficiency will be discussed in Section 6.9. These factors included particle electric characteristics (particle conductivity and particle relative permittivity), particle initial displacements, ion mobility, current levels and particle size distributions. The detailed influence on particle dynamics and particle collection efficiency on electrostatic precipitators will also be discussed in Section 6.9.

6.2 Equations of Particle Dynamics

The particle dynamics model was developed based on the coaxial topology of the electrostatic precipitator. The coaxial topology electrostatic precipitator has been introduced and discussed in previous chapters. The design of the coaxial electrostatic precipitator is shown in Figure 6-1. In the model, the dynamics of a single particle was

simulated. The particle was assumed to have a spherical shape and was moving inside the coaxial electrostatic vertically positioned precipitator. The force on the particle is shown in Figure 6-1.

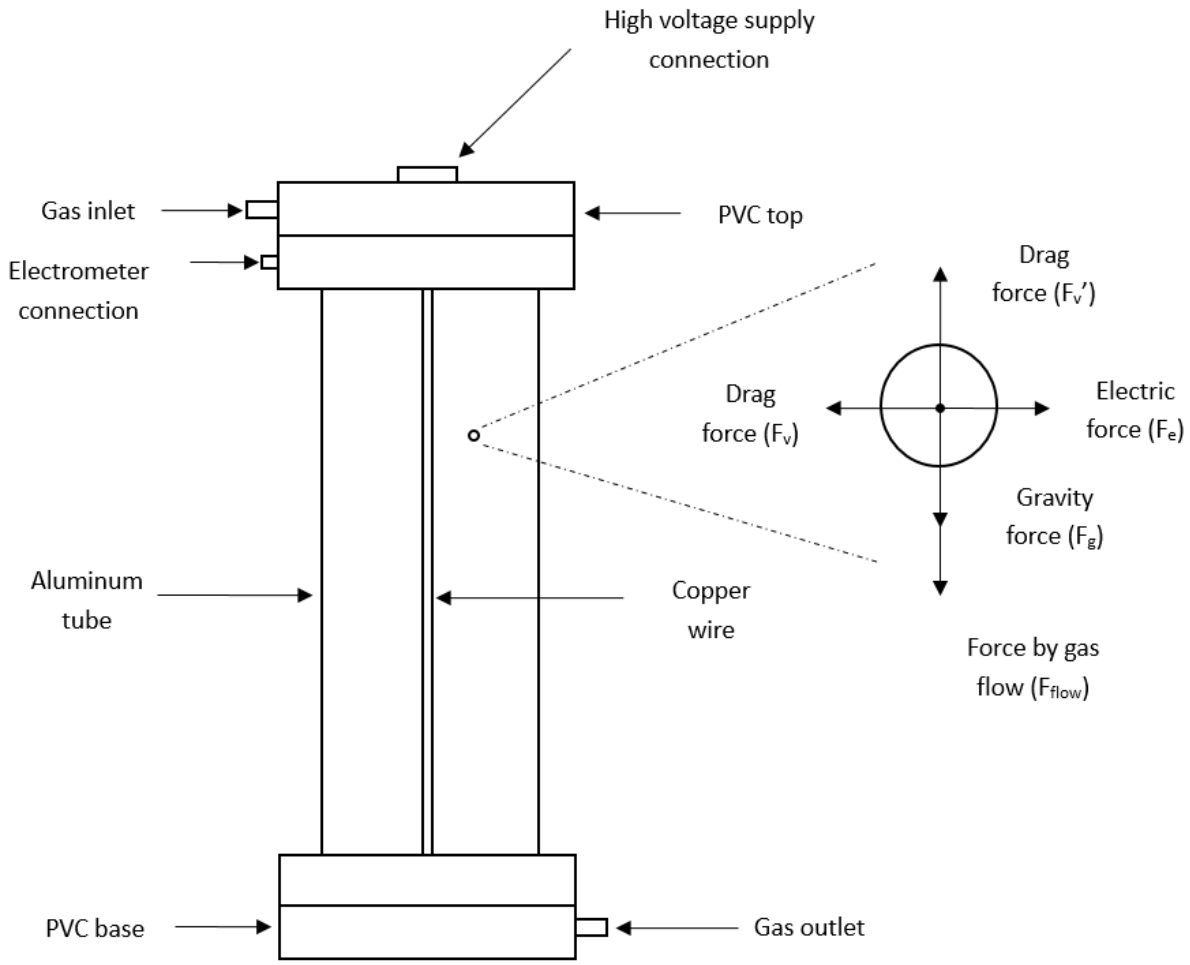

Figure 6-1. Particle inside the particle electrostatic precipitator. (Electrostatic precipitator is from the design shown in Chapter 4).

As shown in Figure 6-1, when the particle is moving inside the electrostatic precipitator, there are several forces acting on the particles in both horizontal and vertical directions. Vertically, the force gravity, F_g, and force, $F_v^{'}$, of gas flow act on the particle in the same direction while the drag force act on the particle in the opposite direction. Horizontally, the

electric force, F_e, and drag force, F_v, act on the particle in opposite directions. In electrostatic precipitators, since charged particles are moving to the collection plate (the aluminium tube) due to the electric force on particles, the horizontal movement of the particle will be investigated in this research and the model in this chapter will be based on this movement.

Therefore, horizontally, the electric force (F_e) and the drag force (F_v) act on the particle in opposite directions, which gives the total force, $F_{Total\text{-}horizontal}$, as

$$F_{Total-horizontal} = -\frac{F_v}{Co} + F_e = -\frac{F_v}{Co} + EQ_{Total}(t) \tag{29}$$

where F_e is the electric force on the particle, E is the electric field strength, Co is Cunningham correction factor, $Q_{Total}(t)$ is the total charge on particle at time t and F_v is the drag force.

The drag force is due to viscosity between a body and a fluid (liquid or gas) when the particle is moving past the gas in this chapter's situation and acts in the direction opposite to the moving direction of the particle when passing through the gas. The drag force caused by viscosity medium, according to Stoke's law, shows the drag force on particles with a very small Reynolds numbers, i.e. particles with a small size, due to the viscosity of the medium. There are some assumptions with the use of Stoke's law: 1) particles are spherical and with smooth surface; 2) interaction between the particles is neglected; 3) medium flows in parallel layers and there is no disruptions between layers (known as laminar flow in fluid dynamics theory); 4) material of particles and medium are assumed to be uniform in composition. The drag force is given by

$$F_v = 6\pi\eta R_p V \tag{30}$$

where η is the viscosity of the gas ($1.8\text{x}10^{-5}$ Ns/m^3 used for simulationm^2), R_p is the radius of particle (m) and V is the migration velocity of particle (m/s).

The drag force is corrected by the Cunningham correction factor, Co, as shown in Equation (29). The Cunningham correction factor is used in the case when there is a non-continuum effect when the particle size is small. The drag force derived by Stoke's law has a critical assumption; the relative velocity of gas molecules at the surface of the particle is zero. The assumption is not correct when the particle size is very small. When the particle size is small, gas molecules may miss the particles without collision. In this situation, the medium is non-continuum. Since the collision of particles and gas molecules is the source of drag force, the missing collisions result in a higher particle velocity when compared with the particle velocity calculated by Stoke's law. Therefore, Stoke's law should be corrected by the Cunningham factor to provide more precise results. The Cunningham factor is given by

$$Co = 1 + 1.246 \times \lambda / R_p + 0.42 \times \lambda \times \exp(-0.87 R_p / \lambda) \quad (31)$$

where λ is mean free path of gas molecules (6.67 x 10^{-8} m for air which is used for simulation).

The mean free path of gas molecules means the average distance a gas molecule travels between collisions with other gas molecules. When the particle size is much smaller than the mean free path of gas molecules, the missing collisions between particles and gas molecules is more likely.

Total time-dependent charge, $Q_{Total}(t)$, accumulated on the particle is given by

$$Q_{Total}(t) = Q_c(t) + Q_p(t) + Q_{diffusion}(t) \quad (32)$$

where $Q_C(t)$ is the conduction charge, $Q_P(t)$ is the polarisation charge and $Q_{diffusion}(t)$ is the diffusion charge (introduced in the following section).

6.3 Charging Mechanisms

In the theory of electrostatic precipitation, particle charging plays an important role as the process provides particles with electric charge, and this charged particle is then subjected to the electric force and moves in the electric field. Particles are charged due to two different mechanisms, as discussed in Chapter 2: field charging and diffusion charging. These mechanisms will be discussed in this section.

6.3.1 Field Charging

In the field charging process, as mentioned, the charge transfer is due to the collision of the particles and ions and the process is influenced by the external electric field. When the particle is stressed with the electric field there are also ions which are travelling along the electric field lines. Thus, the ionic flux can transfer the electric charge on the particle by collision.

The ions continue to bombard the particle until the charge on that particle is saturated. When the charge on the particle becomes saturated, the electric field lines will be repelled from the particle and the field charging process stops. The total field charge is the combination of conduction charge, ($Q_c(t)$), and polarisation charge, ($Q_p(t)$). Conduction charge, ($Q_c(t)$), is given by [87]

$$Q_c(t) = 6\pi R_p^{\,2} E(r)\varepsilon_0 \frac{\varepsilon_m\sigma_p - \sigma_m\varepsilon_p}{2\sigma_m + \sigma_p}(1 - e^{-t/\tau_{MW}}) \tag{33}$$

where E(r) is the electric field strength where the particle locates, ε_0 is the vacuum permittivity (8.85 x 10^{-12} F/m), ε_m is the relative permittivity of the medium, ε_p is the relative permittivity of the particle, σ_m is the conductivity of the medium and σ_p is the conductivity of the particle. τ_{MW} is the Maxwell-Wagner relaxation time.

The time dependant polarisation charge, ($Q_p(t)$), is given by [87]

$$Q_p(t) = 6\pi R_p^2 E(r)\varepsilon_0\varepsilon_p\left(1 - \frac{\varepsilon_p + \varepsilon_m}{\varepsilon_p + 2\varepsilon_m} e^{-t/\tau_{MW}}\right) \quad (34)$$

The Maxwell-Wagner polarisation effect is the polarisation process which takes place at the interface between two dielectric materials stressed with the external electric field. The model describes the inhomogeneous structure of the particle and medium using their respective relative permittivity and conductivity. The Maxwell-Wagner relaxation time, which characterises electric field relaxation, is given by [87]

$$\tau_{MW} = \frac{2\varepsilon_m + \varepsilon_p}{2\sigma_m + \sigma_p}\varepsilon_0 \quad (35)$$

6.3.2 Diffusion Charging

Diffusion charging is the charging mechanism where diffusing ions collide with particles due to random Brownian motion, then particles are charged due to collision with ions. In a diffusion charging mechanism, there is no external field applied. The ionisation source ionises air or gas molecules and the ions collide with particles resulting in charge transfer. The charging rate decreases with the increase of charge on particles.

The gas ions have a Boltzmann distribution of velocities so the collisions of ions with particles are expected to result in a Boltzmann distribution of charges. Charge, $Q_{diffusion}(t)$, which is transferred to the particle due to diffusion charging, is given by [87]

$$Q_{diffusion}(t) = \frac{2\pi\varepsilon_0 kTd}{e}\ln\left(1 + \frac{e^2 Ntd}{2\varepsilon_0\sqrt{2m\pi kT}}\right) \quad (36)$$

where k is the Boltzmann constant (1.38×10^{-23} m^2 kg s^{-2} K^{-1}), T is the temperature (300 K for room temperature), d is the diameter of particle (m), N is the ion number density (1×10^6 $/m^3$) and m is the mass of particle (kg).

6.3.3 Comparison of the Charging Mechanisms

The field charging mechanism and the diffusion charging mechanism dominate for different particle size ranges. For particles with a diameter larger than 1 μm, field charging is more significant than diffusion charging. On the contrary, for particles with diameter smaller than 1 μm, diffusion charging is more significant than field charging.

To compare the difference in charging mechanisms for particle with different sizes, a simple comparison with randomly selected parameters was made using the developed model. The parameters used in this study were as follow: ε_p = 2, ε_m =1, σ_m = 3×10^{-15} S/m, σ_p = 1×10^{-10} S/m, R_p = 2.5×10^{-6} m, T = 300 K, I(t) = 2×10^{-4} A, displacement r = 0 and ion mobility μ = 1.8×10^{-4} m^2/Vs. The result of the analysis using Equation (33), Equation (34) and Equation (36) are shown in Figure 6-2.

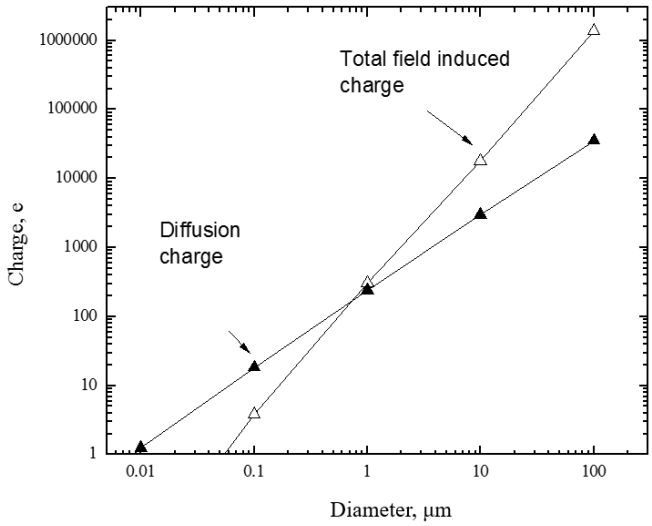

Figure 6-2. Comparison of field charging and diffusion charging for different particle dimensions.

As can be seen from Figure 6-2, diffusion charging is significant for particles smaller than 1 μm and field charging is significant for particles larger than 1 μm.

6.4 Space Charge Influenced Electric Field

In this research the influence of space charge was considered. In cylindrical topology, as simulated in this model, the electric field with space charge is given by

$$E(r)^2 = \left(A + \frac{R_w^2}{r^2} \left(E_r^2 - A \right) \right) \tag{37}$$

where R_W is the radius of the wire (0.0002 m), r is the particle displacement and E_r is the critical electric field of ionisation in atmospheric air (2.9×10^6 V/m).

The parameter A in the equation above is defined as

$$A = \frac{I(t)}{2\pi r \varepsilon_0 \varepsilon_m \mu} \tag{38}$$

where *I(t)* is the corona current (A) and μ is the ion mobility (m^2/Vs)

6.5 Final Equations of Particle Dynamics

The final equation of motion which describes the dynamics of particles in the electrostatic precipitators is given by

$$\frac{d^2 r}{dt^2} = \frac{1}{C}[E^2(r,t)(\varepsilon_0 \frac{\sigma_m \varepsilon_p - \varepsilon_m \sigma_p}{2\sigma_m + \sigma_p}(1 - e^{-t/\tau_{MW}}) + \varepsilon_0 \varepsilon_p (1 - \frac{\varepsilon_p + \varepsilon_m}{\varepsilon_p + 2\varepsilon_m} e^{-t/\tau_{MW}}) + \frac{Q_{diffusion}}{6\pi R^2 E(r)}) - D\frac{dr}{dt}] \tag{39}$$

where the coefficient C and D are given by

$$C = \frac{m}{6\pi R_p^2} \qquad D = \frac{\eta}{R_p Co} \tag{40}$$

6.6 Ion Mobility Measurement

The measurement of an important parameter, ion mobility (μ) as used in the model for diffusion charging in Equation (36), is illustrated in this section. Ion mobility is the ability of ions to move through a medium in response to an electric field. The method of measurement for ion mobility is using a curve fitting which will be discussed in Section 6.6.1. In the research, a test cell was designed to measure ion mobility using both positive and negative energisation and for different distances between needle and plane. The influence of humidity on ion mobility was also investigated.

6.6.1 Methodology of the Ion Mobility Measurement

Ion mobility is measured using the method of current-voltage (I-V) curve fitting. The I-V curve is measured using a tip-plane topology test cell in which ionisation occurs. There is an I-V curve for hyperboloid approximation for electrical field along the central point-plane. The ion mobility and the electrical field serve as the two fitting parameters in the theoretical equation. When the best fitting of the experimental I-V curve and the theoretical I-V curve is found, the two fitting parameters are determined. The parameters used for theoretical I-V curve for tip-plane configuration is shown in Figure 6-3.

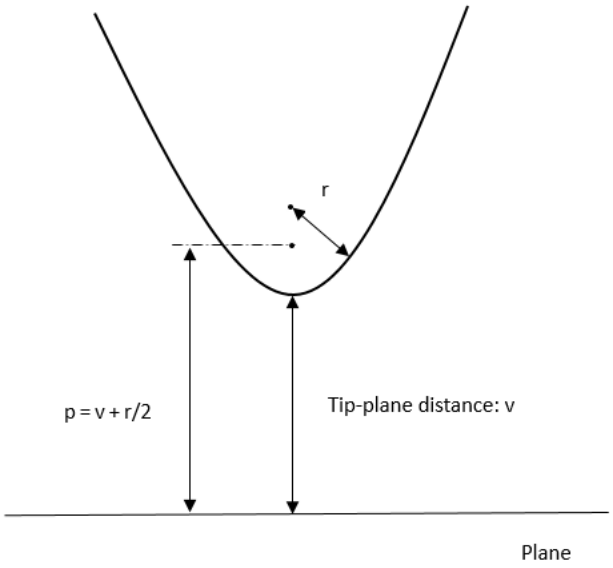

Figure 6-3． Parameters used for theoretical I-V curve for needle-plane configuration.

The hyperboloid approximation for electrical field along the central point-plane is given by

$$E(v) = \frac{[p^2(2-p)E_p^2 - Av\{p(2-p) + (1-p)v - v^2/3\}]^{1/2}}{(v+p)(2-v-p)} \tag{41}$$

where v is the distance from the needle tip (for example, when v=0 it means the apex of the needle) p is given by

$$p = \frac{r}{2a} \tag{42}$$

where r is radius of needle, which is 0.2mm for gramophone needle in this case. a is the combination of tip-plane distance and r/2.

In Equation (41), A is given by

$$A = \frac{2I}{\pi a \varepsilon_0 \mu} \tag{43}$$

where I is the steady-state corona current and μ is ion mobility serve as one fitting parameter.

In Equation (41), E_p is the electric field at the apex of the needle (when v=0) and is given by

$$E_p = \frac{2V_0}{(r \ln(4\frac{a}{r}))} \tag{44}$$

where V_0 is voltage at the apex of the needle (when v=0) and serves as the other fitting parameter.

The integration of E(v) links voltage and current, which is given by

$$\int_0^{1-p} E(v)dv = -\frac{V}{a} \tag{45}$$

Therefore, Equation (41) and its relation to Equation (45) is the theoretical I-V curve in which ion mobility μ and electric field at the apex of the needle Ep serve as fitting parameters.

6.6.2 Test Cell Design

A test cell was designed and developed to measure I-V curves to obtain ion mobility in air. The test cell was with tip-plane configuration. A gramophone needle was used for the HV electrode for the ionisation of air and development of corona discharge. The distance between the tip of the needle and the plane was precisely controlled. The design of the test cell is shown in Figure 6-4.

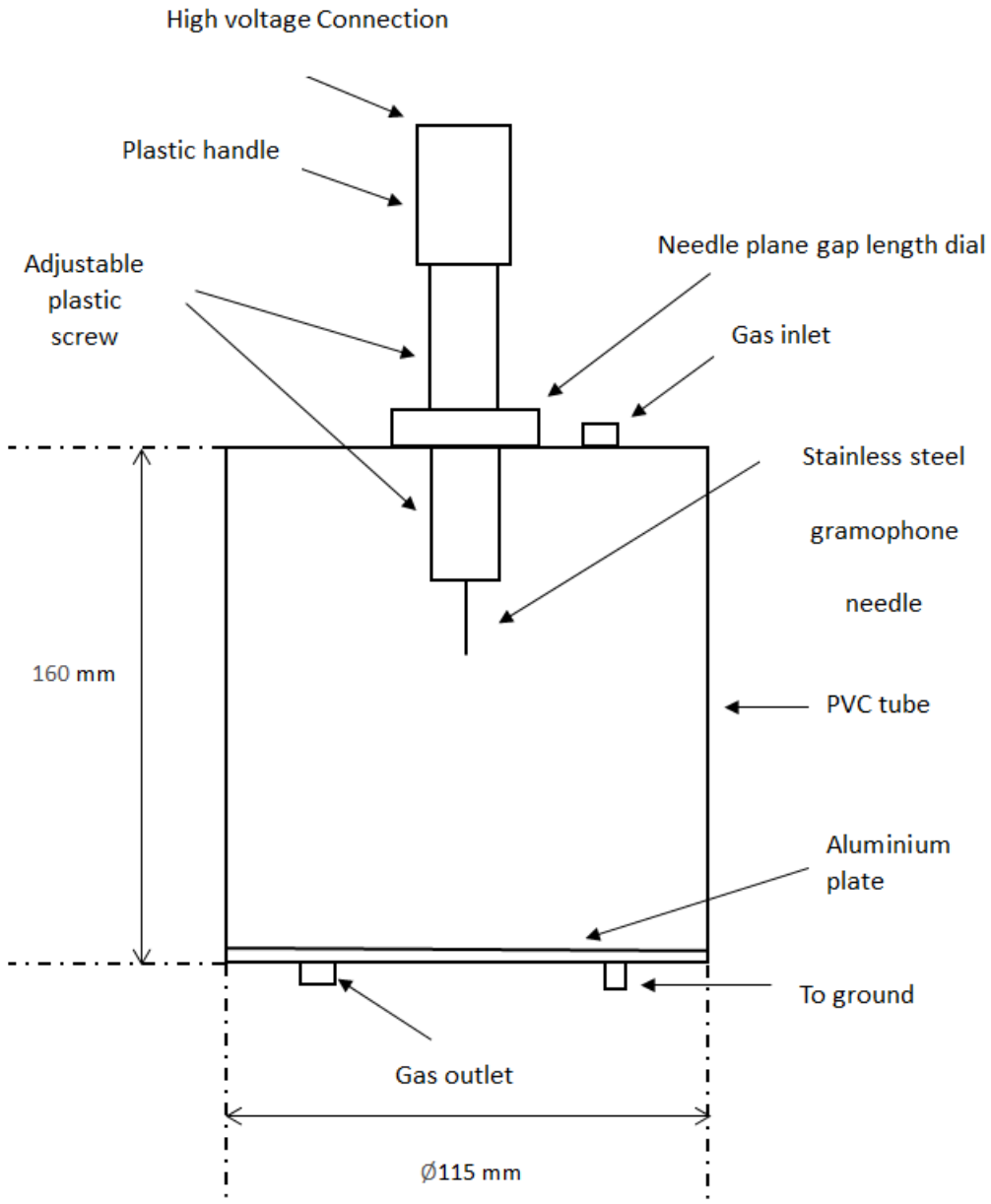

Figure 6-4. Design of the ion mobility measurement test cell.

The test cell was with a tip-plane configuration and the HV electrode was made of a gramophone needle. The reason for the use of the gramophone needle is that they are manufactured to specific standards and have reasonable consistency in their tip radius, thus, the replacement of needles in the test cell does not change the experimental conditions which offers precise measurements. These characteristics make gramophone needles a more suited choice for the generation of ionisation.

The gramophone needle was made of stainless steel (conductivity of stainless steel: 1.45×10^6 S/m) and was located at the central top of the cylindrical tube. A high voltage can be applied to the needle. The needle was connected with a tuneable plastic handle, and a length dial was located at the bottom of the handle to measure the length between the tip of the needle and the plane. The reason for the dial was due to the inconvenience of measuring the length inside the tube. Therefore, the dial placed externally gives the flexibility of the measurement and the adjustment of the length. The dial was divided into eight sections for each turn of the handle and each turn of the handle was 1 mm in distance. Pre-experiments, the needle was adjusted to reach the plane (when needle-plane distance was zero). Then the handle was turned to adjust to the required distance.

The plane was made of aluminium (conductivity of aluminium: 36.9×10^6 S/m). The tube was PVC (relative permittivity of PVC: 3.9) and the tube was transparent for better observation. There was a gas inlet on top of the test cell and a gas outlet on bottom of the test cell. The test cell is shown in Figure 6-5.

Figure 6-5. Ion mobility measurement test cell.

In the measurement of ion mobility, the influence of increased humidity was investigated. In order to investigate the influence of increased humidity, a humidifier was designed which can be used to increase the humidity of the experimental system. The design is shown in Figure 6-6.

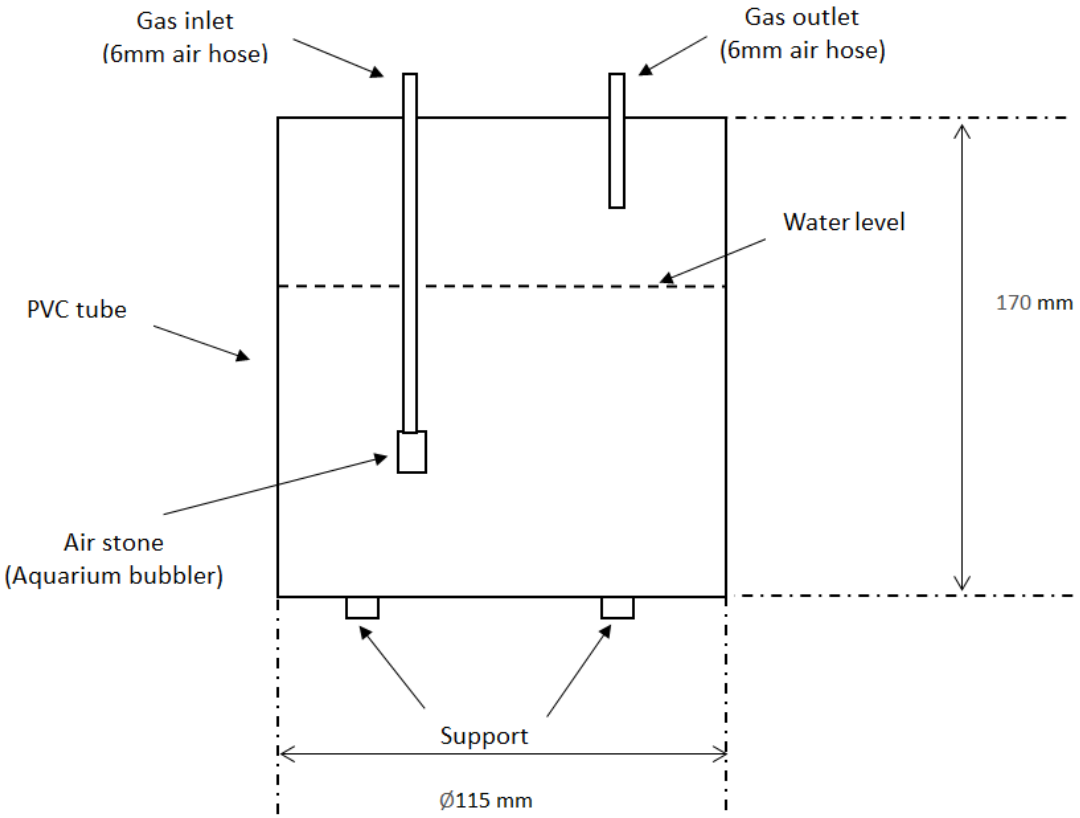

Figure 6-6. Design of the humidifier.

In the design of the humidifier, air flow was guided into the humidifier from the gas inlet. An air stone (bubbler for aquarium) was used and was located under the water level. The air stone allowed air flow to pass through and generate large and stable bubbles, then air with increased humidity was generated above the water level and guided out of the humidifier from the gas outlet.

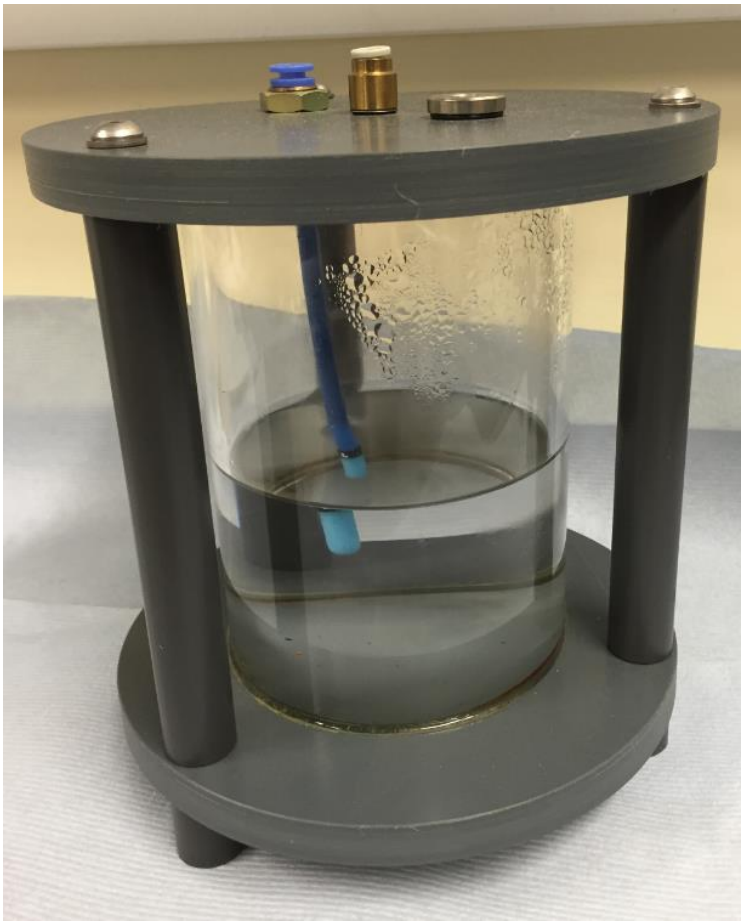

Figure 6-7. Humidifier for the investigation of humidity influence on ion mobility.

Figure 6-7 shows the humidifier for investigation of humidity influence on ion mobility based on the design. The humidity of the air from the humidifier can be as high as 81% in room temperature.

6.6.3 Experimental Setup

The experimental setup of the system is shown in Figure 6-8.

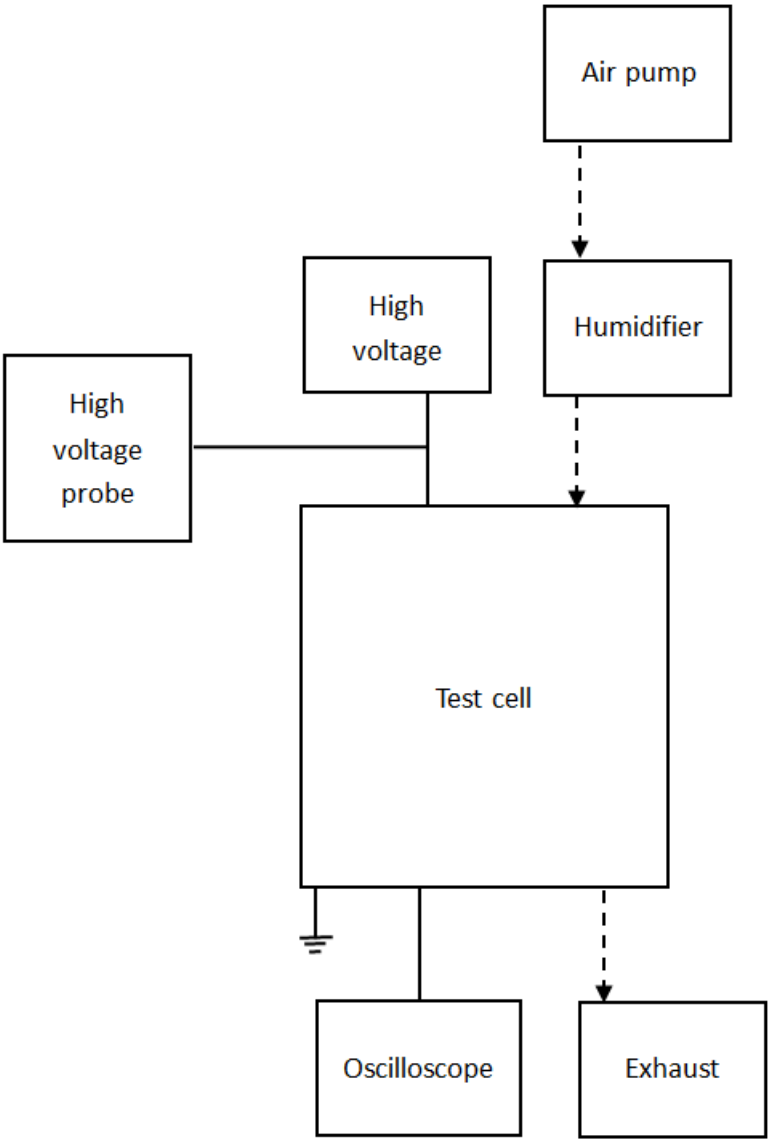

Figure 6-8. Experimental setup of the ion mobility measurement test cell.

As shown, the high voltage (Glassman INC) was applied to the test cell. The high voltage supply used for the measurement was both positive and negative DC high voltage. The voltage level (V) was measured by the high voltage probe (TES TEC HVP-40). An oscilloscope was applied to the plane of the test cell to measure corona current (I) (Tektronix TDS 2024 200 MHz, 2 GS/s). An air pump was used to pump air into the test cell from the gas inlet, and the gas was pumped out of the test cell through the gas outlet to the exhaust.

6.6.4 Ion Mobility Measurement Procedures

The procedure of ion mobility measurement is as follows:

1) Experimental components were connected electrically.

2) Needle-plane distance was adjusted to certain required value.

3) Air pump was switched on.

4) High voltage was applied to the test cell.

5) Voltage was increased step by step and for each voltage level, the current was measured.

6) An experimental I-V curve was plotted.

7) Curve fitting of experimental I-V curve to the theoretical I-V curve was conducted to find the best fit.

8) When the best fit was found, ion mobility was determined.

6.6.5 Measurement Results

Ion mobility measurement results are shown in this section. Both negative and positive DC energisations were used for the measurement, and the influence of increased humidity on ion mobility was investigated. Different gap distances were compared for the measurement to investigate the influence of gap distance on ion mobility. Relative humidity for ambient air was 31%. Relative humidity for increased humidity case was 81%.

6.6.5.1 Curve Fitting Results for Negative DC Energisation

The fitting of the theoretical I-V curve and experimental I-V curve was conducted using the fitting procedure using Origin 9.0 graphing software. The goodness of fitting parameter R^2 (coefficient of determination) obtained in Origin 9.0 was given for all fitted lines. For negative DC energisation, 5 mm, 10 mm and 14 mm gap distances were used. The results of the fitting and the obtained values of ion mobility are shown as follows.

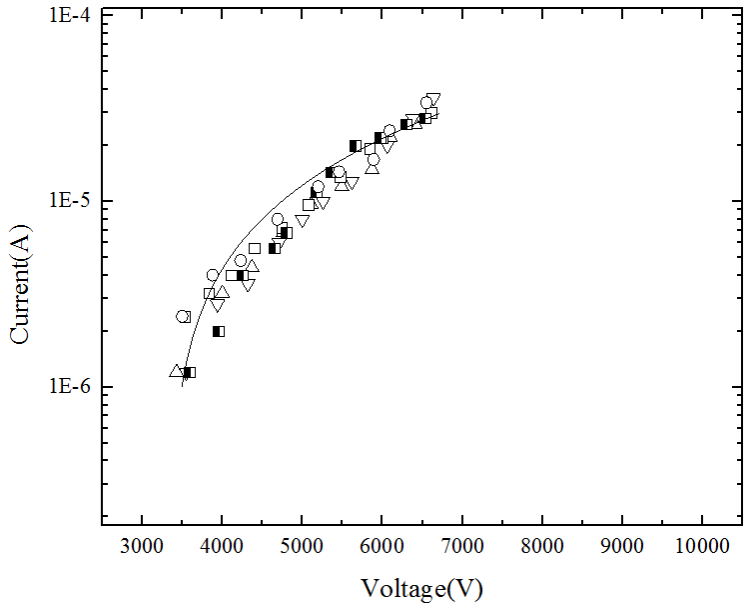

Figure 6-9. Fitting of I-V curve for dry air. (Negative DC, 5mm gap)

$E_P = 1.7\times10^8$ V/m, $\mu = 2.1\times10^{-4}$ m^2/Vs.$V_0 = 11.5$ kV, Goodness of fitting $R^2 = 0.99918$.

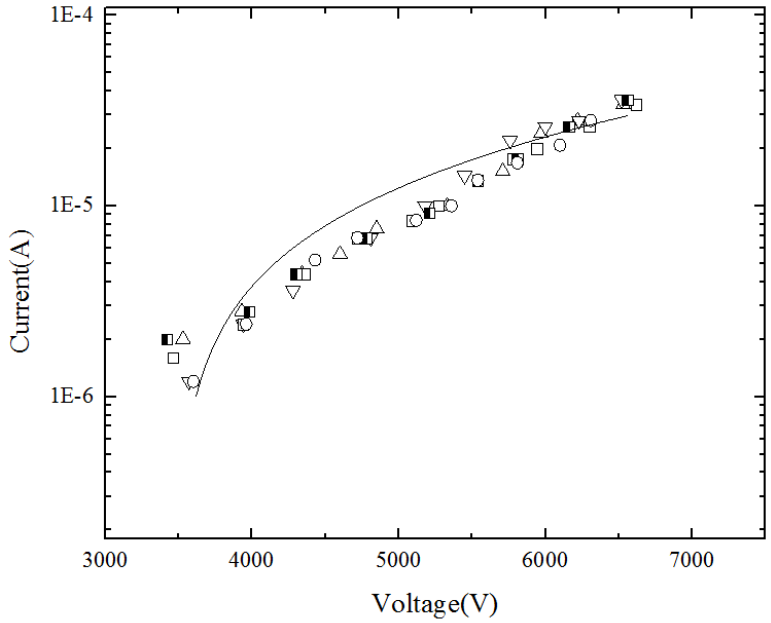

Figure 6-10. Fitting of I-V curve for humid air. (Negative DC, 5mm gap)

E_P = 1.7×10^8 V/m, μ = 2.3×10^{-4} m^2/Vs.V_0 = 12 kV, Goodness of fitting R^2 = 0.99821.

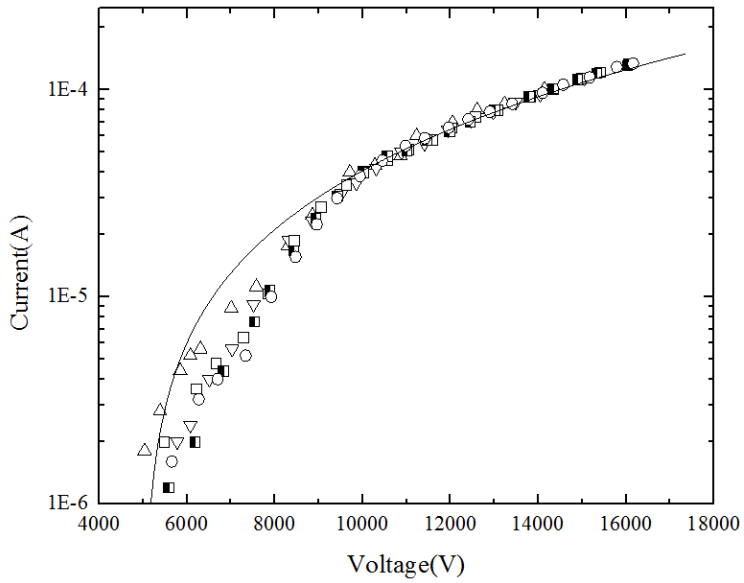

Figure 6-11. Fitting of I-V curve for dry air. (Negative DC, 10mm gap)

E_P = 2.5×10^8 V/m, μ = 2.6×10^{-4} m^2/Vs. V_0 = 19 kV, Goodness of fitting R^2 = 0.99937.

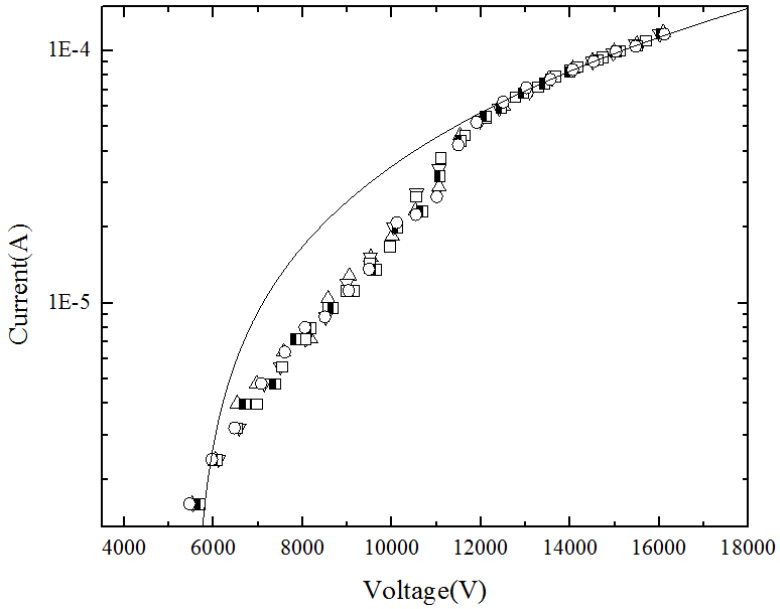

Figure 6-12. Fitting of I-V curve for humid air. (Negative DC, 10mm gap)

$E_P = 2.8\times10^8$ V/m, $\mu = 2.4\times10^{-4}$ m^2/Vs. $V_0 = 21$ kV, Goodness of fitting $R^2 = 0.97911$.

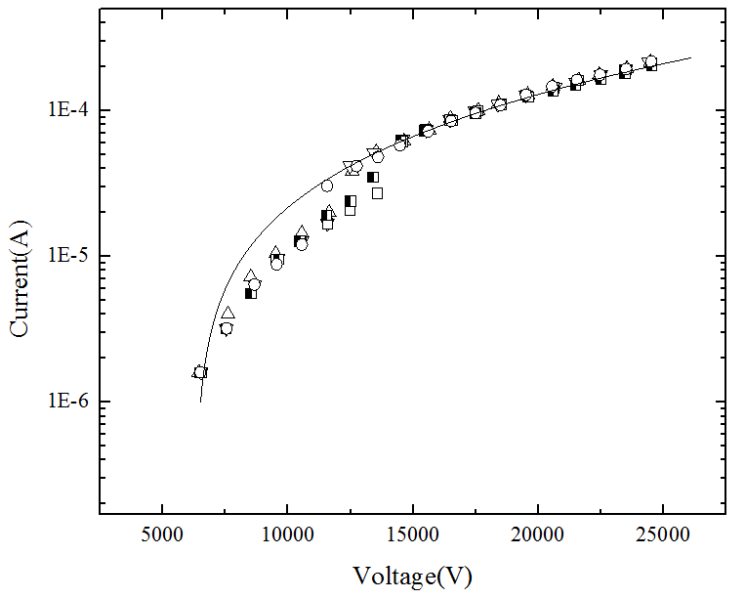

Figure 6-13. Fitting of I-V curve for dry air. (Negative DC, 14mm gap)

$E_P = 3.1\times10^8$ V/m, $\mu = 2.4\times10^{-4}$ m^2/Vs. $V_0 = 25$ kV, Goodness of fitting $R^2 = 0.99812$.

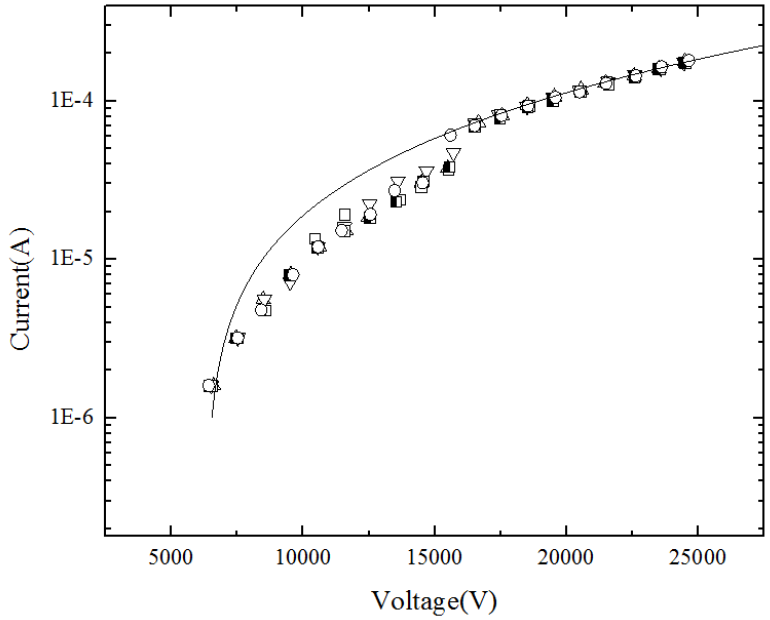

Figure 6-14. Fitting of I-V curve for humid air. (Negative DC, 14mm gap)

$E_P = 3.1\times10^{8}$ V/m, $\mu = 2.1\times10^{-4}$ m^2/Vs. $V_0 = 25$ kV, Goodness of fitting $R^2 = 0.98911$.

6.6.5.2 Curve Fitting Results for Positive DC Energisation

For positive DC energisation, only 10mm and 14 mm gap distances were used. 5mm gap distance was not used as it was found that there was no steady-state current for different voltage levels for this gap.

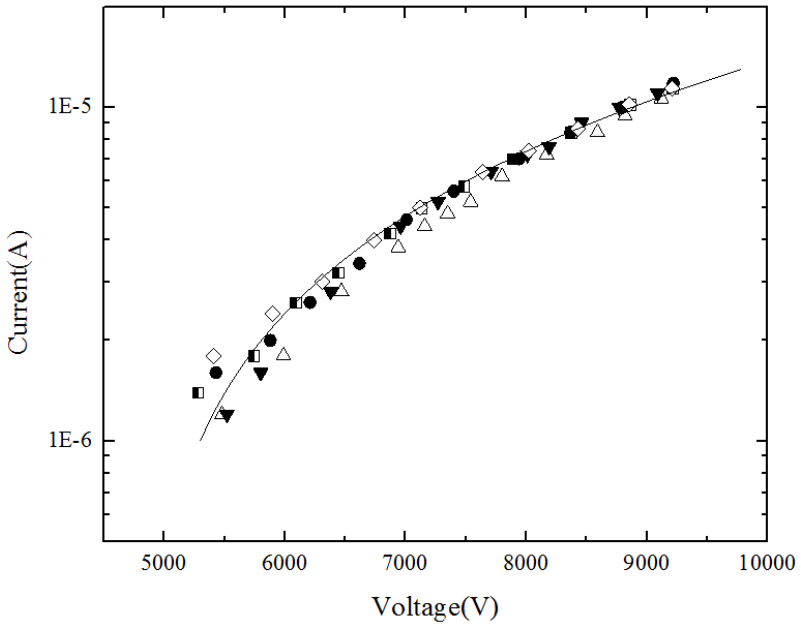

Figure 6-15. Fitting of I-V curve for dry air. (Positive DC, 10mm gap)

$E_P = 2.4\times10^{8}$ V/m, $\mu = 0.85\times10^{-4}$ m^2/Vs. V0 = 18 kV, Goodness of fitting $R^2 = 0.99977$.

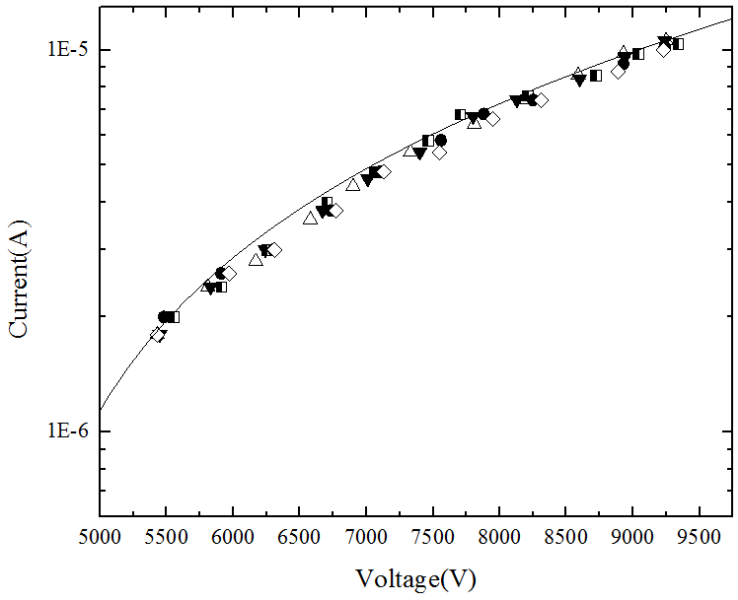

Figure 6-16. Fitting of I-V curve for humid air. (Positive DC, 10mm gap)

$E_P = 2.1\times10^{8}$ V/m, $\mu = 0.75\times10^{-4}$ m^2/Vs. V0 = 16 kV, Goodness of fitting $R^2 = 0.97911$.

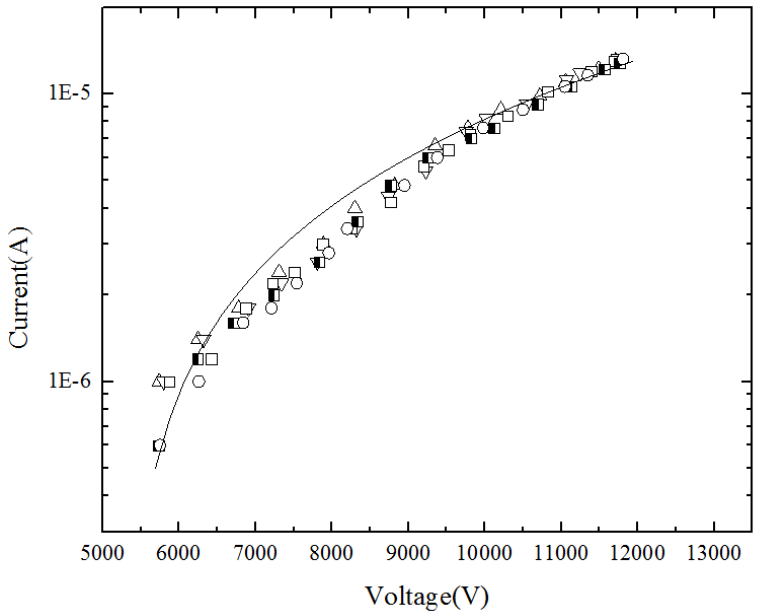

Figure 6-17. Fitting of I-V curve for dry air. (Positive DC, 14mm gap)

$E_P = 2.6\times10^{8}$ V/m, $\mu = 0.74\times10^{-4}$ m^2/Vs. V_0 = 21 kV, Goodness of fitting R^2 = 0.99921.

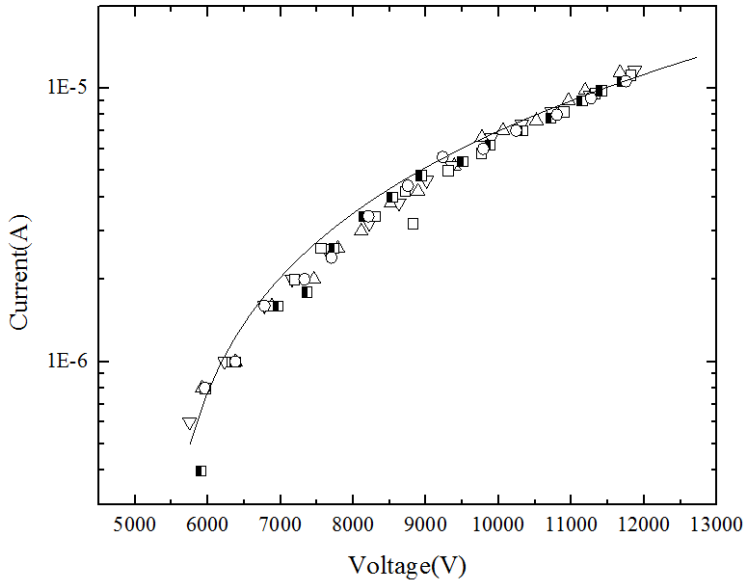

Figure 6-18. Fitting of I-V curve for humid air. (Positive DC, 14mm gap)

$E_P = 2.6\times10^{8}$ V/m, $\mu = 0.65\times10^{-4}$ m^2/Vs. V0 = 21 kV, Goodness of fitting R^2 = 0.99932.

6.6.5.3 Discussions on the Ion Mobility Measurement Results

The results of ion mobility measurement is shown in Table 6-1.

Table 6-1. Ion mobility measurement result. (a) Negative DC energisation. (b)Positive DC energisation.

	5 mm	10 mm	14 mm
Ambient air (31%) (m^2/Vs)	2.2×10^{-4} $\pm1.1\times10^{-5}$	2×10^{-4} $\pm1\times10^{-5}$	1.7×10^{-4} $\pm0.7\times10^{-5}$
Humid air (81%) (m^2/Vs)	1.9×10^{-4} $\pm0.9\times10^{-5}$	1.8×10^{-4} $\pm1\times10^{-5}$	1.5×10^{-4} $\pm0.8\times10^{-5}$

(a)

	5 mm	10 mm	14 mm
Ambient air (31%) (m^2/Vs)	No steady-state current	0.75×10^{-4} $\pm0.05\times10^{-5}$	0.62×10^{-4} $\pm0.04\times10^{-5}$
Humid air (81%) (m^2/Vs)	No steady-state current	0.58×10^{-4} $\pm0.04\times10^{-5}$	0.54×10^{-4} $\pm0.06\times10^{-5}$

(b)

In Table 6-1, the ion mobility is measured and the results are shown. Ion mobility was measured for negative and positive DC energisation, and for two gas (air) environments with different relative humidity (31% and 81%), and three different tip-plane distances (5 mm, 10 mm and 14 mm).

It was found that for negative energisation, negative ion mobility ranged from 1.7×10^{-4} m^2/Vs to 2.2×10^{-4} m^2/Vs for ambient humidity and from 1.5×10^{-4} m^2/Vs to 1.9×10^{-4} m^2/Vs for increased humidity. For positive energisation, positive ion mobility ranged from 0.62×10^{-4} m^2/Vs to 0.75×10^{-4} m^2/Vs for ambient humidity and from 0.54×10^{-4} m^2/Vs to 0.58×10^{-4} m^2/Vs for increased humidity.

According to the results, three significant findings have been established in this part of study:

a) Increased tip-plane distance resulted in decreased ion mobility for positive and negative energisation and for different humidity.

b) Increased humidity of air resulted in decrease in ion mobility for positive and negative energisation and for different tip-plane distances.

c) Ion mobility for negative energisation was higher than ion mobility for positive energisation for different tip-plane distances and for different humidity.

The ion mobility is very important in electrostatic precipitator design and operation because the ion mobility will change due to different energisation polarities and due to different humidity. As a result, particle dynamics and particle collection efficiency will be influenced by the change of ion mobility, which will be discussed later in this chapter.

6.7 Particle Collection Efficiency Calculation

The efficiency of particle collection can be calculated using Equation (46), which is based on the Deutsch-Anderson equation.

$$\eta_{efficiency} = 1 - e^{-SV/w} \tag{46}$$

where S is the area of the collecting plate (m^2) and w is the gas flow rate (m^3/s), V is migration velocity of particle (m/s).

The efficiency is calculated by taking the migration velocity for particle with different sizes, then the efficiency can be calculated using Equation (46).

6.8 Simulation Parameters

With the measured ion mobility, a simulation of the model can be conducted.

The equation of motion was solved for particles with low conductivity and relative permittivity, particles with intermediate conductivity and relative permittivity and particles with high conductivity and relative permittivity. Particle velocity, particle saturation velocity and particle displacement have been obtained.

The simulation parameters were based on typical particles emitted by coal power plants: soot, salt and COC (Condensable Organic Compounds). The parameters for particles are as follows [88] [89] [90] [91]:

Soot: ρ= 1.2x10^3 kg/m^3; ε_p = 2.6; ε_m =1;σ_p = 2 x 10^{-2} S/m.

Salt: ρ= 2.17x10^3 kg/m^3; ε_p = 15; ε_m =1;σ_p = 1.25 x 10^{-4} S/m.

COC (Condensable Organic Compounds): ρ= 1x10^3 kg/m^3; ε_p = 2; ε_m =1; σ_p = 1 x 10^{-8} S/m.

Water: ρ= 1x10^3 kg/m^3; ε_p = 80; ε_m =1; σ_p = 5 x 10^{-2} S/m.

Medium (air): ε_m =1; σ_m = 3x10^{-15} S/m.

The ion mobility was selected randomly from the result obtained in Section 6.6.5.3.

6.9 Simulation Results

Using the parameters listed above, analysis of the dynamics of particles in the cylindrical electrostatic precipitator has been conducted.

The developed model was capable of simulating particle dynamics (particle velocity and particle displacement) and calculating the precipitation (collection) efficiency. Parameters can be controlled to compare the results and investigate the influences of mobility, particle initial displacement, current level and particle size on particle dynamics. The influences of these on particle collection efficiency were also investigated.

6.9.1 Particle Dynamics for Different Types of Particles (Influence of Electrical Parameters)

As mentioned, the model was capable of simulating particle dynamics inside the electrostatic precipitator which included particle velocity and particle displacement. In order to compare the simulation results, four types of particles were selected: soot particles, salt particles, COC particles and water particles, with the parameters of these particles listed in Section 6.8. The simulation was conducted with negative energisation. The ion mobility for negative energisation is 1.8 x10^{-4} m^2/Vs. Current magnitude is 200 μA which is a typical value during actual routine experiments as discussed in previous chapters and particle diameter is 2.5 μm (PM 2.5) which is a typical value in emission control. The simulation results are shown in Figure 6-19 and Figure 6-20.

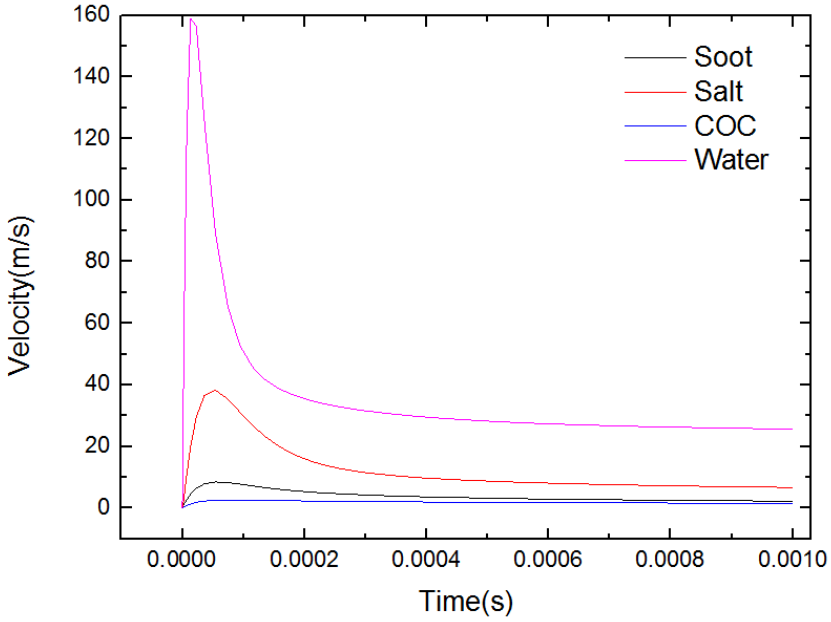

Figure 6-19. Particle velocity (soot, salt, COC and water particles) as a function of time for negative energisation. Ion mobility: 1.8 x10^{-4} m^2/Vs. Current magnitude: 200 µA. Particle diameter: 2.5 µm.

Figure 6-19 shows particle velocity (soot, salt, COC and water particles) as a function of time for negative energisation. Essentially, the velocity of different particles follows a similar tendency; particles which are being charged accelerate at first due to the electric force on particles, and the velocity of particle reaches its peak value in a very short time. Meanwhile particles move towards the collection plate of the electrostatic precipitator. According to Equation (37), the electric field in the electrostatic precipitator depends on the distance from the HV electrode, in other words, the electric field decreases with the increase in particle displacement from the central HV electrode towards the grounded collection electrode. When the particles are moving away from the central HV electrode, the electric field at the particles location decreases, therefore, the electric force on particles also decreases. The drag force, according to Equation (30), acts as the force which makes particle movement more difficult and depends on the particles velocity. When particle velocity increases, the corresponding drag force also increases. Therefore, the increase of drag force

and the decrease of electric force acting on the moving particles are due to the displacement of particles and result in a decrease of the resultant force. With the decrease in the resultant force, the particle velocity decreases to a saturated value as shown in the figure. The saturated velocity shows that the charge on particles is also saturated and the particles are far away from the central HV electrode. Therefore, the resulting electric force which acts on the particles is also saturated and is significantly lower than the resulting force acting of the particles when they are close to the HV charging electrode. This velocity is called the saturation velocity and the variation in the saturation velocity is so small it can be neglected. The velocity which particles have at the moment when they reach the collection electrode of the electrostatic precipitator is called the migration velocity. The migration velocity is a very important factor in the calculation of the collection efficiency of the electrostatic precipitators, as will be shown in Section 6.9.6.

This figure shows the comparison between velocities of different types of particles. Although particles are of the same size and the current levels are the same, the velocity as a function for different particle shows the influence of electrical parameters on particle velocity. In general, particles with a higher conductivity and relativity permittivity have larger velocity when compared with particles with lower conductivity and relativity permittivity while in the electrostatic precipitator. The velocity includes the peak velocity, saturation velocity and migration velocity. Particles with higher conductivity and relativity permittivity (for example water droplets) are easy to be charged and the total charge on particles is higher, which increases the electric force on particles. The increase of electric force causes the increase of the acceleration of particles and finally results in a higher velocity of particles. On the contrary, Particles with lower conductivity and relativity permittivity (for example COC particles) are more difficult to be charged and the total charge on particles is lower, which decreases the electric force on particles. The decrease of electric force causes the decrease of the acceleration of particles and finally results in a lower velocity of particles. The particle

velocity curve is very important, especially as the migration velocity can be obtained from this curve which can be used for calculating the collection efficiency.

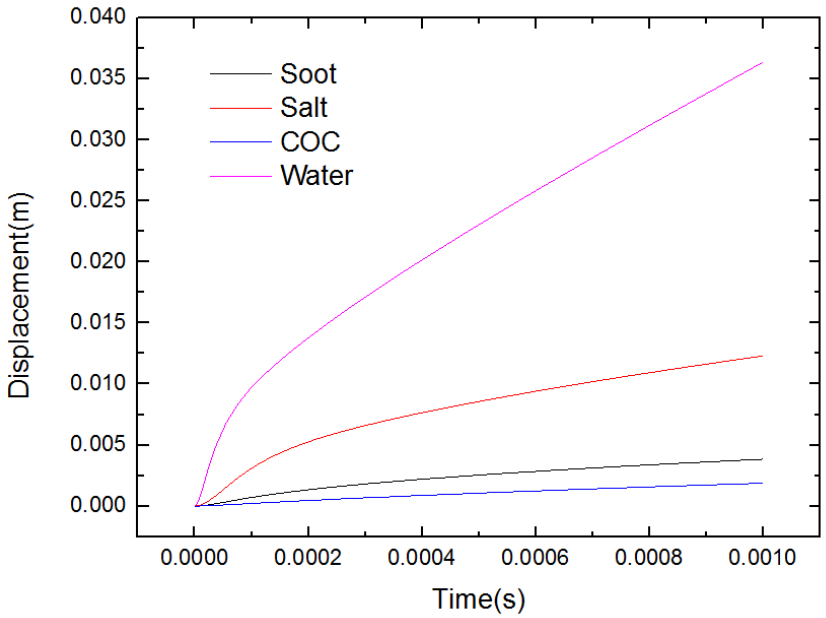

Figure 6-20. Particle displacement (soot, salt, COC and water particles) as a function of time for negative energisation. Ion mobility: 1.8 x10^{-4} m^2/Vs. Current magnitude: 200 µA. Particle diameter: 2.5 µm.

Figure 6-20 shows particle displacement (soot, salt, COC and water particles) as a function of time for negative energisation. The general tendency is that particle displacement starts from zero and increases further. Similar to a velocity-time curve, although particles are of the same size and current levels, the displacement-time curve for different particles shows the influence of electrical parameters on particle displacement. In general, particles with higher conductivity and relativity permittivity have larger displacements when compared with particles of lower conductivity and relativity permittivity while in the electrostatic precipitator. Particles with higher conductivity and relativity permittivity (for example water particles) are easy to be charged and the total charge on particles is higher, which increases the electric force on particles. The increase of electric force causes the increase of the

acceleration of particles and velocity of particles and finally results in higher displacement of particles. On the contrary, particles with lower conductivity and relativity permittivity (for example COC particles) are more difficult to be charged and the total charge on particles is lower, which decreases the electric force on particles. The decrease of electric force causes the decrease of the acceleration and velocity of particles and finally results in lower displacement of particles. Particle displacement is also very important in determination of migration velocity. As mentioned, when the displacement of particles increases to the value of the inner radius of the electrostatic precipitator (0.0475 m in the simulation), particles reach the collection plate of the electrostatic precipitator. The velocity when particles reach the collection plate is the migration velocity. The influence of initial displacement will be discussed in the follow section.

6.9.2 Influence of Particle Initial Displacement

The model was capable of simulating particle dynamics for different particle displacements, and the influence of particle initial displacement can be investigated. The influence of particle initial displacement on particle dynamics is discussed in this section. The simulation results are shown in Figure 6-21 and Figure 6-22. The velocity-time curves and displacement-time curves for salt particles, COC particles and water particles are very similar so they are not shown.

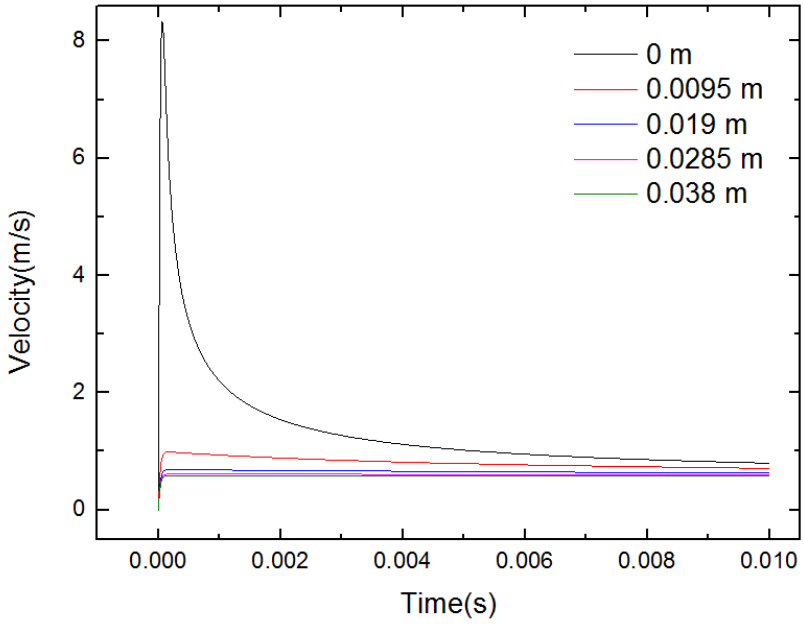

Figure 6-21. Particle velocity (soot) as a function of time for different initial displacements for negative energisation. Ion mobility: 1.8 x10^{-4} m^2/Vs. Current magnitude: 200 µA. Particle diameter: 2.5 µm.

Figure 6-21 shows particle velocity (soot) as a function of time for different initial displacements for negative energisation. In the model, the initial displacements were set for different values prior to the simulation, and the simulation was conducted simultaneously for particles with different initial displacements. The figure shows the influence of initial displacement of particles. As shown in this figure, the velocity tendencies for small initial displacements and for large displacements are different. Therefore, velocity-time curves for small initial displacements and for large displacements were conducted separately to evaluate the difference. One thing worth noting is that the velocity-time curves for different particle initial displacements never cross.

For small initial displacements, as discussed in Section 6.9.1, particles accelerate at first and then velocity increases. The velocity of particles increases to its peak value in a very short time then decreases rapidly and, finally, decreases to the saturation velocity. Since small

initial displacements are close to zero initial displacement, which means particles are close to the central charging electrode, the behaviour of particle velocity of small initial displacements is close to that of zero initial displacement. Larger initial displacement causes lower peak velocity and lower saturation velocity. The velocity-time curves for larger initial displacements essentially follow a similar tendency when compared with smaller initial displacements. However, the difference between peak velocity and saturation velocity for larger initial displacement is much smaller. For example, when the initial displacement is 0.001 m, the difference between peak velocity and saturation velocity is 4 m/s. When initial displacement is 0.008 m, the difference between peak velocity and saturation velocity is 0.8 m/s. That is due to the electric field in the model depends on displacement, according to Equation (37) and Equation (38). The field charge on particles is also influenced by the electric field, according to Equation (33) and Equation (34). When particles are close to the central charging electrode, the electric field is very strong and charge on particles is high, therefore, at first, the electric force on particles is strong and particle velocity is high. The viscosity force, according to Equation (30), acts as the force which prohibits particles from moving and the viscosity force depends on velocity of particles. When the particle velocity increases, the corresponding viscosity force also increases. Therefore, the increase of viscosity force and the decrease of electric force on particles due to the displacement of particles make the resultant force on particles to decrease. The higher the velocity, the higher the viscosity force, therefore the force balance can be reached more rapidly, and under a balanced force the velocity decrease to a stable value. For larger initial displacements, particles are far away from the central charging electrode. The electric field and electric force on particles are both relatively weak. Meanwhile, particles are charged relatively more slowly. Therefore, the initial velocity of particles with larger initial displacements is not as high as those with smaller initial displacements. The corresponding viscosity force is not high, so the saturation velocity is close to the peak velocity. It takes a longer time for the resultant force to reach the balance which means it takes a longer time for particles to reach their saturation velocity.

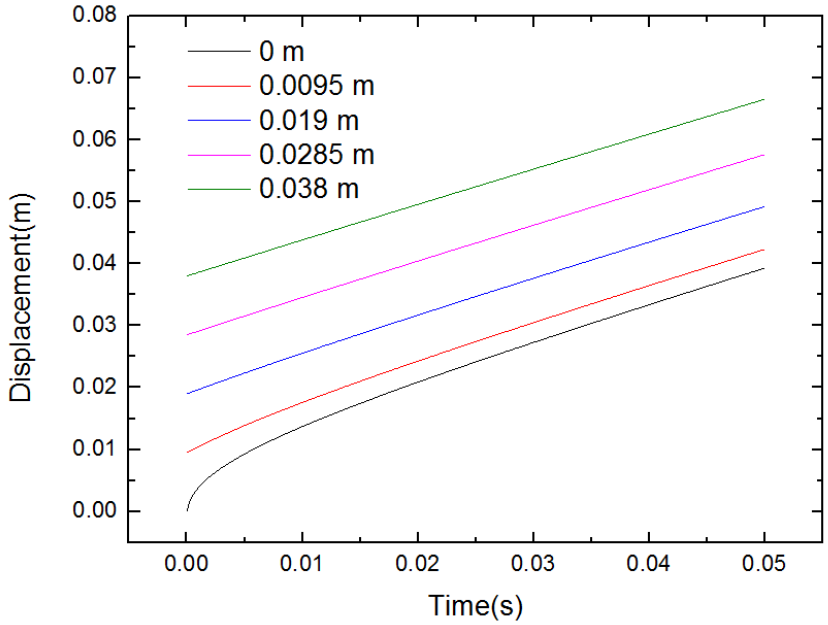

Figure 6-22. Particle displacement (soot) as a function of time for different initial displacement for negative energisation. Ion mobility: 1.8 x10^{-4} m^2/Vs. Current magnitude: 200 µA. Particle diameter: 2.5 µm.

Figure 6-22 shows particle displacement (soot) as a function of time for different initial displacement for negative energisation. One thing worth noting is that the displacement-time curves for different particle initial displacements never cross. Since the displacement of particles is dependent on particle velocity, and mainly on velocity which are close to saturation velocity, the displacement-time curves show that particles with larger initial displacement have a larger final displacement. This result is very important as it shows that particle initial displacement is one of the key factors on particle migration time while inside electrostatic precipitators. In other words, under the same electrical parameters, particles with larger initial displacement always take a shorter time to be collected by the collection plate than particles with smaller initial displacement.

The influence of initial displacement is very important in designing an electrostatic precipitator. The velocity-time curve and the displacement-time curve show that particles

which are close to the central charging electrode take the longest time from charging to collection. Therefore, in order to achieve the best particle collection performance with the highest efficiency, the optimisation of design should take particles with zero initial displacement into consideration when determining particle travel time. The particle travel time is important as it could give the optimum length of electrostatic precipitator. For example, for a given type of particle, when these particles with zero initial displacement take five seconds to be collected, the total travel time inside the electrostatic precipitator is also five seconds. Suppose the electric force acts on particles horizontally, the gas flow direction is perpendicular to the direction of electric force. Suppose the gas flow speed is 0.1 m/s, then the minimum electric length should be 0.5 m to achieve the best performance.

6.9.3 Influence of Ion Mobility (Influence of the Polarity of Energisation)

According to Section 6.6, ion mobility of positive and negative energisation are different. In fact, the ion mobility for negative energisation is more than double than the ion mobility for positive energisation. In the model, the influence of ion mobility was investigated by simulation of the model for ion mobility under positive and negative energisation. The ion mobility for positive energisation is 0.75 $x10^{-4}$ m2/Vs and the ion mobility for negative energisation is 1.8 $x10^{-4}$ m2/Vs with the results shown in Figure 6-23 and Figure 6-24. The velocity-time curves and displacement-time curves for salt particles, COC particles and water particles are very similar so they are not shown.

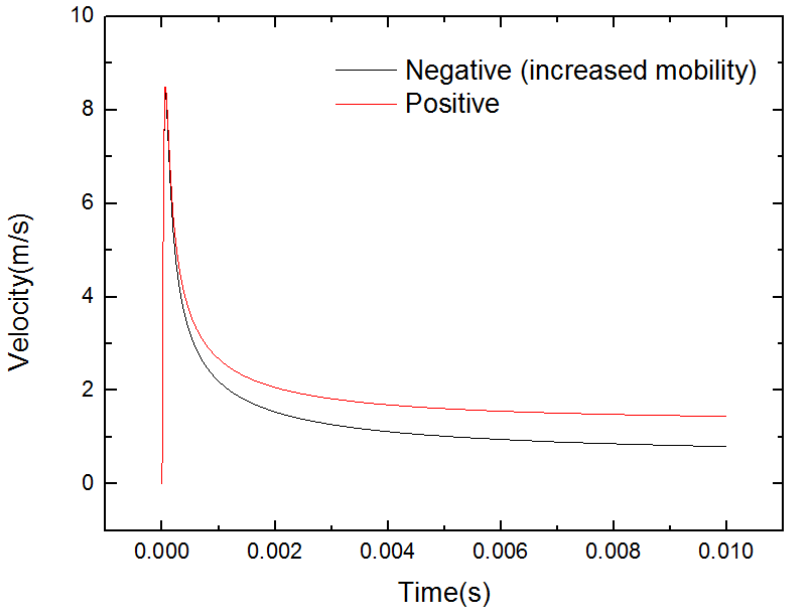

Figure 6-23. Particle velocity (soot) as a function of time for negative energisation and for positive energisation. Ion mobility: 1.8 x10^{-4} m^2/Vs for negative energisation, 0.75 x10^{-4} m^2/Vs for positive energisation. Current magnitude: 200 µA. Particle diameter: 2.5 µm.

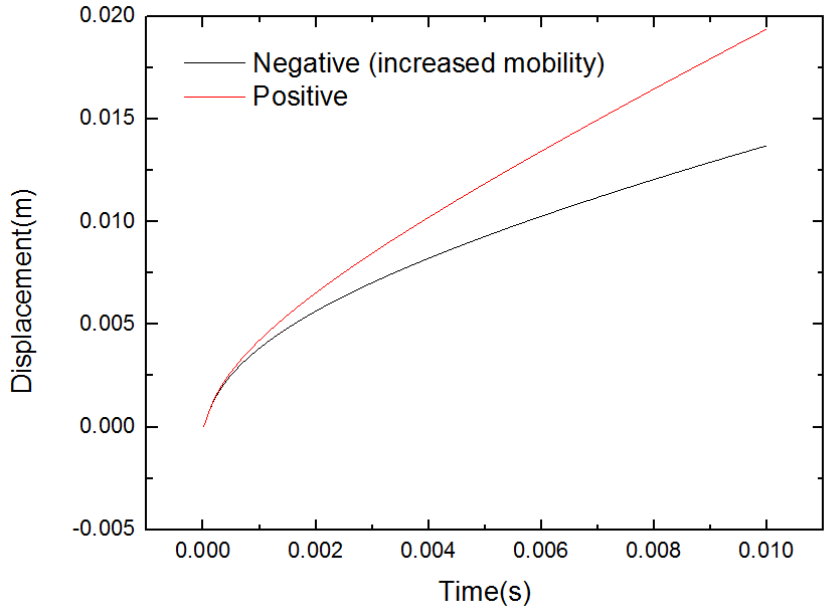

Figure 6-24. Particle displacement (soot) as a function of time for negative energisation and for positive energisation. Ion mobility (1.8 x10^{-4} m^2/Vs) for negative energisation, 0.75 x10^{-4} m^2/Vs for positive energisation. Current magnitude (200 µA). Particle diameter (2.5 µm).

Figure 6-23 shows particle velocity (soot) as a function of time for negative energisation and for positive energisation. Figure 6-24 shows particle displacement (soot) as a function of time for negative energisation and for positive energisation. For a velocity-time curve, the result shows that particle velocity for ion mobility under positive energisation and particle velocity for ion mobility under negative energisation are very similar in tendency, particularly the peak velocity value under the two conditions are almost the same. The difference is that a higher ion mobility results in lower saturation velocity and lower migration velocity. According to Equation (37) and Equation (38), ion mobility can influence the electric field. The increase of ion mobility results in the decrease of electric field. According to Equation (33) and Equation (34), the field charge on particles is also influenced by the electric field, so particle field charge is reduced with decreased electric field. The decrease of electric field and particle field charge cause the decrease of electric force on charged particles, so the velocity is decreased. Since the displacement depends on velocity,

with higher saturation velocity and higher migration velocity the displacement is larger for lower ion mobility, as shown in the displacement-time curve.

The simulation results for the influence of ion mobility show that both particle velocity and particle displacement for positive polarity are larger than particle velocity and particle displacement for negative polarity. One important note is that the results are simulated using the same current level which shows the influence of ion mobility clearly without the interference of different current level influences. However, the behaviours of positive and negative corona are different both in ion mobility and in current level during experiments. In fact, the ion mobility for positive polarity is larger than the ion mobility for negative polarity, and the current level for positive polarity is lower than the current level for negative polarity for the same voltage. Therefore, the influence of current level must be considered when analysing the influence of polarity, which will be discussed in Section 6.9.4.

6.9.4 Influence of Current Levels

The current level is one of the most important factor which can influence the collection efficiency and the performance of electrostatic precipitators. The influence of current level was investigated using the model. The current levels are set as 10 μA, 50 μA, 100 μA, 500 μA, and 1000 μA to see the difference. The results are shown in Figure 6-25 and Figure 6-26. The velocity-time curves and displacement-time curves for salt particles, COC particles and water particles are very similar so they are not shown.

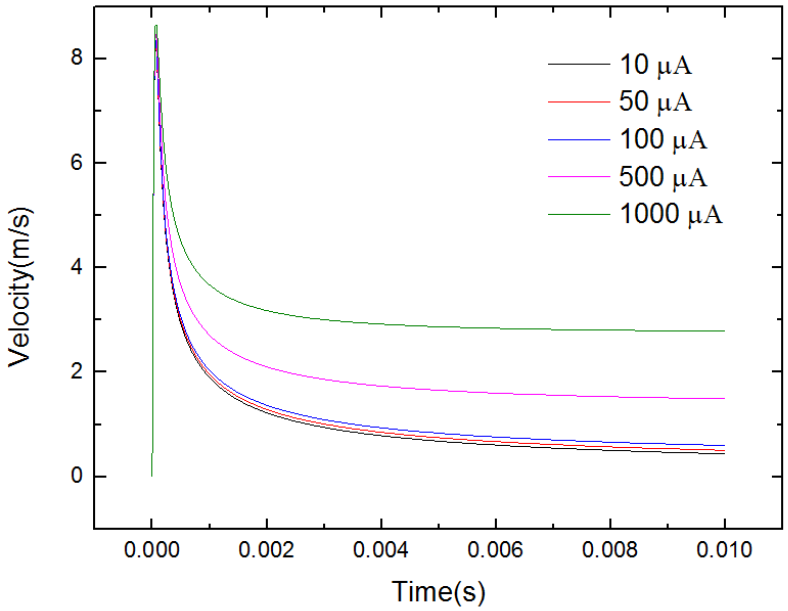

Figure 6-25. Particle velocity (soot) as a function of time for different current levels for negative energisation. Ion mobility: 1.8 x10^{-4} m^2/Vs. Particle diameter: 2.5 µm.

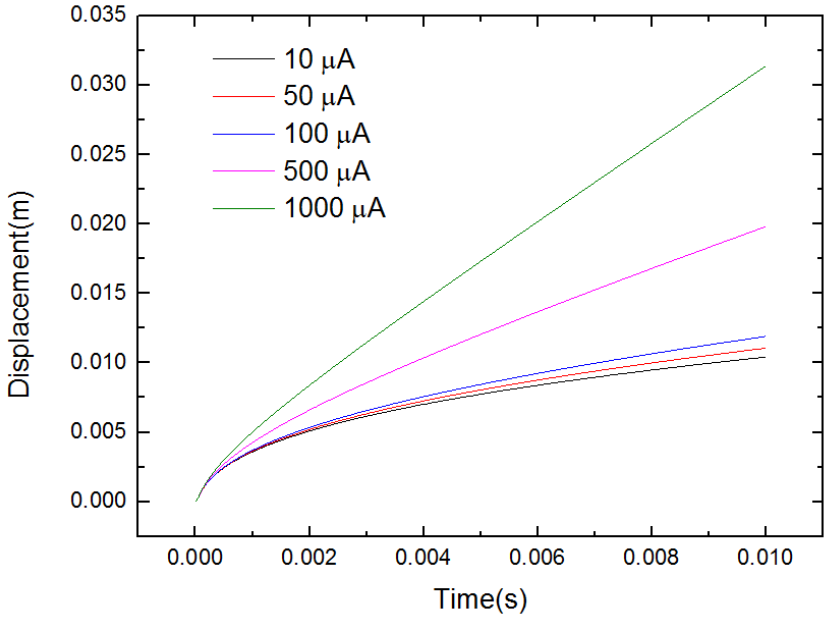

Figure 6-26. Particle displacement (soot) as a function of time for different current levels for negative energisation. Ion mobility: 1.8 x10^{-4} m^2/Vs. Particle diameter: 2.5 µm.

Figure 6-25 shows particle velocity (soot) as a function of time for different current levels for negative energisation. Figure 6-26 shows particle displacement (soot) as a function of time for different current levels for negative energisation. As shown in the velocity-time curve, particle velocity for different current levels follow a similar tendency. The current level influences particle velocity in two aspects: according to Equation (37) and Equation (38), the electric field increases with an increasing current level. According to Equation (33) and Equation (34), the field charge on particles increases with the increase of electric field. Therefore, when the current level is increased, particle velocity is also increased. Particle velocity includes particle peak velocity, saturation velocity and migration velocity. Since the displacement depends on velocity, with higher saturation velocity and higher migration velocity, the displacement is larger for increased current levels as shown in the displacement-time curve.

6.9.5 Influence of Particle Size

Particle size distribution is one of the most important factors which can influence the collection efficiency and the performance of electrostatic precipitators. The influence of particle size was investigated using the model. The particle diameters are set as 0.01 μm (PM 0.01), 0.1 μm (PM 0.1), 1 μm (PM 1), 2.5 μm (PM 2.5) and 10 μm (PM 10) to see the difference. The particle size selected for simulation generally includes particles of all ranges for emission control. The results are shown in Figure 6-27 and Figure 6-28. The velocity-time curves and displacement-time curves for salt particles, COC particles and water particles are very similar so they are not shown.

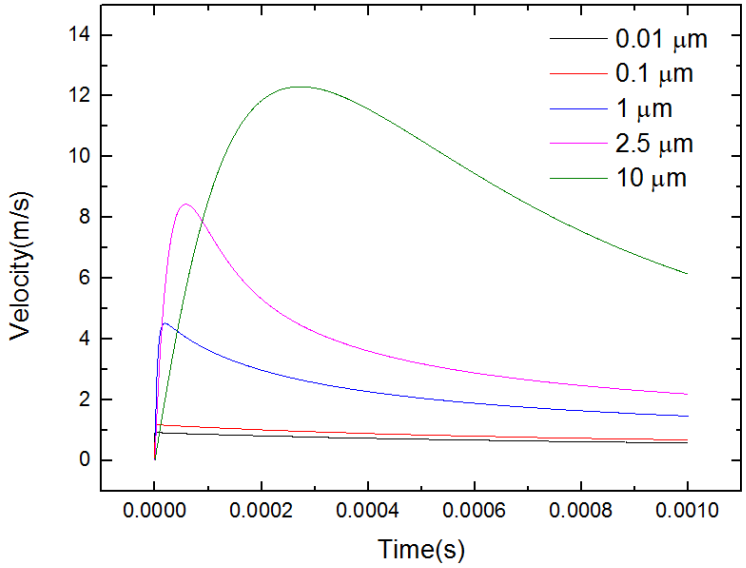

Figure 6-27. Particle velocity (soot) as a function of time for different particle diameters for negative energisation. Ion mobility: 1.8 x10^{-4} m^2/Vs. Current magnitude: 200 µA. Particle diameter: 2.5 µm.

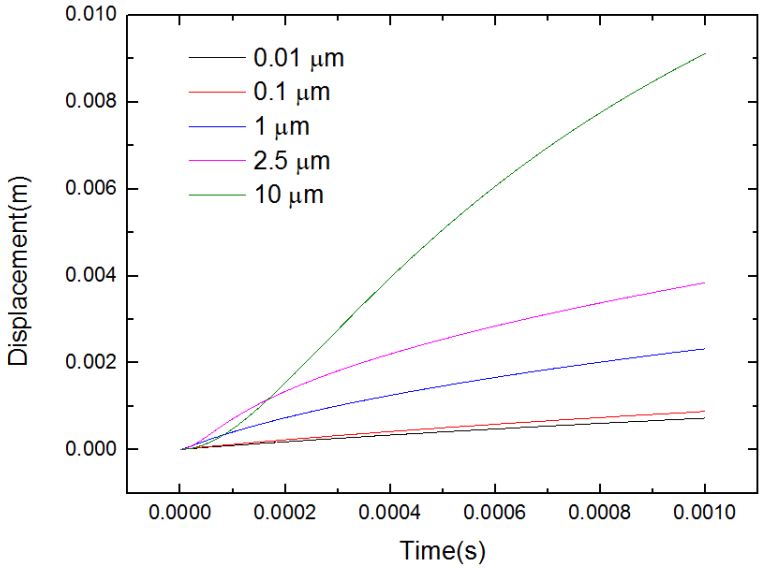

Figure 6-28. Particle displacement (soot) as a function of time for different particle diameters for negative energisation. Ion mobility: 1.8 x10^{-4} m^2/Vs. Current magnitude: 200 µA. Particle diameter: 2.5 µm.

Figure 6-27 shows particle velocity (soot) as a function of time for different particle diameters for negative energisation. Figure 6-28 shows particle displacement (soot) as a function of time for different particle diameters for negative energisation. In general, the velocity-time curve shows that particles of all sizes follow a similar tendency. However, there are two differences for the velocity-time curve of larger particles when compared with smaller particles: particle velocity is higher for larger particles including peak velocity, saturation velocity and migration velocity. The time for particle velocity to reach peak velocity and time for particle velocity to reduce to saturation velocity are longer for larger particles when compared with smaller particles. According to Equation (33), Equation (34) and Equation (36), when particle size increases the total charge on particles increases. Therefore, the corresponding electric force increases. However, the increased particle size results in a larger particle mass, which decrease the acceleration. In other words, the electric force and particle mass both increase. The influence of increased particle size on electric force is more obvious than the influence of increased particle size on particle mass. This is why the velocity for larger particles is higher than the velocity for smaller particles. Besides, since particle mass is increased for increased particle size, it takes a longer time for the particle velocity to reach peak velocity as acceleration is decreased. This reason can also explain the longer time for particle velocity to reduce to saturation velocity. Since the displacement depends on velocity, with a higher saturation velocity and higher migration velocity the displacement is larger for increased particle sizes as shown in the displacement-time curve. When the simulation time is short, the displacement is smaller for increased particle sizes. For example, when simulation time is 0.002 seconds, the particle displacement with diameters of 10 μm (green line) is smaller than particle displacement with diameters of 2.5 μm (pink line) as shown in the figure. This is due to the acceleration of larger particles is lower than the acceleration of smaller particles for a shorter time. When the simulation time increases, the final displacement for larger particles is higher than the final displacement for smaller particles.

6.9.6 Particle Collection Efficiency

As discussed, particle collection efficiency is calculated using Equation (46). In order to calculate collection efficiency, the migration velocity should be determined. As discussed in Section 6.9.1, when the displacement of particles increases to the value of the inner radius of the electrostatic precipitator, particles reach the collection plate of the electrostatic precipitator. The velocity when particles reach the collection plate is migration velocity. Therefore, a simulation was conducted and the simulation time when displacement increased to 0.0475 (inner radius) for different sizes of particles were recorded separately for different particle sizes. Then, the corresponding velocity for different particle sizes was recorded for the calculation of collection efficiency. The collection efficiency for different particles and the influence of different factors are shown and discussed in this section. The influence of increased gas flow rate was also compared. Note that different points of efficiency are shown in figures in this section, and straight lines are used to connect these points just for better visualisation.

6.9.6.1 Ion Mobility Influence, Particle Size Influence and Particle Electric Parameter Influence

The particle collection efficiency as a function of particle diameter for different ion mobility was obtained in this section. The particles for simulation are soot particles, salt particles, COC particles and water particles. Particle diameters are simulated from 0.01 μm (PM 0.01) to 10 μm (PM 10). Gas flow rates for simulation are 1000 L/min and 10000 L/min to show the influence of gas flow on particle precipitation efficiency. The ion mobility for positive energisation is 0.75 $x10^{-4}$ m^2/Vs and the ion mobility for negative energisation is 1.8 $x10^{-4}$ m^2/Vs. The results are shown in Figure 6-29, Figure 6-30, Figure 6-31 and Figure 6-32.

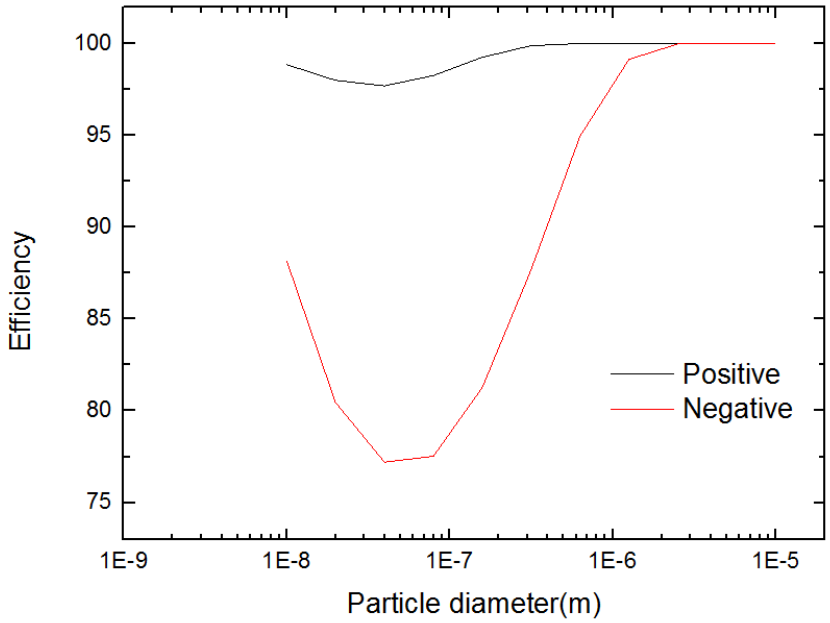

(a)

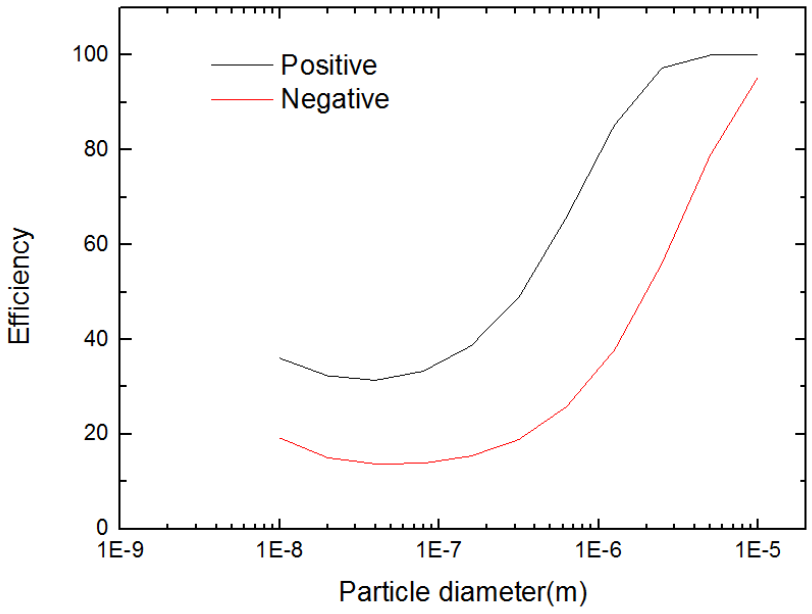

(b)

Figure 6-29 Particle (soot) collection efficiency as a function of particle diameter for positive and negative energisation for different gas flow rates: (a) 1000 L/min. (b) 10000 L/min. Ion mobility: 1.8 x10^{-4} m^2/Vs for negative energisation, 0.75 x10^{-4} m^2/Vs for positive energisation. Current magnitude: 200 μA. The efficiency is in percentage.

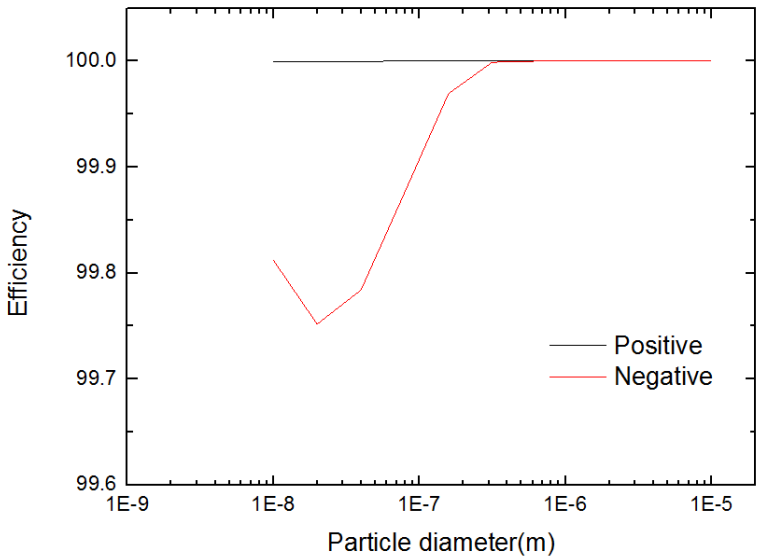

(a)

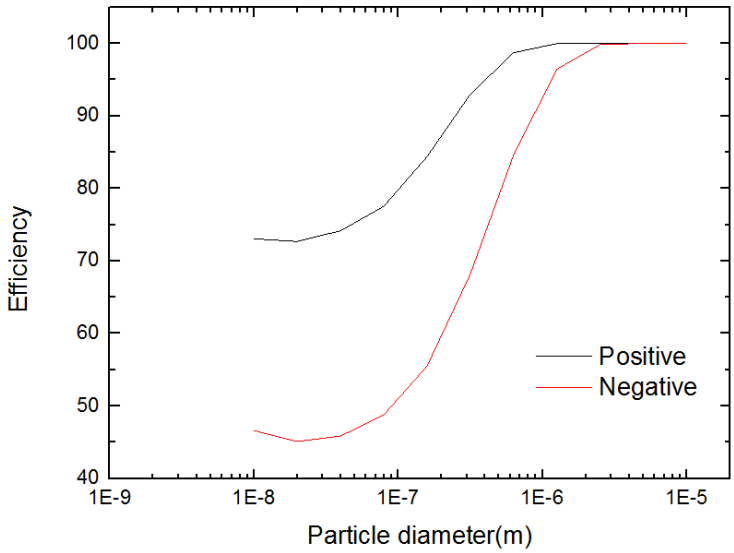

(b)

Figure 6-30 Particle (salt) collection efficiency as a function of particle diameter for positive and negative energisation for different gas flow rates: (a) 1000 L/min. (b) 10000 L/min. Ion mobility: 1.8 x10^{-4} m^2/Vs for negative energisation, 0.75 x10^{-4} m^2/Vs for positive energisation. Current magnitude: 200 µA. The efficiency is in percentage.

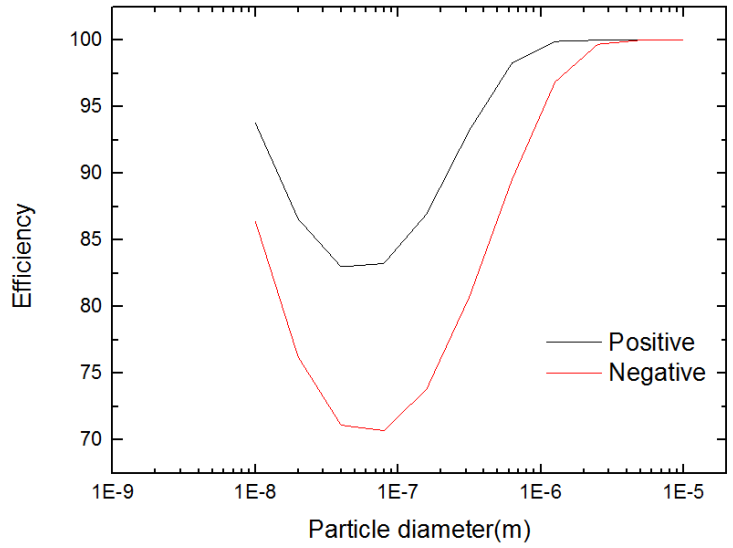

(a)

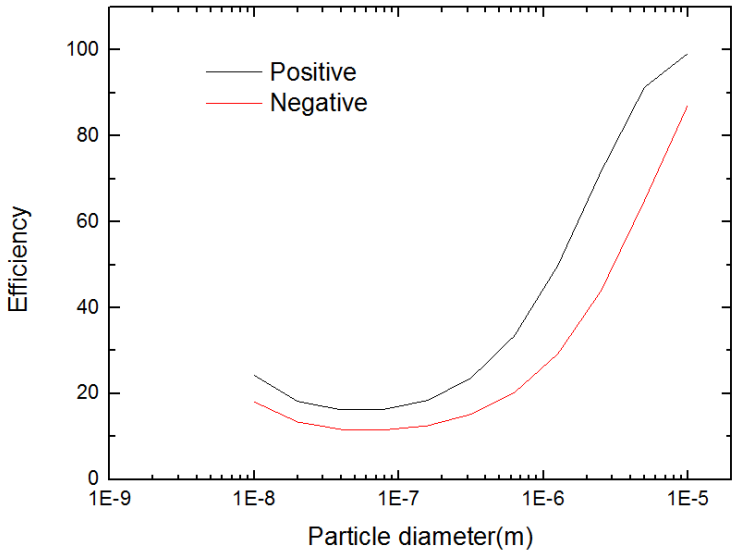

(b)

Figure 6-31 Particle (COC) collection efficiency as a function of particle diameter for positive and negative energisation for different gas flow rates: (a) 1000 L/min. (b) 10000 L/min. Ion mobility: 1.8 x10^{-4} m^2/Vs for negative energisation, 0.75 x10^{-4} m^2/Vs for positive energisation. Current magnitude: 200 µA. The efficiency is in percentage.

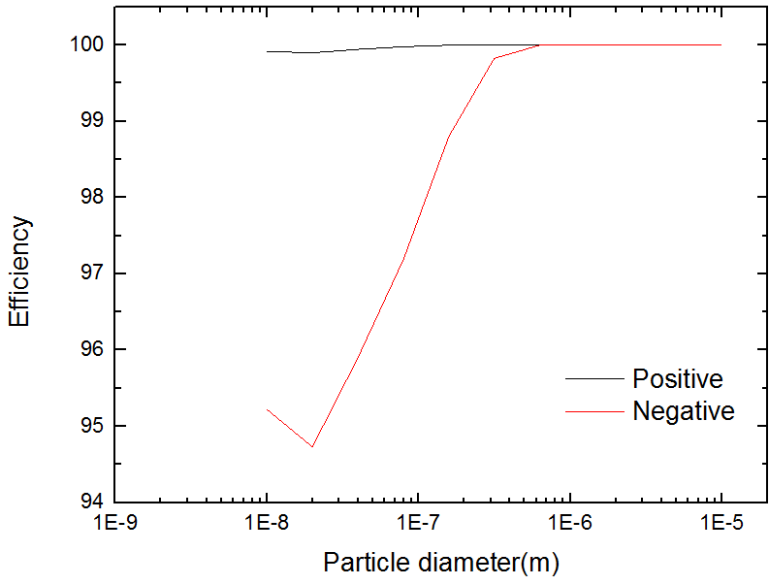

(a)

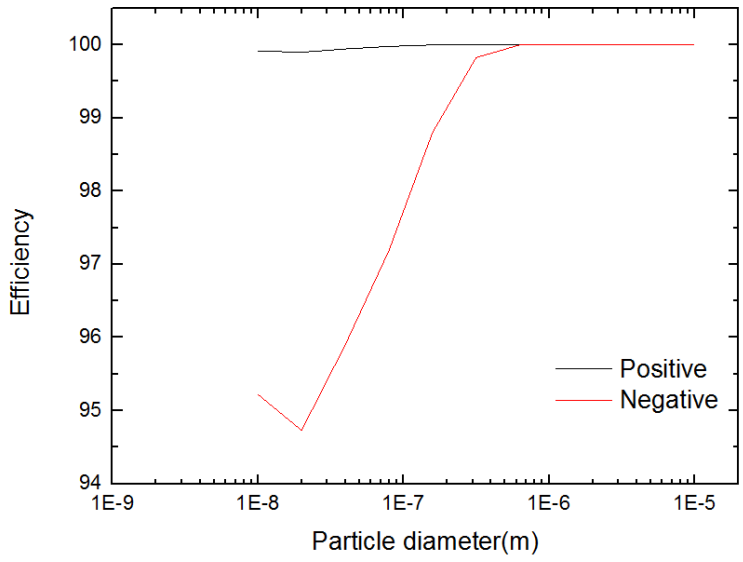

(b)

Figure 6-32 Particle (water) collection efficiency as a function of particle diameter for positive and negative energisation for different gas flow rates: (a) 1000 L/min. (b) 10000 L/min. Ion mobility: 1.8 x10^{-4} m^2/Vs for negative energisation, 0.75 x10^{-4} m^2/Vs for positive energisation. Current magnitude: 200 μA. The efficiency is in percentage.

Figure 6-29, Figure 6-30, Figure 6-31 and Figure 6-32 show particle collection efficiency as a function of particle diameter for different particles (soot, salt, COC and water droplets) for different ionic mobility and for different gas flow rates. The important findings are listed as:

1) There is a minimum collection efficiency for certain particle diameters for different particles. The minimum collection efficiency occurs when the particle diameter is between 0.01 μm (PM 0.01) and 0. 1 μm (PM 0.1) for all types of particles.

2) Increased ion mobility results in a decreased collection efficiency for all types of particles. This can be explained by the decreased particle migration velocity for increased ion mobility, which has been discussed in Section 6.9.3.

Similar to the influence of polarity on particle dynamics, as discussed in Section 6.9.3, the simulation results for the influence of ion mobility show that particle collection efficiency for positive polarity is higher than the particle collection efficiency for negative polarity. One important fact should be noted that the results are simulated using the same current level. The use of the same current level is to show the influence of ion mobility clearly without the interference of different current level influences. However, the behaviours of positive and negative corona are different both in ion mobility and in current level in experiments. In fact, the ion mobility for positive polarity is larger than the ion mobility for negative polarity, and the current level for positive polarity is lower than the current level for negative polarity for the same voltage. Therefore, the influence of current level must be considered when analysing the influence of polarity, which will be discussed in Section 6.9.6.2.

3) Increased gas flow rate results in decreased collection efficiency. Theoretically, according to Equation (46), the increase in gas flow rate can decrease the final efficiency result. In practical experiments, this is due to the particle exposure time to the electric field for higher gas flow rate is lower, which makes charging and migration time for particles lower and the efficiency of collection is reduced.

4) Increased electric parameters of particles (particle conductivity and relative permittivity) result in increased collection efficiency. As discussed in Section 6.9.1, particles with higher conductivity and relativity permittivity (for example water particles) are easy to be charged and the total charge on particles is higher, which increases the electric force on particles. The increase of electric force causes the increase of the acceleration of particles and, finally, results in higher migration velocity of particles so the collection efficiency is increased.

5) Collection efficiency for positive energisation is greater than for negative energisation for specific size ranges.

6.9.6.2 Current Level Influence

Particle collection efficiency as a function of particle diameter for different current levels is shown in this section. The particles for simulation are soot particles, salt particles, COC particles and water particles. Particle diameters are simulated from 0.01 μm (PM 0.01) to 10 μm (PM 10). Gas flow rates for simulation are 1000 L/min and 10000 L/min. The current levels used in the simulation are 200 μA and 1000 μA. The results are shown in Figure 6-33, Figure 6-34, Figure 6-35 and Figure 6-36.

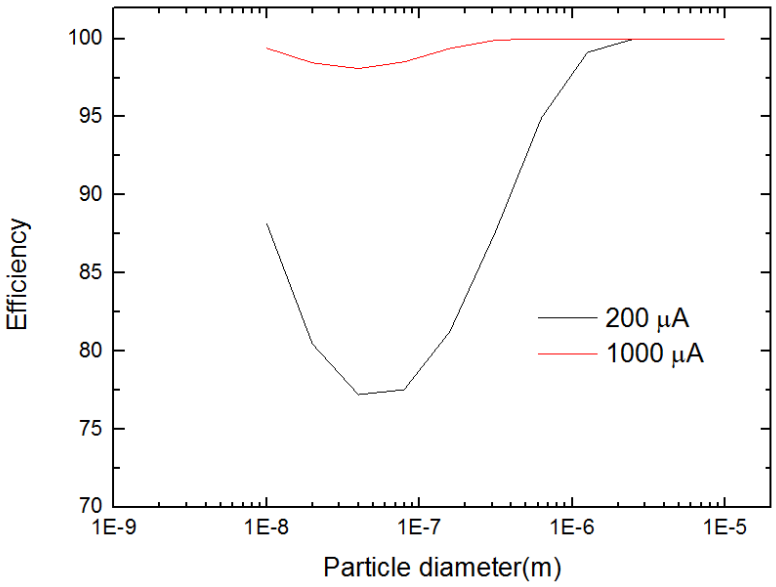

(a)

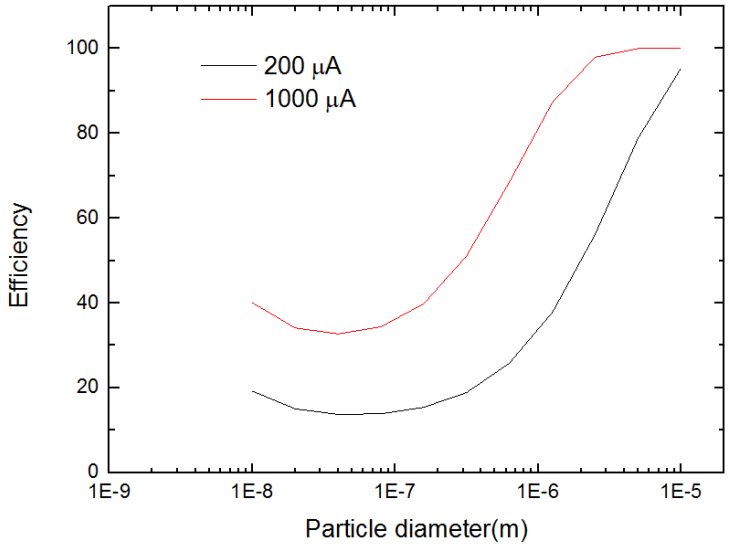

(b)

Figure 6-33 Particle (soot) collection efficiency as a function of particle diameter for different current levels for different gas flow rates: (a) 1000 L/min. (b) 10000 L/min. Ion mobility: 1.8 x10^{-4} m^2/Vs. The efficiency is in percentage.

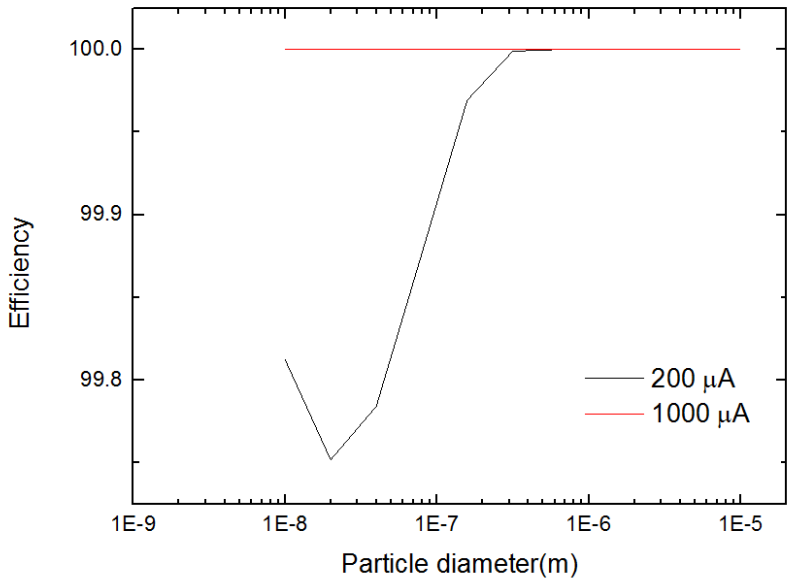

(a)

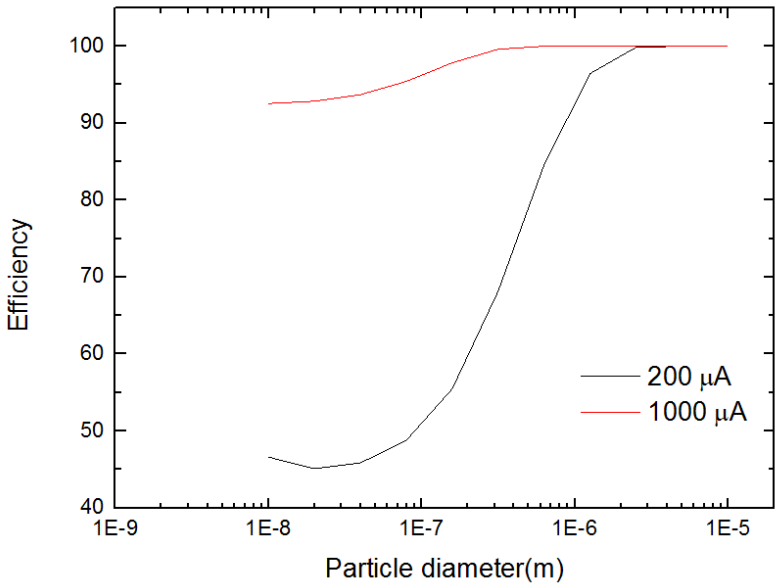

(b)

Figure 6-34 Particle (salt) collection efficiency as a function of particle diameter for different current levels for different gas flow rates: (a) 1000 L/min. (b) 10000 L/min. Ion mobility: 1.8 x10^{-4} m^2/Vs. The efficiency is in percentage.

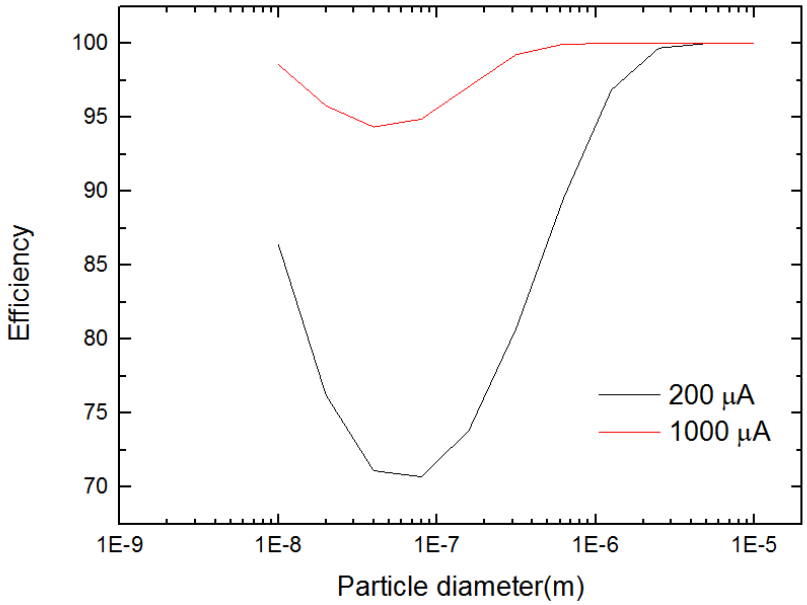

(a)

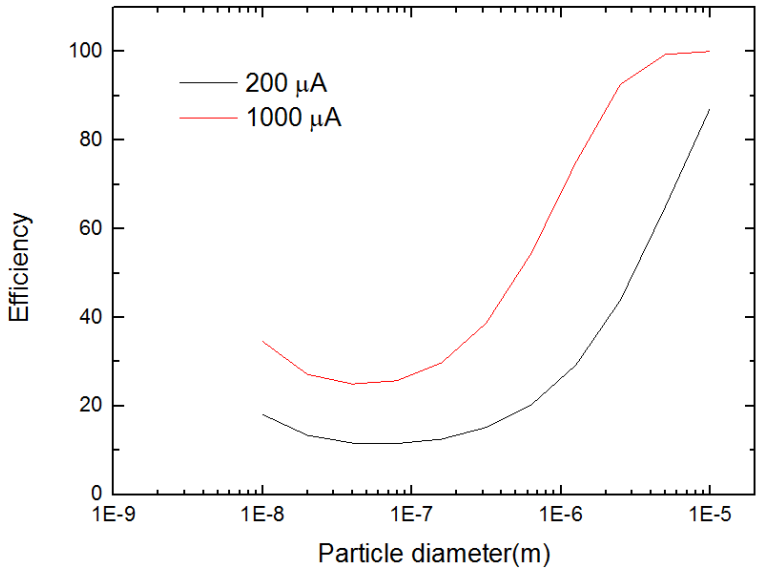

(b)

Figure 6-35 Particle (COC) collection efficiency as a function of particle diameter for different current levels for different gas flow rates: (a) 1000 L/min. (b) 10000 L/min. Ion mobility: 1.8 x10^{-4} m^2/Vs. The efficiency is in percentage.

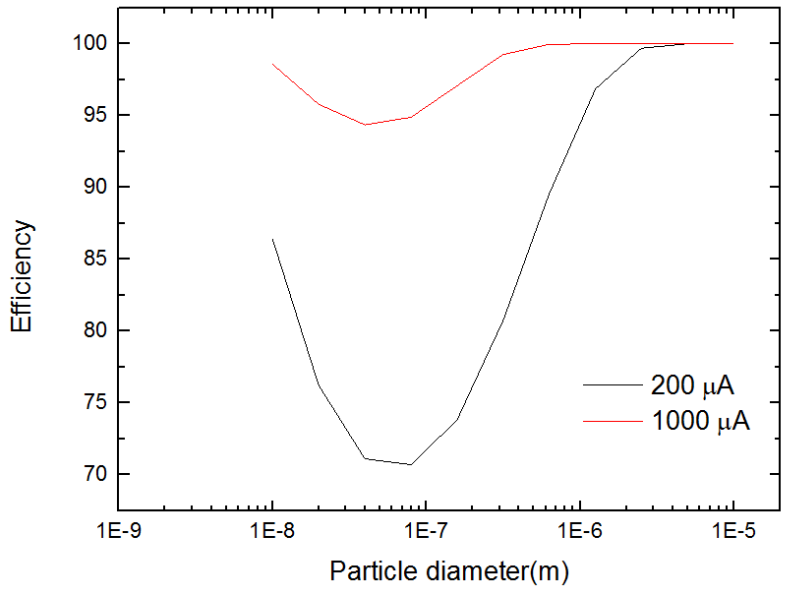

(a)

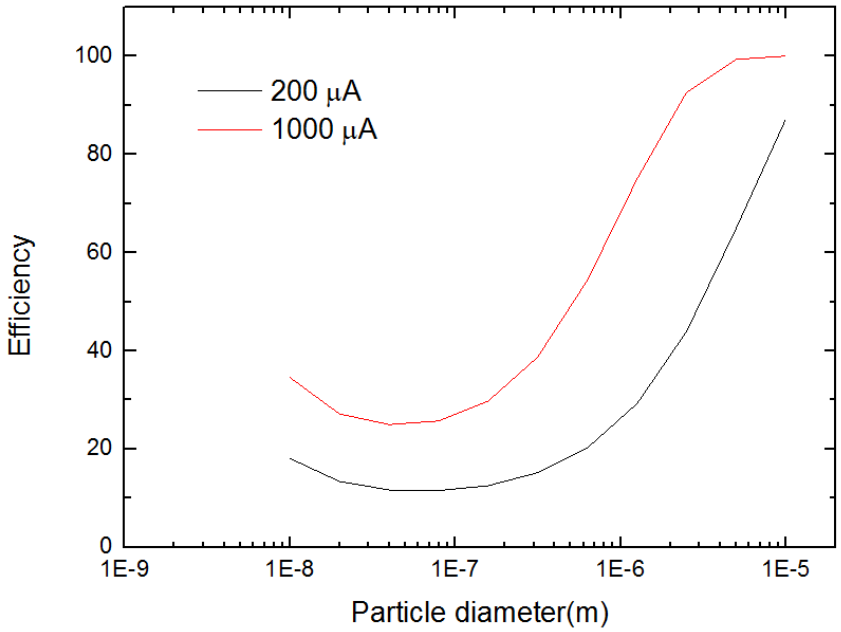

(b)

Figure 6-36 Particle (water) collection efficiency as a function of particle diameter for different current levels for different gas flow rates: (a) 1000 L/min. (b) 10000 L/min. Ion mobility: 1.8 x10^{-4} m^2/Vs. The efficiency is in percentage.

Figure 6-33, Figure 6-34, Figure 6-35 and Figure 6-36 show particle (soot, salt, COC and water respectively) collection efficiency as a function of particle diameter for different current levels and for different gas flow rates. Generally, the tendency of the efficiency-particle-diameter curves follow similar tendencies when compared with the results as shown in Section 6.9.6.1: There is a minimum collection efficiency for certain particle diameter for different particles which occurs when the particle diameter is between 0.01 μm (PM 0.01) and 0. 1 μm (PM 0.1) for all types of particles. Increased gas flow rate results in decreased collection efficiency. Increased electrical parameters of particles (particle conductivity and relative permittivity) result in increased collection efficiency. There is an important finding in this section:

Increased current level results in increased collection efficiency. As discussed in Section 6.9.4, the current level influences particle velocity in two aspects: according to Equation (37) and Equation (38), the electric field increases with the increase of current level. According to Equation (33) and Equation (34), the field charge on particles increases with the increase of electric field. Therefore, when the current level is increased, particle migration velocity is also increased which, in turn, increases the collection efficiency.

6.10 Conclusions

In this chapter, a model was designed and presented with an analytical investigation into the dynamics of airborne particles in electrostatic precipitators stressed with DC energisation and particle collection efficiency.

There were two important features of the model developed in this chapter. First, the space charge influenced electric field has been taken into consideration when compared with modelling approaches for electrostatic precipitation, such as the research in the paper [61]. In the paper, the electric field used was without the influence of the space charge, which was not as accurate as the model developed in this chapter as the space charge effect

occurred during the process of ionisation and particle charging. The existence of space charge decreased the electric field of the charging electrode and the particle collection efficiency can be reduced by the influence of the space charge [62]. Therefore, it is very important to include the influence of the space charge for simulations of electrostatic precipitators to reflect a more real environment inside electrostatic precipitators as has been achieved by the model developed in this chapter.

Second, electric parameters of conductivity and relative permittivity for both particles and medium were considered and included in the model developed in this chapter. Charging mechanisms of field charging and diffusion charging have been considered in the model. In some approaches such as [62] and [51], the only electric parameter considered was the relative permittivity of particles. The conductivity of particles, the conductivity of medium and the relative permittivity of medium in the papers were neglected, which was not as accurate as the model developed in this chapter. The conductivity and relative permittivity of particles and medium were the nature of particles and medium and cannot be neglected. Therefore, similar to the space charge influenced electric field, it is very important to include the conductivity and relative permittivity of particles and medium for simulation to reflect the real situation in electrostatic precipitators as has been achieved by the model developed in this chapter.

In this model, an important parameter, the ion mobility, was measured and used for simulations. The measurement of the ion mobility was conducted through the current-velocity curve fitting of the theoretical and experimental curve. A test system was designed to measure ion mobility and experiments have been conducted to measure ion mobility for different tip-plane distances, humidity and polarity of energisation. Three important findings are:

1) Increased tip-plane distance resulted in decrease in ion mobility for positive and negative energisation and for different humidity.

2) Increased humidity resulted in decreased ion mobility for positive and negative energisation and for different tip-plane distances.

3) Ion mobility for negative energisation was higher than ion mobility for positive energisation for different tip-plane distances and for different humidity.

With the measured ion mobility, the model was designed. The model was capable of:

a) Simulating particle dynamics while inside electrostatic precipitators.

b) Calculating the collection efficiency of the electrostatic based on the Deutsch-Anderson equation.

The simulation of the model has taken particles in real world with real parameters into consideration. These particles are commonly emitted by industries, such as coal power stations, and the particles include soot, salt , COC and water particles. The influences of different factors which may affect particle dynamics are investigated using the model, which includes:

1) Particle electric parameters (conductivity and relative permittivity): increased particle conductivity and relative permittivity result in higher particle velocity and larger particle displacement.

2) Initial particle displacement: particles with larger initial displacement have higher velocity and larger final displacement.

3) Ion mobility: increased ion mobility results in lower particle velocity and smaller particle displacement.

4) Current level: increased current level results in higher particle velocity and larger particle displacement.

5) Particle size distribution: increased particle size results in higher particle velocity and larger particle corresponding displacement. The time for particle velocity to reach peak velocity and time for particle velocity to reduce to saturation velocity are longer for increased particle size. Particle displacement is smaller for larger particles when the simulation time is short. There is a minimum collection efficiency for certain particle diameter for different particles. The minimum collection efficiency occurs when the particle diameter is between 0.01 μm (PM 0.01) and 0. 1 μm (PM 0.1) for all types of particles.

6) Gas flow rate: increased gas flow rate results in decreased collection efficiency due to the reduced plasma exposure time.

The findings in this chapter have shown the influences of different parameters on particle dynamics inside electrostatic precipitators and influences of different parameters on particle collection efficiency of electrostatic precipitators. These findings are important as they will help for optimisation of electrostatic precipitation.

7 Conclusions and Future Work

7.1 Conclusions

This section includes the conclusions of this thesis and significant investigation results. The conclusions of the research discussed in this thesis will be divided into four sections, which are the needle-mesh electrostatic precipitation system, the coaxial electrostatic precipitation system, the biological decontamination system and the simulation on particle charging & removal.

7.1.1 Needle-Mesh Electrode Electrostatic Precipitation System

A novel needle-mesh precipitation system has been designed and developed in Chapter 3. A gauge 14 hypodermic needle and two metallic meshes were used in the electrostatic precipitation system and the detailed design of the system has been introduced in Chapter 3.

To prove the feasibility of the proposed design, precipitation tests were conducted to obtain the precipitation performance of the system. Different types of particles (indoor particles, street airborne particles, bee wax candle particles and cigarette smoke particles) have been used in the precipitation tests. A balloon system has been designed for the street particle collection. The particle number and particle mass of cigarette smoke particles recorded during tests is close to the particle number and particle mass which have been commonly reported in weather reports in heavily polluted areas.

The particle precipitation routine test results show that the performance of the system is excellent and stable. The particle precipitation efficiency for different particles can be as high as almost 100% and can be achieved in very short system running time (less than 30 seconds).

The precipitation operations can be conducted using both a positive and negative DC high voltage energisation. It was found that the performances of both polarities of energisation were very good with almost 100% particle precipitation efficiency within a short time (less than 30 seconds), especially when particle concentration was not high (indoor particles, street airborne particles and bee wax candle particles). When particle concentration was very high (cigarette smoke particles), the performance of the system was also good and stable. For negative energisation, the voltage level used (-10 kV) was similar to the situation when particle concentration is relatively lower, which was just above the corona ignition voltage. However, it required the increase of the voltage level for positive energisation (from 7 kV to 15 kV) to achieve almost 100% particle precipitation efficiency when particle concentration is high.

The energy consumption of the designed system was obtained. In this research, a method of calculating energy consumption based on the current-time waveform was developed. The energy consumption was calculated by the integration of current-time waveforms recorded during particle precipitation tests, which was close to the real situation inside the precipitator. This method has provided another way to calculate energy consumption, which can be more accurate. With the developed method, energy consumptions for different situations were calculated and compared with the energy consumptions in literature. It was found that the electrostatic precipitation system developed was with very low energy consumption for both both positive DC energisation (0.01 Wh/m^3 and 0.353 Wh/m^3) and negative DC energisation (0.258 Wh/m^3).

Ozone concentration level was also considered in the research. The design of the system also included an ozone concentration control section in which a catalyst MnO_2 was used. The ozone level was then lowered to ground level after control which is also environmental friendly.

The results in Chapter 3 have shown the needle-mesh topology electrostatic precipitation system is satisfactory with high particle precipitation efficiency and with low energy consumption. One of the features of this system is that the gas can pass through the hypodermic needles and particles can be charged at the tip of the hypodermic needles, and that is one of the reasons for high particle precipitation efficiency of the system because particles can be charged evenly for the best results in this design. This feature can potentially provide a possible design for research and for practical application of electrostatic precipitation system. Another feature of this system is that the system is very small and portable, which makes the system easy to fit in different environment. The system in Chapter 3 is with low gas flow rate, so potentially it can be used in situations where small volume of gas or particulate matter are needed to be precipitated. Although the system was not tested with higher gas flow rate in this chapter, it is expected that the performance of the system is still satisfactory (high particle precipitation efficiency and low energy consumption) with higher gas flow rate to be used in a wider range of environment.

7.1.2 Coaxial Electrostatic Precipitation System

Two suggestions on the improvement of electrostatic precipitation performance were made and explored in Chapter 4 for the coaxial topology electrostatic precipitators which are widely used in industry. The electrostatic precipitation system with coaxial topology (larger than the needle-mesh system in Chapter 3) has been designed in this project and the details of the system have been illustrated in Chapter 4.

Similar to the research in Chapter 3, particle precipitation tests were conducted to obtain the performance of the developed systems. Different types of particles (indoor particles, bee wax candle particles and cigarette smoke particles) were used in the conducted precipitation tests.

Results show that the designed electrostatic precipitation system was capable of removing almost all the particles from the atmosphere with relatively lower particle concentration (indoor particles and bee wax candle particles). The particle precipitation test results show that the performance of the system was excellent and stable. The particle precipitation efficiency for indoor particles and bee wax candle particles can be as high as ~100% and can be achieved in a very short system running time (tens of seconds). The system can be conducted by both positive and negative DC high voltage energisation. Similar to the needle-mesh system developed in Chapter 3, it was found that the performances of both polarities of energisation are very good, especially when particle concentration was not high (indoor particles and bee wax candle particles). The difference was that the voltage level for positive energisation (20.79 kV) was higher than the voltage level for negative energisation (-14.37 kV) to achieve 100% particle precipitation efficiency. For negative energisation, the voltage level used was just above the corona ignition voltage. However, it required the increase of the voltage level for positive energisation to achieve almost 100% particle precipitation efficiency.

However, the precipitation performance of the system was unsatisfactory when the particle concentration was high, as in the case of cigarette smoke particles. In the worst case, there was > 10% particle penetration. Although 90% of precipitation efficiency was a reasonable result for the electrostatic precipitation system, the aim of this investigation was to develop the system which will provide a maximum of, ideally, 100% precipitation efficiency. Therefore, further steps were made in this research project to improve the electrostatic precipitation efficiency.

The first improvement which was implemented in this research project was an additional precipitation stage in the electrostatic precipitation system. Thus, the double stage system was designed and developed. The precipitation results obtained using this double stage system was compared with the precipitation efficiency of the single stage precipitator. The double stage design aimed at increasing the particle exposure time to the ion flux and

electric field in the electrostatic precipitation system, thus, the second stage can be used to precipitate particles which penetrate the first stage of electrostatic precipitator.

In order to increase the extra stage of the system, a similar coaxial topology electrostatic precipitator was designed and developed. Experiments have been conducted to compare the performance of the single stage and double stage system on particle precipitation when particle concentration is high. The results show that the increase of the stage can provide the system with improved performance, which was the increase of particle precipitation efficiency. The particle precipitation efficiency with a double stage system increases to almost 100% when particle concentration was high (cigarette smoke particles), which has achieved the aim of the research. The better performance can also be reflected from a voltage level aspect. The increase of stage of the system has decreased the voltage level needed for the system to have 100% particle precipitation efficiency (positive: 25 kV to 20.79 kV and negative: -20.29 kV to -14.37 kV). With the two stages of the system, the voltage levels for both positive and negative energisation were just above the corona ignition voltage (20.79 kV for positive energisation and -14.37 kV for negative energisation) which can broaden the usage of the system in certain situations. For example, when there is a limitation in power supply to reach higher voltage levels and there is a need for particle precipitation efficiency, the suggestion of using a double stage system can be made.

The second improvement was the increase in humidity inside the electrostatic precipitator to achieve a better performance of the system. The design of this improvement aimed to use the effect of increased humidity to increase the particle precipitation efficiency. Initially the effect of increased humidity on particle precipitation efficiency of electrostatic precipitators was to be investigated. To investigate the influence of increased humidity on particle precipitation, a humidifier system which can provide the electrostatic precipitator with increased humidity has been designed. The inlet air contaminated with PM (cigarette smoke particles) was mixed with water mist prior to the mixture being pumped into the electrostatic precipitator.

The investigation of the precipitation performance with air flow and increased humidity provided the following results: (1) the magnitude of corona ignition voltage was lowered for both positive and negative energisation (positive energisation: 20.79 kV to 16 kV, negative energisation: -14.37 kV to -9 kV). (2) The magnitude of breakdown voltage was lowered for both positive and negative energisation (positive energisation: 26 kV to 24 kV, negative energisation: -27 kV to -23 kV). (3) The frequency of the corona current was visually much more intensive for both positive and negative energisation. However, there were some differences between positive and negative energisation: (1) in the case of positive energisation, the corona current was quite unstable. It was observed frequently in the tests that there was a variation in current level for a certain value of voltage level which is difficult for measurements. There were also frequent spark breakdowns during the precipitation tests for positive energisation. For negative energisation, the corona current was stable and the measurement of current is simple. The breakdown voltage level was stable. The system worked well as long as the voltage level was kept within the working range (from corona ignition voltage to breakdown voltage). (2) For positive energisation, the performance of the electrostatic precipitation system was not improved when air flow with an increased humidity was used. While for negative energisation, the performance of the electrostatic precipitation system was improved with the increase of humidity (rh 90%). The particle precipitation efficiency was increased to 100% when particle concentration was high (cigarette smoke particles). The voltage level used for increased humidity with 100% precipitation efficiency was lower than the corona ignition voltage in normal humidity (-9 kV compared to -14 kV).

With the results of the investigation, the second suggestion on designing electrostatic precipitators to improve the performance can be made. For a negative DC energised electrostatic precipitation system, the increase of humidity can improve the performance of the system and the applied voltage level can be lowered.

The energy consumption of the precipitation process was also obtained in this research. With the developed method of energy consumption in Chapter 3, the energy consumption for different situations were calculated and compared with the energy consumptions in literature. It was found that the electrostatic precipitation system developed was with very low energy consumption for both positive and negative DC energisation. The system with improvements of double stage and increased humidity was with a very low energy consumption. For positive energisation (100% particle precipitation efficiency), the energy consumption for indoor particles and candle particles are both 0.145 Wh/m^3, and the energy consumption for cigarette smoke particles is 1.665 Wh/m^3 (double stage system). For negative energisation (100% particle precipitation efficiency), the energy consumption for indoor particles and candle particles were both 0.19 Wh/m^3, and the energy consumption for cigarette smoke particles was 1.168 Wh/m^3 (double stage system) and 2.703 Wh/m^3 (increased humidity)

The ozone concentration level was also measured in the research. The design of the system also included an ozone concentration control section, in which a catalyst was used. The ozone level was then lowered to ground level after control which was also environmental friendly.

The most important findings of the research in Chapter 4 are the two solutions to the decrease of the performance of the electrostatic precipitation system when particulate matter concentration is high. The two solutions are important because they can provide possible designs or optimisations of the electrostatic precipitation systems in practical applications. When particulate matter becomes too high to be precipitated in some environment, increasing particulate matter exposure time to plasma (double stage) and increasing humidity to the precipitation environment (increase of humidity) are both possible solutions. The research in Chapter 4 is based on the coaxial system which is commonly used in industry, which provides the research more practical meanings and values. Another important finding that needs to be considered is that the voltage levels used for

best system performance for both double stage system and for increased humidity system are both lower than the single stage system, which gives another possible applications of the two solutions in the situations where there are voltage level limitations.

7.1.3 Biological Decontamination System

The effect of high voltage plasma on biological decontamination has been investigated in Chapter 5. The aim of this research was to prove the possibility of biological decontamination in atmosphere air by corona discharge. The confirmation of the result can establish the corona discharge for wider usage in research and in industry. The biological decontamination system developed for the investigation can be a suggestion of design for biological decontamination by corona discharge, especially for small volumes of gas.

To investigate the possibility of biological decontamination in atmosphere air by corona discharge, a biological decontamination system was designed and developed. The system was altered from the electrostatic precipitation system developed in Chapter 3, which is the needle-mesh topology system.

The experiments were conducted in two groups for comparison (without corona discharge and with corona discharge). The experiments were conducted using negative DC energisation. The results of the CFU show that the corona discharge was effective in biological decontamination of microorganisms and these effects were very clear. The biological decontamination efficiency can be over 90%. As discussed in Chapter 3, the corona reactor was also very efficient in particle precipitation.

Two parameters were controlled to investigate the influence on biological decontamination efficiency: gas flow rate and high voltage level. Different gas flow rates and different high voltage levels were used for comparison. The experimental results show that decreased gas flow rate can increase the exposure time of microorganisms under corona discharge, so the

biological decontamination efficiency was increased. From a voltage level aspect, the increased high voltage level caused the increase of biological decontamination efficiency.

Energy consumption was also considered in this research as the design of the system also aimed to be environmental friendly. With the developed method of energy consumption in Chapter 3, energy consumptions for different situations were calculated and compared with the energy consumptions in literature. It was found that the biological decontamination system developed was with very low energy consumption.

The investigation of biological decontamination in Chapter 5 has provided corona discharge with a potential wider usage. The system can be used not only to control particles in flue gas, but also to control pathogenic microorganisms which can be treated by corona discharge. The research in Chapter 5 can either be a method of controlling certain types of microorganisms emission or provide an extra advantage of using electrostatic precipitation for particulate matter emission control. For the needle-mesh topology system itself, when there is a need for both particles and microorganisms to be controlled, the system can be a suggestion design to meet both demands.

7.1.4 Simulation on Particle Charging and Particle Collection Efficiency

A model was designed and presented in Chapter 6 with an analytical investigation into the dynamics of airborne particles in electrostatic precipitators stressed with DC energisation and particle collection efficiency.

There are two important features of the model developed in this chapter. First, the space charge influenced electric field has been taken into consideration when compared with modelling approaches for electrostatic precipitation. Second, electric parameters of conductivity and relative permittivity for both particles and medium are considered and

included in the model developed in this chapter. Charging mechanisms of field charging and diffusion charging have also been considered in the model.

In this model, ion mobility, which is an important parameter, was measured. The measurement of the ion mobility was through the current-velocity curve fitting of the theoretical and experimental curve. A test system was designed to measure ion mobility and experiments have been conducted to measure ion mobility for different tip-plane distances, humidity and polarity of energisation. Three significant findings are:

1) Increased tip-plane distance results in decreased ion mobility for positive and negative energisation and for different humidity.

2) Increased humidity results in decreased ion mobility for positive and negative energisation and for different tip-plane distances.

3) Ion mobility for negative energisation is higher than ion mobility for positive energisation for different tip-plane distances and for different humidity.

With the measured ion mobility, the model is designed. The model is capable of:

a) Simulating particle dynamics while inside electrostatic precipitators.

b) The collection efficiency of the electrostatic, which is based on the Deutsch-Anderson equation, can be calculated using the model.

The simulation of the model takes particles in the real world with real parameters into consideration. These particles are commonly emitted by industries, such as coal power stations, and the particles include soot, salt, COC and water particles. The influences of different factors which may affect particle dynamics are investigated using the model. These factors include:

1) Particle electric parameters (conductivity and relative permittivity): increased particle conductivity and relative permittivity result in higher particle velocity and larger particle displacement.

2) Initial particle displacement: particles with larger initial displacement have higher velocity and larger final displacement.

3) Ion mobility: increased ion mobility results in lower particle velocity and smaller particle displacement.

4) Current level: increased current level results in higher particle velocity and larger particle displacement.

5) Particle size distribution: increased particle size results in higher particle velocity and larger particle final displacement. The time for particle velocity to reach peak velocity and time for particle velocity to reduce to saturation velocity are longer for increased particle size. Particle displacement is smaller for larger particles when the simulation time is short. There is a minimum collection efficiency for certain particle diameter for different particles. The minimum collection efficiency occurs when the particle diameter is between 0.01 μm (PM 0.01) and 0. 1 μm (PM 0.1) for all types of particles.

6) Gas flow rate: increased gas flow rate results in decreased collection efficiency.

The findings in Chapter 6 have shown the influences of different parameters on particle dynamics inside electrostatic precipitators and influences of different parameters on particle collection efficiency of electrostatic precipitators. Since the design of electrostatic precipitation systems are based on the parameters which have been discussed in Chapter 6, these findings are important as they will help for optimisation of electrostatic precipitation. From research aspect, there is no such model which can simulate particle dynamics and calculate particle collection efficiency with considerations of space charge influenced electric

field and different electric and dielectric parameters of particle and medium, which makes the research in Chapter 6 more important as it provides a more accurate model for further research.

7.2 Future Work

Followed by the conclusions of these innovative techniques proposed for particle electrostatic precipitation, biological decontamination and simulation in this thesis, the potential directions for future research are defined in this section.

Electrostatic precipitation with pulsed power should be investigated in the future as it may be more energy efficient when compared with DC power. If electrostatic precipitation test results of pulsed power are better than those with DC power, and the energy consumption of pulsed power is lower than the energy consumption of DC power, then pulsed power could be used more widely in industry.

Simulation models for electrostatic precipitation with pulsed power should be developed for particle behaviours investigation and precipitation efficiency calculations to provide suggestions on electrostatic precipitator design.

The application of the developed systems to the practical environment in this thesis (the needle-mesh system, the increased humidity coaxial system and the double stage coaxial system) should be investigated. Since the three systems all show good performance in particle precipitation and in energy efficiency in laboratories, it is important to test the performance in a more practical environment.

The performance of the biological decontamination system developed in this thesis should be examined using other types of microorganisms, especially pathogenic microorganisms.

8 References

[1] J Howie, S Tong, K Verrall, R Gerber, and R Wolff, "Air Pollution and Cardiopulmonary Diseases in Australia: A Review of Epidemiological Evidence," *Environmental Health (Aust)* , vol. 5, pp. 23-36, 2005.

[2] E Samoli et al., "Acute Effects of Ambient Particulate Matter on Mortality in Europe and North America: Results from the APHENA Study," *Environ Health Perspect* , vol. 116(11), pp. 1480-1486, 2008.

[3] Y Guo, Y Jia, X Pan, L Liu, and E H Wichmann, "The Association Between Fine Particulate Air Pollution and Hospital Emergency Room Visits for Cardiovascular Diseases in Beijing, China," *Sci Total Environ*, vol. 407(17), pp. 4826-4830, 2009.

[4] D R Brook et al., "Particulate Matter Air Pollution and Cardiovascular Disease: An Update to the Scientific Statement from the American Heart Association," *Circulation*, vol. 121(21), pp. 2331-2378, 2010.

[5] R Chen et al., "Ambient Air Pollution and Hospital Admission in Shanghai, China," *J Hazard Mater* , vol. 181(1-3), pp. 234-240, 2010.

[6] K Schuepp and D P Sly, "The Developing Respiratory Tract and Its Specific Needs in Regard to Ultrafine Particulate Matter Exposure," *Paediatric Respiratory Reviews*, vol. 13(2), pp. 95-99, 2012.

[7] J Heinrich and R Slama, "Fine Particles, A Major Threat to Children," *Int J Hyg Environ Health* , vol. 210(5), pp. 617-622, 2007.

[8] A C Pope and W D Dockery, "Health Effects of Fine Particulate Air Pollution: Lines that Connect," *Journal of the Air & Waste Management Association*, vol. 56(6), pp. 709-742, 2006.

[9] R Brugha and J Grigg, "Urban Air Pollution and Respiratory Infections," *Paediatr Respir Rev* , vol. 15(2), pp. 194-199, 2014.

[10] Air Quality Expert Group, "Particulate Matter in the UK: Summary," Defra, London, 2005.

[11] Department for Environment Food & Rural Affairs, "Air Pollution in the UK 2015," UK, 2016.

[12] T K Whitby, B R Husar, and Benjamin Y.H. Liu, "The Aerosol Size Distribution of Los Angeles Smog," *Journal of Colloid and Interface Sciences* , vol. 39, pp. 177-204, 1972.

[13] J Heintzenberg, "Fine Particles in the Global Troposphere A Review," *Tellus B*, vol. 41(2), pp. 149-160, 1989.

[14] J Cao, "Evolution of PM2.5 Measurements and Standards in the U.S. and Future Perspectives for China.," *Aerosol and Air Quality Research*, vol. 13, pp. 1197-1211, 2013.

[15] W Chen and W D Fryrear, "Aerodynamic and Geometric Diameters of Airborne Particles," *Journal of Sedimentary Research*, vol. 71, pp. 365-371, 2001.

[16] Kok de, MCM Theo, A H Driece, G J Hogervorst, and J J Briede, "Toxicological Assessment of Ambient and Traffic-related Particulate Matter: A Review of Recent Studies," *Mutation Research/Reviews in Mutation Research*, vol. 613.2, pp. 103-122, 2006.

[17] C Reche et al., "New Considerations for PM, Black Carbon and Particle Number Concentration for Air Quality Monitoring Across Different European Cities," *Atmospheric Chemistry and Physics*, vol. 11(13), pp. 6207-6227, 2011.

[18] W C Hinds, *Aerosol Technology: Properties, Behavior, and Measurement of Airborne Particles*. Hoboken, New Jersey, USA: ohn Wiley & Sons, 2012.

[19] US EPA, "Integrated Science Assessment for Particulate Matter," Research Triangle Park, North Carolina, USA, 2009.

[20] C Y Chan, G McTainsh, J Leys, H McGowan, and K Tews, "Influence of the 23 October 2002 Dust Storm on the Air Quality of Four Australian Cities," *Water, Air, and Soil Pollution* , vol. 164, pp. 329-348, 2005.

[21] N Hime, C Cowie, and G Marks, "Review of the Health Impacts of Emission Sources, Types and Levels of Particulate Matter Air Pollution in Ambient Air in NSW ," NSW, Australia, 2015.

[22] W John, S Wall, J Ondo, and W Winklmayr, "Modes in the Size Distributions of Atmospheric Inorganic Aerosol," *Atmospheric Environment*, vol. 24A, pp. 2349-2359, 1990.

[23] H J Seinfeld and N S Pandis, *Atmospheric Chemistry and Physics: From Air Pollution to Climate Change*. Hoboken, NJ, USA: John Wiley & Sons Inc, 2006.

[24] L Morawska, R M Moore, and D Z Ristovski, "Health Impacts of Ultrafine Particles," Canberra, Australian Government, 2004.

[25] M Lippmann, "Toxicological and Epidemiological Studies of Cardiovascular Effects of Ambient Air Fine Particulate Matter (PM2.5) and Its Chemical Components: Coherence and Public Health Implications," *Crit Rev Toxicol* , vol. 44(4), pp. 299-347, 2014.

[26] K Donaldson et al., "Nanoparticles and the Cardiovascular System: A Critical Review," *Nanomedicine*, vol. 8(3), pp. 403-423, 2013.

[27] S Weichenthal, "Selected Physiological Effects of Ultrafine Particles in Acute Cardiovascular Morbidity," *Environ Res* , vol. 115, pp. 26-36, 2012.

[28] R Li et al., "Ambient Ultrafine Particles Alter Lipid Metabolism and HDL Anti-oxidant Capacity in LDLR-null Mice," *Journal of lipid research*, vol. 54(6), pp. 1608-1615, 2013.

[29] R Ruckerl et al., "Air Pollution and Markers of Inflammation and Coagulation in Patients with Coronary Heart Disease," *Am J Respir Crit Care Med*, vol. 173(4), pp. 432-441, 2006.

[30] O J Anderson, G J Thundiyil, and A Stolbach, "Clearing the Air: A Review of the Effects of Particulate Matter Air Pollution on Human Health," *J Med Toxicol* , vol. 8(2), pp. 166-175, 2012.

[31] B G Hamra et al., "Outdoor Particulate Matter Exposure and Lung Cancer: A Systematic Review and Meta-analysis," *Environ Health Perspect*, vol. 122(9), pp. 906-911, 2014.

[32] O Raaschou-Nielsen et al., "Air pollution and lung cancer incidence in 17 European cohorts: Prospective analyses from the European Study of Cohorts for Air Pollution Effects (ESCAPE)," *The Lancet Oncology* , vol. 14(9), pp. 813-822, 2013.

[33] A C Pope III et al., "Lung Cancer, Cardiopulmonary Mortality, and Long-term Exposure to Fine Particulate Air Pollution," *JAMA*, vol. 287(9), pp. 1132-1141, 2002.

[34] Gerald T Joseph and David S Beachler, *Scrubber Systems Operation Review*, Second Edition ed. North Carolina State University , United States: Instructional Designer , 1998.

[35] CR Clean Air. [Online]. https://www.crcleanair.com/uncategorized/wet-scrubbers-high-energy-venturi-scrubbers-packed-bed-scrubbers-solve-most-air-pollution-challenges-in-the-textile-industry/

[36] Honghong Yi et al., "Fine particle and trace element emissions from an anthracite coal-fired power plant equipped with a bag-house in China," *Fuel*, vol. 87, pp. 2050-2057, August 2008.

[37] Rebecca M Maertens, Jennifer Bailey, and White A Paul, "The mutagenic hazards of settled house dust: a review," *Mutation Research/Reviews in Mutation Research*, vol. 567, pp. 401-425, November 2004.

[38] (2015) https://emis.vito.be. [Online]. https://emis.vito.be/en/techniekfiche/fabric-filter

[39] Zhongchao Tan and Yuanhui Zhang, "A Review of Effects and Control Methods of Particulate Matter in Animal Indoor Environments," *Journal of the Air & Waste Management Association* , vol. 54, pp. 845-854, July 2004.

[40] Suvis. [Online]. https://suvis-gmbh.de/en/abscheider/gaszyklon/

[41] http://www.hitachi.com.sg/. [Online]. http://www.hitachi-infra.com.sg/services/energy/dustcollection/dry_type/index.html

[42] Dustin Mulvaney, *Green Technology: An A-to-Z Guide*, 1st ed.: SAGE Publications, Inc, 2011.

[43] http://www.dartmouth.edu. [Online]. http://www.dartmouth.edu/~cushman/courses/engs37/ESPs.pdf

[44] (2013, November) http://nanocontrol.se. [Online]. http://nanocontrol.se/onewebmedia/Advantages%20and%20disadvantages%20of%20particulate%20removal%20devices%202013%2011%2020.pdf

[45] E Kuffel, W S Zaengl, and J Kuffel, *High Voltage Engineering Fundamentals*, Second edition ed. Woburn, USA: Butterworth-Heinemann, 2000.

[46] SOF THESE, "ELECTROSTATIC PRECIPITATION OF FLY ASH FROM AUSTRALIAN BITUMINOUS COALS," Australian, 1998.

[47] Jacob Katz, "Factors Affecting Resistivity in Electrostatic Precipitation," *Journal of the Air Pollution Control Association*, vol. 30, pp. 195-201, February 1980.

[48] U.S. Environmental Protection Agency, "EPA Air Pollution Control Cost Manual (Sixth Edition)," Washington DC, USA, 2002.

[49] James H Turner et al., "Sizing and Costing of Electrostatic Precipitators," *JAPCA*, vol. 38, pp. 458-471, 1988.

[50] Guan-Yu Lin, Tzu-Ming Chen, and Chuen-Jinn Tsai, "A Modified Deutsch-Anderson Equation for Predicting the Nanoparticle Collection Efficiency of Electrostatic Precipitators," *Aerosol and Air Quality Research*, vol. 12, pp. 697–706, 2012.

[51] J Sid Clements et al., "Development of an Electrostatic Precipitator to Remove Martian Atmospheric Dust From ISRU Gas Intakes During Planetary Exploration Missions," *IEEE Transactions on Industry Applications*, vol. 49, pp. 2388-2396, November-December 2013.

[52] Zhuangbo Feng, Zhengwei Long, and Qingyan Chen, "Voltage-current characteristics of needle-plate system with different media on the collection plate," *Journal of Electrostatics*, vol. 72, pp. 129-135, 2014.

[53] H Kawakami, T Inui, T Sato, Y Ehara, and A Zukeran, "Investigation Of Electrode Arrangement On Ionic Wind Velocity For Hole-type Electrostatic Precipitator," *WIT Transactions on Ecology and The Environment*, vol. 183, pp. 177-187, 2014.

[54] Kazuo Shimizu, "Indoor air Quality Improvement Using Atmospheric Plasma," in *Current Air Quality Issues*.: InTech, 2015, ch. 21.

[55] Xuming Zhang, Yifan Huang, Zhen Liu, and Keping Yan, "Aerosol emission and collection in styrene-contaminated air remediation with a multi-stage plasma system," *Journal of Electrostatics*, vol. 76, pp. 31-38, August 2015.

[56] Guan-Yu Lin et al., "High-efficiency wet electrocyclone for removing fine and nanosized particles," *Separation and Purification Technology*, vol. 114, pp. 99-107, August 2013.

[57] Myong-Hwa Lee et al., "Enhanced Collection Efficiency of Nanoparticles by Electrostatic Precipitator with Needle-Cylinder Configuration," *Journal of Nanoscience and Nanotechnology*, vol. 16, pp. 6884-6888, July 2016.

[58] A Bologa, H R Paur, H Seifert, and K Woletz, "Novel Wet Electrostatic Precipitator for Sub-Micron Particles," in *DustConf* , Maastricht, The Netherlands, 2007.

[59] Jong-Ho Kim, Hwa-Su Lee, Hyun-Ha Kim, and Atsushi Ogata, "Electrospray with electrostatic precipitator enhances fine particles collection efficiency," *Journal of Electrostatics*, vol. 68, pp. 305-310, August 2010.

[60] Liqian Wang, Jining Wei, Weimin Zhou, Jianrong Feng, and Lisheng Ji, "An Energy Management System for Electrostatic Precipitator," in *International conference on Electrostatic Precipitation (ICESP VI)*, Budapest, Hungary, 1996.

[61] Bao-Yu Guo, Ding Yang, Yin-Biao Su, and A B Yu, "Process modelling of low temperature electrostatic precipitators," *Powder Technology*, vol. 314, pp. 567-576, June 2017.

[62] White J H, "Particle Charging in Electrostatic Precipitation," *Transactions of the American Institute of Electrical Engineers*, vol. 70, pp. 1186-1191, July 1951.

[63] Jian Guo, Kang Huang, and Jianping Wang, "Bactericidal effect of various non-thermal plasma agents and the influence of experimental conditions in microbial inactivation: A review," *Food Control*, vol. 50, pp. 482-490, April 2015.

[64] Kanako Sekimoto, Rena Gonda, and Mitsuo Takayama, "Effects of H3O+, OH-, O2-, NOx- and NOx for Escherichia coli inactivation in atmospheric pressure DC corona discharges," *Journal of Physics D: Applied Physics*, vol. 48, August 2015.

[65] Danil Dobrynin, Gary Friedman, Alexander Fridman, and Andrey Starikovskiy, "Inactivation of bacteria using dc corona discharge: role of ions and humidity," *New Journal of Physics*, vol. 13, October 2011.

[66] Elena Sysolyatina et al., "Role of the Charged Particles in Bacteria Inactivation by Plasma of a Positive and Negative Corona in Ambient Air," *Plasma Processes and Polymers*, vol. 11, pp. 315-334, January 2014.

[67] Igor V Timoshkin et al., "Bactericidal Effect of Corona Discharges in Atmospheric Air," *IEEE Transactions on Plasma Science*, vol. 40, pp. 2322 - 2333, Oct. 2012.

[68] G Mainelis et al., "Collection of Airborne Microorganisms by Electrostatic Precipitation," *Aerosol Science and Technology*, vol. 30, pp. 127-144, February 1999.

[69] A CK Lai, A CT Cheung, M ML Wong, and W S Li, "Evaluation of cold plasma inactivation efficacy against different airborne bacteria in ventilation duct flow," *Building and Environment*, vol. 98, pp. 39-46, March 2016.

[70] H H Ku, "Notes on the Use of Propagation of Error Formulas," *JOURNAL OF RESEARCH of the National Bureau of Standards - C. Engineering and Instrumentation*, vol. 70C, pp. 264-273, May 1966.

[71] A Bologa, H R Paur, H Seifert, Th Wa¨scher, and K Woletz, "Novel wet electrostatic precipitator for collection of fine aerosol," *Journal of Electrostatics*, vol. 67, pp. 150-153, May 2009.

[72] Gleb Lobov, *Study of the corona discharge phenomenon for application in pathogen and narcotic detection in aerosol*. Stockholm, Sweden: Microsystem Technology KTH Royal Institute of Technology, 2012, Master Thesis.

[73] Arthur Miller, Garrett Frey, Grant King, and Carl Sunderman, "A Handheld Electrostatic Precipitator for Sampling Airborne Particles and Nanoparticles," *Aerosol Science and Technology* , vol. 44, pp. 417-427, 2010.

[74] V Schmatloch and S Rauch, "Design and characterisation of an electrostatic precipitator for small heating appliances," *Journal of Electrostatics*, vol. 63, pp. 85-100, 2005.

[75] Tsuneo Watanabe et al., "Submicron particle agglomeration by an electrostatic agglomerator," *Journal of Electrostatics*, vol. 34, pp. 367-383, 1995.

[76] A Jaworek, A Marchewicz, A T Sobczyk, A Krupa, and A Czech, "Two-stage electrostatic precipitator with co- and counter-flow particle prechargers," *Journal of Electrostatics*, vol. 87, pp. 180-194, June 2017.

[77] Xiang Wang et al., "Electrical characteristics of electrostatic precipitator with a wet membrane-based collecting electrode," *Journal of Electrostatics*, vol. 80, pp. 85-94, April 2016.

[78] Steven A Jaasund, "Control of fine particle emissions with wet electrostatic precipitation," *Environment International*, vol. 6, pp. 233-238, 1981.

[79] Artit Yawootti, Panich Intra, Nakorn Tippayawong, and Phadungsak Rattanadecho, "An experimental study of relative humidity and air flow effects on positive and negative

corona discharges in a corona-needle charger," *Journal of Electrostatics*, vol. 77, pp. 116-122, October 2015.

[80] Gediminas Mainelis et al., "Collection of airborne microorganisms by a new electrostatic precipitator," *Journal of Aerosol Science*, vol. 33, pp. 1417-1432, October 2002.

[81] Caroline Duchaine, "Assessing microbial decontamination of indoor air with particular focus on human pathogenic viruses," *American Journal of Infection Control*, vol. 44, pp. S121-S126, September 2016.

[82] Jae-Seung Jung and Jin-Gyu Kim, "An indoor air purification technology using a non-thermal plasma reactor with multiple-wire-to-wire type electrodes and a fiber air filter," *Journal of Electrostatics*, vol. 86, pp. 12-17, April 2017.

[83] Stefan Schmid et al., "Studying the fate of non-volatile organic compounds in a commercial plasma air purifier," *Journal of Hazardous Materials*, vol. 256-257, pp. 76-83, July 2013.

[84] Kazuo Shimizu, Yusuke Kurokawa, and Marius Blajan, "Basic Study of Indoor Air Quality Improvement by Atmospheric Plasma," *IEEE Transactions on Industry Applications*, vol. 52, pp. 1823-1830, November 2015.

[85] Hyeong Rae Kima, Ji-woon Park, Hyung Sun Kim, Dongeun Yong, and Jungho Hwang, "Comparison of lab-made electrostatic rod-type sampler with single stage viable impactor for identification of indoor airborne bacteria," *Journal of Aerosol Science*, vol. 115, pp. 190-197, Janurary 2018.

[86] Jarotwan Koiwanit, Anastassia Manuilova, Christine Chan, Malcolm Wilson, and Paitoon Tontiwachwuthikul, "Human health risks of post- and oxy-fuel combustion carbon dioxide capture technologies: Hypothetically modeled scenarios," *International Journal of Greenhouse Gas Control*, vol. 47, pp. 279-290, April 2016.

[87] Athanasios C Mermigkas et al., "Removal of Fine and Ultrafine Particles from Air by Microelectrostatic Precipitation," *IEEE TRANSACTIONS ON PLASMA SCIENCE*, vol. 41, pp. 2842-2850, Octover 2013.

[88] A Malik et al., "A Potential Soot Mass Determination Method from Resistivity Measurement of Thermophoretically Deposited Soot," *Aerosol Sci. and Tech*, vol. 45, pp. 284-294.

[89] T Nussbaumer. Characterisation of particles from wood combustion with respect to health relevance and electrostatic precipitation. [Online]. Available:http://www.ieabcc.nl/workshops/task32_2011_graz_aerosols/07_Nussbaumer.pdf

[90] M Maricq and N Xu, "The effective density and fractal dimension of soot particles from premixed flames and motor vehicle exhaust," *Journal of Aerosol Science*, vol. 35, pp. 1251-1274, October 2014.

[91] A Silvestre Ferron, T Reess, J Paillol, L Pecastaing, and P Domens, "Measurement of the treatment efficiency on soot particles flowing into a wire/cylinder filter energized by a repetitive impulse voltage generator," in *15th IEEE International Pulsed Power Conference*, Monterey, California, 2005, pp. 501-504.

[92] J Hautanen et al., "Brownian agglomeration of bipolarly charged aerosol particles," *Journal of Aerosol Science*, vol. 26, pp. S21-S22, 1995.

[93] S H Huang and C C Chen, "Ultrafine aerosol penetration through electrostatic precipitators," *Environmental Science and Technology*, vol. 36, pp. 4625-4632, 2002.

[94] M Jang and R M Kamens, "Atmospheric secondary aerosol formation by heterogeneous reactions of aldehydes in the presence of a sulfuric acid aerosol catalyst," *Environmental Science and Technology*, vol. 35, pp. 4758–4766, 2001.

[95] J H Ji, N G Hwang, and G Y Kim, "Particle charging and agglomeration in DC and AC electric fields," *Journal of Electrostatics*, vol. 61, pp. 57-68, 2004.

[96] A Laitinen, J Hautanen, and J Keskinen, "Bipolar charged aerosol agglomeration with alternating electric field in laminar gas flow," *Journal of Electrostatics*, vol. 38, pp. 303-315, 1996.

[97] B Tan, L Wang, and X Zhang, "The effect of an external DC electric field on bipolar charged aerosol agglomeration," *Journal of Electrostatics*, vol. 65, pp. 82-86, 2007.

[98] M T Nielsen et al., "Formation and emission of fine particles from two coal-fired power plants," *Combustion Science and Technology*, vol. 174, pp. 79-113, 2002.

[99] K Adamiak and P Atten, "Simulation of corona discharge in point-plane configuration,"

Journal of Electrostatics, vol. 6, pp. 85-98, 2004.

[100] K Adamiak, "Numerical models in simulating wire-plate electrostatic precipitators: A review," *Journal of Electrostatics*, vol. 8, pp. 673-680, 2013.

[101] Q Lancereau, J Roux, and J Achard, "Electrohydrodynamic flow regimes in a cylindrical electrostatic precipitator," *IEEE Transactions on Dielectrics and Electrical Insulation*, vol. 8, pp. 1409-1420, 2013.

[102] J Podlinski, J Dekowski, J Mizeraczyk, D Brocilo, and J Chang, "Electrohydrodynamic gas flow in a positive polarity wire-plate electrostatic precipitator and the related dust particle collection efficiency," *Journal of Electrostatics*, vol. 3, pp. 259-262, 2006.

[103] N Farnoosh, K Adamiak, and G S.P Castle, "3-D numerical simulation of particle concentration effect on a single-wire ESP performance for collecting polydispersed particles," *IEEE Transactions on Dielectrics and Electrical Insulation*, vol. 2, pp. 211-220, 2011.

[104] M Alonso and F J Alguacil, "Electrostatic precipitation of ultrafine particlesenhanced by simultaneous diffusional deposition on wire screens," *Air & Waste Manage*, vol. 52, pp. 1342-1347, 2002.

[105] E Barreto and K Martinot, "Nonthermal ionization caused by aerodynamic discontinuities in charged aerosol jets," *Phys. Fluids*, vol. 10, pp. 2155-2163, 1967.

[106] G Biskos, K Reavell, and N Collings, "Electrostatic characterisation of corona-wire aerosol chargers," *Journal of Electrost*, vol. 63, pp. 69-82, 2005.

[107] J Hao, K He, and H Chao, "Calculation of electric field strength distributions fornew electrostatic precipitator discharge electrode designs," *Air Waste and Manage*, vol. 40, pp. 1510-1513, 1990.

[108] C H Huang and M Alonso, "Influence of particle location on the number ofcharges per charged nanoparticle at the outlet of a needle charger," *Air Waste and Manage*, vol. 62, pp. 87-91, 2012.

[109] L Li and D R Chen, "Performance study of a DC-corona-based particle charger for charge conditioning," *Aerosol Sci*, vol. 42, pp. 87-99, 2011.

[110] W Y Lin, Y Y Chang, C T Lien, and C W Kuo, "Separation characteristics of submicron particles in an electrostatic precipitator with alternating electric field corona charger," *Aerosol Sci. Technol*, vol. 45, pp. 393-400, 2011.

[111] Yihan Liu et al., "Analysis of influences of dielectric and electrical properties on particle charging," in *2013 19th IEEE Pulsed Power Conference (PPC)*, San Francisco, CA, USA, 2013.

[112] Yihan Liu, Igor Timoshkin, Mark Wilson, Martin Given, and MacGregor Scott, "Charging and dynamics of fine air-borne particles in impulsive electric fields," in *2014 IEEE International Power Modulator and High Voltage Conference (IPMHVC)*, Santa Fe, NM, USA, 2014.

[113] L Morawska, V Agranovski, Z Ristovski, and M Jamri, "Effect of face velocity and the nature of aerosol on the collection of submicrometer particles by electrostatic precipitator," *Indoor air*, vol. 12, pp. 129-137, 2002.

[114] A Niewulis, J , A Berendt, and J Mizerac, "Investigation of narrow transvers and longitudinal electrostatic precipitator," *Plasma Environ. Sci.Technol.*, vol. 6, pp. 172-176, 2012.

[115] A Zukeran, Y Ikeda, Y Ehara, T Ito, and T Takahas, "Agglomeration of particles by AC corona discharge," *Electr. Eng. Jpn*, vol. 130, pp. 30-37, 2000.

[116] I P Chung and D Dunn-Rankin, "In situ light scattering measurements of mainstream and sidestream cigarette smoke," *Aerosol Sci. Technol*, vol. 24, pp. 85-101, 1996.

[117] L Unger, D Boulaud, and J P Borra, "Unipolar field charging of particles by electrical discharge: Effect of particle shape," *J. Aerosol Sci.*, vol. 35, pp. 965-979, August 2004.

[118] K Adamiak, "Rate of charging of spherical particles by monopolar ions in electric fields," *IEEE Trans. Ind. Appl*, vol. 38, pp. 1001-1008, 2002.

[119] X Li, X Zhang, J Zhu, W Feng, and K Yan, "Sensitivity analysis on the maximum ash resistivity in terms of its compositions and gaseous water concentration," *J. Electrostat*, vol. 70, pp. 83-90, 2012.

[120] J P Borra, "Nucleation and aerosol processing in atmospheric pressure electrical discharges: powders production, coatings and filtration," *J. Phys. D. Appl.Phys*, vol. 39, pp. R19-R54, 2006.

[121] H H Kim, H Kobara, and A Ogata, "Comparative assessment of different non-thermal plasma reactors on energy efficiency and aerosol formation from the decomposition of gas-phase benzene," *IEEE Trans. Ind. Appl*, vol. 41, pp. 206-214, 2005.

[122] D J Bayless, M K Alam, and R Radcliff, "Membrane-based wet electrostatic precipitation," *Fuel Process. Technol*, vol. 85, pp. 781-798, 2004.

[123] Agung Sudrajad and Ahmad Fitri Yusof, "Review of electrostatic precipitator device for reduce of diesel engine particulate matter," in *2nd International Conference on Sustainable Energy Engineering and Application, ICSEEA 2014*, 2014, pp. 370-380.

[124] R Boichot, "Agglomeration of diesel particles by an electrostatic agglomerator under positive DC voltage: Experimental study," *Journal of Electrostatics*, vol. 66, pp. 235-245, 2008.

[125] J S Townsend, *Electricity in Gases*.: Oxford: Clarendon Press, 1915.

[126] Bingxian Lu, Hongyu Sun, Ying Yang, and Qiukun Wu, "The role of negative corona in charged particle dynamics," *Simulation Modelling Practice and Theory*, vol. 74, pp. 64-79, 2017.

[127] A Mizuno, "Electrostatic precipitation," *IEEE Transactions on Dielectrics and Electrical Insulation*, vol. 7, pp. 615-624, 2000.

[128] W Liang and T Lin, "The characteristics of ionic wind and its effect on electrostatic precipitator," *Aerosol Science & Technology*, vol. 2, pp. 330-344, 1994.

[129] S H Huang and C C Chen, "Filtration characteristics of a miniature electrostatic precipitator," *Aerosol Sci. Technol*, vol. 35, pp. 792-804, 2001.

[130] K Thimsen and T J Kotz, "The performance of an electrostatic agglomerator as a diesel soot emission control device," *SAE Trans*, vol. 99, pp. 728-737, 1990.

Appendix

List of Publications

Y. Liu, I. V. Timoshkin, S. J. MacGregor, M. P. Wilson, M. J. Given and T. Wang, "Analysis of influences of dielectric and electrical properties on particle charging," *The 19th IEEE Pulsed Power Conference*, San Francisco, CA, 2013, pp. 1-6.

Y. Liu, I. V. Timoshkin, M. P. Wilson, M. J. Given and S. J. MacGregor, "Charging and dynamics of fine air-borne particles in impulsive electric fields," *The IEEE International Power Modulator and High Voltage Conference*, Santa Fe, NM, 2014, pp. 435-438.

Y. Liu, I. V. Timoshkin, S. J. MacGregor, M. P. Wilson, M. J. Given, “Particle Dynamics and Precipitation Efficiency in Electric Fields,” The UK Technological Plasma Workshop, Coventry, UK, 2014.